UNIVERSITY OF OKLAHOMA

GRADUATE COLLEGE

TECTONICS AND ALTERATION OF OKLAHOMA BASEMENT ROCKS

A DISSERTATION

SUBMITTED TO THE GRADUATE FACULTY

in partial fulfillment of the requirements for the

Degree of

DOCTOR OF PHILOSOPHY

By

MATTHEW HAMILTON
Norman, Oklahoma
2021

Downloaded from SHAREOK. Persistent Handle URL: https://hdl.handle.net/11244/332307

TECTONICS AND ALTERATION OF OKLAHOMA BASEMENT ROCKS

A DISSERTATION APPROVED FOR THE
SCHOOL OF GEOSCIENCES

BY THE COMMITTEE CONSISTING OF

Dr. R. Douglas Elmore, Chair

Dr. Barry L. Weaver

Dr. Brett M. Carpenter

Dr. Zulfiquar A. Reza

© Copyright by MATTHEW HAMILTON 2021
All Rights Reserved.

ACKNOWLEDGMENTS

My thanks to my advisor, Dr. Doug Elmore, for the years of guidance, encouragement, and support. I am also grateful for feedback, discussions, and support from my committee members, Drs. Weaver, Carpenter, and Reza. Several other faculty in the School of Geosciences have also been extremely helpful – Drs. Mike Engel, Shannon Dulin, and Andy Elwood-Madden in particular provided abundant technical assistance and insightful discussions. Emeritus professor Charles Gilbert has also been an excellent source of information on the igneous geology of Oklahoma, as has Dr. Andrew Cullen.

Many thanks go to fellow students I have had the pleasure of working with and/or alongside. I have particularly benefited from discussions with Gerhard Heij, Katie Garrett, and Fola Kolawole, and field work with the latter two as well. Undergraduate student Candace Johnston also performed a substantial amount of lab work that was partially incorporated into Chapter 3.

I am additionally grateful to many outside of the department who have been of great help. Stacey Evans (formerly of the Oklahoma Geological Survey) was a collaborator in the work presented in Chapter 3 and assisted with sampling related to Chapters 2-5, as did the staff at the Oklahoma Petroleum Information Center. Mike Jackson (IRM) and Martin Chadima (AGICO, Inc.) have been extremely helpful as collaborators on the project presented in Chapter 4. Dario Bilardello and Peter Solheid (both at the IRM) provided extensive technical assistance with magnetic measurements and some very informative discussions. Will Deaton assisted greatly with field work in the Wichita Mountains area.

The Institute for Rock Magnetism (IRM) at the University of Minnesota provided a visiting fellowship award which facilitated many of the rock magnetic measurements included

here. Research in the Wichita Mountains area was supported by a graduate student research award from the Geological Society of America with an additional award from its Geophysics & Geodynamics division.

My mother, grandparents, and other family members have encouraged me throughout this, and my friends helped maintain what sanity I can lay claim to. I am also grateful for the 11 years I had with my dog Sansha, who passed as I finished the final edits on this dissertation. They all have my gratitude for their longstanding support.

TABLE OF CONTENTS

ACKNOWLEDGMENTS iv
LIST OF FIGURES ix
LIST OF TABLES xiii
ABSTRACT xiv
CHAPTER 1: INTRODUCTION 1
REFERENCES 6
CHAPTER 2: THE TEXACO KOHPAY L 16-WS: THE OSAGE MICROGRANITE REVISITED 11
OVERVIEW 11
GEOLOGICAL CONTEXT 12
CORE DESCRIPTION AND PETROGRAPHY 14
GEOCHEMISTRY 26
MAGNETIC SUSCEPTIBILITY 29
DISCUSSION 30
CONCLUSIONS 34
REFERENCES 34
CHAPTER 3: FRACTURED, ALTERED, AND FAULTED BASEMENT IN NORTHEASTERN OKLAHOMA: IMPLICATIONS FOR INDUCED SEISMICITY 38
ABSTRACT 38
INTRODUCTION 39
GEOLOGIC SETTING 41
Basement Lithology 41
Tectonic History and Basement Structure 44
MATERIALS AND METHODS 46
OBSERVATIONS AND RESULTS 48
Fractures 48
Secondary Minerals in Fractures 53
Other Fracture Fills 59
Slip 60
Basement Alteration 64
ANALYSIS AND DISCUSSION 71
SUMMARY 74
REFERENCES 75

CHAPTER 4: MAGNETIC CHARACTERISTICS OF ROCKS WITH STRONGLY NEGATIVE FIELD-DEPENDENCE OF SUSCEPTIBILITY FROM THE BASEMENT-COVER INTERFACE OF NORTHEASTERN OKLAHOMA 85
ABSTRACT 85
INTRODUCTION 85
MATERIALS AND GEOLOGICAL CONTEXT 89
METHODS 90
RESULTS 91
Room-Temperature Bulk Susceptibility 91
Hysteresis 93
Low-Temperature Remanence 96
High Temperature Susceptibility and Effects of Heating 98
Low-Temperature Susceptibility 100
Field-Dependence Variation with Temperature 103
DISCUSSION 105
CONCLUSION 108
REFERENCES 110
CHAPTER 5: RECONNAISSANCE PALEOMAGNETIC AND MAGNETIC FABRIC STUDY OF THE SPAVINAW GRANITE 116
ABSTRACT 116
INTRODUCTION 117
GEOLOGICAL SETTING 118
METHODS AND MATERIALS 122
RESULTS 123
Petrographic Observations 123
Bulk Magnetic Susceptibility and Anisotropy 125
High-Temperature Susceptibility 128
Hysteresis 130
Low-Temperature Remanence Cycling 133
Paleomagnetic Results and Interpretations 134
DISCUSSION 141
CONCLUSION 148
REFERENCES 149

CHAPTER 6: PALEOMAGNETISM AND MAGNETIC FABRICS OF THE EARLY CAMBRIAN GLEN MOUNTAINS LAYERED COMPLEX AND ASSOCIATED MAFIC-INTERMEDIATE UNITS, WICHITA MOUNTAINS, OKLAHOMA 156
ABSTRACT 156
INTRODUCTION 156
GEOLOGICAL BACKGROUND 158
METHODS 162
RESULTS AND INITIAL INTERPRETATIONS 164
Site CS1520, Cold Springs Granitoid 166
Sites RP-1 and RP-3, Glen Creek Gabbro 172
Site GM19-1, Unnamed Roosevelt Gabbro 179
Site RP-2, Glen Mountains Layered Complex 184
Site GM19-2, GMLC 188
Site GM19-3, GMLC 193
Site GM1535, GMLC 197
Site GM1530, GMLC 200
Site GM1480-1, GMLC 204
Site GM1480-2, GMLC 208
Site GM54-1, GMLC 213
Site GM54-2, GMLC 217
Sites GM1500-1 and GM1500-2, GMLC 222
Site GM2160-1, GMLC 228
Site GM2160-2, GMLC or Unnamed Roosevelt Gabbro 234
DISCUSSION 238
In-Situ Paleomagnetism 238
Evaluation of Tilting 242
SUMMARY 245
REFERENCES 247
CHAPTER 7: SUMMARY AND SYNTHESIS 259

LIST OF FIGURES

CHAPTER 2

Figure 1. Generalized map of northeast Oklahoma basement subcrop lithology with location of the Kohpay core. 13

Figure 2. Whole-rock photographs from the Kohpay core. 15

Figure 3. Photomicrograph mosaic of thin section from 2843-2844' core interval. 17

Figure 4. Photomicrograph mosaic of thin section from 2844-2847' core interval. 18

Figure 5. Porphyritic texture and groundmass character. 19

Figure 6. Characteristics of quartz phenocrysts. 20

Figure 7. Altered feldspar phenocryst showing abundant chlorite and oxide inclusions. Cross-polarized light, 2844-47' interval. 21

Figure 8. Zircons from the Kohpay core. 22

Figure 9. Backscattered electron images of zircons from 2844-47' interval. 23

Figure 10. Mineralogical examples of hydrothermal alteration. 24

Figure 11. Deformation lamellae in quartz, cross-polarized light. 25

Figure 12. Normalized multi-element variation diagrams for the Kohpay core. 28

Figure 13. Variation of magnetic susceptibility of three sub-samples from the Kohpay core. 30

CHAPTER 3

Figure 1. Generalized map of upper basement rocks in the study area. 40

Figure 2. Mineralogical and chemical classification of study area basement rock units. 43

Figure 3. Rose plots of regional orientations of faults, fractures and surface lineaments. 46

Figure 4. Steeply-inclined mineralized fractures from various basement cores. 49

Figure 5. Abundance and inclination-frequency distribution of mineralized fractures in the Amoco SHADS 4 vs. depth below basement unconformity 51

Figure 6. Porosity hosted in basement fractures. 53

Figure 7. Variable mineralogy in basement fractures. 55

Figure 8. Multiple stages of mineralization in fractures. 57

Figure 9. Slip indicators in NE Oklahoma basement fractures. 61

Figure 10. Microscopic features associated with sheared veins and injectites. 63

Figure 11. Basement alteration adjacent to fractures in core material. 67

Figure 12. Relative element mobility in altered granitoids. 69

CHAPTER 4

Figure 1. Location of general study area and individual cores, with representative plots of susceptibility vs. field and depth profiles of susceptibility, its frequency-dependence and field-dependence across the unconformity of the SHADS 4. 88

Figure 2. (a) Relationship between field-dependence and frequency-dependence of susceptibility for northeastern OK specimens. (b) Field-dependence at multiple frequencies for a sandstone sample from the SHADS 4, showing dependence of χ_{HD} on frequency. (c) Correlation of out-of-phase susceptibility parameter X_{ON} with normalized frequency-dependence χ_{FN}. (d-f) Relationships of χ_{HD} to χ_{FD} from each core. 93

Figure 3. Representative slope-corrected high-field (1-2 T) hysteresis loops of specimens with negative χ_{HD}, showing range of coercivities and shapes. Inset plots show data before and after slope-correction. 95

Figure 4. Low-field hysteresis measurements of a specimen from the Jones 46. 96

Figure 5. Low-T remanence curves showing the range of behaviors observed. 98

Figure 6. High-T susceptibility measurements (left) and calculated derivatives of heating curves(right). 99

Figure 7. Temperature variation of in-phase (χ') and out-of-phase (χ'') AC susceptibility at 3 frequencies from 10 to 400 Kelvin. 102

Figure 8. Temperature variation of χ_{HD}. 104

Figure 9. Temperature variation of χ_{HD} adjusted for temperature variation of bulk susceptibility. 105

CHAPTER 5

Figure 1. Uppermost basement lithology, regional structure, and topography of northeastern Oklahoma. 120

Figure 2. Classification of the Spavinaw Granite Group using the Quartz-Alkali Feldspar-Plagioclase scheme. 121

Figure 3. Petrographic character of the Spavinaw Granite. 125

Figure 4. AMS of the Spavinaw Granite. 128

Figure 5. High-temperature magnetic susceptibility behavior of Spavinaw Granite samples. 130

Figure 6. Hysteresis measurements and backfield coercivity spectra of Spavinaw Granite Samples. 132

Figure 7. Low-temperature cycling of room-temperature saturation remanence. 133

Figure 8. Demagnetization analysis of the Spavinaw Granite. 138

Figure 9. Virtual geomagnetic poles from in-situ and tilt-corrected directions from the Spavinaw Granite compared to the Phanerozoic apparent polar wander path for North America. 140

CHAPTER 6

Figure 1. Generalized map of igneous unit outcrops in the study area, with sampling locations indicated. 160

Figure 2. Hysteresis and backfield remanence data for a sample of Cold Springs granitoid at site CS1520. 167

Figure 3. Low-temperature remanence data for Cold Springs granitoid, site CS1520. 168

Figure 4. AMS results for site CS1520. 169

Figure 5. Paleomagnetic results from site CS1520. 171

Figure 6. Hysteresis and backfield remanence data for samples of Glen Creek Gabbro at sites RP-1 and RP-3. 174

Figure 7. AMS results for Glen Creek Gabbro sites RP-1 and RP-3. 176

Figure 8. Bulk susceptibility (left) and Q-factor (right) as a function of depth below the outcrop surface at site RP-3. 177

Figure 9. Paleomagnetic results from Glen Creek Gabbro, site RP-3. 179

Figure 10. Hysteresis loop and remanent coercivity spectrum for Roosevelt Gabbro at site GM19-1. 180

Figure 11. AMS results for Roosevelt Gabbro at site GM19-1. 181

Figure 12. Paleomagnetic results from unnamed Roosevelt Gabbro, site GM19-1. 183

Figure 13. Hysteresis and coercivity spectra of anorthosite samples from site RP-2. 185

Figure 14. AMS data from Glen Mountains Layered Complex anorthosite at site RP-2. 186

Figure 15. Paleomagnetic results for GMLC anorthosite at site RP-2. 187

Figure 16. Hysteresis and coercivity spectrum for GMLC anorthosite at site GM19-2. 188

Figure 17. AMS results for site 19-2, GMLC. 190

Figure 18. Paleomagnetic results for GMLC site GM19-2. 192

Figure 19. Hysteresis and remanence coercivity spectrum for anorthosite at site GM19-3. 194

Figure 20. AMS results for GMLC site 19-3. 194

Figure 21. Paleomagnetic results from GMLC site GM19-3. 196

Figure 22. Hysteresis loop and coercivity spectrum for sample from GMLC site GM1535. 197

Figure 23. AMS Results from GMLC site GM1535. 198

Figure 24. Paleomagnetic results from site GM1535. 199

Figure 25. Hysteresis and backfield coercivity results for site GM1530. 201

Figure 26. AMS results for GMLC site GM1530. 202

Figure 27. Paleomagnetic results for GMLC site GM1530. 203

Figure 28. Hysteresis and coercivity spectrum for a sample from GMLC site GM1480-1..... 205
Figure 29. AMS results from site GM1480-1. 206
Figure 30. Paleomagnetic results from site GM1480-1. 207
Figure 31. Hysteresis and remanence coercivity spectrum for sample from site GM1480-2..... 208
Figure 32. Low-temperature remanence curves for sample from site GM1480-2. 210
Figure 33. AMS results for GMLC site GM1480-2. 211
Figure 34. Paleomagnetic results from site GM1480-2. 212
Figure 35. Hysteresis and remanent coercivity spectrum for anorthosite from site GM54-1..... 213
Figure 36. Low-T remanence data for anorthosite sample from site GM54-1. 214
Figure 37. AMS results for anorthosite at site GM54-1. 215
Figure 38. Paleomagnetic results for GMLC anorthosite at site GM54-1. 216
Figure 39. Hysteresis and coercivity spectrum for anorthosite from site GM54-2. 218
Figure 40. Low-T remanence curves for anorthosite from site GM54-2. 219
Figure 41. AMS results for GMLC anorthosite at site GM54-2. 220
Figure 42. Paleomagnetic results from site GM54-2. 221
Figure 43. Hysteresis and remanent coercivities from samples of the anorthosite hill at sites GM1500-1 and GM1500-2. 224
Figure 44. AMS results for anorthosite hill sites GM1500-1 and GM1500-2. 225
Figure 45. Paleomagnetic results for site GM1500-1.. 226
Figure 46. Paleomagnetic results for site GM1500-2. 228
Figure 47. Hysteresis and remanence coercivity data for anorthosite from site GM2160-1. 230
Figure 48. Low-temperature remanence data for anorthosite from site GM2160-1. 231
Figure 49. AMS results from anorthosite at site GM2160-1. 232
Figure 50. Paleomagnetic results for anorthosite at site GM2160-1. 233
Figure 51. Hysteresis and remanent coercivity data from gabbro at site GM2160-2. 235
Figure 52. AMS results from gabbro at site GM2160-2. 236
Figure 53. Paleomagnetic results for site GM2160-2.. 237
Figure 54. Compiled in-situ VGPs for all sites in this study, with interpreted trends and primary mean VGP. 239
Figure 55. Comparison of in-situ VGPs to those recalculated using various structural corrections. 244

LIST OF TABLES

CHAPTER 2

Table 1: Whole-rock geochemistry of sample from 2844-47' interval of Kohpay core 27
Table 2: Whole-rock geochemistry of Wichita Granites for comparison 29

CHAPTER 3

Table 1: Core locations, Lithologies, and Depths 47
Table 2: Whole-rock analyses of highly-altered vs. less-altered granitoids 69

CHAPTER 5

Table 1: Bulk magnetic properties of the Spavinaw Granite Group 136
Table 2: Directional magnetic properties of Spavinaw Granite outcrop samples 137

CHAPTER 6

Table 1: Paleomagnetic Results of GMLC and Associated Sites 164
Table 2: Magnetic Susceptibility and NRM Intensity of GMLC and Associated Sites .. 165
Table 3: AMS Mean Tensor Parameters of GMLC and Associated Sites 165

ABSTRACT

The igneous and metamorphic rocks which underlie the sedimentary section of an area (colloquially referred to as “basement” rocks) exert substantial influence on the overlying younger rocks. Large structural features are rooted in basement rocks, and additionally the basement usually contains the only available information regarding the pre-sedimentary geological history. Secondary alteration processes in basement rocks can significantly change their mineralogy and mechanical properties. Understanding of geological history and regional structures within a given area therefore requires study of its basement rocks.

This dissertation utilizes petrographic, geochemical, structural, and magnetic approaches to study the basement rocks of Oklahoma. New petrographic observations of the Mesoproterozoic Osage Microgranite in northeastern Oklahoma provide evidence of deformation and secondary alteration and suggest a possible extrusive origin for this unit. Geochemical data additionally suggest a subduction-related origin. Study of several cores in northeastern Oklahoma shows that fracturing and hydrothermal alteration are pervasive in the area’s basement rocks, in contrast to common assumptions of intact granite used in modeling studies of induced/triggered seismicity. Magnetic susceptibility measurements of some altered basement rocks and overlying clastic sediments show highly unusual properties, including a strongly negative relationship between susceptibility and the strength of the measuring field. Detailed study shows this is likely due to an unknown magnetic mineral which saturates at very low fields and has a Curie temperature near 85 °C.

Paleomagnetic study of the ~1370 Ma Spavinaw Granite yields evidence of remagnetization in the early Cambrian and in the middle Paleozoic. Magnetic fabric data suggests it is either strongly tilted relative to its original emplacement or was emplaced as a dike

rather than a horizontal sill. Paleomagnetic data from intermediate and mafic rocks associated with the early Cambrian Glen Mountains Layered Complex in southwestern Oklahoma provide a new constraint on the paleogeography of Laurentia, with implications for various hypotheses relating to early Cambrian geomagnetic behavior. Additionally, some sites show evidence of partial to complete remagnetization in the middle and late Paleozoic.

CHAPTER 1

INTRODUCTION

The igneous and metamorphic rocks which underlie the sedimentary section of an area exert substantial influence on the distribution and characteristics of the younger rocks above. These units (colloquially referred to as "basement" rocks) control the distribution of the lowermost sediments through paleotopography, and in many cases these sediments are themselves derived from the underlying basement. Large-scale structural features originate from movement within the basement that is then propagated into the overlying sections. Additionally, these rocks are often the only source of information regarding geological history prior to deposition of the oldest preserved sediments. Understanding of geological history and regional structures within a given area therefore requires study of its basement rocks.

Within the state of Oklahoma, the basement rocks are of two distinct age groups. The older group consists mainly of Mesoproterozoic granites and rhyolites which underlie most of the state but are only exposed in the Arbuckle Uplift and a tiny area in northeastern Oklahoma (Ham et al., 1964; Denison, 1966, 1981); these rocks date to ~1400-1370 Ma (ages compiled in Bickford et al., 2015). Most knowledge of these rocks in the northern and central parts of the state comes from petrographic and radiogenic isotope study of borehole samples (Denison, 1981; Bickford et al., 2015). The younger group is exposed in the south-central and southwestern parts of the state and is of early Cambrian age (Ham et al., 1964; Gilbert, 1983); its exposures consist mainly of granite and rhyolite with associated mafic igneous rocks, though mafic units constitute the bulk of the associated rock in the subsurface (e.g., Hanson et al., 2013). Both groups are comprised almost entirely of igneous rocks, though the older group contains units with contact metamorphic features in the subsurface (Denison, 1981).

Petrographic examination is a crucial part in study of igneous rocks, particularly when attempting to determine the conditions under which they formed (e.g., Shelley, 1993). This approach also allows identification of minerals and textures formed from secondary alteration processes as well as microstructures associated with deformation (Vernon, 2004). Chapter 2 provides a petrographic study of material from the Osage Microgranite, a Precambrian unit known only from subsurface samples described by Denison (1966, 1981). This work provides new descriptions of mineralogy and textures of this rock as well as a detailed geochemical analysis. The new data provide new insights regarding the formation of this rock as well as later episodes of alteration and deformation. A version of this chapter was previously published in the Oklahoma City Geological Society's journal *The Shale Shaker* with co-authors Barry Weaver and Doug Elmore.

Hydrothermal alteration (noted in Chapter 2) can significantly affect the mineralogy and the mechanical properties of rocks (e.g., Bruhn et al., 1994; Callahan et al., 2019). Prior history of fracturing has an even larger effect (Bruhn, 1994), and the presence of fractures significantly changes the hydraulic properties of basement rocks (e.g., Holdsworth et al., 2019). In northern and central Oklahoma, the abundance of earthquakes began to increase exponentially in 2008. These earthquakes follow pre-existing faults in the basement rocks and are triggered due to wastewater injection in the overlying Arbuckle Group carbonates (Keranen et al., 2013, 2014). The mechanisms by which they are triggered remain a subject of research, and due to the extremely limited exposures, most models assume properties of intact crystalline granite. Chapter 3 presents direct observations of basement rock in cores recovered from the subsurface of northeastern Oklahoma. Fractures and alteration characteristics seen in the subsurface are documented via petrography, fracture characterization methods, and geochemical analysis. These

data are then integrated with known regional structural trends to provide a more realistic description of the basement rocks in the area. A version of Chapter 3 was published in the *Journal of Structural Geology* with co-authors Brett Carpenter, Candace Johnston, Folarin Kolawole, Stacey Evans and Doug Elmore.

In addition to mechanical properties, secondary alteration by fluid activity can also significantly affect the magnetic properties of rocks. Magnetic susceptibility is perhaps the most convenient of these to measure, and changes in susceptibility directly relate to variations in mineralogy (Lapointe et al., 1986; Dunlop and Özdemir, 1997). Additionally, changes in magnetic susceptibility with the amplitude of the measuring field can be used to make inferences about magnetic mineralogy (Hrouda et al., 2006) and variation with the frequency of an applied AC field can provide information on the particle size of ferrimagnetic minerals (Worm, 1998). Measurements of magnetic susceptibility with the strength and frequency of the measuring field yielded some highly unusual trends for samples of the uppermost basement rocks and lowermost sediments from cores in northeastern Oklahoma. Chapter 4 provides an extensive study of rock magnetic properties associated with these behaviors. Analysis of this data is used to characterize the magnetic mineralogy and identify properties which are specifically linked to this behavior. An extended version of this chapter is being prepared for submission to *Journal of Geophysical Research: Solid Earth* with co-authors Mike Jackson, Martin Chadima, and Doug Elmore.

Additional magnetic techniques which may be of use in deciphering the history of rocks include anisotropy of magnetic susceptibility (AMS) and paleomagnetic analysis of remanent magnetization and its decay. AMS measurements define a second-order tensor (often described as a “fabric”) which in igneous rocks may reflect their emplacement and/or later episodes of deformation and alteration (Tarling and Hrouda, 1993). Remanent magnetization is acquired

during initial cooling and may be partially or completely overprinted by later episodes of heating or fluid alteration (Dunlop and Özdemir, 1997). Analysis of the decay of remanence during demagnetization treatments may yield individual magnetic components which contribute to the bulk remanence direction (Butler, 1992). Analysis of these individual components can be used to determine the age of the magnetizations (e.g., Elmore et al., 1998). Chapter 5 provides the first paleomagnetic and rock magnetic data from the ~1370 Ma Spavinaw Granite outcrop in northeastern Oklahoma in nearly 50 years, as well as the first measurements of AMS. Previous studies (Hawes, 1952; Spall and Noltimier, 1972) found scattered directions which they were unable to interpret. Use of modern experimental and data analysis methods helps to explain some of their findings as well as refine the properties of the magnetic carrier minerals. The AMS data in combination with the paleomagnetic results yield a new interpretation for the magnetization and history of the Spavinaw Granite.

The previously mentioned paleomagnetic method of determining the age of magnetizations in rocks relies on the knowledge of expected magnetic directions through time. This is constructed through paleomagnetic analysis of rocks where the magnetization is well constrained to be of essentially the same age as the rock itself, and apparent geomagnetic poles are calculated. The progression of these apparent magnetic poles through time is used to construct an "apparent polar wander path" for each stable continental block (Butler, 1992), to which apparent poles are compared in order to determine their age. These are well-defined for most of the Phanerozoic, but the early Cambrian pole position for North America remains controversial. The most-accepted apparent polar wander path (Torsvik et al., 2012) only uses a single constraint for North America at ages greater than 510 Ma, that provided by a study of ~530 Ma syenites from Quebec (McCausland et al., 2007). The pole position of that study differs

from several other studies of similarly-aged rocks, including multiple studies from granites and rhyolites of southern Oklahoma (e.g., Spall, 1968; Elmore et al., 1998; Hamilton et al., 2016). In fact, there is a great deal of variation in paleomagnetic studies of Ediacaran to early Cambrian rocks worldwide, which has led to numerous hypotheses including rapid inertial-interchange true polar wander (e.g., Kirschvink et al., 1997), non-uniformitarian geodynamo behavior such as an equatorial dipole (Abrajevitch and van der Voo, 2010), and late Ediacaran to early Cambrian nucleation and growth of the solid inner core (Bono et al., 2019 and refs therein).

Chapter 6 presents new paleomagnetic, rock magnetic and AMS data from the Glen Mountains Layered Complex of southern Oklahoma, recently dated at 532.49 Ma (Wall et al., 2021) and associated mafic and intermediate igneous rocks. This chapter lays out the new data in an effort to provide an additional constraint to the early Cambrian apparent polar wander path and possibly constrain some of the hypotheses for geomagnetic field behavior at that time. Some sites contain partial to complete late Paleozoic overprints similar to those found in many Cambrian rocks and which have historically led to spurious interpretations such as the "Cambrian Loop" of North America's apparent polar wander path (Watts et al., 1980). Results of this study also provide a possible explanation for the discrepancies between prior results from granites and rhyolites of southern Oklahoma relative to other early Cambrian rocks. Additionally, this chapter provides an initial evaluation of the possibility of using AMS data as a tilt correction in igneous rock where paleohorizontal is difficult to constrain, as AMS foliation in layered mafic rocks is generally expected to reflect mineral lamination (e.g., O'Driscoll et al., 2015).

Finally, Chapter 7 summarizes the results of Chapters 2-6, providing an overview of the new findings and a discussion illustrating how they are linked.

REFERENCES

Abrajevitch, A. and Van der Voo, R., 2010. Incompatible Ediacaran paleomagnetic directions suggest an equatorial geomagnetic dipole hypothesis. Earth and Planetary Science Letters, 293(1-2), pp.164-170. https://doi.org/10.1016/j.epsl.2010.02.038

Bickford, M.E., Van Schmus, W.R., Karlstrom, K.E., Mueller, P.A. and Kamenov, G.D., 2015. Mesoproterozoic-trans-Laurentian magmatism: A synthesis of continent-wide age distributions, new SIMS U–Pb ages, zircon saturation temperatures, and Hf and Nd isotopic compositions. Precambrian Research, 265, pp.286-312. https://doi.org/10.1016/j.precamres.2014.11.024

Bono, R.K., Tarduno, J.A., Nimmo, F. and Cottrell, R.D., 2019. Young inner core inferred from Ediacaran ultra-low geomagnetic field intensity. Nature Geoscience, 12(2), pp.143-147. https://doi.org/10.1038/s41561-018-0288-0

Bruhn, R.L., Parry, W.T., Yonkee, W.A. and Thompson, T., 1994. Fracturing and hydrothermal alteration in normal fault zones. Pure and Applied Geophysics, 142(3), pp.609-644. https://doi.org/10.1007/BF00876057

Butler, R.F., 1992. Paleomagnetism: Magnetic domains to geologic terranes. Boston: Blackwell Scientific Publications.

Callahan, O.A., Eichhubl, P., Olson, J.E. and Davatzes, N.C., 2019. Fracture mechanical properties of damaged and hydrothermally altered rocks, Dixie Valley-Stillwater fault zone, Nevada, USA. Journal of Geophysical Research: Solid Earth, 124(4), pp.4069-4090. https://doi.org/10.1029/2018JB016708

Denison, R.E., 1966. Basement rocks in adjoining parts of Oklahoma, Kansas, Missouri, and Arkansas. (Ph.D. dissertation) University of Texas at Austin.

Denison, R.E., 1981. Basement rocks in northeastern Oklahoma. Oklahoma Geological Survey Circular, 84.

Dunlop, D.J. and Özdemir, Ö., 1997, Rock magnetism: Fundamentals and frontiers. Cambridge University Press, Cambridge, UK.

Elmore, R.D., Campbell, T., Banerjee, S. and Bixler, W.G., 1998. Palaeomagnetic dating of ancient fluid-flow events in the Arbuckle Mountains, southern Oklahoma. Geological Society, London, Special Publications, 144(1), pp.9-25. https://doi.org/10.1144/GSL.SP.1998.144.01.02

Gilbert, M.C., 1983. Timing and chemistry of igneous events associated with the Southern Oklahoma Aulacogen. Tectonophysics, 94(1-4), pp.439-455. https://doi.org/10.1016/0040-1951(83)90028-8

Ham, W.E., Denison, R.E., and Merritt, C.A., 1964. Basement Rocks and Structural Evolution of Southern Oklahoma. Oklahoma Geological Survey Bulletin, 95.

Hamilton, E.M., Elmore, R.D., Weaver, B.L., Dulin, S. and Jackson, J., 2016. Paleomagnetic and petrologic study of the age, origin, and significance of early and late Paleozoic events in the Long Mountain Granite, Wichita Mountains, Oklahoma. Geological Society of America Bulletin, 128(1-2), pp.187-202. https://doi.org/10.1130/B31277.1

Hanson, R.E., Puckett Jr, R.E., Keller, G.R., Brueseke, M.E., Bulen, C.L., Mertzman, S.A., Finegan, S.A. and McCleery, D.A., 2013. Intraplate magmatism related to opening of the southern Iapetus Ocean: Cambrian Wichita igneous province in the Southern Oklahoma rift zone. Lithos, 174, pp.57-70. https://doi.org/10.1016/j.lithos.2012.06.003

Hawes, J., 1952. A magnetic study of the Spavinaw granite area, Oklahoma. Geophysics, 17(1), pp.27-55. https://doi.org/10.1190/1.1437738

Holdsworth, R.E., McCaffrey, K.J.W., Dempsey, E., Roberts, N.M.W., Hardman, K., Morton, A., Feely, M., Hunt, J., Conway, A. and Robertson, A., 2019. Natural fracture propping and earthquake-induced oil migration in fractured basement reservoirs. Geology, 47(8), pp.700-704. https://doi.org/10.1130/G46280.1

Hrouda, F., Chlupáčová, M. and Mrázová, Š., 2006. Low-field variation of magnetic susceptibility as a tool for magnetic mineralogy of rocks. Physics of the Earth and Planetary Interiors, 154(3-4), pp.323-336. https://doi.org/10.1016/j.pepi.2005.09.013

Keranen, K.M., Savage, H.M., Abers, G.A. and Cochran, E.S., 2013. Potentially induced earthquakes in Oklahoma, USA: Links between wastewater injection and the 2011 Mw 5.7 earthquake sequence. Geology, 41(6), pp.699-702. https://doi.org/10.1130/G34045.1

Keranen, K.M., Weingarten, M., Abers, G.A., Bekins, B.A. and Ge, S., 2014. Sharp increase in central Oklahoma seismicity since 2008 induced by massive wastewater injection. Science, 345(6195), pp.448-451. https://doi.org/10.1126/science.1255802

Kirschvink, J.L., Ripperdan, R.L. and Evans, D.A., 1997. Evidence for a large-scale reorganization of Early Cambrian continental masses by inertial interchange true polar wander. Science, 277(5325), pp.541-545. https://doi.org/10.1126/science.277.5325.541

Lapointe, P., Morris, W.A. and Harding, K.L., 1986. Interpretation of magnetic susceptibility: a new approach to geophysical evaluation of the degree of rock alteration. Canadian Journal of Earth Sciences, 23(3), pp.393-401. https://doi.org/10.1139/e86-041

McCausland, P.J., Van der Voo, R. and Hall, C.M., 2007. Circum-Iapetus paleogeography of the Precambrian–Cambrian transition with a new paleomagnetic constraint from Laurentia. Precambrian Research, 156(3-4), pp.125-152. https://doi.org/10.1016/j.precamres.2007.03.004

Shelley, D., 1993. Igneous and Metamorphic Rocks under the Microscope: Classification, Textures, Microstructures and Mineral Preferred-Orientation. Chapman & Hall, London.

Spall, H., 1968. Paleomagnetism of basement granites of southern Oklahoma and its implications: Progress report. Oklahoma Geology Notes, 28(2), pp.65–80.

Spall, H. and Noltimier, H.C., 1972. Some curious magnetic results from a Precambrian granite. Geophysical Journal of the Royal Astronomical Society, 28(3), pp.237-248. https://doi.org/10.1111/j.1365-246X.1972.tb06126.x

Tarling, D.H. and Hrouda, F., 1993. The Magnetic Anisotropy of Rocks. Chapman and Hall, London.

Torsvik, T.H., Van der Voo, R., Preeden, U., Mac Niocaill, C., Steinberger, B., Doubrovine, P.V., Van Hinsbergen, D.J.J., Domeier, M., Gaina, C., Tohver, E., Meert, J.G., McCausland, P.J.A., and Cocks, R.M., 2012. Phanerozoic polar wander, palaeogeography and dynamics. Earth-Science Reviews, 114(3-4), pp.325-368. https://doi.org/10.1016/j.earscirev.2012.06.007

Vernon, R.H., 2004. A practical guide to rock microstructure. Cambridge University Press, Cambridge, UK.

Wall, C.J., Hanson, R.E., Schmitz, M., Price, J.D., Donovan, R.N., Boro, J.R., Eschberger, A.M. and Toews, C.E., 2021. Integrating zircon trace-element geochemistry and high-precision U-Pb zircon geochronology to resolve the timing and petrogenesis of the late Ediacaran–Cambrian Wichita igneous province, Southern Oklahoma Aulacogen, USA. Geology, 49(3), pp.268-272. https://doi.org/10.1130/G48140.1

Watts, D.R., Van der Voo, R. and Reeve, S.C., 1980. Cambrian paleomagnetism of the Llano uplift, Texas. Journal of Geophysical Research: Solid Earth, 85(B10), pp.5316-5330. https://doi.org/10.1029/JB085iB10p05316

Worm, H.U., 1998. On the superparamagnetic—stable single domain transition for magnetite, and frequency dependence of susceptibility. Geophysical Journal International, 133(1), pp.201-206. https://doi.org/10.1046/j.1365-246X.1998.1331468.x

CHAPTER 2

THE TEXACO KOHPAY L 16-WS: THE OSAGE MICROGRANITE REVISITED

OVERVIEW

The Texaco Kohpay L 16-WS well was drilled in central Osage County in 1963 to a total depth of 2848 feet (868 m), penetrating approximately 30 ft of igneous basement (Campbell and Weber, 2006). Three pieces of core from the bottom 5 feet of the well, totaling almost two feet, are currently housed at the Oklahoma Petroleum Information Center (OPIC). This is one of very few cores of northern Oklahoma basement material available from outside of the Tri-State Mineral District and is the only one reported from the Osage Microgranite (Denison, 1966, 1981). A radiometric age of 1,183 ± 48 million years was determined for this core using the Rb-Sr isotopic system (Denison, 1981; recalculated from Muehlburger et al., 1966, using the updated ^{87}Rb decay constant). This age is most likely an underestimate – all radiometric age determinations from northeast Oklahoma basement rocks using U-Pb analyses of zircons indicate ages close to 1,370 million years (Bickford et al., 2015), whereas the corresponding Rb-Sr age determinations are consistently younger and show a wider range (Denison, 1981).

The name of this core appears differently in multiple sources. Muehlberger et al. (1966) report the core as the "Texaco No. 1 Kohpay" whereas it is listed as "Texaco 16 W.S. Kohpay" by Denison (1966, 1981) and as "Texaco L Kohpay 16WS" by Campbell and Weber (2006). The Oklahoma Geological Survey lists the name as "Texaco Kohpay L 16-WS" (API: 35113069160000) in their oil & gas core database. That name is retained herein, should a reader wish to locate the core for their own inspection. For brevity, it will be referred to as the Kohpay core for the remainder of this chapter.

The Kohpay core was recently sampled as part of a study of alteration and deformation in northeastern Oklahoma's basement. This article presents new observations and analytical data in order to expand the limited information available to date regarding these rocks. The new results may prove useful in understating the origin and history of the Osage Microgranite.

GEOLOGICAL CONTEXT

The igneous rocks of northeastern Oklahoma are broadly grouped within the 1400-1350 Ma Southern Granite-Rhyolite Province, a Proterozoic granite-rhyolite terrane which comprises the uppermost basement of northern Arkansas, southwestern Missouri, southern Kansas, southeasternmost Colorado, eastern New Mexico, parts of west Texas and nearly all of Oklahoma (Van Schmus et al., 1996). The origins of this province remain uncertain – some authors have favored an intraplate extensional or rift setting (e.g., Lidiak, 1996), while others have suggested the origins may be related to subduction or back-arc extension (e.g., Bickford et al., 2015).

As the basement rocks of northern Oklahoma are only exposed in a very small area in and near the town of Spavinaw, detailed study is only possible using samples recovered by drilling operations. While some specimens have been incorporated into large-scale isotopic studies (reviewed in Bickford et al., 2015), the only major efforts to describe and map the rocks on a petrographic basis are those of Denison (1966, 1981). Denison identified four major units in the northeastern Oklahoma basement – the Central Oklahoma Granite Group (coarse, two-feldspar granites similar to those exposed in the eastern Arbuckle Mountains), the Spavinaw Granite Group (micrographic to graphic granites similar to those exposed at Spavinaw), the Washington Volcanic Group (rhyolites with minor dacites and andesites, locally metamorphosed), and the Osage Microgranite (a porphyritic body present in much of south-central Osage County,

interpreted as a sill). He considered these units to represent related magmas erupted or emplaced at different depths within a single igneous complex.

Petrographically, many upper basement specimens from south-central Osage County are strongly similar and appear to form a continuous body when plotted on a map. Denison therefore concluded that they comprise a rapidly-cooled thin sill, which he dubbed the Osage County Microgranite (Denison, 1966; shortened to Osage Microgranite by Denison, 1981). The Osage Microgranite is characterized by red coloration due to disseminated hematite, anhedral to subhedral phenocrysts of alkali feldspar, the presence of rounded and sparingly embayed quartz phenocrysts, a groundmass of alkali feldspar and acicular quartz, and virtually complete replacement of primary iron-magnesium silicate (femic) minerals by chlorite (Denison, 1981). The Kohpay core is from the northwestern part of the microgranite (Fig. 1); to date, no additional cores have been reported from this body.

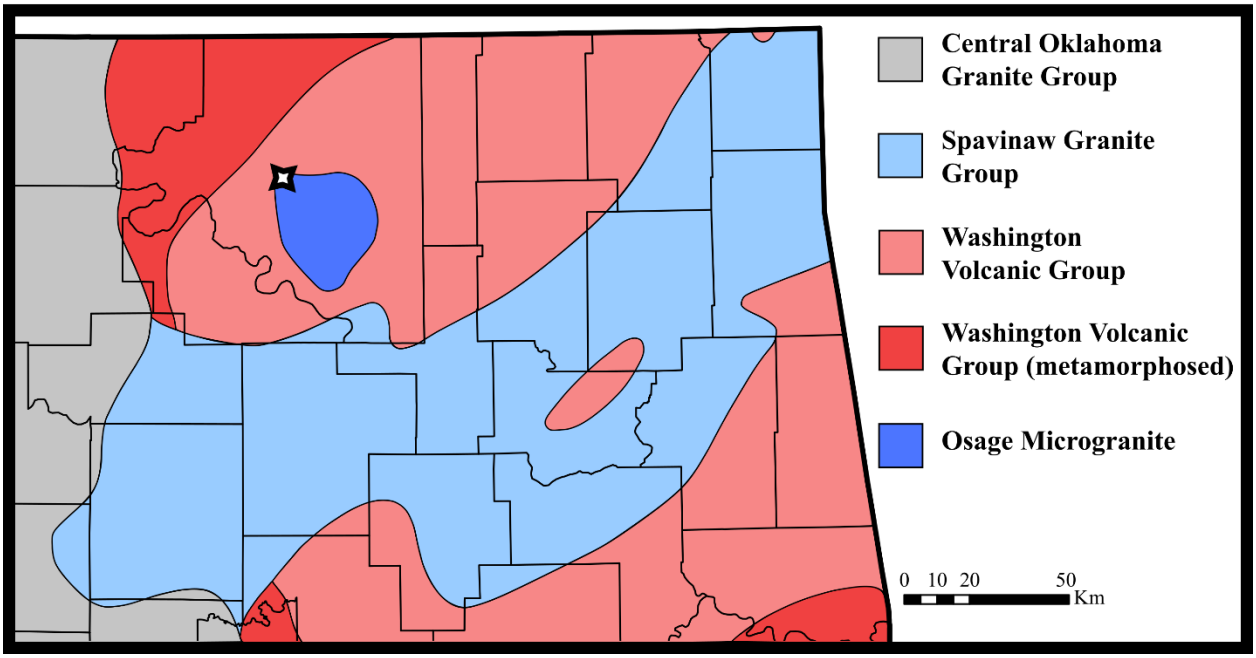


Figure 1. Generalized map of northeast Oklahoma basement subcrop lithology, redrawn after Denison (1981) with location of the Kohpay core indicated by the star.

For this study, two new samples of the Kohpay core were taken at OPIC. These specimens were used for petrographic analysis, as well as measurements of geochemical composition and magnetic properties. Petrographic observations have been made via polarizing microscope and scanning electron microscope; magnetic susceptibility measurements were made were made using a MFK1-FA Kappabridge manufactured by AGICO, Inc.

CORE DESCRIPTION AND PETROGRAPHY

In hand sample, the core is a deep red color with clearly visible lighter-colored rounded phenocrysts (Fig. 2A). Denison (1981) reports these are composite grains of alkali feldspar up to 2.3 cm in size. Looking closer (Fig. 2B), feldspar phenocrysts of various shapes are present in the 1-5 mm range, as well as rounded quartz in the 1-3 mm size range. Dark phenocrysts of up to 1-2 mm represent Fe-Mg silicates minerals replaced by chlorite. No preferred orientation is apparent in the phenocrysts. Very fine healed fractures are seen in the rock (Fig. 2B).

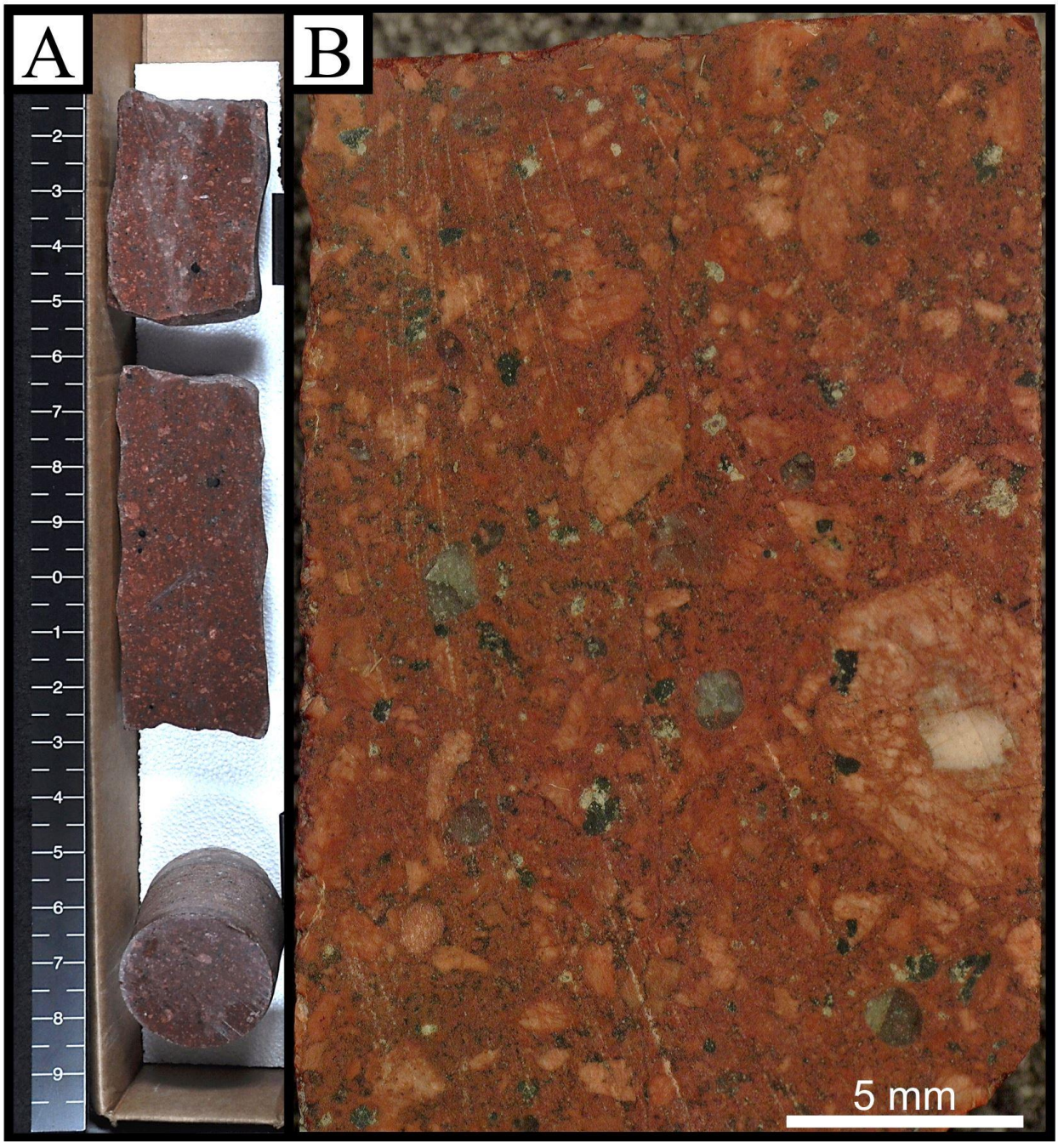


Figure 2. Whole-rock photographs from the Kohpay core. (A) Box photo courtesy of OPIC showing the entire remaining core interval. Scale is in tenths of feet. (B) Magnified photo of a sample fragment showing the character of the phenocrysts and presence of fine, healed fractures (horizontal, center).

Broad views of thin sections (Figs. 3, 4) show the same characteristics noted in hand sample as well as highlighting the composite nature of the feldspar phenocrysts previously noted

by Denison (1966, 1981). It is also apparent that several of the larger feldspar phenocrysts visible in hand sample are glomerocrysts of feldspar, chlorite, opaque minerals, and accessory minerals such as apatite and zircon (see large one in Fig. 3A). The large composite feldspars may also represent monomineralic glomerocrysts. Bulk mineralogy is largely consistent with that reported by Denison (1981), except that fluorite and epidote are largely absent in the new thin sections and apatite seems more abundant than indicated by Denison. Thin sections from both new samples contain fractures mineralized by quartz, chlorite and sparse alkali feldspar.

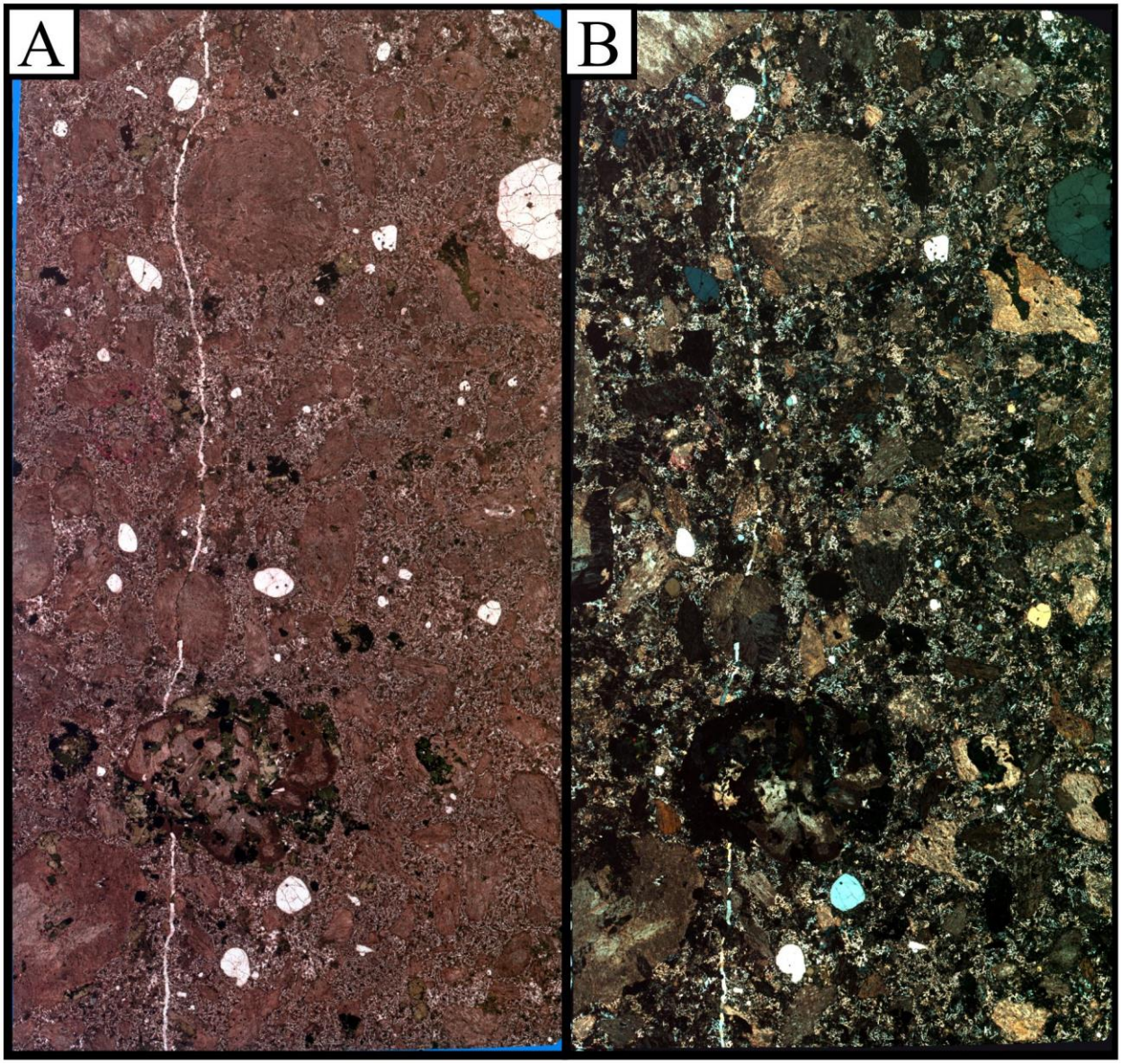


Figure 3. Photomicrograph mosaic of thin section from 2843-2844' core interval in (A) Plane-polarized light, (B) Cross-polarized light. Note composite feldspar phenocrysts and glomerocrysts as well as rounded, fractured quartz phenocrysts and mineralized fracture. No preferred orientation is apparent.

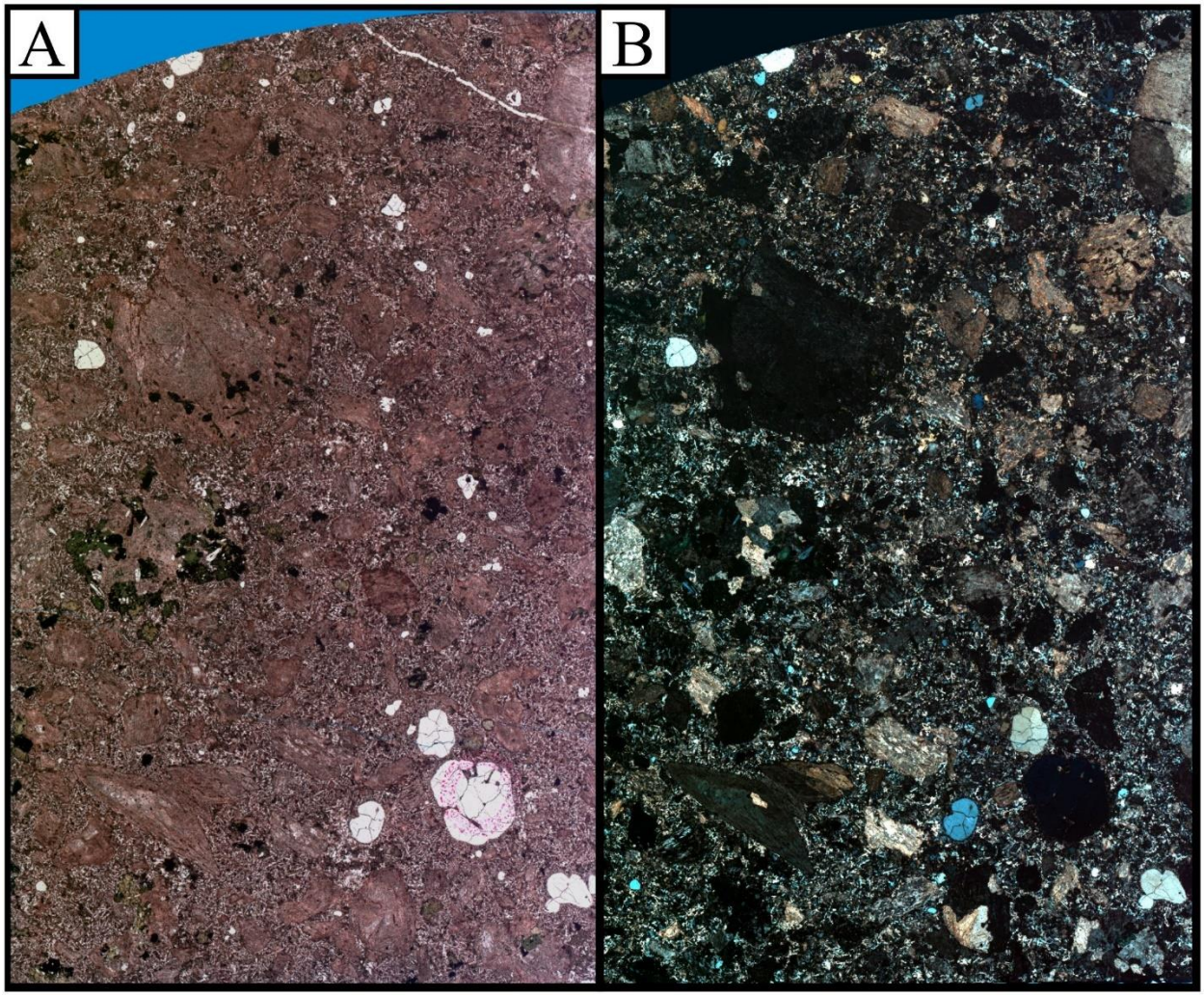


Figure 4. Photomicrograph mosaic of thin section from 2844-2847' core interval in (A) Plane-polarized light, (B) Cross-polarized light. Note composite feldspar phenocrysts and glomerocrysts as well as rounded, fractured quartz phenocrysts and mineralized fracture. No preferred orientation is apparent.

The distinctive texture of the Osage Microgranite is apparent, with randomly oriented, highly acicular crystals of quartz up to 1 mm in length (Fig. 5). This habit is here interpreted as a pseudomorph after tridymite, similar to that reported in the Carlton Rhyolite by Hanson and Eschberger (2014). Similar texture is common in the rhyolites of the Washington Volcanic Group, though the crystal size is typically smaller (Denison, 1981).

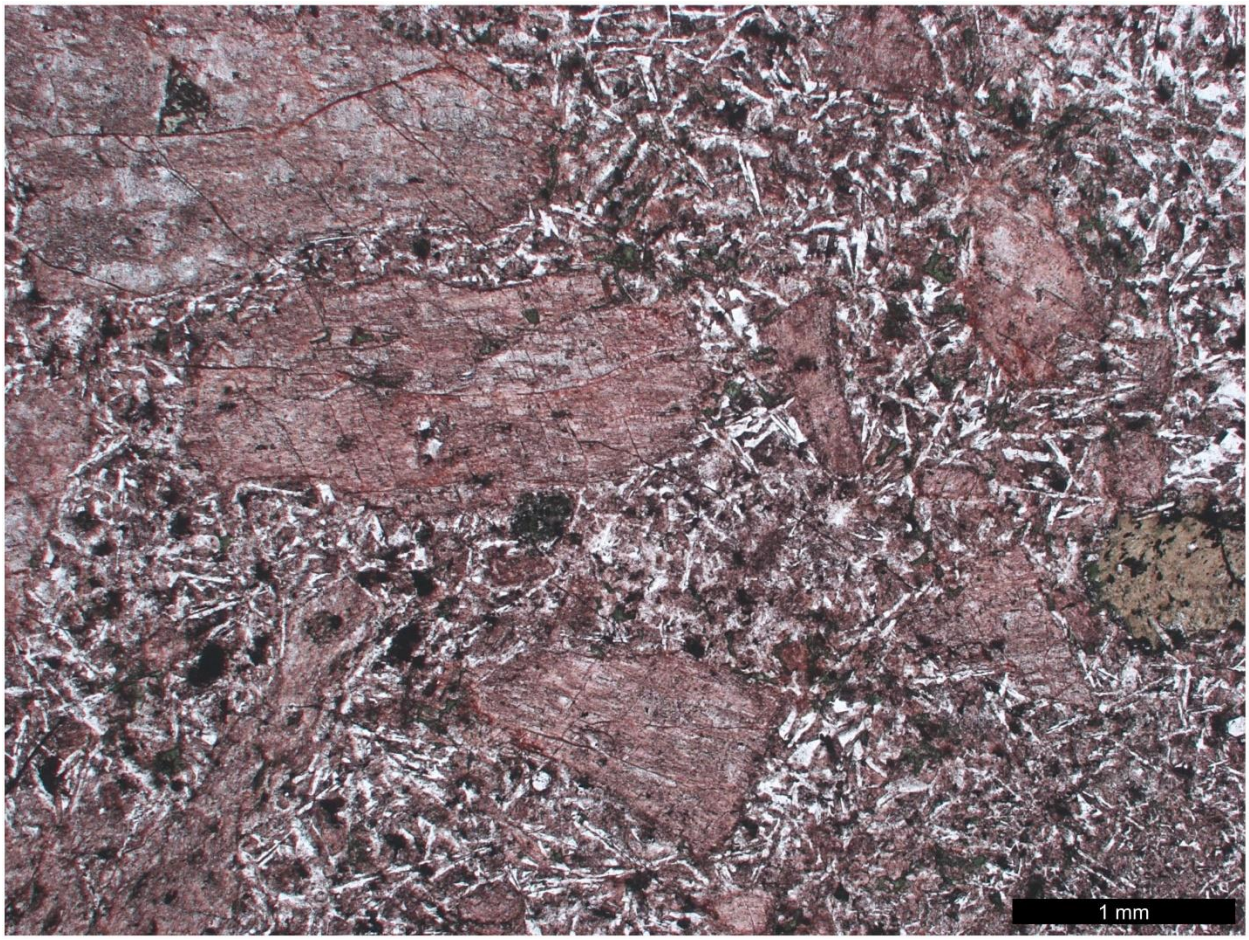


Figure 5. Porphyritic texture and groundmass character. Note acicular, slightly wedge-shaped habit of groundmass quartz. Plane light, 2843-44' interval.

Quartz phenocrysts are universally rounded, though the edges are typically ragged (Fig. 6) and many of the phenocrysts show optical continuity with groundmass quartz (Fig. 6A) as previously noted by Denison. The phenocrysts also commonly contain abundant fractures and fluid inclusion lines (Fig. 6B), and inclusions of chlorite, opaque minerals, and groundmass are common, with a few also containing zircon inclusions. Many of the quartz phenocrysts show incomplete or undulatory extinction.

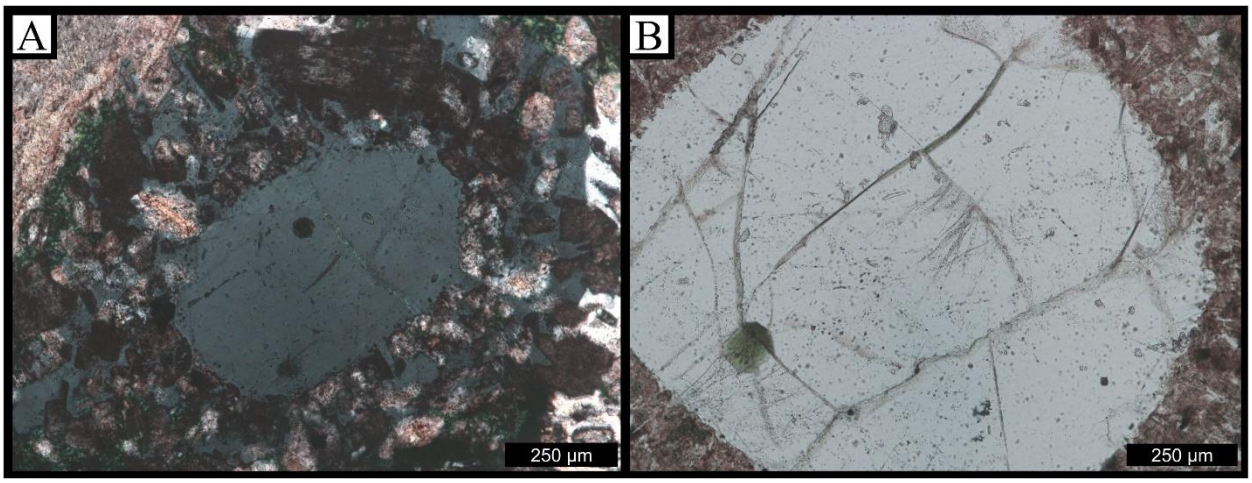


Figure 6. Characteristics of quartz phenocrysts. (A) Quartz phenocryst in cross-polarized light near extinction showing optical continuity with groundmass quartz. Also note ragged edges of the phenocryst and abundant fractures and inclusions. (B) Quartz phenocryst in plane light showing ragged edges, abundant fractures (some mineralized with chlorite) and numerous fluid inclusion trails. Thin section from 2843-44' interval.

Feldspar phenocrysts are commonly sericitized and are subhedral to anhedral in habit; many are also fragmented. They may occur individually or in the larger rounded glomerocrysts previously mentioned. While most are intact, several contain inclusions of opaque minerals and chlorite (e.g., Fig. 7). Cleavage is commonly well-developed and highlighted by hematite staining (e.g., Figs. 5, 7). Denison, (1966, 1981) reports these feldspars are perthitic in thin section. Inspection by scanning electron microscope (SEM) shows that this is true for many grains, however, in many others the compositional variation is blocky and associated with fractures rather than lamellar exsolution. Energy-dispersive spectroscopy shows many of the fracture-associated areas lack detectable K (if Na-feldspar) or Na (if K-feldspar). This suggests that, while the primary feldspar was likely perthitic, the compositional segregation was affected by alteration processes.

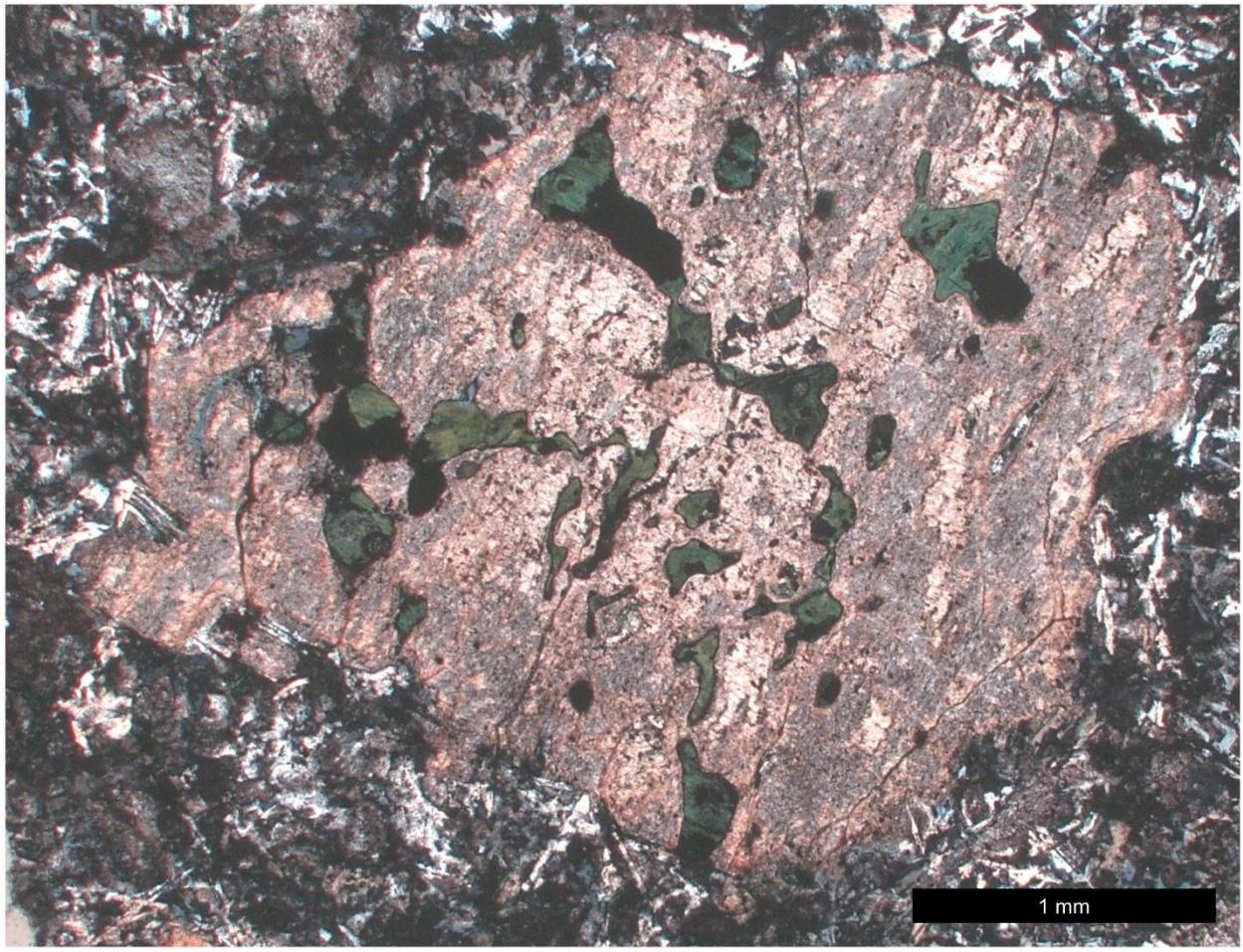


Figure 7. Altered feldspar phenocryst showing abundant chlorite and oxide inclusions. Cross-polarized light, 2844-47' interval.

The most abundant minor and accessory minerals are chlorite, opaque minerals, apatite and zircon. The most abundant is chlorite, which has replaced all primary femic minerals and shows a large range of colors from translucent olive-brown to intense deep green. Grain shapes are largely anhedral, making it difficult to identify the original minerals, which likely consisted of biotite and amphibole (consistent with Denison, 1981). Opaque minerals are former exsolved titanomagnetites which have been altered to leucoxene (a mixture of iron oxides and titanium oxide minerals such as anatase). Apatite is present as euhedral to subhedral grains, and faint compositional zoning is visible in several crystals when examined using backscattered electrons on an SEM. Zircon is abundant and exhibits a variety of shapes; square sections, prismatic, and

highly elongate grains are all present, as are fragments (Fig. 8). Many zircon grains contain hollow spaces that may originally have been melt or vapor inclusions (cf. Corfu et al., 2003); others contain mineral inclusions such as apatite, chlorite, pyrite, and monazite (Fig. 9).

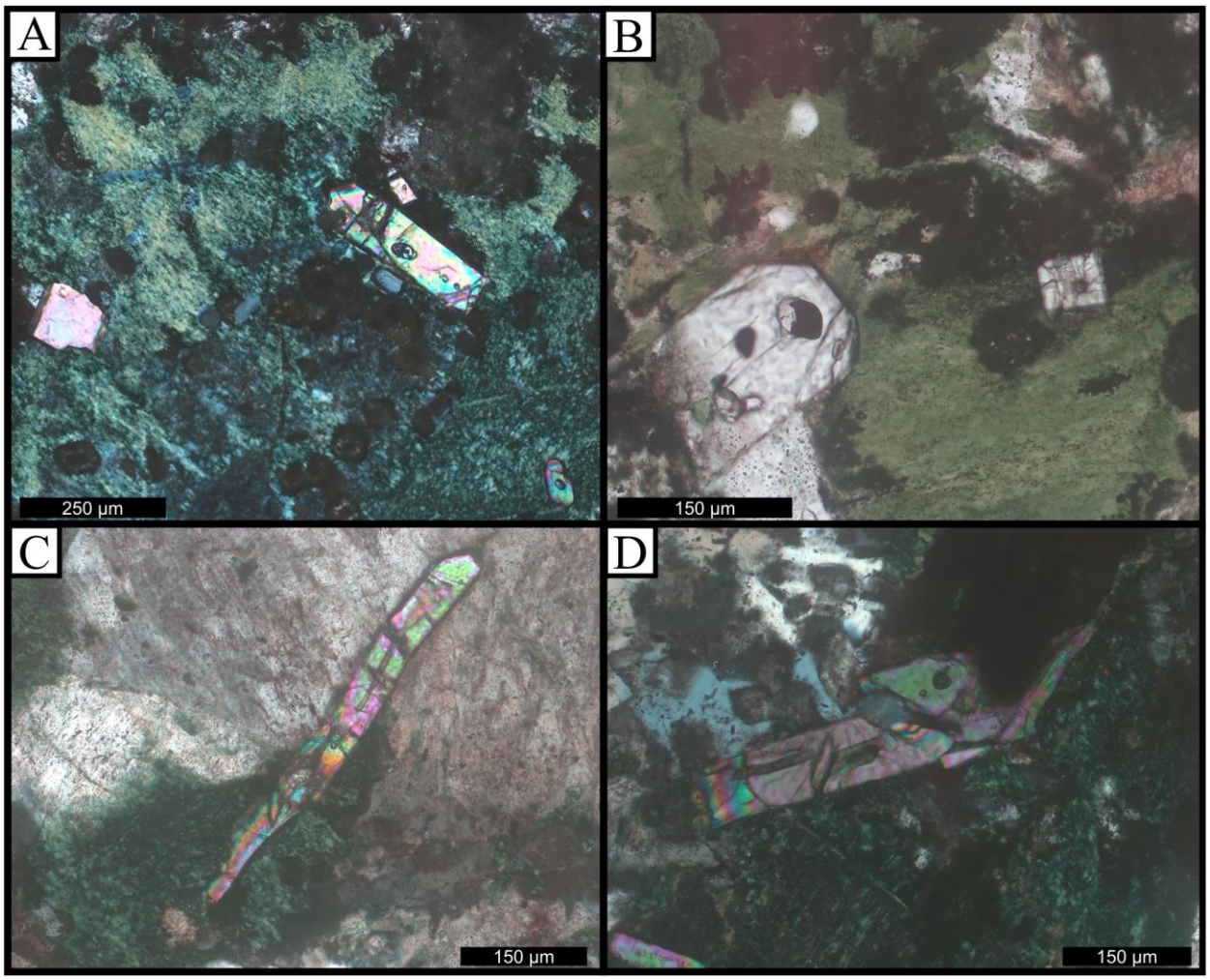


Figure 8. Zircons from the Kohpay core. (A) Prismatic zircon with inclusions, also smaller euhedral zircons (top adjacent, bottom right) and fragmented zircon (left). Matrix is chlorite with leucoxene and possibly synchysite. Cross-polarized light'. (B) Partial euhedral zircon with opaque and translucent inclusions (left) and square-section zircon (right). Square zircon is partly metamict. Plane light. (C) Elongate fractured zircon with inclusions, possibly altered from primary gas or melt inclusions. (D) Rectangular fractured zircon with similar inclusions as (C). A and B from 2843-44' interval, C and D are in cross-polarized light and from 2844-47' interval.

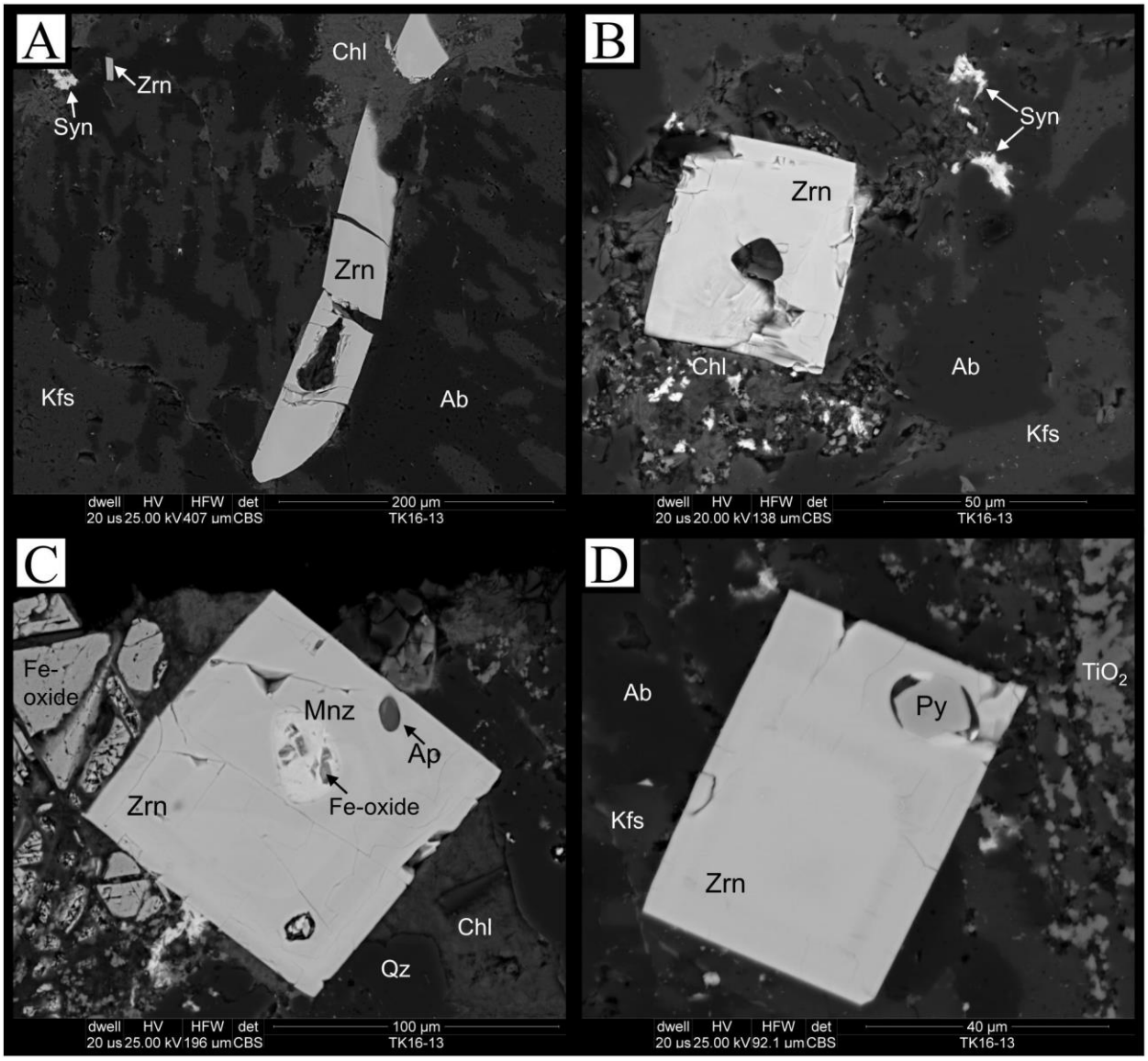


Figure 9. Backscattered electron images of zircons from 2844-47' interval. (A) and (B): zircons with void inclusions partially filled by chlorite (C) Zircon with inclusions of apatite, monazite and iron oxides. (D) Zircon with pyrite inclusion in void. Note faint zoning in C and D. Mineral abbreviations: Ab = Albite, Ap = Apatite, Chl = Chlorite, Kfs = K-feldspar, Mnz = Monazite, Py = Pyrite, Qz = Quartz, Syn = Synchysite, Zrn = Zircon.

A few zircon crystals show anomalously low interference colors and are more intensively fractured and appear zoned. Denison (1981) suggested that some of the zircon may be metamict (radiation damaged). Under the electron microscope, these show substantial zoning, with bands containing detectable amounts of non-formula elements such as Ca, Al, and Fe (Fig. 10A). This combination of texture and chemistry is considered to be a consequence of diffusion-reaction

processes resulting from interaction of substantially metamict zircons with aqueous fluids, potentially even under weathering conditions (Geisler et al., 2007).

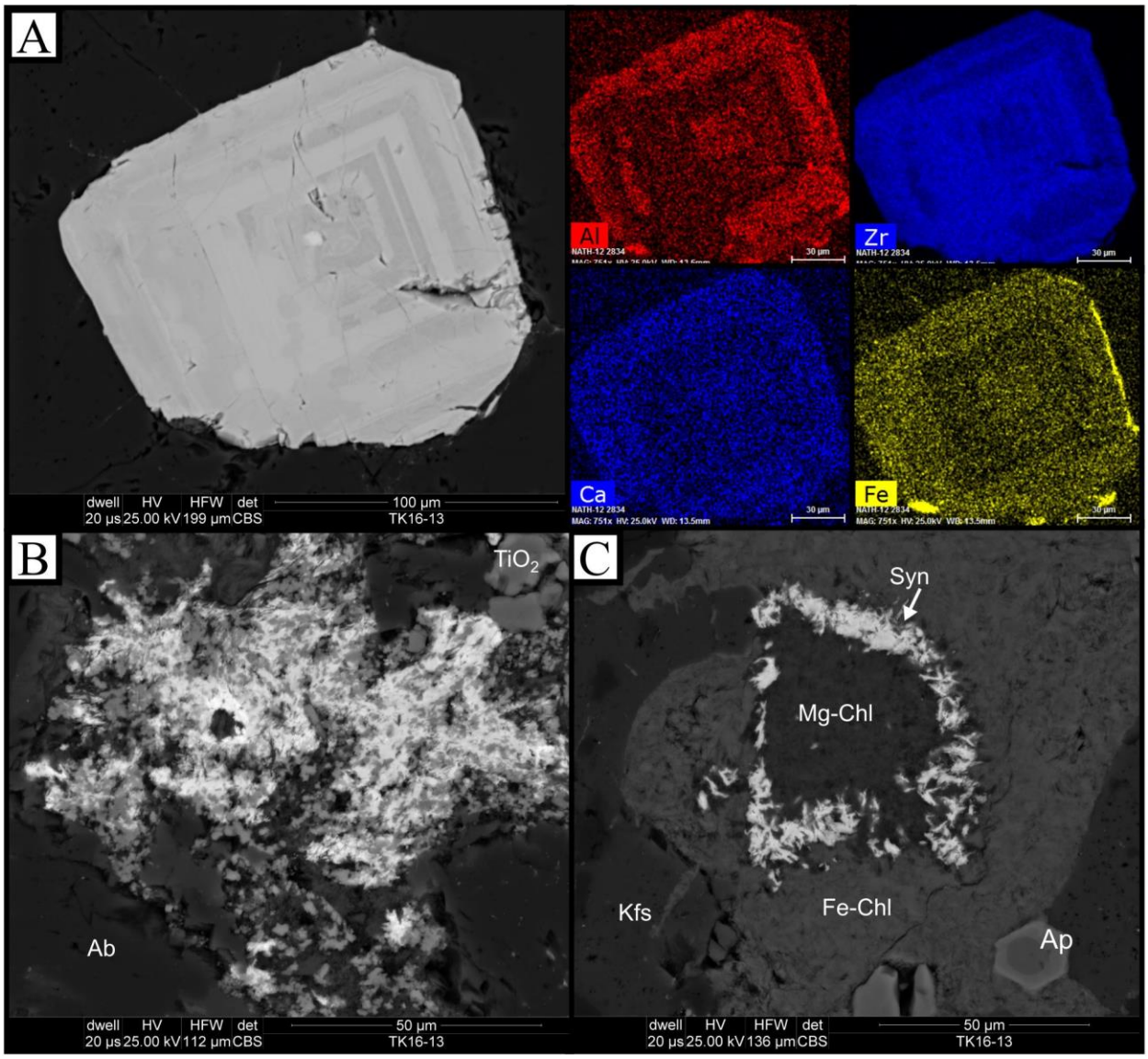


Figure 10. Mineralogical examples of hydrothermal alteration. (A) Zoned zircon in quartz showing central inclusion of HREE-rich Xenotime (bright spot) and convolute zoning in the center. Elemental abundance maps from energy-dispersive spectroscopy (right) indicate darker bands are due to substitution of non-formula elements such as Ca, Al, and Fe. (B) Synchysite (bright fibrous material) intergrown with a TiO2 mineral. (C) Synchysite corona around Mg-rich chlorite in a matrix of Fe-rich chlorite; also note zoned apatite. Backscattered electron images of specimen from 2844-47' core interval. Mineral abbreviations as in Fig. 9.

Scanning electron microscopy also reveals the presence of a Ca-REE carbonate mineral, most likely synchysite, $Ca(Ce,La,Nd)(CO_3)_2F$, which is commonly intergrown with either

titanium oxide in leucoxene or with chlorite (Fig. 10B, 10C). Identification of this phase is difficult due to the common intergrowths with Fe-bearing minerals, as Fe obscures the F peak in energy-dispersive analysis, but some iron-free spectra do show a fluorine peak. Given that it is a carbonate and exhibits high birefringence, it is plausible that at least some of the "calcite blebs" noted as replacement minerals by Denison (1981) may be synchysite. Synchysite is also present in trace amounts in at least three other northeastern Oklahoma basement cores as an alteration product (see Chapter 3).

As previously noted, the thin sections all contain fractures cemented by quartz, chlorite, and sparse feldspar (where the fractures cross-cut phenocrysts). Fracture-cementing quartz is commonly in optical continuity with adjacent groundmass quartz, much like the phenocrysts. Additionally, much like the phenocrysts, the quartz in fractures is commonly decorated with fluid inclusions (Fig. 11A); this is also true for some groundmass quartz. Scattered quartz grains, particularly in phenocrysts and fractures, also display thin, slightly arcuate features (Fig. 11) that commonly contain very small fluid inclusions. These are deformation lamellae – a feature associated with slow, ductile deformation and also commonly associated with fluid inclusions (Vernon, 2004).

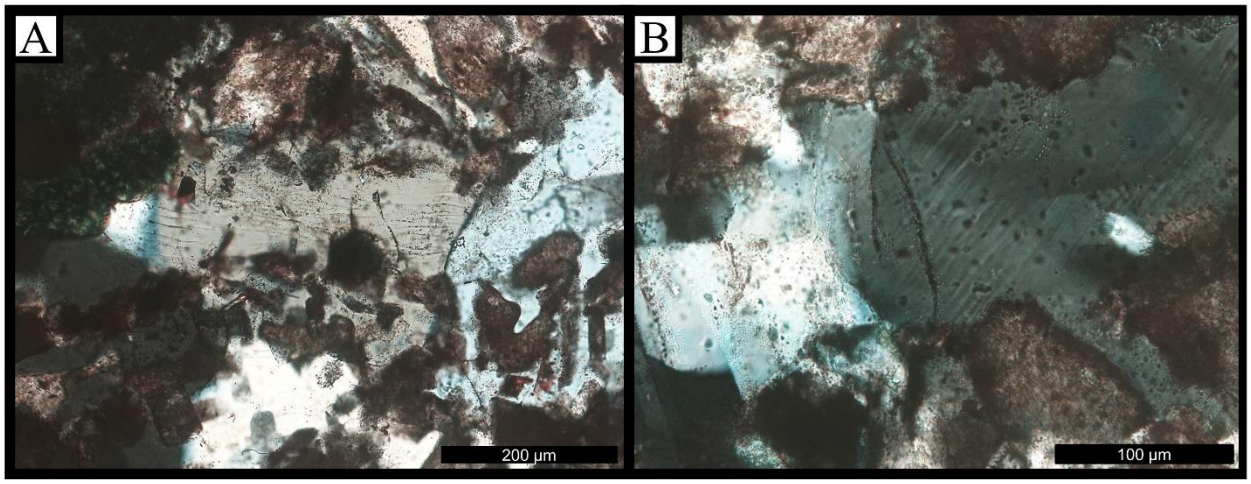


Figure 11. Deformation lamellae in quartz, cross-polarized light. (A) 2843-44' interval, (B) 2844-47' interval. Note decoration by fluid inclusions, particularly in (A).

GEOCHEMISTRY

One specimen of the Kohpay core was sent for whole-rock geochemical analysis at Activation Labs (Ancaster, Ontario). Major and trace elements were determined by ICP-MS, with ferrous iron determined by titration. Results are given in Table 1.

The rock is a granitoid (chemically classified as rhyolite, normative mineralogy of an alkali feldspar granite), with high K_2O, Na_2O, and low CaO. Although the major element chemistry is broadly similar to that published by Denison (1981), the new analysis has larger amounts of total Fe and MgO, with lower TiO_2, Al_2O_3, CaO, and Na_2O. In comparison to the Mount Scott Granite (Table 2), a well-characterized Cambrian rift A-type granite from the Wichita Mountains of southwestern Oklahoma with similar (slightly higher) silica content, the Kohpay chemistry is slightly richer in Al_2O_3, MgO and P_2O_5, considerably higher in K_2O, comparable in Na_2O, P_2O_5, total Fe and TiO_2, and is considerably lower in CaO.

Table 1: Whole-rock geochemistry of sample from 2844-47' interval of Kohpay core

Analyte	wt. %	Analyte	ppm	Analyte	ppm	Analyte	ppm
SiO_2	69.97	Sc	8	Nb	16.4	Tb	2.45
TiO_2	0.479	Be	4	Mo	< 2	Dy	14.2
Al_2O_3	13.38	V	6	Ag	1.3	Ho	2.73
FeO	0.63	Cr	< 20	In	0.1	Er	8.11
Fe_2O_3	2.80	Co	< 1	Sn	3	Tm	1.24
MnO	0.072	Ni	< 20	Sb	< 0.2	Yb	8.83
MgO	0.75	Cu	< 10	Cs	1.7	Lu	1.37
CaO	0.26	Zn	80	Ba	912	Hf	13.3
Na_2O	3.61	Ga	23	La	110	Ta	1.62
K_2O	5.59	Ge	1.2	Ce	238	W	< 0.5
P_2O_5	0.09	As	< 5	Pr	27.6	Tl	0.63
LOI	0.64	Rb	179	Nd	103	Pb	6
Total	98.58	Sr	30	Sm	19.8	Bi	< 0.1
$Fe_2O_3(T)$	3.75	Y	70.3	Eu	2.86	Th	17.7
Fe^{3+}/Fe_{TOT}	0.092	Zr	579	Gd	16.2	U	4.14

The trace element chemistry of the Kohpay core shows enrichment in many incompatible elements (Ba, Rb, Th, light rare earth elements). Use of multi-element diagrams normalized to the compositions of primitive mantle and chondrite, commonly referred to as spider diagrams, shows several relative anomalies in element abundances (Fig. 12). Reduced abundances relative to similarly-compatible elements (similar field strength and ionic radius) are referred to as negative anomalies. Prominent negative anomalies are present for Cs, Ba, Nb, Ta, Pb, Sr, P, Eu, and Ti. Light rare earth elements (REE) are enriched, while for REE heavier than Ho, the normalized slope is flat to slightly positive with increasing atomic number.

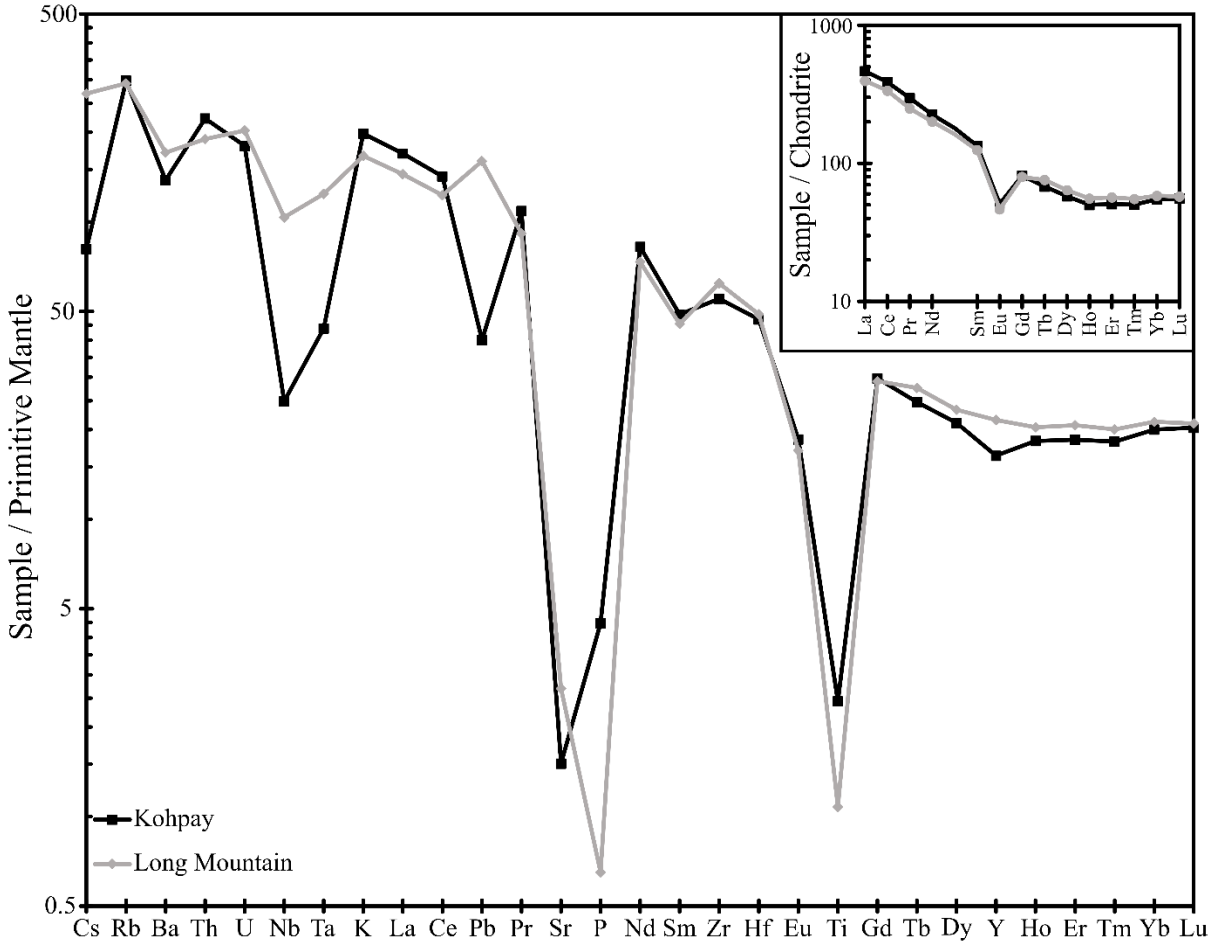


Figure 12. Normalized multi-element variation diagrams for the Kohpay core (Table 1), with data from fresh Long Mountain Granite (Hamilton et al., 2016) plotted for comparison. Normalization factors from McDonough & Sun (1995).

For purposes of comparison, chemical data from the Long Mountain Granite of the Wichita Mountains area are also plotted in Fig. 12 and given in Table 2. The trace element chemistry of the Long Mountain Granite is similar to that of the Mount Scott Granite (Hamilton et al., 2016), and in this case the analyses cover the same range of elements and were performed by the same laboratory. Despite their age differences (~1,370 Ma for the Kohpay; ~530 Ma for the Long Mountain Granite), their trace element patterns are remarkably similar, though the Kohpay sample has distinct negative Nb-Ta and Pb anomalies while the Long Mountain Granite shows stronger depletions in Ti and P.

Table 2: Whole-rock geochemistry of Wichita Granites for comparison

Mount Scott Granite		Long Mountain Granite					
Analyte	wt. %	Analyte	wt. %	Analyte	ppm	Analyte	ppm
SiO_2	72.3	SiO_2	75.12	Sc	2	Nd	91.7
TiO_2	0.44	TiO_2	0.216	Be	5.3	Sm	18.4
Al_2O_3	12.3	Al_2O_3	12.01	Cr	50	Eu	2.62
Fe_2O_3(T)	3.9	FeO	1.54	Zn	140	Gd	15.8
MnO	0.08	Fe_2O_3	1.11	Ga	26.7	Tb	2.74
MgO	0.31	MnO	0.045	Ge	2.2	Dy	15.7
CaO	1.2	MgO	0.14	Rb	175.3	Ho	3.04
Na_2O	3.8	CaO	0.65	Sr	53.7	Er	9.07
K_2O	4.3	Na_2O	3.87	Y	92.7	Tm	1.36
P_2O_5	0.08	K_2O	4.80	Zr	653	Yb	9.38
LOI	0.34	P_2O_5	0.01	Nb	68.1	Lu	1.42
Total	99.06	F	0.14	Mo	5	Hf	13.8
		LOI	0.29	Ag	2.4	Ta	4.59
		Total	99.94	Sn	15	W	2.5
				Cs	5.7	Tl	0.64
		Fe^{3+}/Fe_{TOT}	0.392	Ba	1128	Pb	24
				La	93.7	Bi	0.2
				Ce	206	Th	15.1
				Pr	23.2	U	4.66

MAGNETIC SUSCEPTIBILITY

Magnetic susceptibility of sub-specimens from the 2843-44’ interval using the default settings of the MFK1-FA Kappabridge (measuring field of 976 Hz and field strength of 200 A/m) indicate an average mass-normalized susceptibility of 4.85×10^{-7} m^3/kg. Using the average density of 2.61 g/cm^3 reported by Denison (1966), this equates to a value of 1.28×10^{-3} SI. This value is lower than the value of 1.63×10^{-3} SI reported by Denison (1966) by ~22%, though it is still comparable.

Measurements of susceptibility using varying measuring fields between 5 and 700 A/m at constant frequency (976 Hz) show a systematic decrease of susceptibility with increasing applied field. Measurements using a constant 200 A/m field at frequencies of 976, 3904 and 15616 Hz also indicate significant decreases of susceptibility with increasing frequency. The total loss of susceptibility is on the order of 5% from low to high measuring fields and approximately 13% from low to high frequency (Fig. 13).

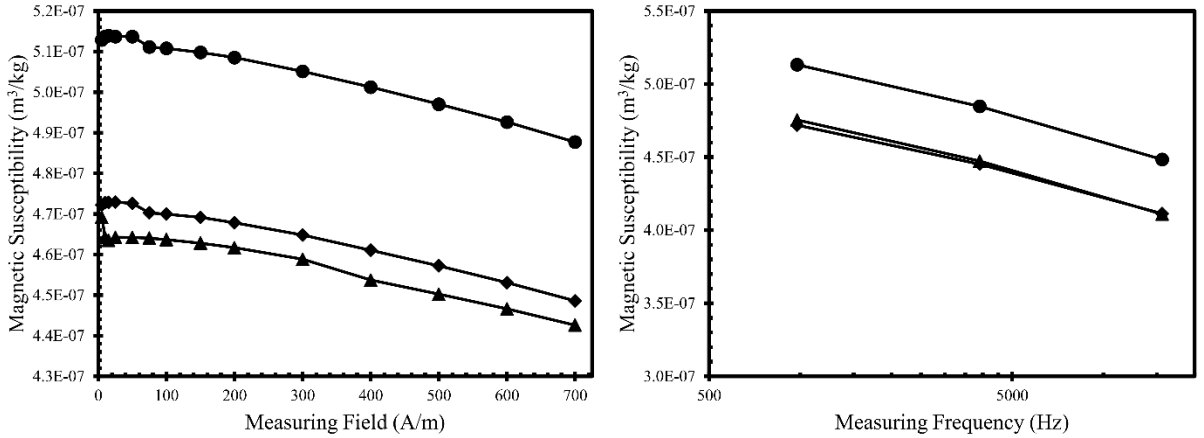


Figure 13. Variation of magnetic susceptibility of three sub-samples from the Kohpay core. Left: Variation as a function of measuring field at a frequency of 976 Hz. Right: Variation as a function of measuring frequency using a field of 200 A/m.

DISCUSSION

Petrographically, the Kohpay core shows features more characteristic of an extrusive rather than an intrusive rock. These features include: 1) fragmented crystals, 2) lack of euhedral phenocrysts of major minerals, 3) embayed and/or spongy phenocrysts, 4) glomerocrysts, and most importantly, 5) apparent quartz pseudomorphs after tridymite. The highly elongate shapes of some zircon crystals and the presence of relict melt or vapor phase inclusions indicate rapid crystallization (Corfu et al., 2003), which supports a volcanic or, as proposed by Denison (1981), a shallow intrusive origin. Overall, textures are similar to rhyolites of the Washington Volcanic

Group described by Denison (1981). The only major difference is that the groundmass quartz needles of the Osage Microgranite are significantly larger.

A potential argument against a volcanic origin for the Kohpay sample is the lack of an apparent preferred flow fabric seen in intervals of clearly volcanic material in other cores, though some cores of volcanic rock from northeastern Oklahoma contain intervals which lack flow textures. Overall, the available evidence seems to suggest that the material from the Kohpay core represents a rhyolite flow of the Washington Volcanic Group rather than an intrusive rock, and by extension it may be that the Osage Microgranite itself represents a distinct group of rhyolite flows rather than a single intrusion. Alternatively, the extrusive-like textures of the Kohpay core could result from a shallow granitic intrusion breaching the paleosurface, similar to the interpreted origin of the gradation from intrusive to extrusive textures in the Saddle Mountain Granite of the Wichita Mountains (Gilbert, 1986). This would be worthy of further research, though lack of available materials is likely to impede such work.

It is obvious petrographically that the rock in the Kohpay core has undergone secondary alteration. The universal replacement of former femic minerals by chlorite, the replacement of primary titanomagnetite by leucoxene, the formation of quartz-chlorite-feldspar veins, the dissemination of hematite and intense red color, alteration textures in zircon, and the presence of authigenic synchysite are all indications of significant fluid-rock interaction. The fact that virtually all fracture-hosted quartz shows evidence of fluid inclusion trails (as do many of the phenocrysts and much of the quartz in the groundmass) and that phenocryst and fracture-hosted quartz is commonly in optical continuity with adjacent groundmass suggests that most, if not all, of the quartz in this rock has been recrystallized.

Geochemically, evidence of alteration is also apparent from the negative Pb anomaly. Pb always shows a positive anomaly in unaltered igneous rocks whether from subduction or continental settings; however, it is a highly mobile element under weathering and hydrothermal conditions (Winter, 2010), and removal by fluid-rock interaction is the only plausible cause for a negative anomaly. For comparison, a (less severely) negative Pb anomaly is also present in the carapace of altered red granite at Long Mountain (Hamilton et al., 2016). This fluid-rock interaction is also likely responsible for the relative depletion of Cs (and possibly also the very low CaO) and could explain the anomalously young Rb-Sr age estimate for the Kohpay core. Curiously, despite the abundant disseminated hematite and the consequent intense red color of the rock, ferric iron makes up less than ten percent of the total iron.

The geochemical patterns in the Kohpay core rock are intriguing. While many authors have broadly considered the igneous rocks in this area to represent extensional A-type granitoids (Lidiak, 1996; summary in Bickford et al., 2015), and the Kohpay rock shares many chemical similarities with them, the strong negative Nb-Ta anomaly is much more typical of magmas produced in subduction-related environments (Winter, 2010). Negative anomalies in Sr and Eu are associated with crystallization and removal of plagioclase, the negative anomaly in Ba is likely due to removal of K-feldspar, and the negative anomaly in P is associated with removal of apatite. The negative Ti anomaly is linked to removal of ilmenite or magnetite, though strong negative Ti anomalies are also characteristic of subduction zone magmas. Strong enrichment in light rare-earth elements is typically associated with small degrees of melting and/or the presence of garnet in the magma source, however, the flat to slightly upward slope of the REE diagram in the heavy REE is strongly inconsistent with a melt that was ever in equilibrium with garnet. The implications for the source of the magma remain to be determined.

Likewise, the broad similarity of the trace element characteristics with those of the Wichita Granite Group pose some interesting questions. The general trends are nearly identical with the exception of Nb and Ta, which are much more abundant in A-type Wichita granite. Possible genetic links between the Cambrian Wichita Granite Group and the Proterozoic Southern Granite-Rhyolite Province have been speculated on before (e.g., Weaver and Gilbert, 1986), but to date the data from the Precambrian rocks has been lacking. It may be that both groups are at least partially derived from the same sources; alternatively, the Wichita Granite Group may be partially derived from more basic to intermediate rocks of the Southern Granite Rhyolite Province. Further geochemical analysis of related rocks in northeastern Oklahoma may shed light on the origins of both groups.

The deformational microstructures in the Kohpay core may also be worth further investigation. Interest in the structure and deformational history of Oklahoma's Proterozoic basement rocks has been elevated due to the abundant seismic activity in the northern and central areas of the state over the past decade. Spacing and orientation of deformation lamellae in quartz have been tentatively linked to the magnitude and orientation of differential stresses (Vernooij and Langenhorst, 2005). Detailed analysis of these and related structures could potentially prove useful in understanding the tectonic history of this area as well as its modern seismic hazards. The variations of magnetic susceptibility are unusual and difficult to interpret. Decreases in susceptibility with increasing frequency are associated with extremely fine-grained magnetite, referred to as superparamagnetic (e.g., Worm, 1998). Production of superparamagnetic magnetite could conceivably be due to the fluid alteration mentioned previously. The decrease of susceptibility with increasing field is harder to explain – while this has previously been observed in rocks and soils from multiple localities (Hrouda et al., 2006), it has never been explained, and

the magnitude of this decrease in the Kohpay specimens is similar to the largest reported in the literature. Research into this phenomenon is ongoing and is further explored in Chapter 4.

CONCLUSIONS

Core from the Texaco Kohpay L 16-WS well has yielded a wealth of scientific information and is likely to be of continued value. Petrographic observations suggest that this rock is volcanic rather than intrusive, which opens questions regarding the nature (or even existence) of the Osage Microgranite. Observed microstructures may prove relevant to stress analysis and seismic hazards. Both petrography and geochemistry show substantial evidence for fluid alteration, and further work may yield estimates of the conditions of this event. Geochemical analysis appears inconsistent with the oft-presumed rift setting for the origin of the Southern Granite-Rhyolite Province magmas, yet abundant similarities with the Long Mountain Granite may provide clues to the origins of the magmas that produced the Wichita Granite Group during rifting some 840 million years later. The unusual magnetic susceptibility variations of this rock also make it relevant to open questions in rock magnetism. Despite containing less than two feet of recovered material, the Kohpay core has proven pertinent to issues of basic petrography and mapping, seismic hazards, rock magnetism, and the Proterozoic assembly of what has become North America.

REFERENCES

Bickford, M.E., Van Schmus, W.R., Karlstrom, K.E., Mueller, P.A. and Kamenov, G.D., 2015. Mesoproterozoic-trans-Laurentian magmatism: A synthesis of continent-wide age distributions, new SIMS U–Pb ages, zircon saturation temperatures, and Hf and Nd isotopic compositions. Precambrian Research, 265, pp.286-312. https://doi.org/10.1016/j.precamres.2014.11.024

Campbell, J.A. and Weber, J.L., 2006, Wells Drilled to Basement in Oklahoma. Oklahoma Geological Survey Special Publication 2006-1.

Corfu, F., Hanchar, J.M., Hoskin, P.W. and Kinny, P., 2003. Atlas of zircon textures. Reviews in Mineralogy and Geochemistry, 53(1), pp.469-500. https://doi.org/10.2113/0530469

Denison, R.E., 1966. Basement rocks in adjoining parts of Oklahoma, Kansas, Missouri, and Arkansas. (Ph.D. dissertation) University of Texas at Austin.

Denison, R.E., 1981. Basement rocks in northeastern Oklahoma. Oklahoma Geological Survey Circular 84.

Geisler, T., Schaltegger, U. and Tomaschek, F., 2007. Re-equilibration of zircon in aqueous fluids and melts. Elements, 3(1), pp.43-50. https://doi.org/10.2113/gselements.3.1.43

Gilbert, M.C., 1986. Stop 6: Saddle Mountain Granite. Oklahoma Geological Survey Guidebook 23, pp.169-171.

Hamilton, E.M., Elmore, R.D., Weaver, B.L., Dulin, S. and Jackson, J., 2016. Paleomagnetic and petrologic study of the age, origin, and significance of early and late Paleozoic events in the Long Mountain Granite, Wichita Mountains, Oklahoma. Geological Society of America Bulletin, 128(1-2), pp.187-202. https://doi.org/10.1130/B31277.1

Hanson, R.E. and Eschberger, A.M., 2014. An overview of the Carlton Rhyolite Group: Cambrian A-type felsic volcanism in the Southern Oklahoma aulacogen. Oklahoma Geological Survey Guidebook 38, pp.123-142.

Hrouda, F., Chlupáčová, M., and Mrázová, S., 2006. Low-field variation of magnetic susceptibility as a tool for magnetic mineralogy of rocks. Physics of the Earth and Planetary Interiors, 154, pp.323-336. https://doi.org/10.1016/j.pepi.2005.09.013

Lidiak, E.G., 1996. Geochemistry of subsurface Proterozoic rocks in the eastern midcontinent of the United States: Further evidence for a within-plate tectonic setting. Geological Society of America Special Paper 308, pp.45-66. https://doi.org/10.1130/0-8137-2308-6.45

McDonough, W.F. and Sun, S.S., 1995. The composition of the Earth. Chemical Geology, 120(3-4), pp.223-253. https://doi.org/10.1016/0009-2541(94)00140-4

Muehlberger, W.R., Hedge, C.E., Denison, R.E. and Marvin, R.F., 1966. Geochronology of the midcontinent region, United States: 3. Southern area. Journal of Geophysical Research, 71(22), pp.5409-5426. https://doi.org/10.1029/JZ071i022p05409

Myers, J.D., Gilbert, M.C. and Loiselle, M.C., 1981. Geochemistry of the Cambrian Wichita Granite Group and revisions of its lithostratigraphy. Oklahoma Geology Notes, 41(6), pp.172-195.

Price, J.D., Hogan, J.P. and Gilbert, M.C., 1996. Rapakivi Texture in the Mount Scott Granite, Wichita Mountains, Oklahoma. European Journal of Mineralogy, pp.435-452. https://doi.org/10.1127/ejm/8/2/0435

Price, J.D., Hogan, J.P., Gilbert, M.C. and Payne, J.D., 1998. Surface and near-surface investigation of the alteration of the Mount Scott Granite and geometry of the Sandy Creek Gabbro pluton, Hale Spring area, Wichita Mountains, Oklahoma. In Basement Tectonics 12 (pp. 79-122). Springer, Dordrecht. https://doi.org/10.1007/978-94-011-5098-9_4

Van Schmus, W.R., Bickford, M.E. and Turek, A., 1996. Proterozoic geology of the east-central Midcontinent basement. Geological Society of America Special Paper, 308, pp.7–32. https://doi.org/10.1130/0-8137-2308-6.7

Vernon, R.H., 2004. A practical guide to rock microstructure. Cambridge University Press, Cambridge, UK.

Vernooij, M.G.C. and Langenhorst, F., 2005. Experimental reproduction of tectonic deformation lamellae in quartz and comparison to shock-induced planar deformation features. Meteoritics & Planetary Science, 40(9-10), pp.1353-1361. https://doi.org/10.1111/j.1945-5100.2005.tb00406.x

Weaver, B.L. and Gilbert, M.C., 1986. Reconnaissance geochemistry of silicic igneous rocks of the Wichita Mountains: The Wichita Granite Group and the Carlton Rhyolite Group. Oklahoma Geological Survey Guidebook 23, pp.117-125.

Winter, J.D., 2014. Principles of igneous and metamorphic petrology (2nd Edition). Pearson Education, New Jersey.

Worm, H.U., 1998. On the superparamagnetic—stable single domain transition for magnetite, and frequency dependence of susceptibility. Geophysical Journal International, 133(1), pp.201-206. https://doi.org/10.1046/j.1365-246X.1998.1331468.x

CHAPTER 3

FRACTURED, ALTERED, AND FAULTED BASEMENT IN NORTHEASTERN OKLAHOMA: IMPLICATIONS FOR INDUCED SEISMICITY

ABSTRACT

Due to a decade of wastewater injection-triggered seismicity, the crystalline basement of northern Oklahoma has become the subject of intensive research, almost all of which has relied upon remote sensing or analog models and materials due to a near total absence of outcrops. This study reports relevant characteristics of material in drill cores from the area, the best available analog for seismogenic northern Oklahoma basement. Fractures are present in all cores, remain abundant over 100 m below the top of basement, commonly have steep inclinations (≥70°) and are nearly universally mineralized. Many fractures show evidence of slip such as slickenlines, vein offset, brecciation, and, in one core, injectite formation. Fractures are mineralized by carbonates and/or phyllosilicates along with various other minerals, some contain vugs, and many contain multiple generations of minerals. Color changes suggestive of redox processes, including possible paleoweathering, are associated with fractures and proximity to the basement unconformity. Paragenesis of fracture minerals and variations in geochemical analyses of altered rocks indicate complex histories of deformation and fluid activity. The abundance of fractures in cores indicates that the upper basement of northeastern Oklahoma is much less "intact" than commonly assumed; it instead shows similarities to fractured basement plays, which may provide a more reasonable comparison for future work.

INTRODUCTION

Seismic activity in northern Oklahoma began to rapidly increase starting in 2008 and has been linked to wastewater disposal wells (Ellsworth, 2013; Keranen et al., 2013, 2014). These induced/triggered earthquakes occur along pre-existing faults in the crystalline basement (Keranen et al., 2013; McNamara et al., 2015; Kolawole et al., 2019), many of which remain unrecognized until rupture. Most of the earthquakes occur 2-3 km below the top of the basement even though wastewater is commonly injected into the overlying Cambrian-Ordovician carbonates of the Arbuckle Group (Keranen et al., 2013; Schoenball and Ellsworth, 2017). The dramatic increase in seismicity has led to renewed interest in the basement rocks of the area.

As exposures are non-existent aside from a small discontinuous granite outcrop in the town of Spavinaw (Ireland, 1930), direct observations of basement rocks and faults from northern Oklahoma are few and far between. Faults have therefore been primarily identified and studied via well logs or geophysical expressions such as offset of seismic reflectors and/or magnetic anomalies. Direct description of basement fault rocks has been limited to a few observations of sheared and cataclastic material from drill cuttings (Denison, 1966, 1981). Consequently, literature values for intact crystalline granite are commonly assumed for hydrological and mechanical modeling of the basement (e.g., Schoenball et al., 2018), sometimes with modification using empirical crustal permeability relationships (e.g., Barbour et al., 2017; Pollyea et al., 2019).

This study documents numerous features in northeastern Oklahoma basement rocks which are incongruent with the common assumption of intact crystalline granite. As matrix permeabilities of basement rocks are typically extremely low, hydrological properties are usually governed by fractures. Mineralized fractures are present in all recovered cores of basement rock

from the area. Hydrothermal alteration changes the mineralogy of rocks and thus their mechanical properties (e.g., Callahan et al., 2019; Laubach et al., 2019), and this study indicates that all basement rocks of the area have been hydrothermally altered. Fault rocks are found in multiple cores as well, providing the closest available analog to the seismically-active faults. As basement rocks from the main seismically active areas are not currently available as core, sample locations in the current study are mostly east of the main area of seismic activity (Fig. 1), with the closest being approximately 45 km from the 2016 M_w 5.8 Pawnee earthquake.

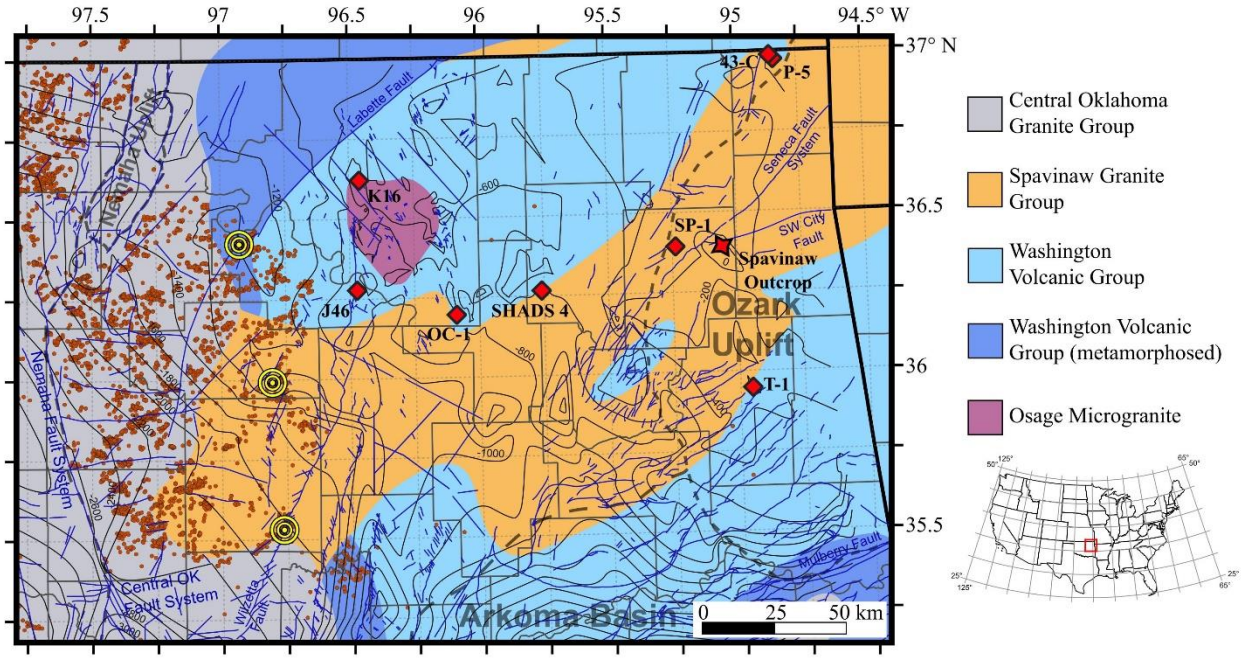


Figure 1. Generalized map of upper basement rocks in the study area, with lithologic groups after Denison (1966, 1981) and tectonic provinces from Northcutt and Campbell (1995). Known faults indicated by blue lines (interpretive database of Marsh and Holland, 2016), with locations of discussed cores shown by red markers (full names in Table 1). Depth contours are elevation in meters with respect to sea level, contoured from data in Campbell and Weber (2006). Orange dots represent magnitude 2.5 or higher earthquakes from Jan. 1, 2009 to Apr. 14, 2020 from the USGS catalog; yellow circles indicate M_w 5.0 or higher events (from north to south: Sept. 2016 M_w 5.8 Pawnee, Nov. 2016 M_w 5.0 Cushing, Nov. 2011 M_w 5.7 Prague).

GEOLOGIC SETTING

Basement Lithology

The basement rocks of the area consist of Mesoproterozoic granites and rhyolites, with minor andesites (Figs. 1, 2) and have been described and categorized into four groups by Denison (1966, 1981). On the basis of occurrence and mineralogy, three of these units are considered to represent a comagmatic volcanic-intrusive complex which forms most of the basement subcrop in the study area (Denison, 1981); recent geochemical data are consistent with this interpretation (Hamilton et al., 2020a). All Volcanic rocks are assigned to the Washington Volcanic Group, which is comprised mainly of rhyolites and alkali-feldspar rhyolites with lesser occurrences of andesitic to trachytic flows. A moderate textural overprint interpreted to result from contact metamorphism is present along the northern and western boundaries of the volcanic rocks. Other than a few penetrations of altered "andesite" that may have originally been close to basaltic composition (Denison, 1966), mafic rocks are absent, though geophysical data strongly suggest their presence (e.g., Shah and Keller, 2017).

The intrusive rocks are mostly assigned to the Spavinaw Granite Group, which is comprised of monzogranites and syenogranites with minor alkali-feldspar granites. These granites are usually fine to medium-grained and almost always show abundant granophyric/micrographic texture. They are interpreted as a suite of sills emplaced at relatively shallow depths beneath and within the volcanic series. A second intrusive unit described from the area is the Osage Microgranite, composed exclusively of alkali-feldspar granite and inferred to be a very shallowly-emplaced sill or sill complex, though the textures are also very similar to some of the extrusive rocks (Denison, 1981; Hamilton et al., 2020b).

The upper basement to the west of the study area is composed of coarse-grained granodiorites to syenogranites belonging to the Central Oklahoma Granite Group, which is broadly similar in character to the Proterozoic granitoids exposed further south in the Arbuckle Mountains area. These rocks are interpreted to have been emplaced at greater (mid-crustal) depth and have been suggested to be responsible for the metamorphism of the volcanic rocks and thus slightly younger (Denison, 1981), though the very limited geochronological data presently available (compiled in Bickford et al., 2015) is indistinguishable from the other units.

U-Pb zircon ages from the Spavinaw and Central Oklahoma Granite Groups and rhyolites of the Washington Volcanic Group consistently yield ages near 1,370 Ma. (Denison et al., 1984; Bickford et al., 2015). No zircon ages have been reported from the Osage Microgranite, nor have any dates been reported for the andesites. All units are considered to be part of the ~1,400-1,340 Ma Southern Granite-Rhyolite Province, the younger of two granite-rhyolite provinces which make up the basement of much of the southern and eastern North American midcontinent (Van Schmus et al., 1996). The tectonic origin of these rocks is poorly constrained, with some authors advocating an intraplate or rift setting (e.g., Lidiak, 1996) and others favoring a collisional or back-arc extensional setting (e.g., Bickford et al., 2015).

Radiometric dates obtained from the basement rocks via the Rb-Sr system are consistently 50 to nearly 200 million years younger than U-Pb zircon ages (Denison, 1981), considered to be a consequence of Precambrian alteration. All basement rocks studied by Denison show petrographic evidence of alteration as well – out of 130 wells, altered feldspars are reported for every location, secondary chlorite in 125, secondary carbonates in 82 and epidote in 64. In the vast majority of locations across all lithologies, the original Fe-Mg silicates (most commonly hornblende and biotite) are mostly to completely replaced by chlorite. Feldspars are

commonly sericitized and usually heavily dusted with hematite. Microfractures filled with chlorite, opaque minerals, carbonate or quartz are reported for many samples as well (Denison, 1981).

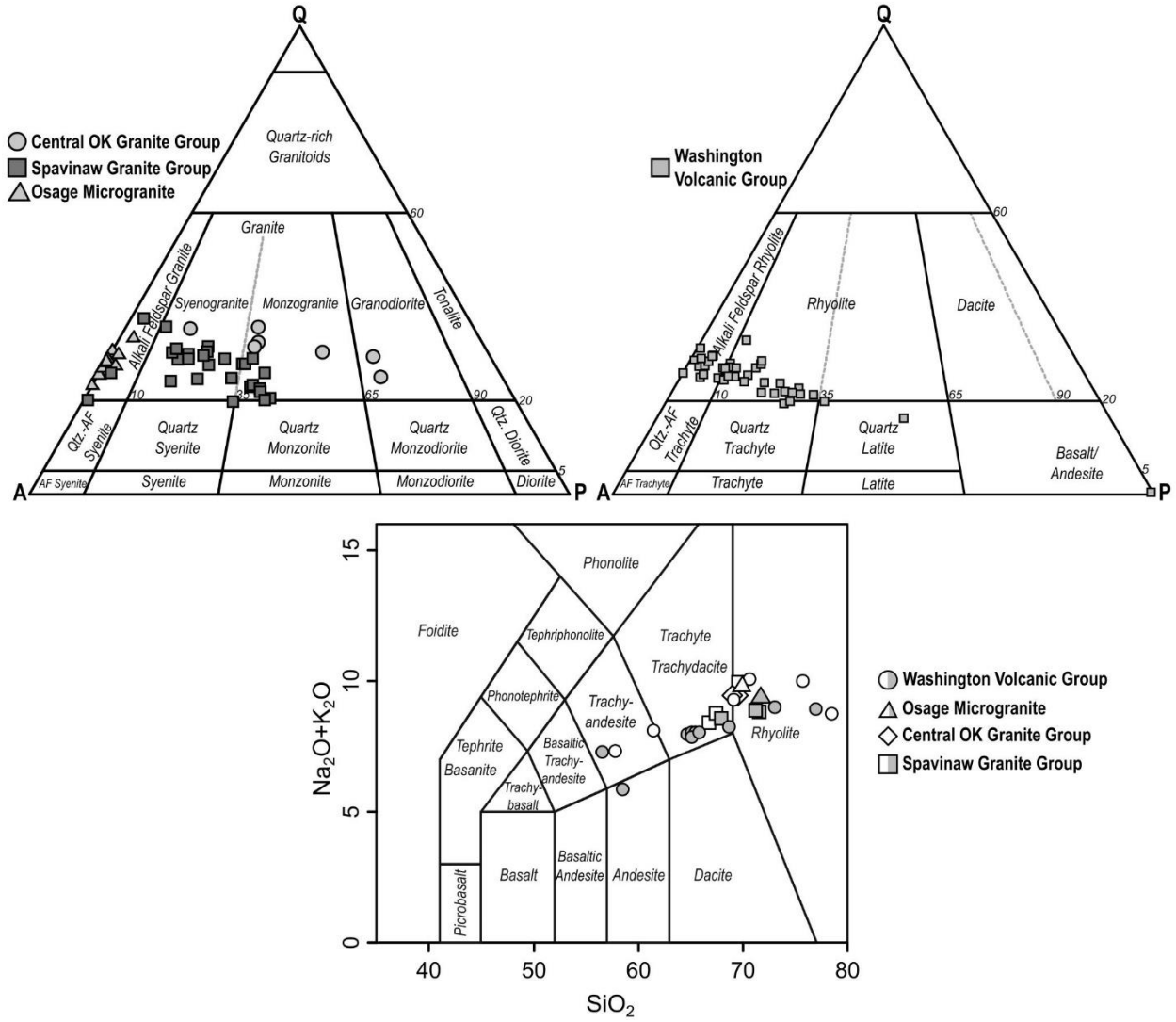


Figure 2. Mineralogical and chemical classification of study area basement rock units. Top: Mineralogical classifications (Streckeisen 1976, 1979) of intrusive units (left) and volcanics (right) derived from modal mineralogy reported by Denison (1981). Bottom: Total alkali-silica classification for extrusives (Le Bas et al., 1986) with analyses from all units for comparison. Open symbols are previously-published analyses (compiled in Denison, 1981); filled symbols are recent analyses (Hamilton et al., 2020a; some reproduced in Table 2).

Tectonic History and Basement Structure

The Precambrian history of the area is largely unknown due to the lack of exposures and absence of Precambrian sediments. Two wells penetrated sediments interpreted to be contemporaneous with the volcanic rocks (Denison, 1981), otherwise the oldest known sedimentary rocks are rare sandstones interpreted to be of middle to upper Cambrian age. The basement was progressively buried throughout the Paleozoic and was mostly covered by Arbuckle Group carbonates in the early Ordovician, though some islands of igneous material appear to have persisted until Mississippian time (Ireland, 1955; McCracken, 1964; Chenoweth, 1968). Several episodes of Phanerozoic folding and uplift have been documented from the late Cambrian (Ireland, 1955; McCracken, 1964), middle Ordovician, middle to late Devonian, and Mississippian to late Pennsylvanian (Ireland, 1955; Huffman, 1958; Rottmann, 2018). The latter is likely related to the Appalachian-Ouachita orogeny and development of the Arkoma basin to the south of the study area, which occurred in Pennsylvanian time and has been associated with significant movements in the Nemaha (Friess, 2005) and Ozark Uplifts (Cox, 2009).

The basement surface is highly irregular in topography, mostly considered to be from the eroded remnants of Precambrian mountains with some contributions from buried fault scarps (Ireland, 1955; McCracken, 1964). These paleotopographic features have been cited as evidence of significant Precambrian deformation (Ireland, 1955; Rottmann, 2018), though it has been noted that at least some could also be early Cambrian (McCracken, 1964). The distribution of basement lithologies, with the Spavinaw Granite Group forming an apparent central axis with volcanics to the northwest and southeast, has also been interpreted as a regional Precambrian anticline (Denison, 1981). The Nemaha Uplift, which lies just to the west of the study area (Fig. 1), is largely considered to be related to the ~1.1 Ga Midcontinent Rift (Adams and Keller, 1994;

Friess, 2005). A northwest-trending transcontinental “fracture zone” of likely Precambrian age has also been claimed to pass through the area (Barosh, 1992) which appears to parallel transform faults associated with late Precambrian to early Cambrian rifting of eastern Laurentia (Thomas, 2011).

A substantial number of faults are recognized in the area (Denison 1966, 1981; Marsh and Holland, 2016) (Fig. 1). Most are recognized from sedimentary offsets in exploration drilling and seismic data, though some (most notably the Seneca Fault System) have surface exposures. Aeromagnetic data also suggest the presence of basement faults which have little to no expression in the overlying Cambro-Ordovician sediments (e.g., Shah and Crain, 2018) and which are therefore likely at least middle Cambrian in age. Seismogenic fault lineations west of the study area most commonly have azimuth orientations near 60°/240° and 120°/300° (Kolawole et al., 2019); similar trends are found in outcrop fractures of the Spavinaw Granite (Kolawole, 2020), in known basement faults immediately north of the study area (Berendsen and Blair, 1991) and in surface lineations in the eastern part of the study area as well as northwestern Arkansas (Labusch, 2016) (Fig. 3). The ~300° trend in particular is also associated with late Paleozoic faults as well as early Cambrian (and possibly Precambrian) diabase dikes in southern Oklahoma (Denison, 1995) and late Precambrian to early Cambrian transform faults across North America (Thomas, 2011).

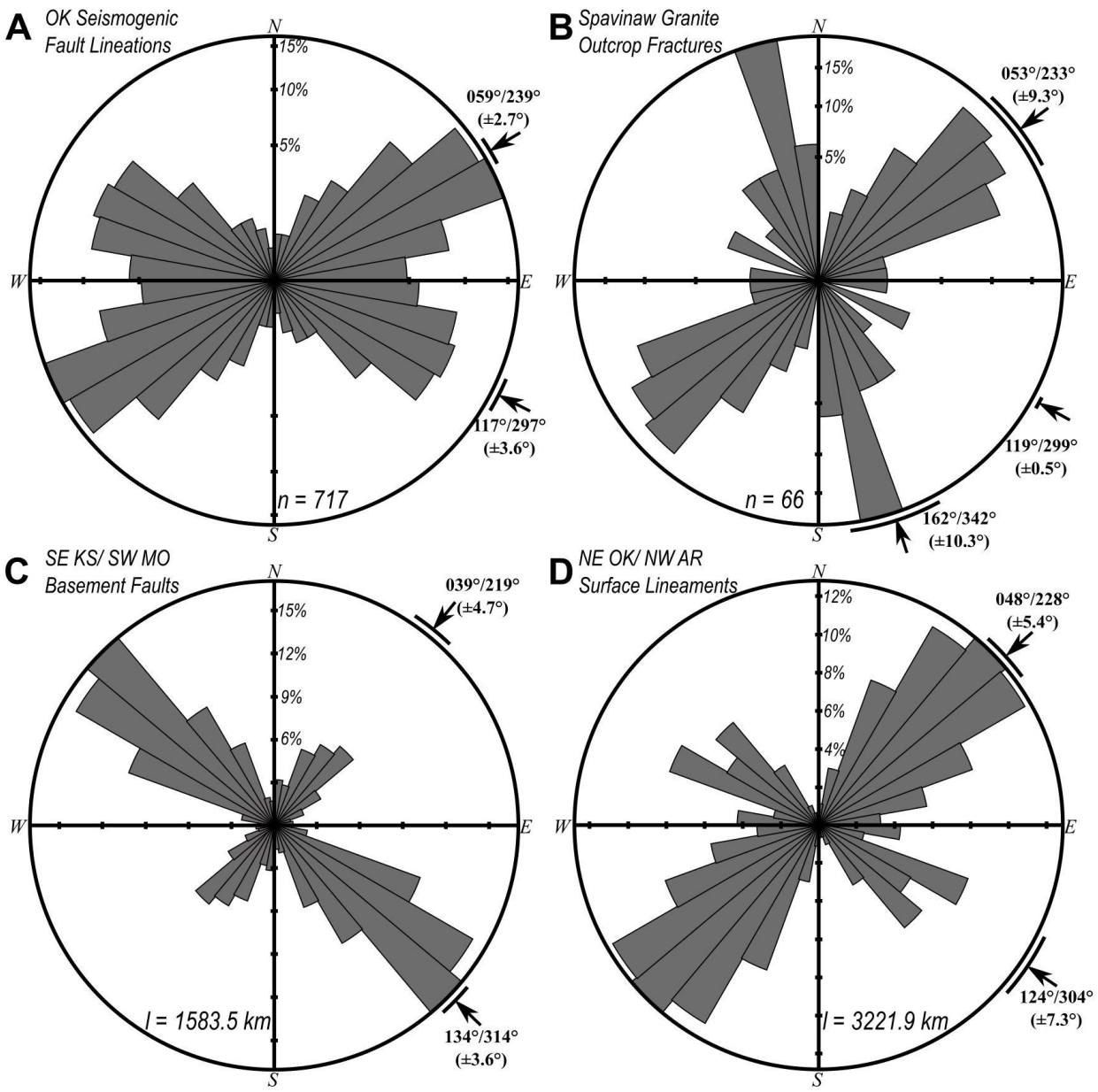


Figure 3. Rose plots of regional orientations of faults, fractures and surface lineaments. (A) Frequency-azimuth plot of seismogenic fault lineations from Oklahoma, after Kolawole et al. (2019). (B) Frequency-azimuth plot of fracture orientations from the Spavinaw Granite outcrop, after Kolawole (2020). (C) Length-azimuth plot of basement faults from southeastern Kansas and southwestern Missouri, immediately north of the study area (Berendsen and Blair, 1991). (D) Length-azimuth plot of surface lineations in northeastern Oklahoma and northwestern Arkansas (Labusch, 2016).

MATERIALS AND METHODS

Materials for this study consist of eight azimuth-unoriented cores housed by the Oklahoma Geological Survey's Oklahoma Petroleum Information Center (OPIC) (Fig. 1, Table

1). These cores represent three of the four basement groups described by Denison (1966, 1981); core from the Central Oklahoma Granite Group was not available. Cored basement sections are typically short (<1 m to a few tens of meters) with the exception of the Amoco SHADS 4, which recovered over 140 meters of basement section (Derby et al., 1991). The Sinclair Louisa M. Jones 46 and the Texaco Kohpay L 16-WS are standard 3.5-inch (88.9 mm) diameter cores, while the SHADS 4 is a 2.5-inch (63.5 mm) diameter core to a depth of 3040 ft. (926.6 m) below which it reduces to 1.75 inches (44.5 mm) in diameter. The others are 1.25-inch (31.75 mm) mineral exploration cores, with portions of the Eagle Picher cores only preserved as partial slabs.

Table 1: Core locations, Lithologies, and Depths

Well Name	Unit	Lat. (°N)	Lon. (°W)	Basement Top (m, MD/SL)	Basement Core Interval (m, MD)
AMAX SP-1	SGG	36.393	95.237	531.9 / -320.1	531.9 – 551.4
AMAX T-1	WVG	35.947	94.952	432.5* / -152.1	432.5 – 449.9
Amoco SHADS 4	WVG	36.266	95.758	918.0 / -688.2	918.0 – 1059.7
Eagle-Picher 43-C Anna Beaver	SGG	36.986	94.854	491.9* / -238.0	491.9 – 505.1
Eagle-Picher P-5 Goldenhawk	WVG	36.973	94.838	528.7* / -275.1	528.7 – 547.6
Sinclair Louisa M. Jones 46	WVG	36.276	96.472	892.8 / -599.9	892.8 – 897.7
Texaco Kohpay L 16-WS	OM	36.621	96.460	857.4 / -525.8	866.5-868.1[D]
Texaco Osage C-1A	WVG	36.193	96.084	1107.6 / -802.2	~1124.2-1124.7[D]

Table 1. Cores discussed in the current study (also see Fig. 1). Locations and depths from Campbell and Weber (2006), except depths marked by asterisk have been adjusted to fit observations. The Texaco cores noted with a [D] are discontinuous and contain less than a meter of material each. Lithologic group assignments from Denison (1981) and Derby et al. (1991). Group abbreviations: OM = Osage Microgranite, SGG = Spavinaw Granite Group, WVG = Washington Volcanic Group (Denison, 1981).

Cores were inspected using the unaided eye and microscopes. Fracture occurrences were noted for the longest core (the Amoco SHADS 4) and inclinations were measured using an angle ruler. Samples were cut from selected intervals by OPIC personnel. Polished thin sections were prepared from many of these samples and inspected by petrographic microscope as well as a FEI Quanta 250 scanning electron microscope (SEM) equipped with a Bruker energy-dispersive spectrometer (EDS) for semiquantitative elemental analysis. Mineral identifications at the

microscopic scale were made on the basis of optical properties and/or elemental compositions. Selected samples were sent to Activation Laboratories of Ancaster, Ontario, Canada for whole-rock elemental geochemical analysis. Major and trace element abundances were determined by mass spectrometry, with ferrous iron determined by titration. Preliminary attempts to orient samples from three larger-diameter cores using paleomagnetism failed, as the rocks carry a near-vertical remanence interpreted to be drilling-induced.

OBSERVATIONS AND RESULTS

Fractures

Every core of northeastern Oklahoma basement rock inspected contains fractures, nearly all of which (aside from those which are clearly artificial) contain secondary minerals. These fractures usually occur throughout the entire recovered sections – for instance, mineralized fractures are still common over 140 meters below the top of basement in the Amoco SHADS 4. The vast majority of fractures appear to have formed as opening-mode fractures, though many show indications of subsequent shear.

In six cores, the most prominent fractures have steep inclinations (commonly 70° to vertical) (Fig. 4); both of the cores where this is not observed contain less than a meter of section each. Multiple sets of steep fractures may be present (Fig. 4C); the relative difference in strike angles was not measured but does not usually appear to be orthogonal. Near-vertical joints are also common in the Spavinaw Granite outcrop (Kolawole, 2020). Many of these fractures have a slight curvature, and the cores are commonly broken along them (e.g., Figs. 4A, 4B). These fractures have not been observed to cross-cut the basement-sediment unconformity in core, though samples of this boundary are quite limited and steep fractures are also found in the overlying Arbuckle carbonates.

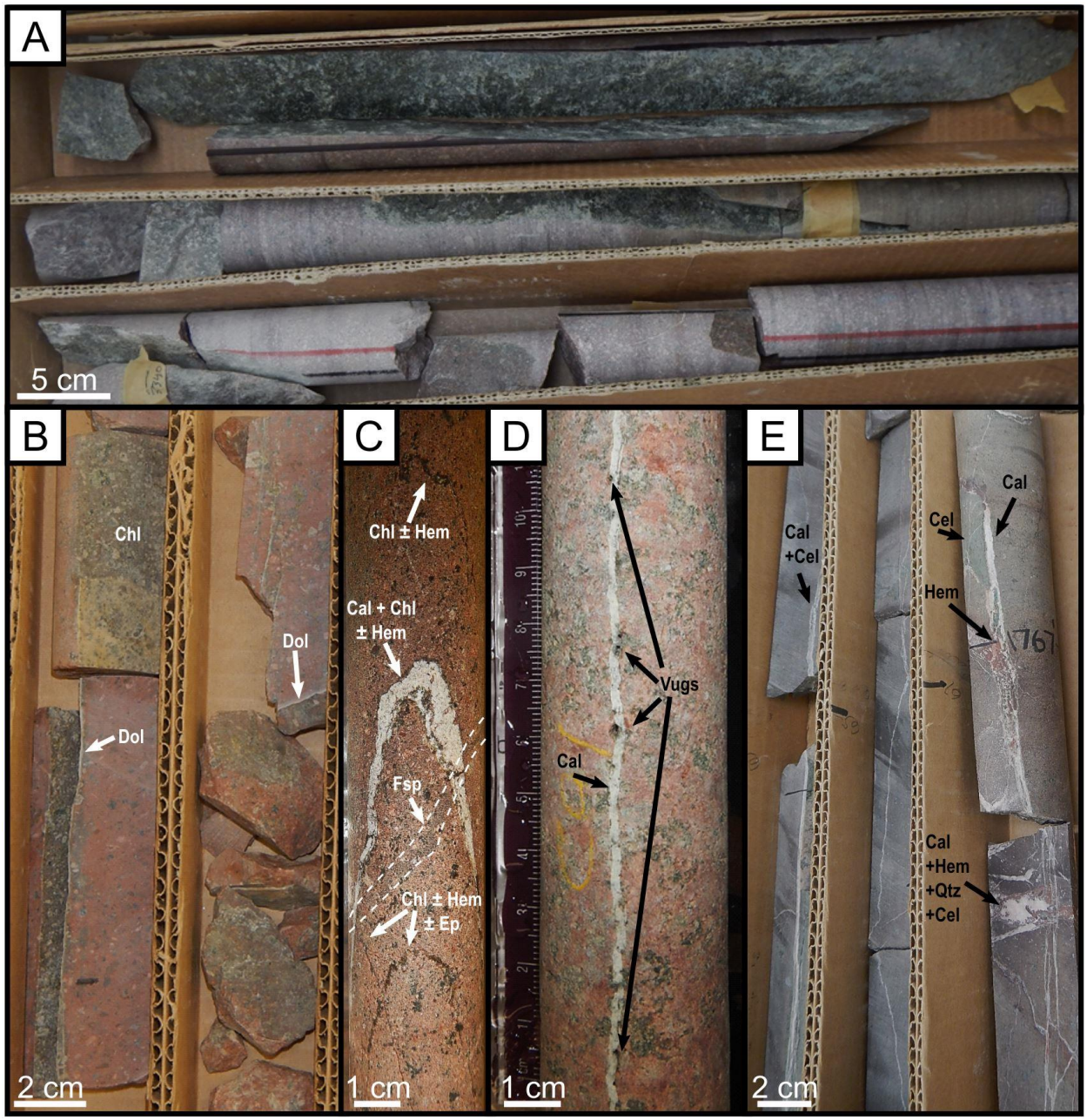


Figure 4. Steeply-inclined mineralized fractures from various basement cores. (A) Steep to vertical chlorite-filled fractures, some with curvature. Amoco SHADS 4, 1018-1020 m MD. (B) Moderately chloritized fractures (some with dolomite). Eagle Picher 43-C Anna Beaver, ca. 500 m MD. (C) Prominent calcite (Cal)-filled fracture cross-cutting thinner feldspar (Fsp) fracture and chlorite (Chl) ± hematite (Hem) ± epidote (Ep) fractures. Note multiple sets of the latter towards the bottom. AMAX T-1, 448.2 m MD. (D) Vertical calcite vein with quartz-bearing vugs. AMAX SP-1, 538.6 m MD. (E) Subvertical carbonate veins with associated celadonite (Cel) and breccia zone. Eagle-Picher P-5 Goldenhawk, ~537-539 m MD.

Fractures with shallower inclinations (30° to horizontal) are also present in all cores examined, though due to core geometry they are not as visually prominent as the steep fractures.

They also lack the curvature found in some steeply-inclined fractures. In the few intervals found where fractures of significantly different inclinations cross-cut each other, the shallower-inclination fractures either cross-cut or truncate against the steeper ones. Exceptions to this trend are found in the Eagle-Picher P-5 Goldenhawk, where some brecciated intervals dominated by subhorizontal fractures are cross-cut by vertical carbonate veins (e.g., Fig. 4E).

Macroscopic fracture abundances were measured on the basement section of the Amoco SHADS 4, which penetrated just over 140 meters of trachyte. A total of 866 fractures were identified, though this count only applies to macroscopic fractures and is almost certainly an underestimate, as many fractures are extremely faint and easy to miss even on a wet smooth surface. Nearly 70% of these have inclinations $\geq 60°$ (Fig. 5), averaging to a rough abundance of four steep fractures per meter of core. Shallow-inclination ($\leq 30°$) fractures make up 24% of those in the SHADS 4, and are most concentrated in the interval from 110-130 meters below the basement unconformity. Overall fracture intensity is relatively consistent in the upper ~60 meters of basement and then begins to increase with depth (Fig. 5). Microfractures are also found in nearly all thin sections prepared from basement material in every core.

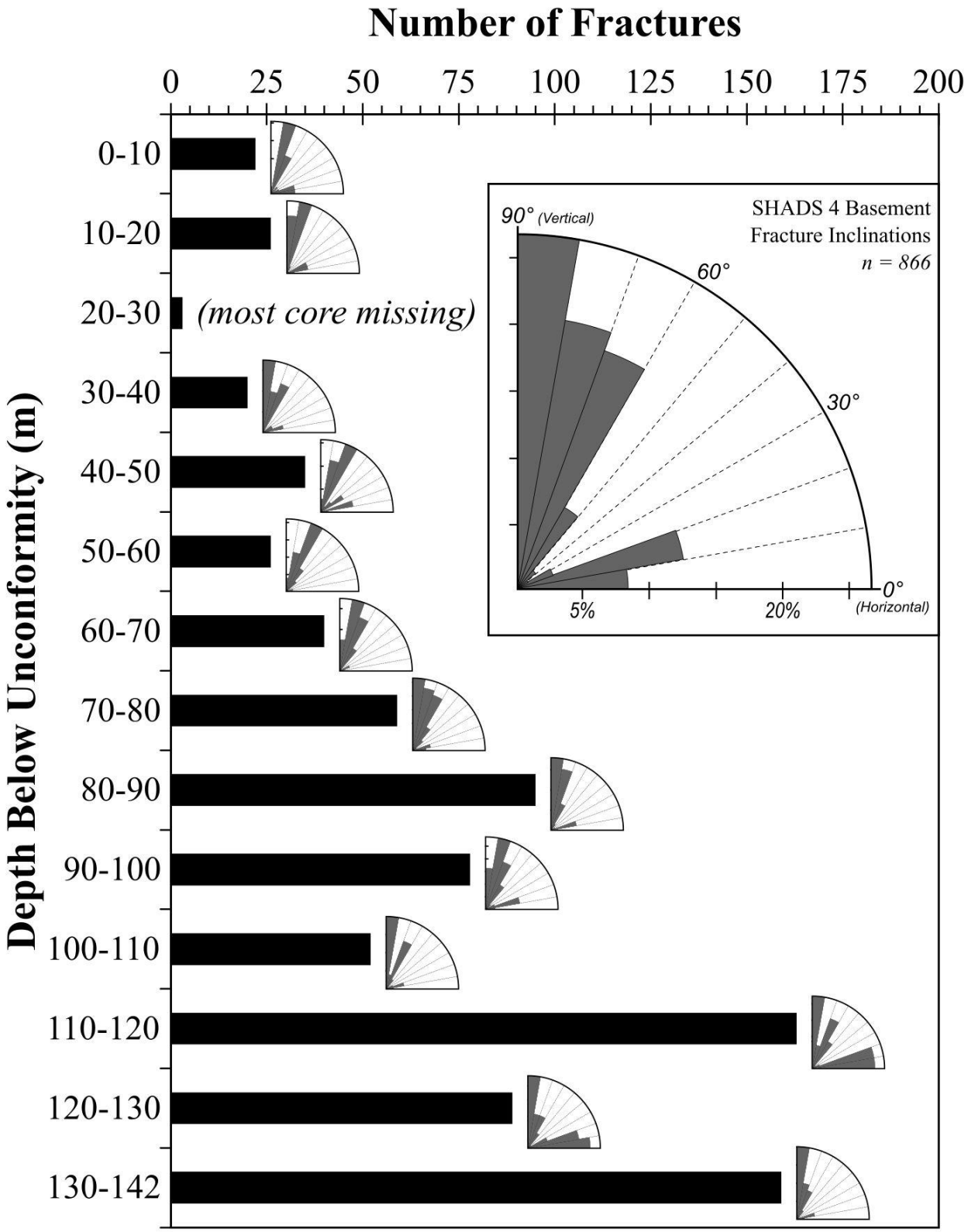


Figure 5. Abundance and inclination-frequency distribution of mineralized fractures in the Amoco SHADS 4 vs. depth below basement unconformity. Steep fractures dominate, with shallow inclinations also prominent between 110 and 130 m below the top of basement.

Vug porosity is present in fractures from several cores (Fig. 4D, Fig. 6), as evidenced by well-developed crystal faces of carbonates and quartz in open spaces within otherwise intact fractures. Macroscopic vugs are mostly found along or within calcite or dolomite veins. Vugs seem most common near the basement unconformity, but this may be biased by the relatively shallow penetrations of most cores – for instance, vug porosity is found in a calcite vein over 110 meters below the basement unconformity in the SHADS 4 (Fig. 6C), well beyond the penetration of other cores from the area.

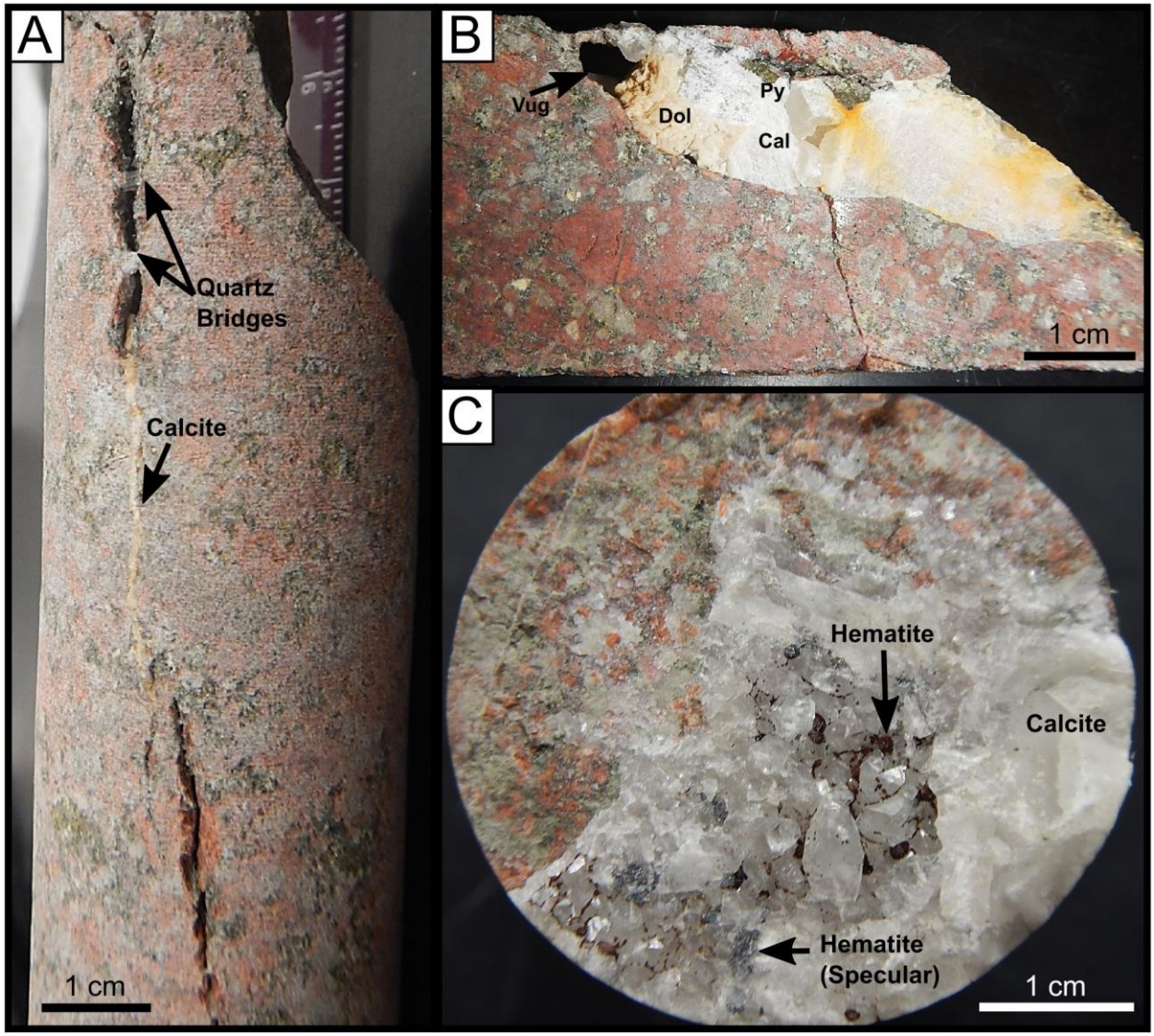


Figure 6. Porosity hosted in basement fractures. (A) Quartz bridging porosity in calcite fracture. AMAX SP-1, 538.6 m MD. (B) Dolomite (Dol) in fracture with pore space, calcite and pyrite. AMAX SP-1, 540 m MD. (C) Euhedral calcite with hematite in fracture vug. Amoco SHADS 4, 1030.5 m MD.

Secondary Minerals in Fractures

The secondary mineralogy of basement fractures is highly variable (Figs. 4, 7-8). Macroscopic chlorite-filled fractures are found in seven of the eight cores studied (absent only in the Kohpay 16, though chlorite fills microfractures in that core as well). Calcite fills fractures in six, only absent in the two cores containing <1 m of section. Quartz-filled fractures are present in all cores, but are usually much thinner than the chlorite and carbonate veins and therefore often

hard to see. Quartz also fills a few N-S trending veins of ~1 cm thickness in the Spavinaw outcrop. Dolomite veins are present in the 43-C Anna Beaver core (Fig. 4B, Fig. 7D); dolomite also occurs within some black chlorite-filled fractures in the T-1 (Figs. 7B, 7C), and baroque dolomite is present in thick veins near the unconformity of the SP-1 (Fig. 7F). Epidote is abundant in fractures of the SHADS 4 and minor to trace amounts are also found in fractures from the T-1, SP-1, 43-C Anna Beaver and the P-5 Goldenhawk. Pyrite is found in trace amounts in fractures from all cores, with higher abundance in some intervals of the SP-1 and P-5 Goldenhawk. Pyrite and epidote have also been reported from thin veins in the Spavinaw Granite outcrop (Tolman and Landes, 1939). Fractures from several cores show hematite staining. Rare macroscopic fractures cemented by secondary alkali feldspar (e.g., Fig. 4C) are also found in the T-1, 43-C Anna Beaver and the SHADS 4. Celadonite is found only in the P-5 Goldenhawk (which has by far the most mafic lithology inspected), where it is prominent in several veins (Fig. 4E).

Mineralized fractures are also abundant at the microscopic scale, even in intervals that appear intact to the unaided eye. All minerals found macroscopically are present in microfractures, and several more minerals are only found at the microscopic scale. Fluorite is present in microfractures from the Sinclair Louisa M. Jones 46; it has also been reported in fractures from the Spavinaw Granite (Tolman and Landes, 1939). Authigenic albite, K-feldspar, iron oxide and clay minerals are found in fractures from several cores. Traces of zeolites are present in the P-5.

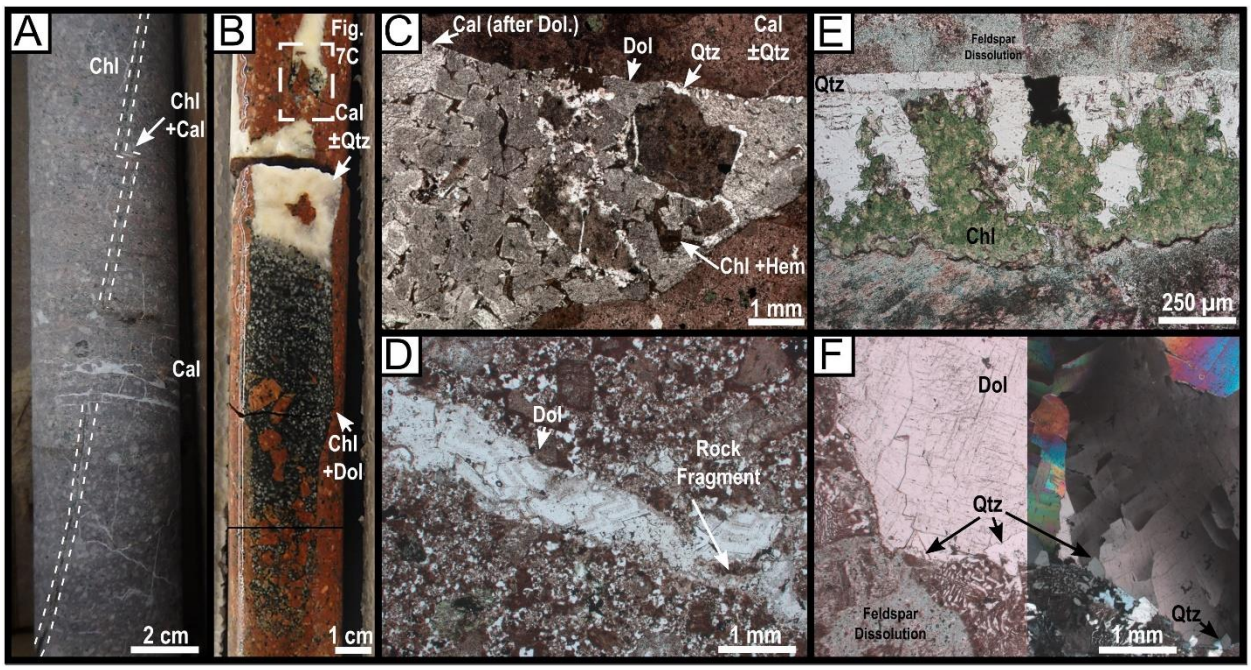


Figure 7. Variable mineralogy in basement fractures. (A) Steep chlorite fracture crosscut and offset by subhorizontal calcite-cemented fractures and breccia, SHADS 4, 1029.6 m MD. (B) Black chlorite with later dolomite (white specks), subsequently replaced uphole by calcite and quartz. AMAX T-1, 444 m MD. (C) Plane-light photomicrograph of thin section from area marked in 7B. Quartz cements rock fragments in breccia. Early dark material (now mostly chlorite + hematite) is progressively replaced by dolomite and subsequently calcite. (D) Dolomite showing growth lines in Eagle-Picher 43-C Anna Beaver, 497.4 m MD. (E) Quartz and chlorite vein, Texaco Osage C-1A ~1124 m MD. Possible crack-seal texture is present in quartz, chlorite has vermiform habit, and groundmass feldspars are partly dissolved (blue staining from epoxy impregnation). Lower vein boundary has stylolitic character. (F) Baroque dolomite and pyramidal quartz in thick vein, with dissolved feldspar in host rock. AMAX SP-1, 535.8 m MD. Left half of image in plane-polarized light, right half in cross-polarized light.

Multiple generations of mineral growth are present in many fractures (Fig. 8). Calcite is commonly found as a later fill in fractures originally mineralized by chlorite and/or epidote (Fig. 8D). Traces of vermiculite are found along fractures re-mineralized by calcite in the SHADS 4 and P-5 Goldenhawk, apparently as an alteration product of chlorite in both cores and also of celadonite in the P-5 (Fig. 8F). Calcite also fills along early feldspar-cemented fractures in the 43-C (Fig. 8C). Dolomite (with zoning and Fe-oxide inclusions) occurs within earlier black chlorite veins in the AMAX T-1, as do small amounts of synchysite and xenotime (Fig. 8B). These same veins are replaced by calcite ± quartz in some intervals of the core (Fig. 7B), and

intermittently by clays along their margins. Traces of synchysite are also present in some fractures near the unconformity in the SHADS 4. Jarosite is present in some fractures of the Jones 46 as an alteration product of pyrite (Fig. 8E). Some intervals of the SHADS 4 contain veins in which epidote and quartz appear to have grown nearly simultaneously; in all other fractures inspected, different minerals do not appear to overlap in time. Successive generations of the same mineral within a single fracture are largely absent with the exception of the P-5 Goldenhawk, which contains some very complex veins housing several generations (and habits) of calcite alongside zeolite, pyrite and multiple phyllosilicates (e.g., Fig. 8F).

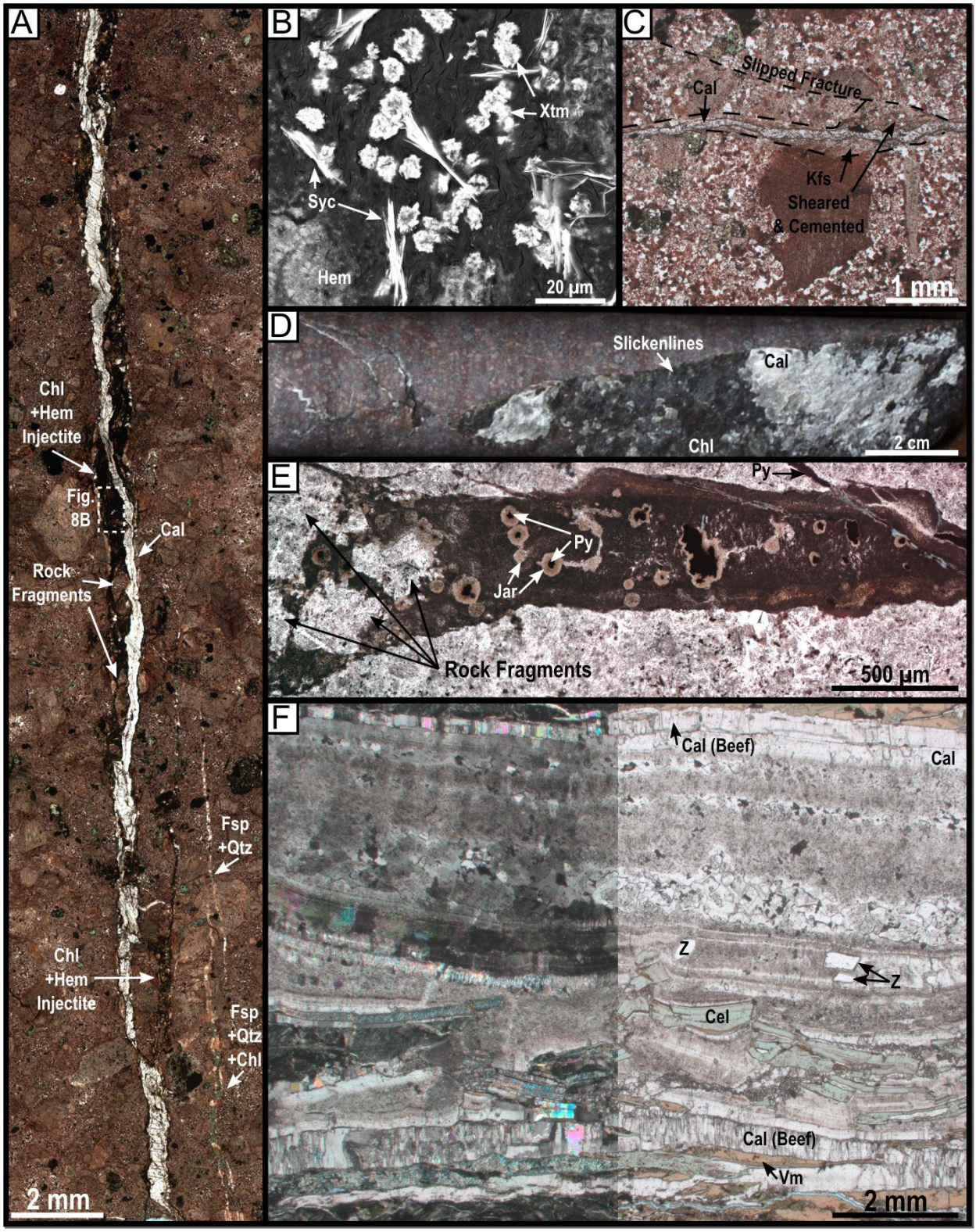


Figure 8. Multiple stages of mineralization in fractures. (A) Plane-light micrograph of black injectite (EDS indicates chlorite + hematite composition) vein containing rock fragments and re-occupied by later calcite with crenulation and prominent twins. Also note subparallel fractures cemented by feldspars and quartz with variable green chlorite. Paler intervals in injectite partly

altered to vermiculite. AMAX T-1, 448.4 m MD. (B) Backscattered electron micrograph of secondary minerals in injectite from Fig. 8A. Matrix has composition of chlorite with later growths of hematite, synchysite (Syc) and xenotime (Xtm). (C) Plane-light micrograph of early sheared fracture cemented by K-feldspar (Kfs) and later re-occupied by calcite. Another fracture branching from this one offsets phenocrysts and appears to have slipped an indeterminate distance. Eagle-Picher 43-C Anna Beaver, 503.8 m MD. (D) Calcite re-occupying earlier chlorite fracture with faint slickenlines. SHADS 4, 1003 m MD. (E) Jarosite (Jar) overgrowths replacing pyrite (Py) in clay-filled fracture with rock fragments. Sinclair Louisa M. Jones 46, 893.4 m MD. (F) Complex vein containing multiple generations of calcite along with brecciated green celadonite (Cel) variably altered to brown vermiculite (Vm). Traces of an unidentified zeolite (Z) are also present. Some calcite appears to have been originally fibrous but has recrystallized. Eagle-Picher P-5 Goldenhawk, 537.2 m MD. Left half of micrograph in cross-polarized light; right half in plane light.

Where fractures of differing mineralogy (not necessarily of different inclinations) cross-cut one another, chlorite and epidote are generally cross-cut by carbonates (e.g., Figs. 4C, 7A). This is consistent with carbonates occurring as late phases in earlier chlorite or epidote-bearing fractures. Authigenic feldspars also appear to be an early phase. Quartz is present in both early fractures and later carbonate veins. Where both are present, pyrite mostly appears to post-date carbonate.

Qualitatively, there are some tentative relationships between fracture properties and mineralogy. In general, chlorite is most common in relatively thin (usually ≤ 0.5 mm) veins of steep inclination. Dolomite is essentially absent in sub-millimeter veins; its occurrence is most common in thick veins (some > 1.5 cm) near the unconformity where the basement is onlapped by dolomitized carbonates; these were likely exposed joints at the time of burial. Dolomite also occurs as crystals growing within thicker (several mm to ~1 cm) black veins of the T-1 (extremely fine-grained and nearly opaque in thin section, identified as chlorite on the basis of EDS analyses showing a composition rich in Mg, Al, Fe and Si and lacking in Ca and alkalis) and in veins of approximately 1-5 mm thickness in the 43-C. Calcite commonly occurs as a later mineral alongside (or replacing) chlorite or dolomite; where it is the sole mineral the veins

(usually < 1 mm, but up to a few mm thickness) are usually of low (horizontal to ≤ 30°) inclination, though numerous exceptions exist.

Quartz bridges across fractures in the SP-1 in some locations (Fig. 6A), though it more commonly lines both sides of the fractures with short pyramidal faces. These fractures are usually filled with carbonate (as is part of the one in Fig. 6A), and small quartz crystals with pyramidal faces oriented roughly orthogonal to vein walls are found in thin sections along thick carbonate veins from SP-1 and T-1. Bridges (found in narrower parts of the veins) are associated with rapid opening relative to crystal growth, and the short pyramidal habit with opening rates too rapid to form bridges (Lander and Laubach, 2015). This suggests that these fractures opened relatively rapidly, and that quartz preceded carbonate in the paragenesis.

Other Fracture Fills

Many fractures in the upper ~8 meters of basement in the AMAX SP-1 appear to have been exposed fissures. In addition to carbonate veins (partly replaced by baroque dolomite similar to that of the overlying Ordovician rocks), some fractures contain very fine-grained silicate among the igneous material. The contacts between this material and the granite are more arcuate/rounded than typical fractures, and in some intervals the material contains a laminated texture – it is interpreted as fissure-fill sediment. One interval about 3 m below the top of basement is composed of cleavage fragments of alkali feldspar along with illite clay; it also contains pyrite and anomalous Sr- and REE-bearing aluminum phosphate-sulfate minerals that may be replacing microfossils. Fissure sediments deeper in the core are composed of mostly rock fragments with some angular detrital quartz. The upper few meters of the SHADS 4 also contain fractures filled by clastic material very similar in appearance to the immediately overlying sandstone. Detrital carbonate is absent in all apparent sediments.

The uppermost basement rocks of the AMAX T-1 are also highly brecciated and re-cemented by dolomite. Below this are fractures containing clay minerals and host rock fragments. These may also be fissure-fill sediment, though they lack the lamination of those in the SP-1 and the fractures are much more regular in shape. The steep chlorite-dolomite veins also contain abundant rock fragments and lack any apparent sedimentary fabric.

Host rock fragments are common in fractures from many cores. In addition to the aforementioned occurrences in the SP-1 and T-1, they occur in both calcite-filled and clay-filled fractures of the Jones 46, in the complex veins of the P-5, and some calcite veins in the SHADS 4. Rock fragments frequently lack apparent contact with vein boundaries or each other and often lack distinctive cement textures; however, rock fragments in some veins of the T-1 show quartz overgrowths similar to early cements in cockade breccias (e.g., Frenzel and Woodcock, 2014) (Fig. 7), and a small minority of rock fragments in the Jones 46 vein appear to have rotated during vein cementation.

Slip

Fractures from several cores contain evidence of slip (Figs. 8-10). Slickenlines, commonly but not always with step structures, are present on several fracture surfaces in the SHADS 4 (e.g., Fig. 8D) and are found mainly on chlorite fractures with secondary carbonate. Some record subhorizontal slip while others appear near vertical; only one set is present on any given surface. These features are also found along host rock and chlorite/clay fractures in the SP-1 and T-1 as well as on a prominent vertical carbonate vein in the Jones 46 (Fig. 9). The host rock contact with the slickenside-bearing vein in the Jones 46 also has locally embayed margins, and calcite near the contact is sheared with reduced grain size, bulged grain boundaries and localities of intense twins consistent with the Type I and II twins of Burkhard (1993). The

sheared contact contains undeformed authigenic dolomite, clays and pyrite, suggesting it served as a fluid conduit subsequent to slip.

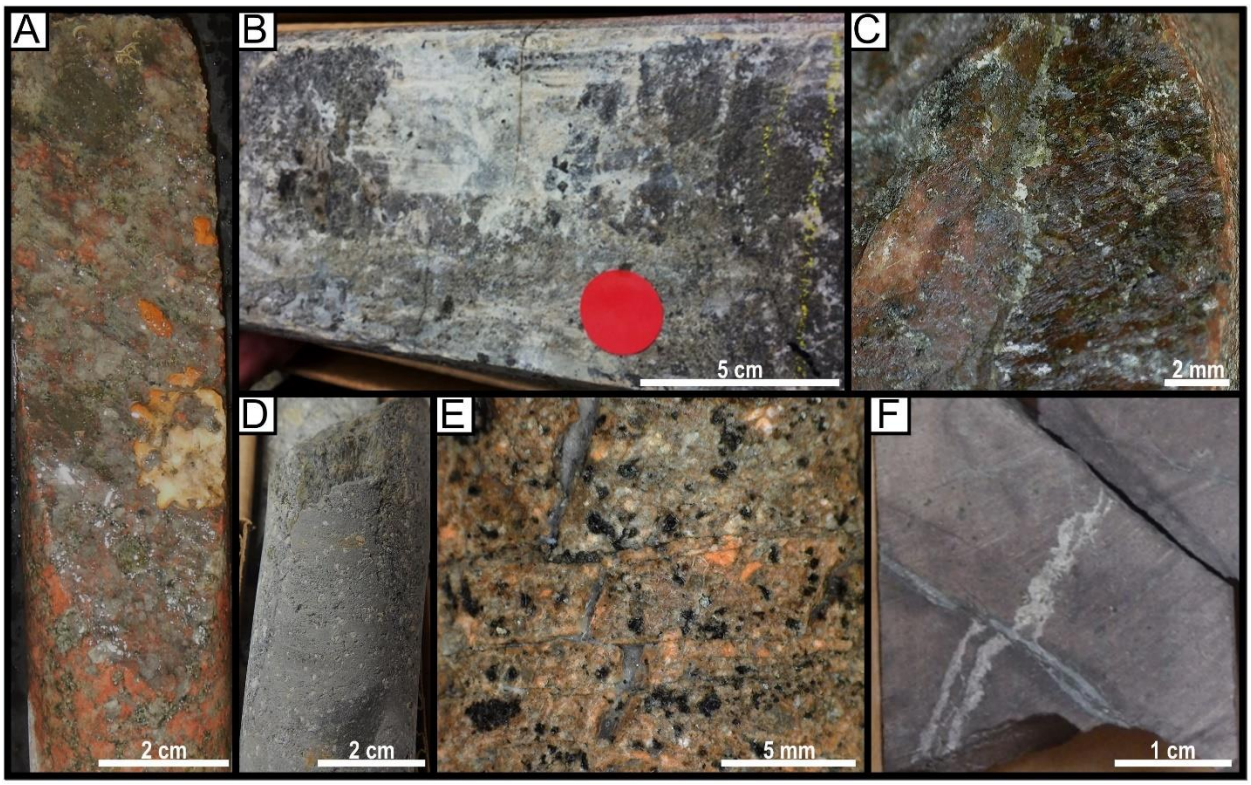


Figure 9. Slip indicators in NE Oklahoma basement fractures (A) Inclined slickenlines on fracture surface mineralized by clays and calcite, SP-1, 536.8 m MD. (B) Striated margin of calcite vein, Jones 46, 895 m MD. (C) Slickenlines and steps on epidote fracture, T-1, 446.2 m MD. (D) Slickenlines along margin of fracture filled with clay (after black chlorite material) and dolomite, T-1, 433.7 m MD. (E) Steep clay-filled fracture with multiple offsets by horizontal fractures, T-1, 442.6 m MD. (F) Calcite vein offset by fracture with undetermined fill, P-5 Goldenhawk, 541 m MD.

Veins are offset by slip along cross-cutting fractures in the SHADS 4, P-5, and T-1 (e.g., Fig. 9E, 9F). In the SHADS 4, abundant subhorizontal fractures are associated with offset of steeper veins and local brecciation, particularly in the interval from 110-130 meters below the unconformity (1028-1048 m measured depth); these offsetting veins and breccias are all cemented with calcite. Early fractures in the 43-C are associated with shearing and feldspar re-cementation, followed by later carbonate (Fig. 8C). Black veins (nearly opaque even in thin section) in the T-1 intrude the host rock along discontinuous small fractures of irregular shape

and various orientations (Figs. 7B-C, 8A-B, 10C); this appears to have been due to dynamic injection, usually considered diagnostic of coseismic rupture (e.g., Rowe et al., 2012; Rowe and Griffith, 2015). Opening-mode microfractures mostly sealed by quartz extend orthogonally from some of these injectite-bearing fractures (Fig. 10C). The original material has been replaced by chlorite and hematite (identified via EDS as Mg-Fe-Al silicate and Fe-oxide, as the material is very dark brown to opaque in thin section) and subsequently overprinted by dolomite and other minerals; primary textures appear completely lost, and it is unclear whether the material was originally sediment fill, gouge or even melt. Late calcite re-using the earlier fractures is crenulated and shows Type II twins (Fig. 8A).

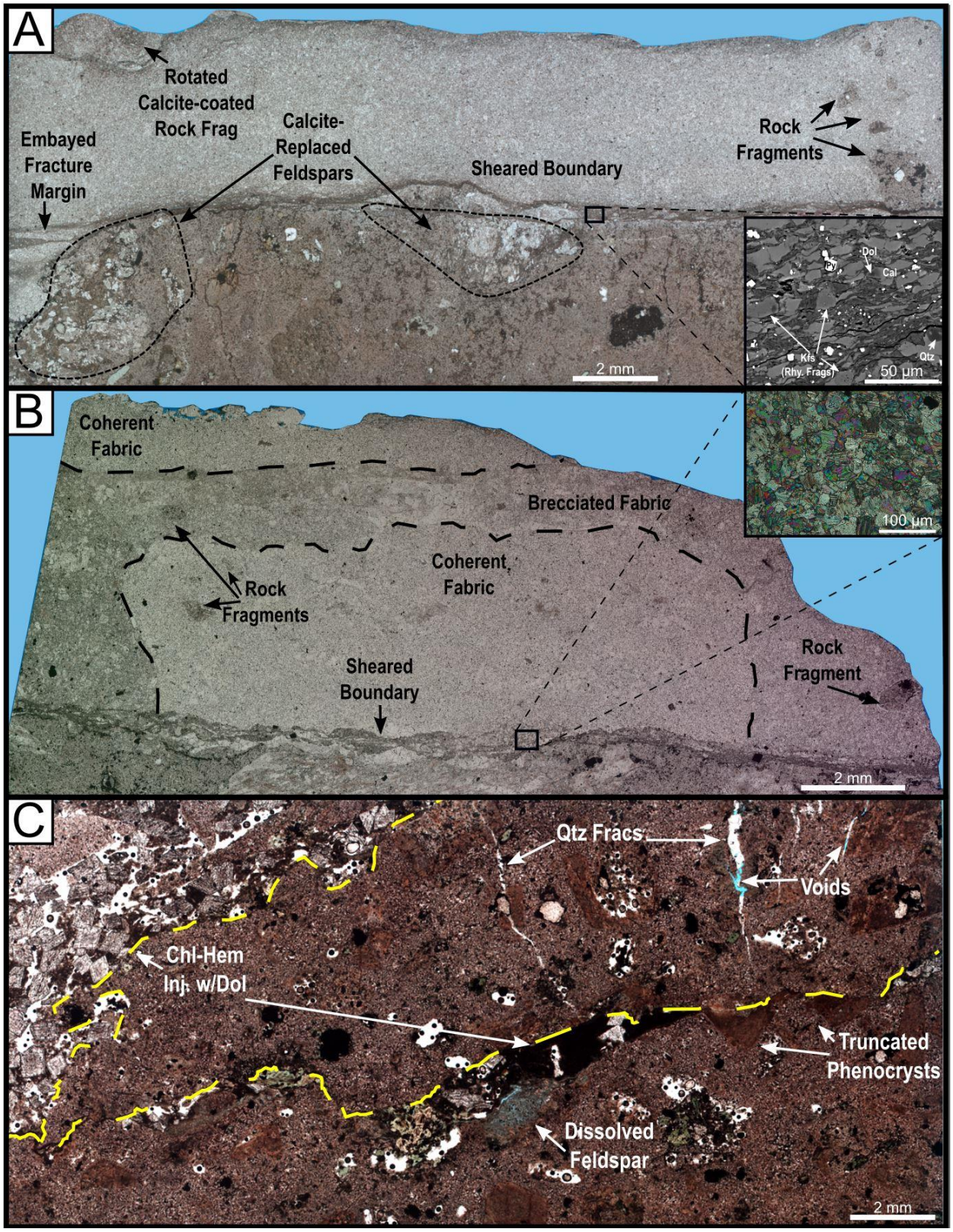


Figure 10. Microscopic features associated with sheared veins and injectites. (A) Plane-light mosaic showing coherent fine-grained calcite with rock fragments (one rotated during cementation), sheared boundary and embayed margin. Calcite grain size is reduced, and

secondary minerals preferentially grow at the boundary (see inset backscattered electron image). Feldspars in the host rock are altered to calcite along the contact. Calcite vein with slickenlines, Jones 46, 895 m MD. (B) Variable fabric in the same vein - some bits are brecciated. Inset XPL micrograph shows abundant fine twins developed near the contact. (C) Microstructures associated with injectite in AMAX T-1, 438 m MD. Injectite propagates along sinuous fractures (traced in yellow) associated with phenocryst truncation. Injectite is partially altered to green chlorite and contains later dolomite even in thin, discontinuous intervals. Thicker areas (e.g., upper left) associated with more extensive dolomite replacement. Also note extensional fractures mostly cemented with quartz between injectite-hosting fractures. Feldspar phenocrysts show some dissolution along fracture margin, and much of the injectite (and parts of some phenocrysts) has been replaced by clays which scoured out during thin section preparation.

Basement Alteration

All basement rocks inspected show petrographic evidence of alteration throughout. Consistent with the observations of Denison (1981), feldspars are commonly turbid and heavily stained by hematite. Many are also partially or completely sericitized, particularly plagioclase. Plagioclase in some intervals of the P-5 and SHADS 4 is partially to completely saussuritized (i.e. replaced by epidote and sericite). Plagioclase grains from the SHADS 4, Jones 46, Kohpay 16, and SP-1 have been analyzed using EDS; the vast majority show no detectible Ca content, indicating they have likely been albitized. Primary biotite and hornblende are completely replaced by chlorite ± titanite, and clinopyroxene (present in the SHADS 4 and P-5) is sometimes partly chloritized as well. Titanomagnetite is largely altered to magnetite (sometimes maghemite) with titanite and/or anatase. Synchysite is also present alongside secondary chlorite and titanite in the Kohpay 16 (Hamilton et al., 2020b) as well as the Jones 46.

Additional alteration is observed in association with macroscopic fractures. Hematite staining of host rock is commonly more prominent in heavily-fractured core intervals. At the microscopic scale, feldspars near mineralized fractures are commonly more altered than the rest, and many appear slightly porous. Dissolution pitting of host rock is visible at the macroscopic scale in the SP-1 (Fig. 11A), particularly adjacent to veins containing pyrite. Plagioclase

phenocrysts within a few mm of calcite veins in the Jones 46 are largely replaced by clays and/or calcite (Fig. 10A). Chlorite near these fractures is also largely altered to clays, and the clays replacing chlorite and calcite are particularly susceptible to scouring during thin section preparation (e.g., Fig. 10C).

Two additional types of alteration are associated with proximity to the basement unconformity. Hematite staining and alteration of feldspars is much more prominent in the uppermost basement sections of the SHADS 4 and 43-C; similar trends are visible but less pronounced in the Jones 46 and the T-1. The upper parts of the SP-1 have a reddened, heavily weathered appearance. In immediate proximity to the unconformity, basement rock in the 43-C, T-1 and Jones 46 is altered from the typical reddish hues to gray (Fig. 11B-D). This color change is also found along fractures in the upper 2-4 meters of basement, as well as in basement boulders in the lower Paleozoic sedimentary sections of the Jones 46 and T-1. Affected rocks have feldspars and chlorite further replaced by clay minerals, and an increased abundance of secondary pyrite. Yellow staining associated with jarosite is present in both gray-altered and non-gray fractures in the Jones 46. The gray alteration style was previously recognized in a now-backfilled quarry of the Spavinaw Granite (Tolman and Landes, 1939) and in the Jones 46 core (Chenoweth, 1968); both studies attributed it to paleoweathering. The fact that it appears to post-date a reddening style of alteration that could also be interpreted as paleoweathering was not noted in these locations.

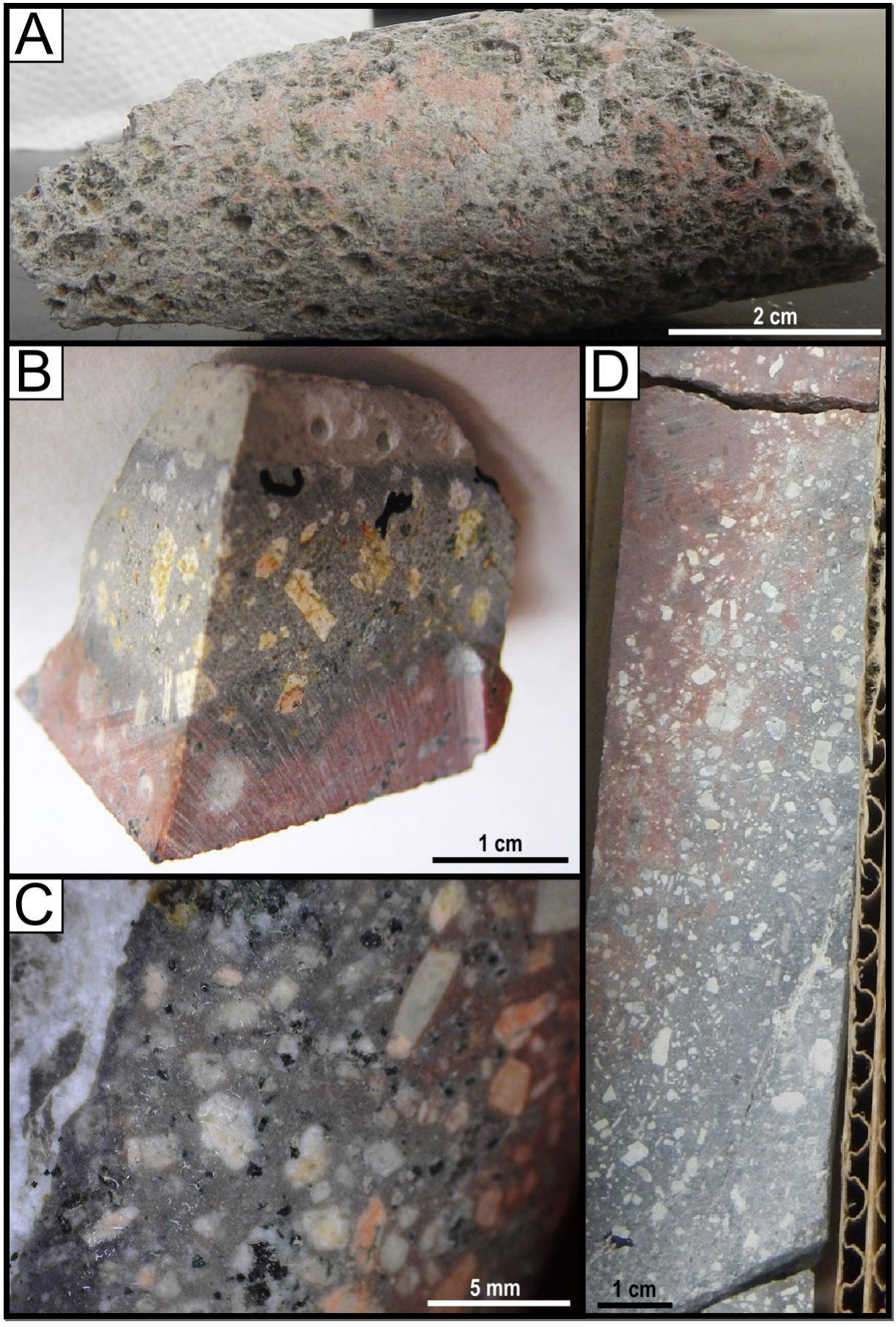

A
2 cm
B
1 cm
C
5 mm
D
1 cm

Figure 11. Basement alteration adjacent to fractures in core material. (A) Dissolution of host rock adjacent to fractures hosting clays, pyrite and carbonate. AMAX SP-1, 535.8 m MD. (B) Host rhyolite around sheared calcite vein (see Figs. 9B, 10A-B) altered with secondary phyllosilicates, calcite, pyrite and jarosite. Jones 46, 895.5 m MD. (C) Similar discoloration of red host rock around calcite-dolomite vein. T-1, 433.1 m MD. (D) Fracture-associated discoloration. 43-C Anna Beaver, 493.8 m MD.

Comparison of geochemical analyses of highly altered vs. less-altered material (Table 2; Fig. 12) indicates a variety of chemical changes, with some consistencies and scattered differences. Altered rocks are typically enriched in volatiles, K, Cs, Tl, Rb and low-mobility trace elements relative to less-altered rock, and typically show loss of Ca, Na, Mn, Fe (particularly Fe^{3+}), Sr, Zn, and Pb. Reduced Pb, Sr and Ca abundances have also been noted in the Kohpay L 16-WS core in the northwestern part of the study area (Hamilton et al., 2020b), though the very limited amount of core did not contain less-altered material for comparison. Other elements (e.g., Mg, P, LREE, W) are more variable in their mobility.

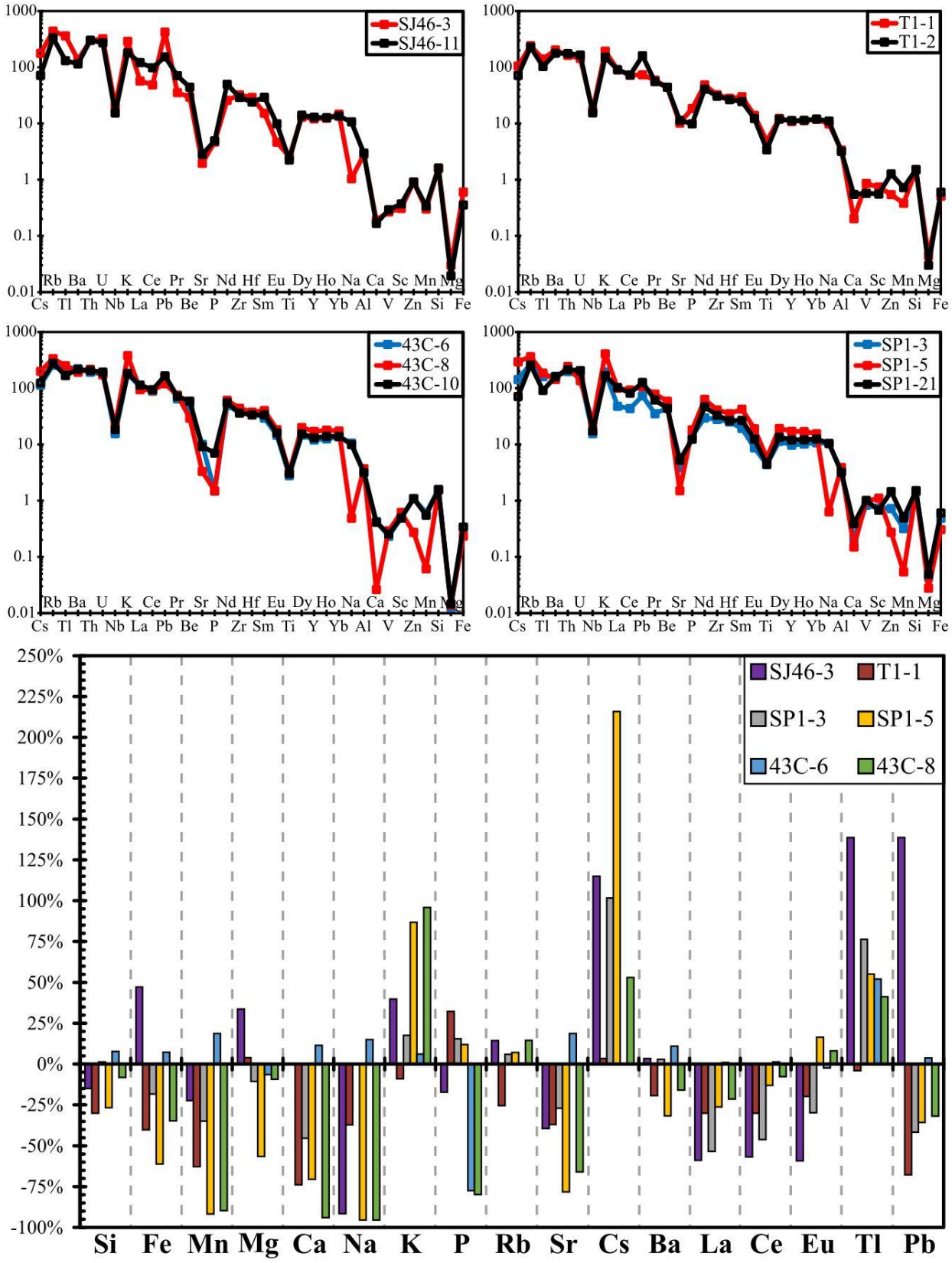

SJ46-3
SJ46-11
T1-1
T1-2
43C-6
43C-8
43C-10
SP1-3
SP1-5
SP1-21
1000
100
10
1
0.1
0.01
Rb Ba U K Ce Pr Sr Nd Hf Eu Dy Ho Na Ca Sc Mn Mg
Cs Tl Th Nb La Pb Be P Zr Sm Ti Y Yb Al V Zn Si Fe
250%
225%
200%
175%
150%
125%
100%
75%
50%
25%
0%
-25%
-50%
-75%
-100%
Si Fe Mn Mg Ca Na K P Rb Sr Cs Ba La Ce Eu Tl Pb

Figure 12. Relative element mobility in altered granitoids (see Table 2 for full data). (Top) Modified spider diagrams with elemental abundances normalized to primitive mantle composition (McDonough & Sun, 1995). Black lines represent least-altered samples; colored lines represent more significantly altered samples. (Bottom) Comparative elemental changes of more-altered rocks relative to least-altered samples, calculated assuming titanium as immobile.

Gray-altered material from the 43-C and T-1 shows a substantial loss of Fe^{3+}/Fe^{T}, while an increase is observed for reddened, weathered-looking material from the 43-C and SP-1. Gray highly-altered material from the Sinclair Louisa M. Jones 46 notably and uniquely shows increased concentrations of Fe^{3+}, Pb, As, and Sb, all of which are compatible in the aforementioned jarosite (Hudson-Edwards, 2019), as well as significant depletion in light rare-earth elements (LREE).

Table 2: Whole-rock analyses of highly-altered vs. less-altered granitoids

Core	Sinclair Louisa M. Jones 46		AMAX T-1		Eagle Picher 43-C Anna Beaver			AMAX SP-1		
Sample	SJ46-3	SJ46-11	T1-1	T1-2	43C-6	43C-8	43C-10	SP1-3	SP1-5	SP1-21
Type	Alt.	Less Alt.	Alt.	Less Alt.	Mod. Alt.	Alt.	Less Alt.	Alt.	Alt.	Less Alt.
Depth (m, MD)	893.4	897.0	430.7	449.9	493.6	494.1	498.7	531.9	532.5	549.1
SiO_2	71.39	73.03	68.11	68.62	71.37	69.31	71.60	68.23	65.14	67.92
TiO_2	0.513	0.447	0.967	0.683	0.558	0.637	0.604	0.875	1.155	0.884
Al_2O_3	12.37	13.09	14.88	14.09	14.32	16.39	14.03	14.80	17.19	14.14
FeO	1.91	1.51	3.47	3.23	2.41	1.95	2.58	2.29	1.45	3.46
Fe_2O_3	3.21	1.48	0.67	1.76	0.30	<0.01	0.15	1.79	1.12	1.51
MnO	0.040	0.045	0.051	0.097	0.081	0.008	0.074	0.043	0.007	0.066
MgO	1.13	0.73	1.67	1.13	0.47	0.52	0.55	1.62	1.05	1.83
CaO	0.67	0.58	0.72	1.93	1.50	0.09	1.45	0.74	0.53	1.36
Na_2O	0.37	3.82	3.51	3.94	3.78	0.17	3.56	3.71	0.23	3.75
K_2O	8.29	5.17	5.57	4.32	5.17	10.88	5.27	5.61	11.77	4.82
P_2O_5	0.10	0.10	0.38	0.20	0.03	0.03	0.14	0.29	0.37	0.25
LOI	4.54	0.83	1.17	0.43	0.54	2.07	0.78	2.16	2.63	1.31
Fe_2O_3 (T)	5.34	3.15	4.53	5.34	2.98	2.17	3.02	4.34	2.73	5.36
$Fe^{3+}/\Sigma Fe$	0.602	0.469	0.149	0.329	0.101	N/A	0.051	0.413	0.41	0.281
Sc	5	6	12	9	8	10	8	12	18	11

Be	2	3	3	3	3	2	4	3	4	3
V	22	24	70	47	19	24	21	68	80	83
Cr	< 20	< 20	< 20	30	< 20	< 20	< 20	30	< 20	30
Co	4	3	8	7	3	2	2	12	7	9
Ni	< 20	< 20	< 20	< 20	< 20	< 20	< 20	< 20	< 20	< 20
Cu	30	10	10	20	< 10	< 10	< 10	< 10	< 10	20
Zn	50	50	30	70	60	< 30	60	40	< 30	80
Ga	16	18	18	19	20	24	20	18	29	19
Ge	1.1	1.2	0.7	1.8	1.4	0.9	1.3	0.8	0.8	1.3
As	85	5	< 5	< 5	< 5	< 5	< 5	< 5	< 5	< 5
Rb	264	201	145	137	155	202	167	164	219	156
Sr	39	56	202	226	201	66	183	76	30	105
Y	52.0	55.6	46.4	48.5	51.8	73.0	56.5	41.7	73.8	51.9
Zr	338	305	340	321	387	463	380	293	432	348
Nb	13.2	10.1	11.3	10.2	10.3	14.3	12.1	10.3	16.1	11.5
Mo	7	< 2	2	< 2	2	< 2	< 2	< 2	5	< 2
Ag	1.4	1.0	0.7	1.2	1.2	1.1	1.0	0.7	0.9	1.1
In	< 0.1	< 0.1	< 0.1	< 0.1	< 0.1	< 0.1	< 0.1	< 0.1	< 0.1	< 0.1
Sn	4	4	2	3	2	2	2	1	3	2
Sb	1.8	< 0.2	< 0.2	0.4	< 0.2	< 0.2	< 0.2	< 0.2	< 0.2	< 0.2
Cs	3.7	1.5	2.2	1.5	2.4	4.2	2.6	3.0	6.2	1.5
Ba	895	754	1338	1169	1468	1272	1431	1076	944	1054
La	37.0	78.3	58.3	58.8	68.8	61.2	73.7	31.0	64.8	67.0
Ce	81.5	164	121	122	148	154	158	73.1	156	137
Pr	9.00	18.0	15.0	14.1	16.4	19.2	18.2	8.97	20.0	15.7
Nd	32.3	62.2	60.7	51.1	62.0	76.3	69.3	37.1	79.1	58.6
Sm	6.15	11.9	12.2	9.91	11.9	16.3	13.6	7.82	17.2	10.9
Eu	0.713	1.52	2.14	1.88	2.24	2.83	2.48	1.34	2.93	1.92
Gd	5.94	10.3	9.92	8.33	10.2	12.6	11.2	7.16	14.3	9.24
Tb	1.26	1.59	1.43	1.36	1.61	2.20	1.77	1.23	2.23	1.51
Dy	8.74	9.46	8.28	8.07	9.92	13.5	10.4	7.64	13.0	9.09
Ho	1.85	1.89	1.68	1.69	1.87	2.68	2.08	1.52	2.52	1.81
Er	5.74	5.77	5.06	4.95	5.63	7.90	6.21	4.59	7.34	5.31
Tm	0.973	0.915	0.751	0.748	0.877	1.18	0.906	0.725	1.04	0.827
Yb	6.44	5.94	5.23	5.29	6.04	7.64	6.14	4.73	6.86	5.50
Lu	1.03	0.933	0.772	0.806	0.960	1.13	0.928	0.728	1.03	0.876
Hf	8.2	6.8	7.9	7.5	10.5	10.6	9.5	7.1	10.0	7.5
Ta	1.44	1.26	1.01	0.92	1.05	1.28	1.25	1.07	1.41	1.05
W	< 0.5	< 0.5	5.4	< 0.5	18.7	< 0.5	1.3	2.3	0.6	< 0.5
Tl	1.26	0.46	0.49	0.36	0.83	0.88	0.59	0.56	0.65	0.32
Pb	63	23	11	24	24	18	25	11	16	19
Bi	0.3	0.2	< 0.1	0.1	0.1	< 0.1	0.2	< 0.1	< 0.1	0.2

Th	23.8	24.0	12.9	13.9	15.3	17.2	16.4	15.8	19.4	17.0
U	7.37	6.24	3.31	3.79	4.09	4.00	4.46	3.62	3.13	4.74

Table 2. Whole-rock analyses of variably-altered granitoid basement rocks. Major element oxide abundances have been recalculated to 100% (volatile-free). Major element oxides and volatiles listed as weight percent, trace elements listed as parts per million. Components not detected are listed as less than detection limit.

ANALYSIS AND DISCUSSION

Mineralized fractures appear to be ubiquitous in the basement rocks of northeastern Oklahoma, with abundant evidence for multiple generations of fracturing and mineralization. A variety of origins are possible, given the age of the rock and what is known of the tectonic history. Some, particularly the epidote-bearing fractures, are likely nearly as old as the rock – for instance, the presence of saussuritized plagioclase (present in several intervals of the Amoco SHADS 4, and at least partially associated with fractures) is usually attributed to greenschist-facies hydrothermal activity, with temperatures approaching or in excess of 300 °C (Shelley, 1993); similar temperatures have been invoked for the transformation of biotite to chlorite (Eggleton and Banfield, 1985), which is present in basement rock throughout the region (Denison, 1981). Such temperatures are in substantial excess of those indicated by diagenetic studies from the area's Phanerozoic sediments; they are therefore likely Precambrian, possibly coinciding with the Rb-Sr ages obtained by Denison (1981).

Most of the various secondary minerals found in the fractures have sufficiently large stability fields that they cannot be directly related to a specific event or set of conditions, and their ages remain unconstrained. Several of them (e.g., feldspars, carbonates, clays, jarosite, pyrite, and xenotime) could potentially be dated using modern radiometric methods, which may yield very interesting results but was beyond the scope of this study. In general, feldspars and epidote seem to be the earliest minerals, followed by chlorite, followed by carbonate and pyrite. Quartz appears in both early and late events. Jarosite is most commonly associated with near-

surface weathering under quite acidic conditions (e.g., Dutrizac and Jambor, 2000). Synchysite has been associated with albitization of basement unconformities by surface weathering and/or exposure to evaporative brines (e.g., Fàbrega et al., 2019); whether this would be of Precambrian age or a result of early Paleozoic exposure and/or interaction with dolomitizing brines is unknown. The variety in geochemical changes indicates alteration was quite heterogeneous, and overprinting of alteration styles within individual cores suggests multiple events. Some localities are likely at least partially influenced by paleoweathering, as suggested by some previous workers (e.g., Tolman and Landes, 1939; Chenoweth, 1968) and consistent with the appearance of altered rock near the unconformity and feldspar dissolution near some fractures in this study (Fig. 11).

The abundance of steeply-dipping (70°-90°) fractures is a major point of interest, as such should have a relatively low chance of being encountered in core unless they are quite abundant. They appear in nearly every core inspected (many < 4 cm in diameter), indicating the upper basement is highly fractured. These fractures are still common well over 100 meters below the top of basement in the SHADS 4 (Fig. 5), in sharp contrast with the common assumption that the upper basement is intact, impermeable crystalline rock.

Instead, the observations from northeastern Oklahoma have more in common with more intensively-studied fractured basement terrains. For instance, abundant subvertical to vertical jointing is prominent in exposed granitic Lewisian basement (e.g., McCaffrey et al., 2020), and the relative paragenesis of fracture mineralogy (early chlorite, epidote, feldspars and quartz followed by late carbonate, clays, pyrite and quartz) is similar to that observed in fractures both from exposed and subsurface Lewisian basement (Holdsworth et al., 2020; McCaffrey et al., 2020). Fissure-fill sediments, cockade breccias and injectites of frictional melt are also

recognized in fractured basement from the Rona Ridge and Lancaster hydrocarbon fields (Holdsworth et al., 2019, 2020). Fractures and dissolution porosity from likely paleoweathering have also been shown to result in quite permeable basement rock in the Norwegian North Sea (Riber et al., 2015).

Data from those localities suggest that cemented fractures and faults near the basement unconformity may prop open fractures and faults at greater depth and allow them to act as conduits and traps for hydrocarbons moving up along faults from source rocks (Holdsworth et al., 2020). In northern and central Oklahoma such structures would likely instead act as conduits for downward transmission of fluid pressure changes, recently implicated as the dominant mechanism of earthquake triggering in the area (Zhai et al., 2019). Injected wastewater itself could potentially be transmitted as well, as the most common rocks to be faulted against basement are those of the Arbuckle Group carbonates (which are often underpressured) and disposal wells commonly penetrate up to ~20 meters of basement.

The ubiquity with which fractures and hydrothermal alteration are found also has implications for the mechanical behavior of faults. Observed fractures and faults are typically mineralized, usually by calcite or dolomite with variable amounts of chlorite and epidote and minor amounts of other minerals. Chlorite and other phyllosilicates undergo approximately a 50% reduction in the coefficient of friction when wet, and chlorite is also susceptible to hydrous diagenetic alteration to other phyllosilicate minerals (Haines and van der Pluijm, 2012); such alteration has been observed in two cores in the present study (Fig. 8F). Phyllosilicates commonly exhibit velocity-strengthening frictional behavior, promoting aseismic creeping rather than earthquake nucleation (Haines and van der Pluijm, 2012), which is consistent with inferred aseismic slip preceding the 2016 Mw 5.8 Pawnee earthquake (Chen et al., 2017). Deformation

lamellae, also considered a sign of creeping rather than dynamic deformation (e.g., Vernooij and Langerhorst, 2005), are observed in quartz veins of the Texaco Kohpay L 16-WS (Hamilton et al., 2020b).

In contrast, carbonate-rich fault rocks tend to recover strength quickly and are more prone to unstable stick-slip behavior (e.g., Carpenter et al., 2016), and carbonate-cemented fractures are found in all cores inspected with more than a meter of available material. Several of these (examples in Figs. 7-10) are also associated with slip. Additionally, recent experimental results from variably-altered Oklahoma basement rocks (including cores in this study) under in-situ P-T conditions have demonstrated that more extensive hydrothermal alteration correlates with shallower transitions to frictionally unstable behavior, with those transitions in altered rocks occurring at simulated depth ranges similar to those of most northern Oklahoma earthquakes (Kolawole et al., 2019). The observations of Denison (1981) as well as those in this study indicate that unaltered rocks are vanishingly rare to absent in the study area. Instead, they exhibit features consistent with early high-temperature hydrothermal activity as well as later, likely lower-temperature hydrothermal alteration.

SUMMARY

Hydrothermal alteration and mineralized fractures are ubiquitous in the northeastern Oklahoma basement. Many of these fractures host multiple generations of minerals, with early silicates followed by carbonate and occasionally pyrite. Near-vertical fractures are present in virtually every core from the area, suggesting a high fracture density. In the only core with a large recovered interval, fracture density remains high well over 100 meters below the basement unconformity – in fact, fracture abundance seems to increase at depth, even below the interval with abundant younger subhorizontal calcite veins.

The rocks present in cores from the upper igneous basement in this area are not consistent with the common assumption of intact, unaltered basement. Instead, they show evidence of high-temperature (possibly very early) alteration as well as lower-temperature hydrothermal events and additional influence from early Paleozoic weathering. The fractures, secondary mineralogy and slip structures, including injectite in the T-1, are instead far more similar to those encountered in fractured basement hydrocarbon plays. While the vast majority of fractures observed in northeastern Oklahoma basement cores are sealed by secondary minerals, comparable structures from the Lancaster and Rona Ridge areas have been shown to result in enhanced porosity and permeability at greater depth.

Further study is required in order to determine how well such a model applies in the study area. This study is admittedly limited – currently, only a small number of cores are available, and these are unoriented and typically quite short. This makes it very difficult to obtain statistically meaningful data, or to compare to the structural trends observed through remote-sensing or geophysical techniques. In the absence of a scientific drilling program, however, the core samples from this area represent the closest available analog to basement rocks and faults affected by induced seismicity in Oklahoma and much of the U.S. midcontinent.

REFERENCES

Adams, D.C. and Keller, G.R., 1994. Possible extension of the Midcontinent Rift in west Texas and eastern New Mexico. Canadian Journal of Earth Sciences, 31(4), pp.709-720. https://doi.org/10.1139/e94-063

Barbour, A.J., Norbeck, J.H. and Rubinstein, J.L., 2017. The effects of varying injection rates in Osage County, Oklahoma, on the 2016 Mw 5.8 Pawnee earthquake. Seismological Research Letters, 88(4), pp.1040-1053. https://doi.org/10.1785/0220170003

Barosh, P.J., 1992. Neotectonic framework of the United States. In Basement Tectonics 7 (pp. 277-288). Springer, Dordrecht. https://doi.org/10.1007/978-94-017-0833-3_19

Berendsen, P. and Blair, K.P., 1991. Interpretive Subcrop Map of the Precambrian Basement in the Joplin 1° x2° Quadrangle. Kansas Geological Survey Subsurface Geology Series 14.

Bickford, M.E., Van Schmus, W.R., Karlstrom, K.E., Mueller, P.A. and Kamenov, G.D., 2015. Mesoproterozoic-trans-Laurentian magmatism: A synthesis of continent-wide age distributions, new SIMS U–Pb ages, zircon saturation temperatures, and Hf and Nd isotopic compositions. Precambrian Research, 265, pp.286-312. https://doi.org/10.1016/j.precamres.2014.11.024

Burkhard, M., 1993. Calcite twins, their geometry, appearance and significance as stress-strain markers and indicators of tectonic regime: A review. Journal of Structural Geology, 15(3-5), pp.351-368. https://doi.org/10.1016/0191-8141(93)90132-T

Callahan, O.A., Eichhubl, P., Olson, J.E. and Davatzes, N.C., 2019. Fracture mechanical properties of damaged and hydrothermally altered rocks, Dixie Valley-Stillwater fault zone, Nevada, USA. Journal of Geophysical Research: Solid Earth, 124(4), pp.4069-4090. https://doi.org/10.1029/2018JB016708

Campbell, J.A. and Weber, J.L., 2006, Wells Drilled to Basement in Oklahoma. Oklahoma Geological Survey Special Publication 2006-1.

Carpenter, B.M., Ikari, M.J. and Marone, C., 2016. Laboratory observations of time-dependent frictional strengthening and stress relaxation in natural and synthetic fault gouges. Journal of Geophysical Research: Solid Earth, 121(2), pp.1183-1201. https://doi.org/10.1002/2015JB012136

Chen, X., Nakata, N., Pennington, C., Haffener, J., Chang, J.C., He, X., Zhan, Z., Ni, S. and Walter, J.I., 2017. The Pawnee earthquake as a result of the interplay among injection, faults and foreshocks. Scientific Reports, 7(1), 4945, pp.1-18. https://doi.org/10.1038/s41598-017-04992-z

Chenoweth, P.A., 1968. Early Paleozoic (Arbuckle) overlap, southern mid-continent, United States. AAPG Bulletin, 52(9), pp.1670-1688. https://doi.org/10.1306/5D25C4C7-16C1-11D7-8645000102C1865D

Cox, R.T., 2009. Ouachita, Appalachian, and Ancestral Rockies deformations recorded in mesoscale structures on the foreland Ozark plateaus. Tectonophysics, 474(3-4), pp.674-683. https://doi.org/10.1016/j.tecto.2009.05.005

Denison, R.E., 1966. Basement rocks in adjoining parts of Oklahoma, Kansas, Missouri, and Arkansas. (Ph.D. dissertation) University of Texas at Austin.

Denison, R.E., 1981. Basement rocks in northeastern Oklahoma. Oklahoma Geological Survey Circular, 84.

Denison, R.E., Lidiak, E.G., Bickford, M.E. and Kisvarsanyi, E.B., 1984. Geology and geochronology of Precambrian rocks in the Central Interior region of the United States. U.S. Geological Survey Professional Paper No. 1241-C. https://doi.org/10.3133/pp1241C

Denison, R.E., 1995. Significance of air-photograph linears in the basement rocks of the Arbuckle Mountains. Oklahoma Geological Survey Circular 97, pp.119-131.

Derby, J.R., Hinch, H.H. and Repetski, J.R., 1991. Lithology, stratigraphy, and age of the Arbuckle Group in the Amoco SHADS No. 4, a continuous core from grassroots into basement, Rogers County, Oklahoma. Oklahoma Geological Survey Special Publication 91-3, pp.69-82.

Dutrizac, J.E. and Jambor, J.L., 2000. Jarosites and their application in hydrometallurgy. Reviews in Mineralogy and Geochemistry, 40(1), pp.405-452. https://doi.org/10.2138/rmg.2000.40.8

Eggleton, R.A. and Banfield, J.F., 1985. The alteration of granitic biotite to chlorite. American Mineralogist, 70(9-10), pp.902-910.

Ellsworth, W.L., 2013. Injection-induced earthquakes. Science, 341(6142). https://doi.org/10.1126/science.1225942

Fàbrega, C., Parcerisa, D., Thiry, M., Franke, C., Gurenko, A., Gòmez-Gras, D., Solé, J. and Travé, A., 2019. Permian–Triassic red-stained albitized profiles in the granitic basement of NE Spain: evidence for deep alteration related to the Triassic palaeosurface. International journal of earth sciences, 108(7), pp.2325-2347. https://doi.org/10.1007/s00531-019-01764-0

Frenzel, M. and Woodcock, N.H., 2014. Cockade breccia: product of mineralisation along dilational faults. Journal of Structural Geology, 68, pp.194-206. https://doi.org/10.1016/j.jsg.2014.09.001

Friess, J.P., 2005. The southern terminus of the Nemaha tectonic zone, Garvin County, Oklahoma. Oklahoma City Geological Society Shale Shaker, 56, pp.55-67.

Haines, S.H. and van der Pluijm, B.A., 2012. Patterns of mineral transformations in clay gouge, with examples from low-angle normal fault rocks in the western USA. Journal of Structural Geology, 43, pp.2-32. https://doi.org/10.1016/j.jsg.2012.05.004

Hamilton, M., Weaver, B.L. and Elmore, R.D., 2020a. Mesoproterozoic magmatism in northeastern Oklahoma: Petrogenetic constraints from trace-element geochemistry.

Geological Society of America Abstracts with Programs, 52(1). https://doi.org/10.1130/abs/2020SC-343743

Hamilton, M., Weaver, B.L. and Elmore, R.D., 2020b. The Texaco Kohpay L 16-WS: The Osage Microgranite Revisited. Oklahoma City Geological Society Shale Shaker, 71(3), pp.108-125.

Holdsworth, R.E., McCaffrey, K.J.W., Dempsey, E., Roberts, N.M.W., Hardman, K., Morton, A., Feely, M., Hunt, J., Conway, A. and Robertson, A., 2019. Natural fracture propping and earthquake-induced oil migration in fractured basement reservoirs. Geology, 47(8), pp.700-704. https://doi.org/10.1130/G46280.1

Holdsworth, R.E., Trice, R., Hardman, K., McCaffrey, K.J.W., Morton, A., Frei, D., Dempsey, E., Bird, A. and Rogers, S., 2020. The nature and age of basement host rocks and fissure fills in the Lancaster field fractured reservoir, West of Shetland. Journal of the Geological Society, 177(5), pp.1057-1073. https://doi.org/10.1144/jgs2019-142

Hudson-Edwards, K.A., 2019. Uptake and release of arsenic and antimony in alunite-jarosite and beudantite group minerals. American Mineralogist: Journal of Earth and Planetary Materials, 104(5), pp.633-640. https://doi.org/10.2138/am-2019-6591

Huffman, G.G., 1958, Geology of the flanks of the Ozark uplift, northeastern Oklahoma. Oklahoma Geological Survey Bulletin 77.

Ireland, H.A., 1930. Oil and gas in Oklahoma: Mayes, Ottawa, and Delaware Counties. Oklahoma Geological Survey Bulletin 40-NN.

Ireland, H.A., 1955. Pre-Cambrian surface in northeastern Oklahoma and parts of adjacent states. AAPG Bulletin, 39(4), pp.468-483. https://doi.org/10.1306/5CEAE163-16BB-11D7-8645000102C1865D

Keranen, K.M., Savage, H.M., Abers, G.A. and Cochran, E.S., 2013. Potentially induced earthquakes in Oklahoma, USA: Links between wastewater injection and the 2011 Mw 5.7 earthquake sequence. Geology, 41(6), pp.699-702. https://doi.org/10.1130/G34045.1

Keranen, K.M., Weingarten, M., Abers, G.A., Bekins, B.A. and Ge, S., 2014. Sharp increase in central Oklahoma seismicity since 2008 induced by massive wastewater injection. Science, 345(6195), pp.448-451. https://doi.org/10.1126/science.1255802

Kolawole, F., 2020. The roles of structural inheritance in areas of induced seismicity and active tectonics. (Ph.D. Dissertation) University of Oklahoma.

Kolawole, F., Johnston, C.S., Morgan, C.B., Chang, J.C., Marfurt, K.J., Lockner, D.A., Reches, Z. and Carpenter, B.M., 2019. The susceptibility of Oklahoma's basement to seismic reactivation. Nature Geoscience, 12(10), pp.839-844. https://doi.org/10.1038/s41561-019-0440-5

Labusch, L., 2016. Linear Trend Analysis: Implications for a Structural Fracture System and Applications of Subsurface Fluid Migration, Northwest Arkansas and Eastern Oklahoma. (M.Sc. Thesis) University of Arkansas.

Lander, R.H. and Laubach, S.E., 2015. Insights into rates of fracture growth and sealing from a model for quartz cementation in fractured sandstones. Geological Society of America Bulletin, 127(3-4), pp.516-538. https://doi.org/10.1130/B31092.1

Laubach, S.E., Lander, R.H., Criscenti, L.J., Anovitz, L.M., Urai, J.L., Pollyea, R.M., Hooker, J.N., Narr, W., Evans, M.A., Kerisit, S.N., Olson, J.E., Dewers, T., Fisher, D., Bodnar, R., Evans, B., Dove, P., Bonnell, L.M., Marder, M.P. and Pyrak-Nolte, L. 2019. The role of chemistry in fracture pattern development and opportunities to advance interpretations

of geological materials. Reviews of Geophysics, 57(3), pp.1065-1111. https://doi.org/10.1029/2019RG000671

Le Bas, M.L., Le Maitre, R.W., Streckeisen, A. and Zanettin, B., 1986. A chemical classification of volcanic rocks based on the total alkali-silica diagram. Journal of Petrology, 27(3), pp.745-750. https://doi.org/10.1093/petrology/27.3.745

Lidiak, E.G., 1996. Geochemistry of subsurface Proterozoic rocks in the eastern midcontinent of the United States: Further evidence for a within-plate tectonic setting. Geological Society of America Special Paper 308, pp.45-66. https://doi.org/10.1130/0-8137-2308-6.45

Marsh, S. and Holland, A.A., 2016. Comprehensive fault database and interpretive fault map of Oklahoma. Oklahoma Geological Survey Open-File Report OF2-2016.

McCaffrey, K.J.W., Holdsworth, R.E., Pless, J., Franklin, B.S.G. and Hardman, K., 2020. Basement reservoir plumbing: fracture aperture, length and topology analysis of the Lewisian Complex, NW Scotland. Journal of the Geological Society, 177(6), pp.1281-1293. https://doi.org/10.1144/jgs2019-143

McCracken, M.H., 1964. The Cambro-Ordovician rocks of northeastern Oklahoma and adjacent areas. Tulsa Geological Society Digest, 32, pp.49-75.

McDonough, W.F. and Sun, S.S., 1995. The composition of the Earth. Chemical Geology, 120(3-4), pp.223-253. https://doi.org/10.1016/0009-2541(94)00140-4

McNamara, D.E., Benz, H.M., Herrmann, R.B., Bergman, E.A., Earle, P., Holland, A., Baldwin, R. and Gassner, A., 2015. Earthquake hypocenters and focal mechanisms in central Oklahoma reveal a complex system of reactivated subsurface strike-slip faulting. Geophysical Research Letters, 42(8), pp.2742-2749. https://doi.org/10.1002/2014GL062730

Northcutt, R.A. and Campbell, J.A., 1995. Geologic provinces of Oklahoma. Oklahoma Geological Survey Open File Report OF5-95.

Pollyea, R.M., Chapman, M.C., Jayne, R.S. and Wu, H., 2019. High density oilfield wastewater disposal causes deeper, stronger, and more persistent earthquakes. Nature Communications, 10(1), e3077. https://doi.org/10.1038/s41467-019-1102

Riber, L., Dypvik, H. and Sørlie, R., 2015. Altered basement rocks on the Utsira High and its surroundings, Norwegian North Sea. Norwegian Journal of Geology, 95(1), pp.57-89. http://dx.doi.org/10.17850/njg95-1-04

Rottmann, K., 2018. Well-log characterization of the Arbuckle Group in central and northern Oklahoma: Interpretation of the impact of its depositional and post-depositional history on injection induced seismicity. Oklahoma Geological Survey Open File Report OF21-2018.

Rowe, C.D., Kirkpatrick, J.D. and Brodsky, E.E., 2012. Fault rock injections record paleo-earthquakes. Earth and Planetary Science Letters, 335, pp.154-166. https://doi.org/10.1016/j.epsl.2012.04.015

Rowe, C.D. and Griffith, W.A., 2015. Do faults preserve a record of seismic slip: A second opinion. Journal of Structural Geology, 78, pp.1-26. https://dx.doi.org/10.1016/j.jsg.2015.06.006

Schoenball, M. and Ellsworth, W.L., 2017. Waveform-relocated earthquake catalog for Oklahoma and southern Kansas illuminates the regional fault network. Seismological Research Letters, 88(5), pp.1252-1258. https://doi.org/10.1785/0220170083

Schoenball, M., Walsh, F.R., Weingarten, M. and Ellsworth, W.L., 2018. How faults wake up: the Guthrie-Langston, Oklahoma earthquakes. The Leading Edge, 37(2), pp.100-106. https://doi.org/10.1190/tle37020100.1

Shah, A.K. and Keller, G.R., 2017. Geologic influence on induced seismicity: Constraints from potential field data in Oklahoma. Geophysical Research Letters, 44(1), pp.152-161. https://doi.org/10.1002/2016GL071808

Shah, A.K. and Crain, K., 2018. Aeromagnetic data reveal potential seismogenic basement faults in the induced seismicity setting of Oklahoma. Geophysical Research Letters, 45(12), pp.5948-5958. https://doi.org/10.1029/2018GL077768

Shelley, D., 1993. Igneous and Metamorphic Rocks under the Microscope: Classification, Textures, Microstructures and Mineral Preferred-Orientation. Chapman & Hall, London.

Streckeisen, A., 1976. To each plutonic rock its proper name. Earth-science reviews, 12(1), pp.1-33. https://doi.org/10.1016/0012-8252(76)90052-0

Streckeisen, A., 1979. Classification and nomenclature of volcanic rocks, lamprophyres, carbonatites, and melilitic rocks: Recommendations and suggestions of the IUGS Subcommission on the Systematics of Igneous Rocks. Geology, 7(7), pp.331-335. https://doi.org/10.1130/0091-7613(1979)<3C331:CANOVR>2.0.CO;2

Thomas, W.A., 2011. The Iapetan rifted margin of southern Laurentia. Geosphere, 7(1), pp.97-120. https://doi.org/10.1130/GES00574.1

Tolman, C. and Landes, K.K., 1939. Igneous Rocks of the Mississippi Valley Lead-Zinc Districts. Geological Society of America Special Paper 24, pp.71-104. https://doi.org/10.1130/SPE24-p71

Van Schmus, W.R., Bickford, M.E. and Turek, A., 1996. Proterozoic geology of the east-central Midcontinent basement. Geological Society of America Special Paper, 308, pp.7–32. https://doi.org/10.1130/0-8137-2308-6.7

Vernooij, M.G.C. and Langenhorst, F., 2005. Experimental reproduction of tectonic deformation lamellae in quartz and comparison to shock-induced planar deformation features. Meteoritics & Planetary Science, 40(9-10), pp.1353-1361. https://doi.org/10.1111/j.1945-5100.2005.tb00406.x

Zhai, G., Shirzaei, M., Manga, M. and Chen, X., 2019. Pore-pressure diffusion, enhanced by poroelastic stresses, controls induced seismicity in Oklahoma. Proceedings of the National Academy of Sciences, 116(33), pp.16228-16233. https://doi.org/10.1073/pnas.1819225116

CHAPTER 4

MAGNETIC CHARACTERISTICS OF ROCKS WITH STRONGLY NEGATIVE FIELD-DEPENDENCE OF SUSCEPTIBILITY FROM THE BASEMENT-COVER INTERFACE OF NORTHEASTERN OKLAHOMA

ABSTRACT

Some rock and soil samples exhibit significant loss of magnetic susceptibility (χ) with increasing applied field even at relatively low (100s of A/m) fields, a behavior which remains unexplained. This study documents exceptionally strong negative field-dependence (χ_{HD}) in sandstones and altered granitoids in several cores from the northeastern Oklahoma subsurface. These same rocks also show elevated frequency-dependence of susceptibility (χFD), with reasonable correlation of χ_{HD} to χ_{FD}, and χ_{HD} itself is frequency-dependent. Using multiple characterization methods, it is shown that strongly negative χ_{HD} in these rocks is linked to a yet-unidentified phase which approaches magnetic saturation in low fields (<1 mT), shows elevated χ_{FD} to very low temperatures, is unstable at high T, and becomes paramagnetic above ~83 °C. Efforts to identify this mineral continue, and clear associations with fluid alteration features indicate that it may be highly relevant to rock alteration, diagenetic, and environmental studies.

INTRODUCTION

The magnetic susceptibility (*k* if volume-normalized, or χ if mass-normalized) of rocks and soils is commonly measured using low-field (tens to hundreds of A/m) alternating current (AC) instruments which operate at frequencies of several hundred to several thousand Hz. While the susceptibilities of diamagnetic and paramagnetic materials are in phase with and independent of the applied AC field, the measured susceptibilities of ferromagnetic *sensu lato* materials may

vary significantly depending on the amplitude and frequency of the measuring field (e.g., Worm 1991, 1998). They may additionally have a susceptibility component that is out of phase with the measuring field (sometimes referred to as out-of-phase, imaginary, or quadrature susceptibility) which is also typically dependent on frequency and/or field strength (Jackson, 2004). Variations of in-phase and out-of-phase susceptibility with changes in frequency and amplitude may provide information on the composition and grain size of the ferromagnetic *s.l.* mineral fraction in natural materials.

The magnetization (M) of diamagnetic, paramagnetic, and (at sufficiently low fields) ferromagnetic *s.l.* materials follows the linear relationship $M = kH$, where k is susceptibility and H is the applied field. For some ferromagnetic *s.l.* minerals, the magnetization is linear (and therefore susceptibility is constant) within the range of field strengths commonly used for measurements. For others, particularly those of multidomain grain size, the magnetization follows the Rayleigh Law $M = k_i H + \alpha H^2$, where k_i is the initial susceptibility, and α is the Rayleigh coefficient (e.g., Hrouda et al., 2006). The magnetic susceptibility is then dependent on the field: $K = \frac{dM}{dH} = k_i + 2\alpha H$, where $\alpha \geq 0$. Measurements at varying fields have shown substantial field-dependent increases in magnetic susceptibilities of geological materials including pyrrhotite (Worm, 1991), titanomagnetite (Jackson et al., 1998), and hematite (Hrouda, 2002; Guerrero-Suarez and Martín-Hernández, 2012), though these do not always follow the linear Rayleigh relation. Consequently, field-dependent variation of susceptibility has found application in rocks as an indicator of magnetic mineralogy (Hrouda et al., 2006). Some environmental and geological materials however exhibit a *negative* field-dependence, i.e. a decrease in susceptibility with increasing applied field (e.g., Hrouda et al., 2006; Chlupáčová et al., 2010). At high fields (tens of thousands of A/m or higher) this behavior results from the

saturation of known ferromagnetic *s.l.* minerals (Borradaile et al., 2008) but its presence at low fields (tens to hundreds of A/m) has not been explained to date. Preliminary models of field-dependent superparamagnetic behavior of magnetite only allow for less than one percent decrease in χ over a field range up to 700 A/m (Hamilton et al., 2019).

This report documents significant negative field-dependence of susceptibility (χ_{HD}) in specimens from the lowermost clastic sediments and uppermost igneous "basement" rocks in the subsurface of northeastern Oklahoma. Preliminary study of the subsurface nonconformity between Mesoproterozoic trachyte and (presumably) Cambrian sandstone in a drill core found that the sandstone and uppermost trachyte near the unconformity lose a significant amount (up to ~10%) of their susceptibility as the measuring field strength is increased from 5 to 700 A/m (Hamilton et al., 2018). The same samples also lose significant susceptibility (some over 14%) at higher frequency (from 976 to 15616 Hz), and there is reasonable correlation between the magnitudes of frequency-dependence (χ_{FD}) and negative field-dependence (Fig. 1).

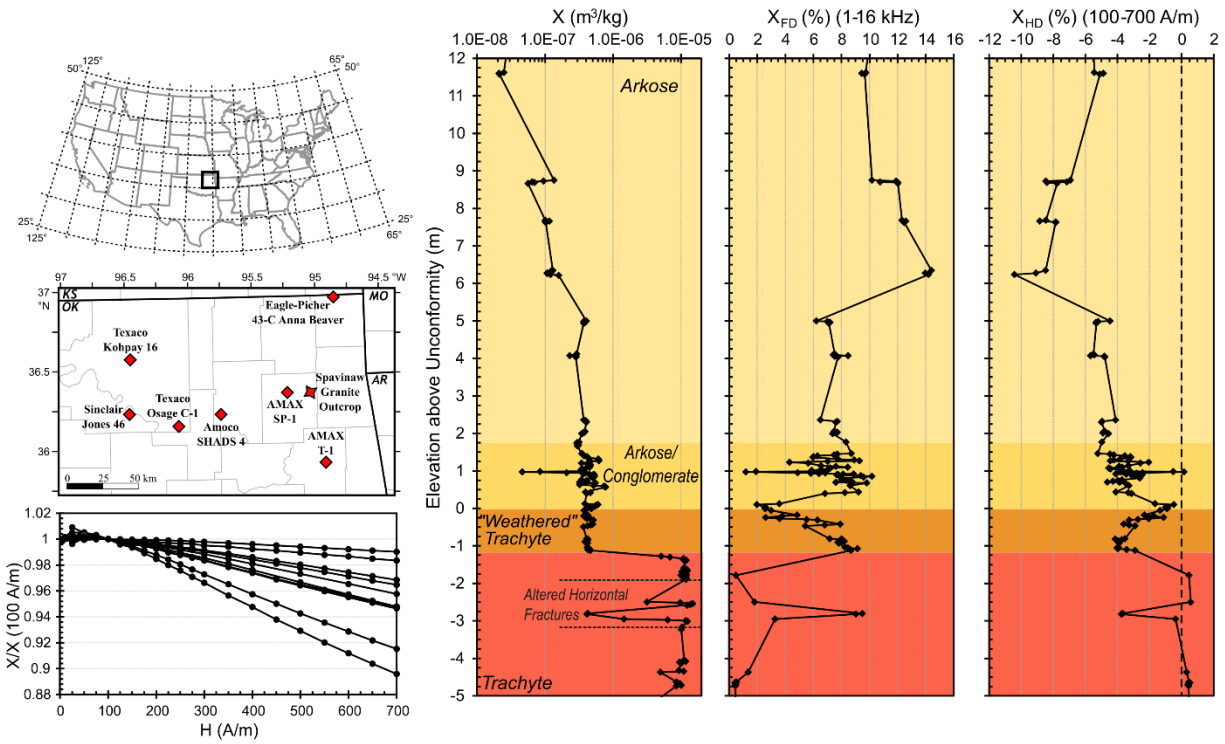


Figure 1.(Left, top and middle) Location of general study area and individual cores. (Left, bottom) Representative plots of susceptibility vs. field for samples near the basement unconformity of the Amoco SHADS 4, normalized to the value at 100 A/m. (Right) Depth profiles of susceptibility, its frequency-dependence and field-dependence across the unconformity of the SHADS 4 (after Hamilton et al., 2018).

Samples from several other subsurface cores in northeastern Oklahoma exhibit similar behavior, indicating that this phenomenon is widespread along the unconformity between Mesoproterozoic igneous basement and overlying Cambro-Ordovician sediments in this area. Elevated χ_{FD} and moderately negative χ_{HD} (~ -2%) are also found alongside altered fractures and fault breccia as much as 100 meters below the basement unconformity in the SHADS 4. These associations suggest that the phenomenon has its origins in some sort of fluid alteration. The upper igneous rocks of this area virtually all show evidence of fluid alteration, particularly near the unconformity (Denison, 1981; Hamilton et al., 2021). Likewise, the materials reported to show negative χ_{HD} in previous studies (e.g., Hrouda et al., 2006; Chlupáčová et al., 2010) are also mostly those which are commonly associated with or highly prone to fluid alteration (e.g.,

peralkaline igneous rocks) or are by definition extensively altered (e.g., soils and keratophyres). In addition to being an outstanding problem in rock magnetism, the origin of negative χ_{HD} in geological materials may therefore also have major implications for chemical conditions of weathering, diagenesis and basement rock alteration.

MATERIALS AND GEOLOGICAL CONTEXT

Rock specimens in this study come from seven subsurface cores of the upper igneous basement and immediately overlying sediments in northeastern Oklahoma (Fig. 1), all of which are owned and housed by the Oklahoma Geological Survey at the Oklahoma Petroleum Information Center (OPIC).

The igneous rocks of this area are comprised of mostly granites and rhyolites which consistently have U-Pb zircon ages of approximately 1,370 Ma (Bickford et al., 2015). Rb-Sr age determinations range from 50 to nearly 200 million years younger than the zircon dates (*Denison*, 1981), indicating some degree of alteration. Clastic sediments (where present) typically lack fossils suitable for biostratigraphy and are therefore of uncertain age; they consist mainly of medium to coarse arkosic sandstones which appear to be derived from the underlying basement, are overlain by early Ordovician carbonates and are generally assumed to be of upper Cambrian age (e.g., McCracken, 1964; Derby et al., 1991).

Igneous rocks in this study are mostly pink to red in appearance, though in some intervals secondary alteration has turned them a gray color. Chlorite is common, and traces of pyrite and/or jarosite have been found in some thin sections (Hamilton et al., 2021). Sedimentary samples are mostly yellowish, gray, or white arkosic sandstones with variable amounts of clay minerals and pyrite. The northeasternmost part of the study area lies within the Tri-State Mineral District, which was exploited for lead and zinc sulfides in the early 20th century. While some of

the cores were drilled by mining exploration companies prospecting for subsurface ores, none contain substantial metal mineralization beyond minor intervals with up to a few percent pyrite. Other cores come from oil and gas wells drilled a fair distance from the mineral district.

METHODS

Room-temperature bulk magnetic susceptibility measurements were made using an AGICO MFK1 Kappabridge; a subset of samples was also measured using the newer MFK2. Field-dependence was measured at a frequency of 976 Hz and peak fields ranging from 5-10 A/m to 700 A/m with a fixed measuring range (sensitivity setting). Field-dependence values are reported as $X_{HD}[\%] = 100 * \left(\frac{X_{Hmax} - X_{Hmin}}{X_{Hmin}}\right)$ with H_{max} = 700 A/m and H_{min} = 100 A/m, as measurements using field amplitudes below 100 A/m sometimes show increased uncertainty. Frequency-dependence was measured using a peak applied field of 200 A/m at frequencies of 976 (f_{min}) and 15616 Hz (f_{max}); values are reported as $X_{FD}[\%] = 100 * \left(\frac{X_{fmin} - X_{fmax}}{X_{fmin}}\right)$ and the normalized frequency-dependence parameter $X_{FN}[\%] = \frac{X_{FD}}{\ln\left({}^{fmax}/_{fmin}\right)}$ (after Hrouda, 2011). Specimen orientation was consistent between frequency-dependent and field-dependent measurements in order to minimize complications from anisotropy. The phase angle ($\delta = tan^{-1}\left[{}^{X_{In-phase}}/_{X_{out-of-phase}}\right]$) at 976 Hz was corrected using regular measurements of a calibration standard (after Hrouda et al., 2015) to calculate out-of-phase susceptibility.

Additional measurements were made using instruments at the Institute for Rock Magnetism (IRM) at the University of Minnesota. High-temperature susceptibility was measured using a Geofyzika KLY-2 Kappabridge at an applied field of 300 A/m and measuring frequency of 920 Hz; data were corrected assuming a constant furnace value and analyzed using in-house IRM software. Princeton Measurements and Lake Shore 8600 vibrating sample magnetometers

(VSMs) were utilized for hysteresis and backfield remanence measurements; hysteresis data processing utilized IRM software and nonlinear high-field fits were used for the paramagnetic slope corrections (Jackson and Sølheid, 2010). Quantum Design Magnetic Property Measurement Systems (MPMS) were used for remanence and AC susceptibility measurements at temperatures from 10 to 300 Kelvin (MPMS-5S) and from 10 to 400 K (MPMS-XL, MPMS3). Remanence measurements were made for three low-T thermomagnetic protocols: on cooling and re-warming after application of a 2.5 Tesla room-temperature saturation isothermal remanent magnetization (RT-SIRM); on warming after cooling in a constant 2.5 T field (field-cooling, FC); and on warming after zero-field cooling (ZFC) followed by a 2.5 T SIRM at low temperatures. Susceptibility measurements were made at several frequencies and a field strength of 3 Oe (238.7 A/m) with the MPMS-5S and MPMS-XL; the MPMS3 used field amplitudes from 1 to 9 Oe (79.6 to 716.2 A/m).

RESULTS

Room-Temperature Bulk Susceptibility

Samples of clastic sediments and uppermost igneous rocks consistently show negative χ_{HD} values, some nearly as low as -15% from 100 to 700 A/m. This decrease is essentially linear above 100 A/m in most samples (Fig. 1), and is sometimes apparent below 20 A/m. Values of χ_{FD} are of comparable to slightly higher magnitude, reaching nearly 16% (χ_{FN} = 5.75%). Comparison of χ_{FD} and χ_{HD} for samples from all seven cores indicates a reasonable correlation ($R^2 \approx 0.7$, Fig. 2a). Additionally, χ_{HD} and χ_{FD} are not independent – measurements of field-dependence at multiple frequencies indicate that χ_{HD} has lower magnitudes at higher *f* (Fig. 2b). Comparison of the normalized frequency-dependence parameter χ_{FN} with the out-of-phase parameter χ_{ON} ($X_{ON} = \frac{200}{\pi} tan\delta_{fmin}$) yields a strong correlation ($R^2 \approx 0.97$) with a slope near 1

and intercept near zero (Fig. 2c), indicating that the vast majority of the out-of-phase component is due to viscous relaxation effects of very fine magnetic particles (Hrouda et al., 2013).

The overall correlation between χ_{FD} and χ_{HD} for the area is skewed by data from the Amoco SHADS 4, which accounts for the overwhelming majority of specimens measured. However, each location appears to have a reasonable correlation when inspected on its own (Fig. 2d-f). The worst correlation is from the Sinclair Louisa M. Jones 46 ($R^2 \approx 0.54$), which may be due to the lack of specimens with low χ_{FD} or χ_{HD}, as $R^2 \geq 0.75$ for each of the other locations. While the apparent slope of the correlation is variable between sites, negative χ_{HD} has not been observed without significant χ_{FD}. This does not however imply that rocks with elevated χ_{FD} will necessarily have significant negative χ_{HD} – reference samples of Tiva Canyon tuff (χ_{FD} = 28.4%) and a paleosol from southwestern Oklahoma (χ_{FD} = 12.5%) yielded χ_{HD} values of -0.1 to -0.2%.

Altered trachyte samples in the SHADS 4 core with significant χ_{FD} and negative χ_{HD} have notably lower bulk susceptibility values than less-altered specimens, which have insignificant χ_{FD} and zero to positive χ_{HD} (e.g., Fig. 1). The same general relationship is found in other cores also containing igneous rock which does not exhibit elevated χ_{FD} or negative χ_{HD}. Unlike the subsurface rocks, samples collected from the Spavinaw Granite outcrop (see Chapter 5) showed no χ_{FD} and weakly positive χ_{HD} and are therefore excluded from this study.

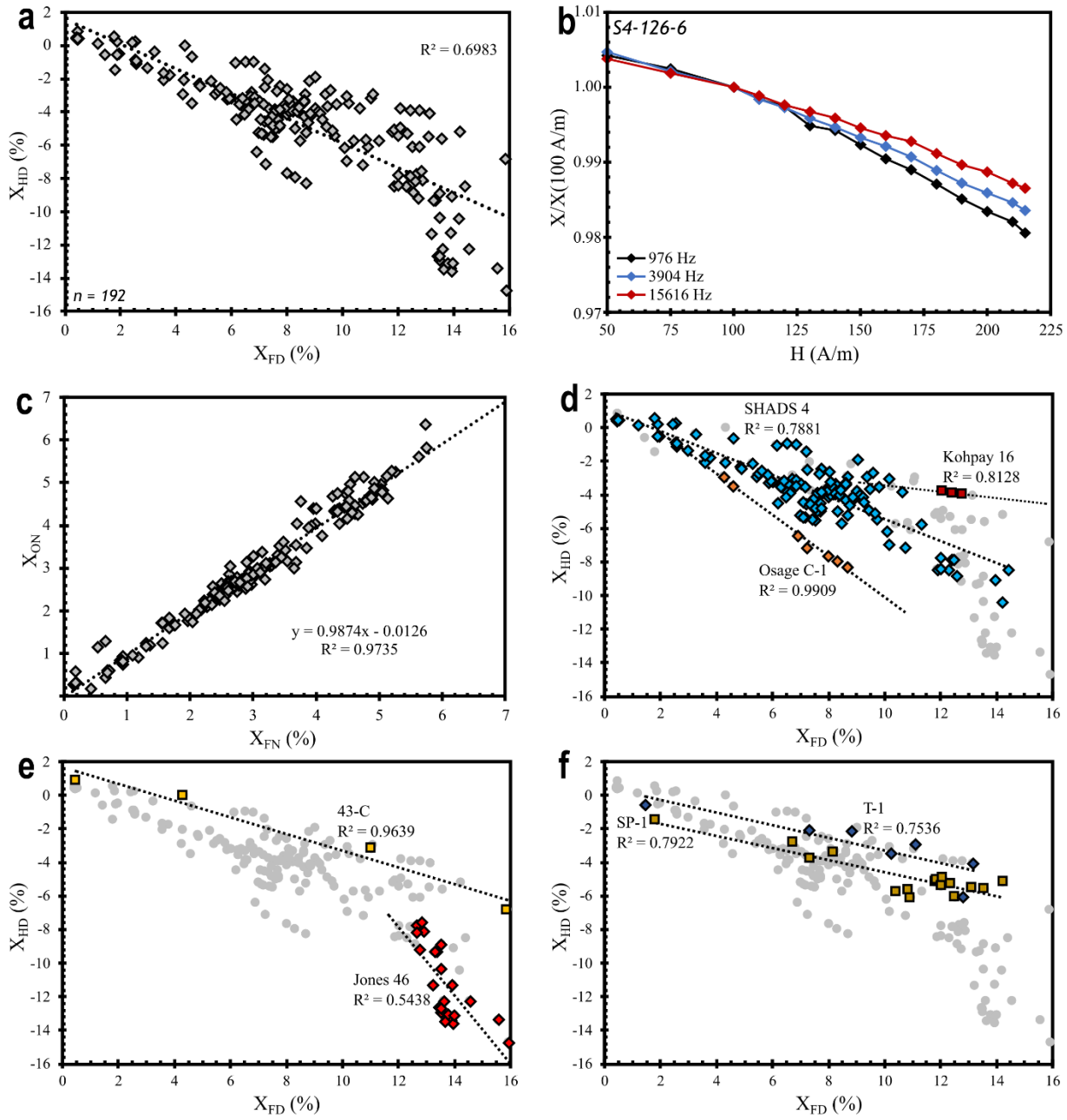


Figure 2. (a) Relationship between field-dependence and frequency-dependence of susceptibility for northeastern OK specimens. (b) Field-dependence at multiple frequencies for a sandstone sample from the SHADS 4, showing dependence of χ_{HD} on frequency. (c) Correlation of out-of-phase susceptibility parameter X_{ON} with normalized frequency-dependence χ_{FN}. (d-f) Relationships of χ_{HD} to χ_{FD} from each core.

Hysteresis

High-field (1-2 T) hysteresis measurements show a range of behaviors (Fig. 3). Most samples have low bulk coercivity (B_C), with values of a few mT to a few tens of mT. Some loops

vary smoothly and saturate at a few hundred mT (Fig. 3a-c), while others are somewhat constricted and do not completely saturate until fields of 1-1.5T or higher (Fig. 3d-f). Values of σ_{hys} are weakly to strongly positive for all samples, indicating a tendency towards constricted, "wasp-waisted" shapes (Fabian, 2003). Samples from the Jones 46 (Fig. 3e-f) are notably different from the other locations – B_C ranges from ~10 to nearly 200 mT, and the loops are moderately to severely constricted with unusual shapes due to the presence of low- B_C and high-B_C components (Tauxe et al., 1996).

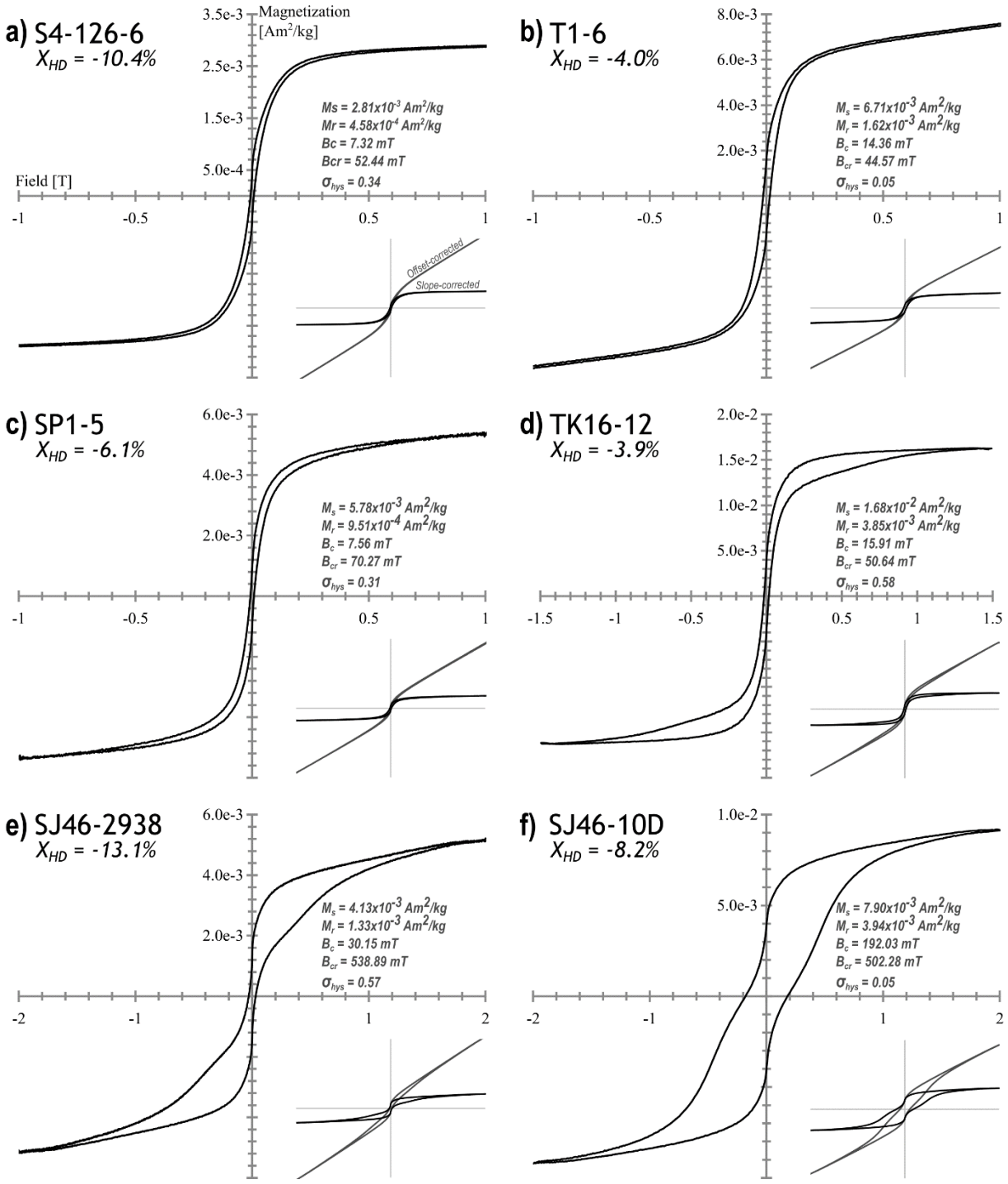


Figure 3. Representative slope-corrected high-field (1-2 T) hysteresis loops of specimens with negative χ_{HD}, showing range of coercivities and shapes. Inset plots show data before and after slope-correction. High-field artefacts from pole saturation are present in most samples (Jackson and Sølheid, 2010), leading to some uncertainties in Ms. Sample names begin with abbreviated core names (see Fig. 1), S4 = Amoco SHADS 4, T1 = AMAX T-1, SP1 = AMAX SP-1, TK16 = Texaco Kohpay 16, SJ46 = Sinclair Louisa M. Jones 46.

Hysteresis measurements at low peak fields (0.1 to 10 mT (≈ 80 to 8000 A/m)) are somewhat noisy but show essentially linear reversible behavior at very low fields (≤0.5 mT) (Fig. 4). Linear regression of data from samples with appreciable negative χ_{HD} yields lower slopes at higher peak fields. At peak fields ≥ 1 mT, nonlinear behavior is visible in M(H) curves for several specimens. These curves shallow at the ends of the field range, suggesting the presence of a phase which is approaching saturation.

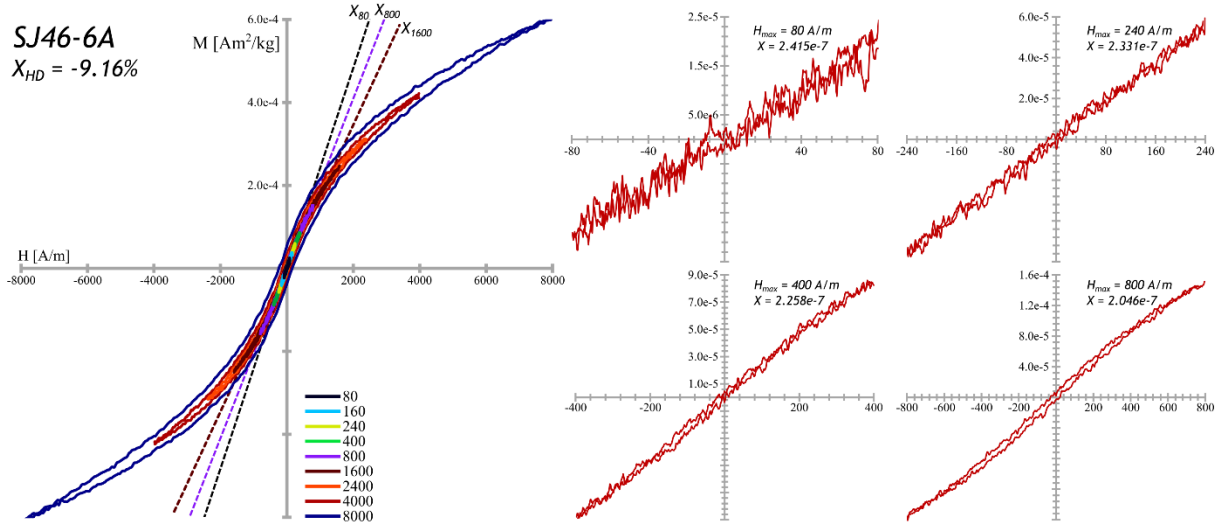


Figure 4. Low-field hysteresis measurements of a specimen from the Jones 46. (Left) Low-field loops from 80 to 8000 A/m, with extended linear regressions showing slope changes. (Right) Low-field data (≤800 A/m) with regression slopes indicating shallowing even where the data appears linear. Curvature is visible by 800 A/m.

Low-Temperature Remanence

Remanence curves indicate a variety of carrier minerals, but show little in the way of consistent results (Fig. 5). Most specimens yield slightly "humped" curves from low-temperature demagnetization (LTD) of room-T SIRM (e.g., Fig. 5a-c, g, i), a feature linked to the presence of maghemite (Özdemir and Dunlop, 2010). LTD-RTSIRM curves from the Jones 46, Kohpay 16 and SP-1 specimens also show prominent remanence drops near 260K, consistent with the Morin transition of hematite (Fig. 5d-e, h). The efficiency of LTD is highly variable, with Osage C-1 specimens losing over 30% of remanence after cycling (Fig. 5f) and the 43-C specimen losing

only 5% (Fig. 5i). The relative loss of remanence during LTD (ΔM_C, after Özdemir and Dunlop, 2010) is averaged from measurements between 290-300 K and expressed as a percentage in Fig. 5.

Low-T remanence changes consistent with the Verwey transition (T_V) of magnetite (e.g., Moskowitz et al., 1998; Carter-Stiglitz et al., 2006) are present in several samples but conspicuously absent in others. Remanence after field-cooling (FC) is stronger than ZFC-LTSIRM remanence at low temperatures in all specimens, though the values become similar in several samples after warming through T_V. Specimens with clear Morin transitions (e.g., Özdemir et al., 2008) in LTD-RTSIRM curves also show remanence increases in FC-ZFC data when approaching 260 K, at which point ZFC remanence may exceed FC (e.g., Fig. 5d). Changes associated with magnetite are very faint in FC-ZFC data from the Jones 46 and SP-1, and are essentially absent in a sample from the 43-C. An unidentified transition appears near 65 K in data from the 43-C (Fig. 5i) and may also be faintly present in the SP-1 sample (Fig. 5e). While all plots in Fig. 5 are truncated at 300 K, FC-ZFC remanences were measured up to temperatures of 400 K for several specimens. No changes from the trends apparent by 300 K were observed.

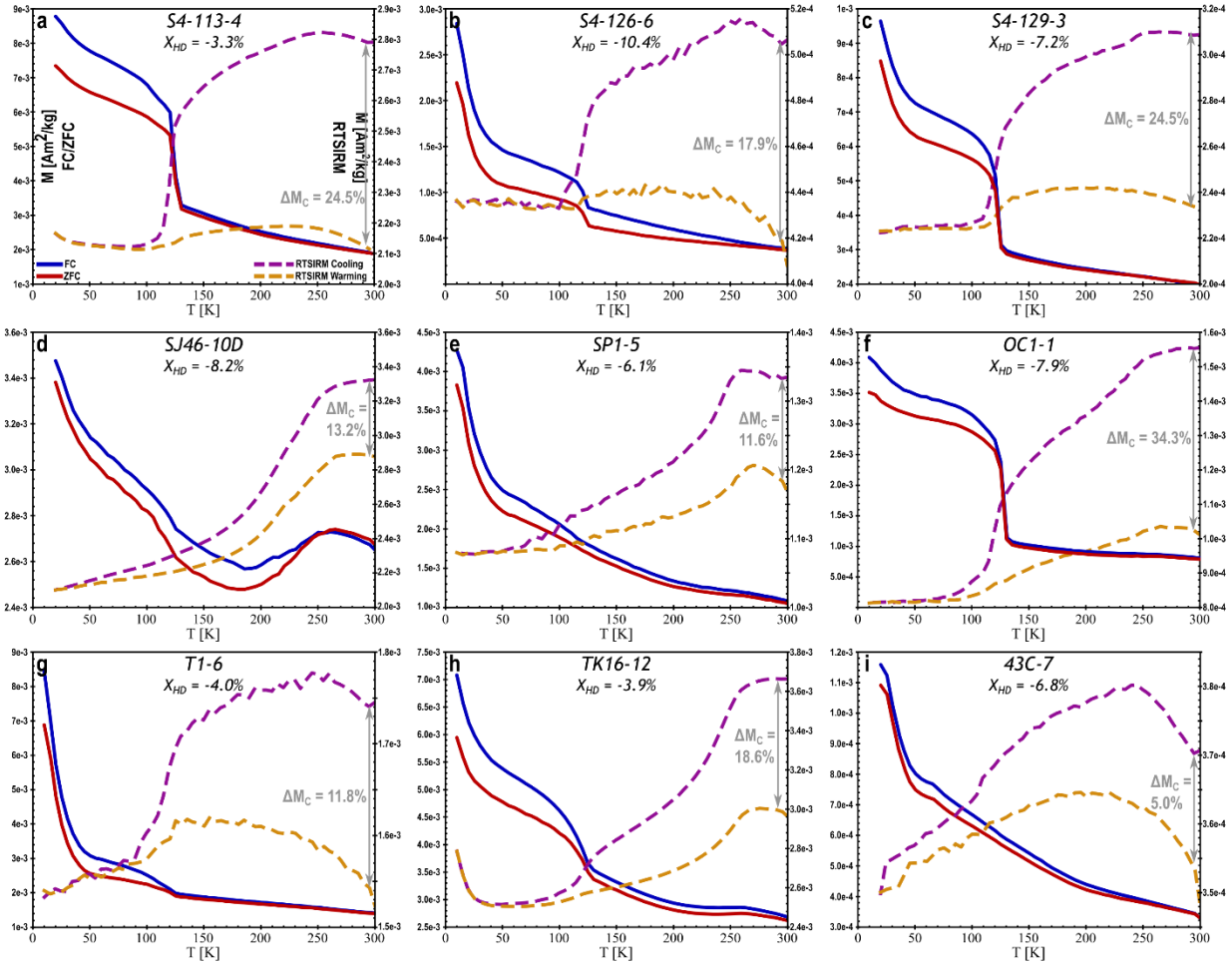


Figure 5. Low-T remanence curves showing the range of behaviors observed. FC-ZFC (solid curves) remanence scaled to left axes, LTD-RTSIRM (dashed curves) scaled to right axes. ΔM_C denotes relative loss of RTSIRM through low-T cycling (after Özdemir and Dunlop, 2010). Core names abbreviated as in Fig. 3, with new abbreviations OC = Texaco Osage C-1 and 43C = Eagle-Picher 43-C Anna Beaver.

High Temperature Susceptibility and Effects of Heating

All samples with negative χ_{HD} show a significant drop in susceptibility before 100 °C (Fig. 6). Most specimens also yield large susceptibility drops near 580 °C (consistent with the Curie point of magnetite) (Fig. 6a, b), though in several this drop is small and gradual. Many samples show large increases above 400-450 °C which then drop at 580 ° (e.g., Fig. 6c) - some of these are likely Hopkinson peaks for magnetite, though in many instances susceptibility is much higher after cooling from T >600 °C, indicating neoformation of magnetite from pre-

existing minerals. Repeated cycles usually result in continued increases, and artificial magnetite growth is particularly pronounced in specimens heated under argon.

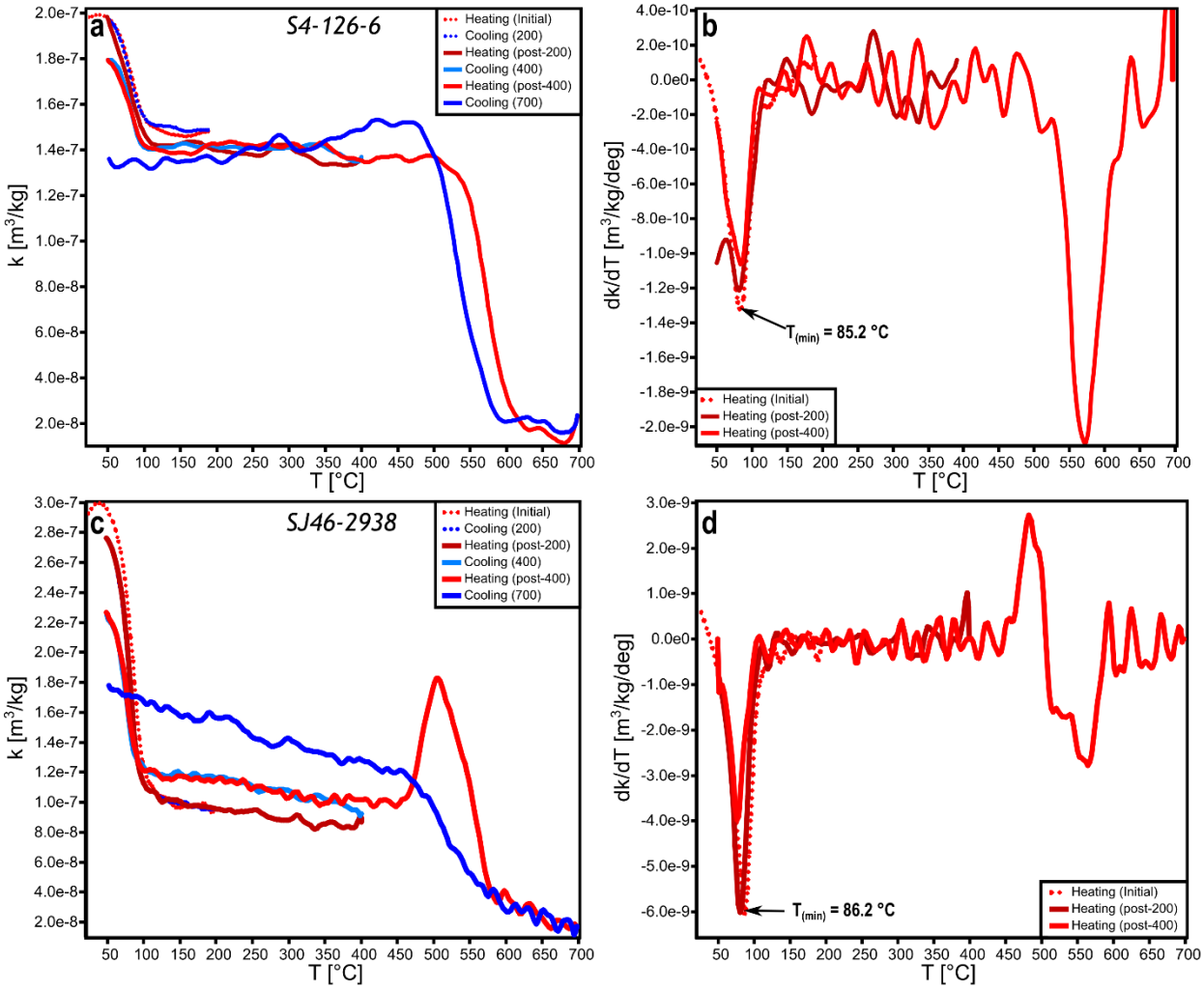


Figure 6. High-T susceptibility measurements (left) and calculated derivatives of heating curves(right).

The pre-100 °C susceptibility drop is irreversibly lost at high temperatures, but in many specimens it is almost completely recoverable at peak temperatures of 200-300 °C. Partial recovery is possible up to 500° or so (Figs. 6a, c). The reversibility indicates that this is likely a magnetic disordering temperature. Determinations of this nominal Curie point using the minima of the temperature-derivative of susceptibility (Petrovský and Kapička, 2006; Fabian et al., 2013)

(Fig. 6b, d) yield values between 75.2 – 90.3 °C, with an average of 83.2° (n = 21, σ = 3.4). Only the initial heating curves were used for this estimate.

While there is essentially no correlation between the relative magnitude of this drop and χ_{HD} of the parent specimens ($R^2 \approx 0.26$), it is of note that preliminary field-dependence measurements of samples after high-temperature (650-700 °C) treatment no longer yield negative values, and in several instances the frequency-dependence is also lost. Small susceptibility drops in this temperature range are also present in specimens from these cores that do not exhibit negative χ_{HD} or identifiable χ_{FD}, but accounts for only a very small proportion of the susceptibility (≤1%) of those samples as opposed to 20-70% in rocks with negative χ_{HD}.

Low-Temperature Susceptibility

AC susceptibility shows significant frequency-dependence at all temperatures and increases hyperbolically below ~70 K, likely at least in part due to paramagnetic mineral content (Fig. 7). Aside from this low-T effect, susceptibility usually has a minimum near 100 K and then increases with temperature with peak values in most samples occurring between 290-315 K (near room temperature). The isotropic point of magnetite is apparent as a small anomaly at 130 K in several susceptibility curves (Fig. 7b-d), but increases upon warming through the Verwey transition are prominent only in data from the Osage C-1 samples (Fig. 7d). The Osage core is also the only locality where the temperature of maximum susceptibility is clearly frequency-dependent. Susceptibility drops above 350 K (average maximum drop at 360 K/ 87 °C) are also present in all samples, consistent with results from high-temperature measurement sequences. This drop in most specimens corresponds to some loss of frequency-dependence and also to diminished frequency-dependence of the out-of-phase susceptibility (Fig. 7). Out-of-phase susceptibility is variable at very low temperatures but typically rises smoothly between ~50 and

200-250 K, at which point it may plateau or continue rising at a reduced rate. While data are noisy, most samples show elevated frequency-dependence of out-of-phase susceptibility from ~175 to 360 K (e.g., Fig. 7a, f).

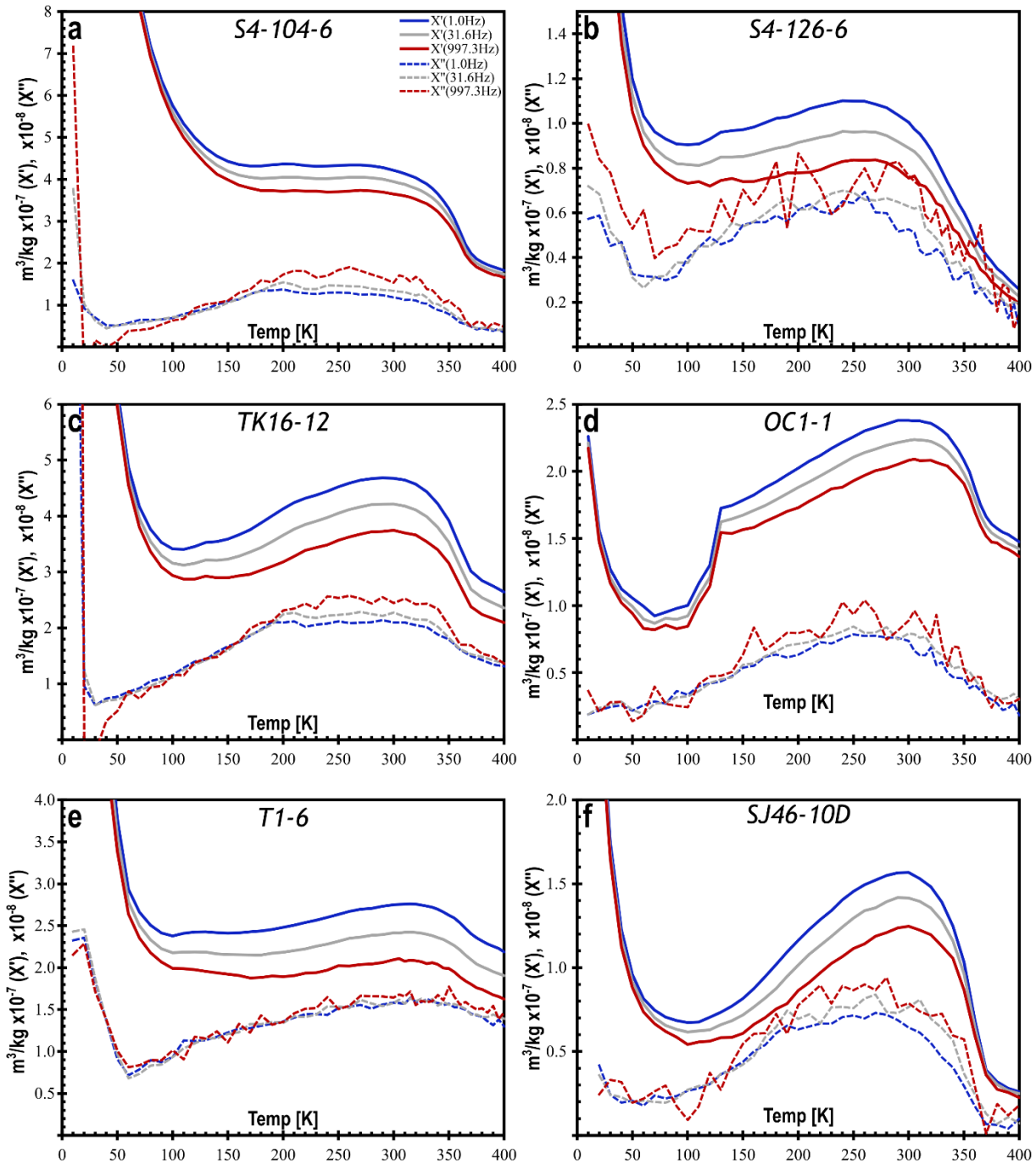


Figure 7. Temperature variation of in-phase (χ') and out-of-phase (χ'') AC susceptibility at 3 frequencies from 10 to 400 Kelvin. While behavior is variable, all samples show elevated frequency-dependence across a large temperature range and loss of both in-phase and out-of-phase susceptibilities at T> ~350 K. In-phase and out-of-phase values are scaled an order of magnitude apart (see left axis).

Field-Dependence Variation with Temperature

Due to the consistent presence of the susceptibility drop at ~83 °C, field-dependence of susceptibility was measured between 10-400 K using the MPMS3. Field-dependence is positive or only weakly negative at very low temperatures. Values become notably negative above ~100 K, and negative χ_{HD} intensifies as temperature rises. As seen in room-temperature measurements from the MFK Kappabridge, χ_{HD} is consistently more negative at lower frequencies. In four of five samples measured, χ_{HD} reaches a minimum near 330-340 K and then begins to rise (Fig. 8, one additional Jones 46 specimen was measured and yielded similar results to Fig. 8a). χ_{HD} becomes positive by 375 K in rhyolite samples from the Jones 46 and is only very weakly negative (≈-1%) in a sandstone from the SHADS 4 (Fig. 8b). Altered granite from the SP-1 loses about half its negative χ_{HD} response between 340 and 400 K (Fig. 8c), while χ_{HD} in the 43C sample uniquely does not begin to disappear at elevated temperature (Fig. 8d).

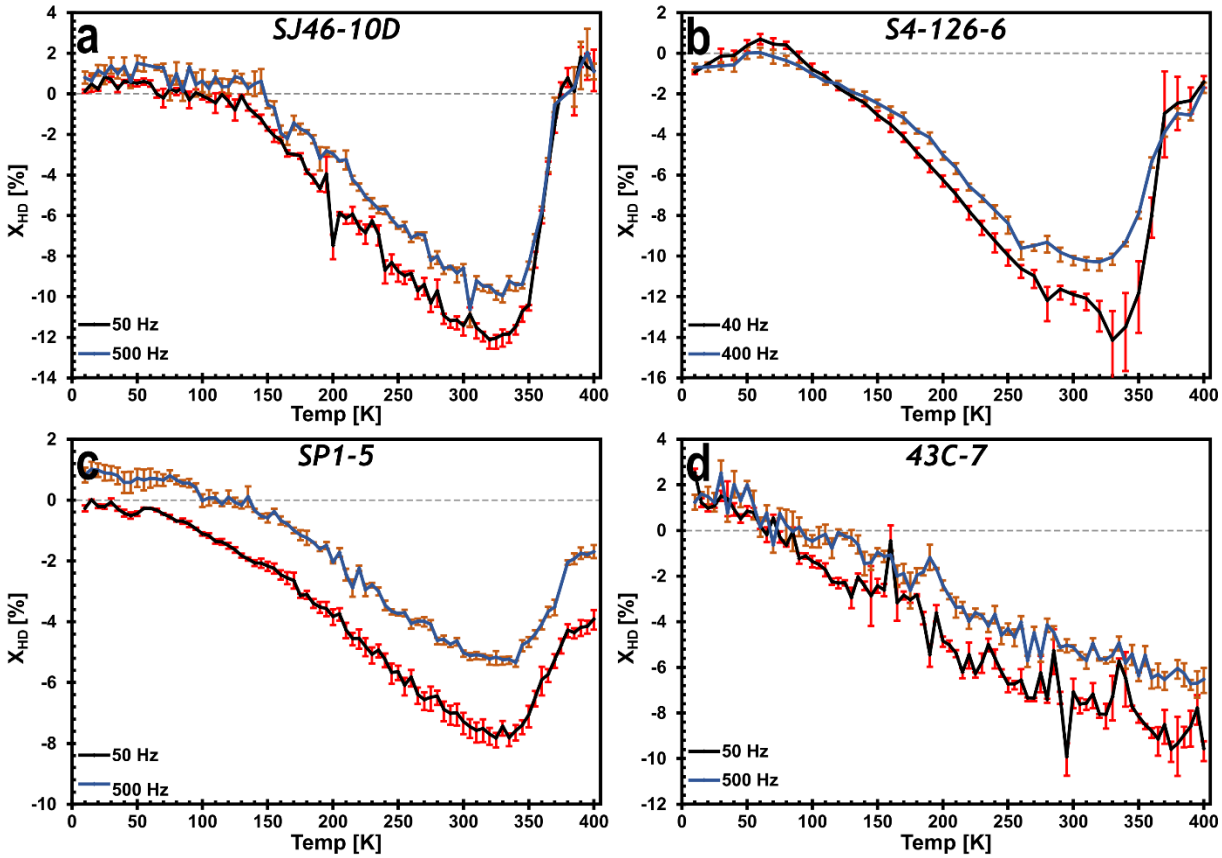


Figure 8. Temperature variation of χ_{HD}. χ_{HD} and error bars are calculated by linear regression of 5 measurements in fields from 1 to 9 Oe (79.6 to 716.2 A/m) at the listed frequencies.

The remaining negative χ_{HD} at 400 K is perhaps slightly misleading, as the same absolute change in χ vs. H becomes a larger percentage due to loss of bulk susceptibility at elevated temperature. Normalizing the regression slopes to susceptibility at H = 1 Oe and T = 300 K helps illustrate the changes in absolute rather than relative χ_{HD} (Fig. 9), and it is apparent that actual loss of χ vs. H is reduced above 350 K in most specimens (Fig. 9a-c). Even in the 43C, where relative χ_{HD} continues to become more negative with temperature (Fig. 8d), the normalized value shows that the slope has levelled off and begun to shallow (Fig. 9d). This treatment also helps show that the loss of negative χ_{HD} does not appear to be an artefact of low-T paramagnetic contributions – in all samples, the slope approaches zero near 70 K, and χ_{HD} is positive in the Jones 46 and 43-C specimens below this temperature. χ_{HD} appears to become negative again

below 40 K in the SHADS 4 sandstone sample (Fig. 9b) and low-frequency data from the SP-1, while the SP-1 high-frequency curve diverges and is increasingly positive at low-T (Fig. 9c). These behaviors are interesting, but further investigation and discussion are presently beyond the scope of this work.

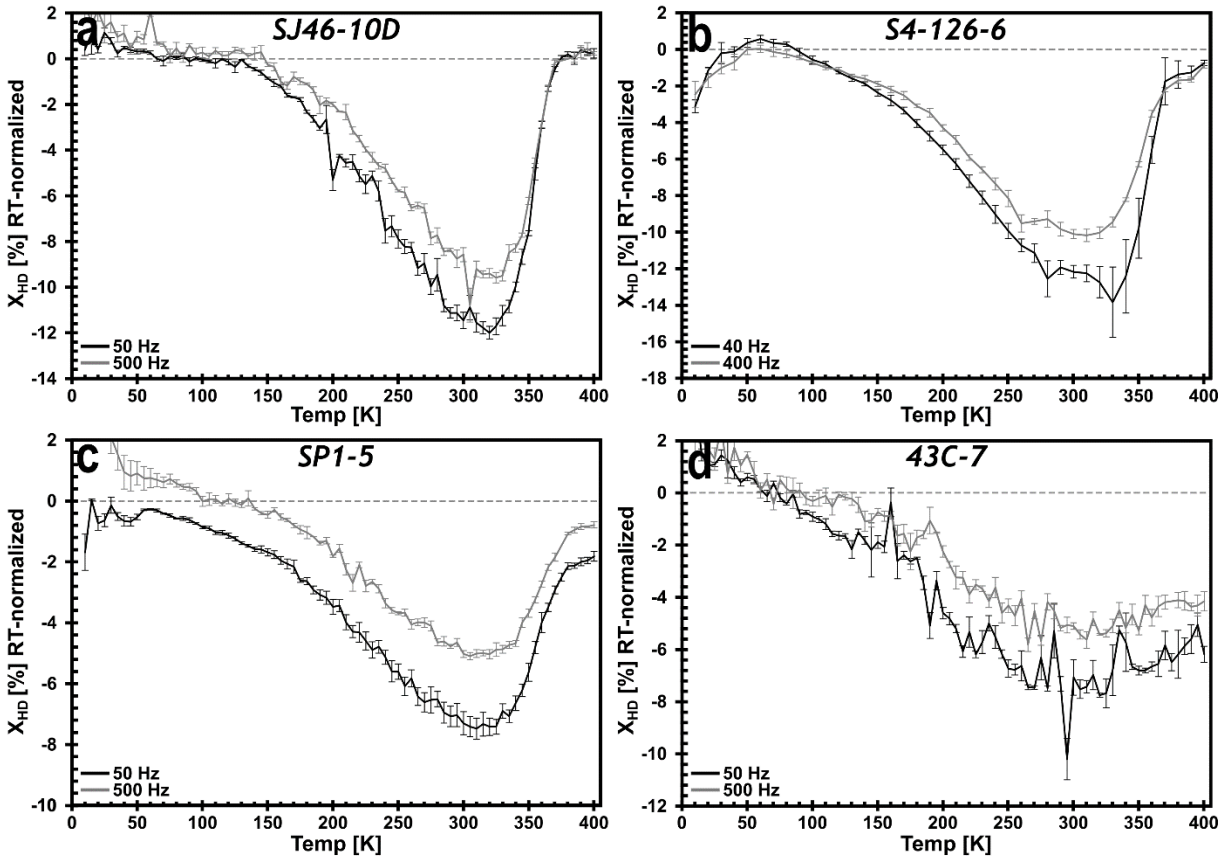


Figure 9. Temperature variation of χ_{HD} adjusted for temperature variation of bulk susceptibility. Data is the same as Fig. 8 but χ_{HD} at all temperatures is recalculated using the ratio of regression slope relative to susceptibility at T = 300 K and H = 1 Oe.

DISCUSSION

The decrease of magnetic susceptibility with increasing fields implies the presence of a mineral which is approaching magnetic saturation, which is supported by low-field hysteresis measurements. In typical ferromagnetic *s.l.* minerals, this occurs at applied field strengths of tens of thousands of A/m or more (e.g., Borradaile et al., 2008), while in the rocks studied here it is apparent at tens of A/m. Remanence curves show behavior consistent with typical magnetic

minerals (magnetite, maghemite, hematite), but none are consistently present and none seem like viable candidates. The particular mineral responsible is still unknown, but several statements can be made about its properties.

The correlation of χ_{HD} with χ_{FD} implies that the phase responsible is frequency-dependent, and this is supported by changes in the magnitude of χ_{HD} at different frequencies. Low-T susceptibility measurements show elevated χ_{FD} at essentially all temperatures with no characteristic low-T phase transitions, and the typical absence of Verwey transitions in susceptibility data suggest that stoichiometric magnetite has only a relatively minor contribution to susceptibility. χ_{HD} remains negative at temperatures down to 100 K or below, and in some samples is negative down to 10 K. Measurements above room temperature clearly indicate a relationship of negative χ_{HD} to a phase which becomes magnetically disordered above ~83 °C, and in multiple samples the negative χ_{HD} response almost or completely vanishes (reversibly) in that temperature range, with notable changes in χ_{FD} of some samples as well. Notably, the two specimens which continue to exhibit significant negative χ_{HD} above this temperature range are also the ones which yielded an apparent phase transition near 65 K in remanence curves, which suggests the possibility that multiple minerals may be responsible for this behavior in some rocks.

In the present study, this behavior is associated with the basement-cover interface and with alteration along fractures, indicating that the responsible phase likely originated from low-temperature fluid-rock interaction. High-T susceptibility measurements indicate that this mineral irreversibly alters at temperatures above 400 °C and may begin to degrade by 200 °C in some specimens. The low disordering temperature, thermal instability and links to alteration suggest that some sort of iron oxyhydroxide may be responsible, though the known non-paramagnetic

ones are poor fits. The Néel temperature of very fine goethite particles is consistent with the observed disordering temperature (Bocquet and Kennedy, 1992), but such particles still require fields of ~200 mT to approach saturation (Brok et al., 2014). The only other non-paramagnetic iron oxyhydroxide is feroxyhyte, which has been suggested to form from rapid oxidation during low-T fluid-rock interaction (Carlson and Schwertmann, 1980). The magnetic properties of natural feroxyhyte do not seem to be well-characterized, but artificial samples are commonly superparamagnetic with a consistent Curie temperature of ~170 °C (Koch et al., 1995), considerably higher than observed here. Unidentified phases with Curie temperatures of ~70 and 120 °C have been reported to form during experimental transformations of ferrihydrite to "hydromaghemite" and hematite (Liu et al., 2008) and may be worth further investigation in this context. In samples which do not produce substantial magnetite during high-T experiments, post-heating susceptibility is usually considerably reduced (e.g., Fig. 6), indicating that the phase alters to either a paramagnetic mineral or a low-susceptibility phase such as hematite.

The properties of the yet-unidentified material responsible for significant values of negative χ_{HD} have implications for other types of analysis. In particular, it is evident that this material is also highly frequency-dependent. Frequency-dependence of susceptibility in most natural materials is attributed to relaxation effects of very small superparamagnetic grains of magnetite and/or maghemite (e.g., Mullins and Tite, 1973; Dearing et al., 1996) which are near the transition between SP and stable single-domain behavior (Worm, 1998). While one or both of these phases are present in at least some samples, the properties of the material responsible for negative χ_{HD} in this study are not consistent with either. Negative χ_{HD} has been reported from environmental materials and soils (Hrouda et al., 2006; Chlupáčová et al., 2010), which are the most common subjects of studies involving frequency-dependence. Field-dependence

measurements are rarely reported in such studies, and without χ_{HD} and/or high-T susceptibility data the presence of this particular magnetic carrier might be easily missed and its χ_{FD} contribution attributed to more common phases. Additionally, preliminary measurements of anisotropy of magnetic susceptibility (AMS) of negative χ_{HD} samples from the SHADS 4 indicate that both in-phase and out-of-phase AMS fabrics are controlled by this unknown phase (Hamilton et al., 2019). Control of out-of-phase AMS likely means that it will control frequency-dependent AMS as well; both approaches are finding increased use in environmental and paleoenvironmental studies (e.g., Hrouda et al., 2017; Bradák et al., 2018).

The clear link between this phase and secondary fluid activity suggests that χ_{FD} and χ_{HD} have value for granite and "basement" alteration studies, and the strongly negative χ_{HD} in some of the sandstones shows potential value for diagenetic studies as well. Understanding the meaning of this particular behavior will however require a great deal more work. Previous reports and the current study clearly show a relationship to secondary processes, but the details are still evasive. Chemical characteristics associated with alteration in this study area are complex and still poorly understood (Hamilton et al., 2021), and negative χ_{HD} is so rarely reported that general comparisons between occurrences are not presently possible. Better understanding will require more recognized occurrences, and obviously would benefit from direct identification through petrographic methods. Initial attempts at magnetic separations made during the course of this study were unsuccessful, but efforts to isolate and identify the responsible mineral(s) are ongoing.

CONCLUSION

Sandstones and altered igneous rocks near the subsurface basement-cover interface in northeastern Oklahoma show pronounced frequency-dependence and negative field-dependence

of susceptibility, with negative χ_{HD} values exceeding any found during a literature search. These parameters are clearly correlated, though the particular relationship varies between localities. Characterization through multiple methods shows that negative χ_{HD} in most of these rocks is linked to the presence of an unidentified superparamagnetic phase which is strongly frequency-dependent down to very low temperatures and approaches saturation at much lower fields than known natural magnetic carriers. This phase has an apparent Curie temperature near 83 °C, and negative χ_{HD} is significantly weakened or completely lost (reversibly) in most specimens near that temperature. One sample stands as an exception, and it is possible that multiple phases may cause this behavior. The properties observed do not fit well with any known mineral but the low Curie point, the irreversible alteration at high temperature and association with fluid alteration are consistent with iron oxyhydroxides.

As measurements of χ_{HD} are still relatively uncommon, the actual abundance and distribution of negative χ_{HD} behavior are essentially unknown. In the absence of field-dependence data, the responsible phase could easily go unrecognized and its χ_{FD} behavior may be erroneously assigned to magnetite or maghemite. To the extent that it is not due to data scarcity, the apparent rarity of significant negative χ_{HD} suggests it could be a very useful indicator of particular chemical and/or thermal conditions. Identification of the responsible mineral is necessary for a clear understanding – while this is still ongoing, the present dataset suggests the possibility of a previously unrecognized magnetic carrier mineral which controls the properties of these rocks.

REFERENCES

Bickford, M.E., Van Schmus, W.R., Karlstrom, K.E., Mueller, P.A., and Kamenov, G.D., 2015. Mesoproterozoic trans-Laurentian magmatism: A synthesis of continent-wide age distributions, new SIMS U–Pb ages, zircon saturation temperatures, and Hf and Nd isotopic compositions. Precambrian Research, 265, pp.286-312. https://doi.org/10.1016/j.precamres.2014.11.024

Bocquet, S., and Kennedy, S.J., 1992. The Néel temperature of fine particle goethite. Journal of magnetism and magnetic materials, 109(2-3), pp.260-264. https://doi.org/10.1016/0304-8853(92)91758-L

Borradaile, G.J., Stupavsky, M., and Metsaranta, D.A., 2008. Induced magnetization of magnetite-titanomagnetite in alternating fields ranging from 400 A/m to 80,000 A/m: Low-field susceptibility (100–400 A/m) and beyond. Pure and Applied Geophysics, 165(7), pp.1411-1433. https://doi.org/10.1007/s00024-008-0361-5

Bradák, B., Seto, Y., Hyodo, M., and Szeberényi, J., 2018. Relevance of ultrafine grains in the magnetic fabric of paleosols. Geoderma, 330, pp.125-135. https://doi.org/10.1016/j.geoderma.2018.05.036

Brok, E., Frandsen, C., Madsen, D.E., Jacobsen, H., Birk, J.O., Lefmann, K., Bendix, J., Pedersen, K.S., Boothroyd, C.B., Berhe, A.A., Simeoni, G.G., and Mørup, S. 2014. Magnetic properties of ultra-small goethite nanoparticles. Journal of Physics D: Applied Physics, 47(36), 365003. http://dx.doi.org/10.1088/0022-3727/47/36/365003

Carlson, L., and Schwertmann, U., 1980. Natural occurrence of feroxyhite (δ′-FeOOH). Clays and Clay Minerals, 28(4), pp.272-280. https://doi.org/10.1346/CCMN.1980.0280405

Carter-Stiglitz, B., Moskowitz, B., Sølheid, P., Berquó, T.S., Jackson, M. and Kosterov, A., 2006. Low-temperature magnetic behavior of multidomain titanomagnetites: TM0, TM16, and TM35. Journal of Geophysical Research: Solid Earth, 111, B12S05. https://doi.org/10.1029/2006JB004561

Chlupáčová, M., Hanák, J. and Müller, P., 2010. Magnetic susceptibility of cambisol profiles in the vicinity of the Vir Dam, Czech Republic. Studia Geophysica et Geodaetica, 54(1), pp.153-184. https://doi.org/10.1007/s11200-010-0008-8

Dearing, J.A., Dann, R.J.L., Hay, K., Lees, J.A., Loveland, P.J., Maher, B.A., and O'Grady, K., 1996. Frequency-dependent susceptibility measurements of environmental materials. Geophysical Journal International, 124(1), pp.228-240. https://doi.org/10.1111/j.1365-246X.1996.tb06366.x

Denison, R.E., 1981. Basement rocks in northeastern Oklahoma. Oklahoma Geological Survey Circular 84.

Derby, J.R., Hinch, H.H., and Repetski, J.R., 1991. Lithology, stratigraphy, and age of the Arbuckle Group in the Amoco SHADS No. 4, a continuous core from grassroots into basement. Rogers County, Oklahoma. Oklahoma Geological Survey Special Publication 91-3, pp.69-82.

Fabian, K., 2003. Some additional parameters to estimate domain state from isothermal magnetization measurements. Earth and Planetary Science Letters, 213(3-4), pp.337-345. https://doi.org/10.1016/S0012-821X(03)00329-7

Fabian, K., Shcherbakov, V.P. and McEnroe, S.A., 2013. Measuring the Curie temperature. Geochemistry, Geophysics, Geosystems, 14(4), pp.947-961. https://doi.org/10.1029/2012GC004440

Guerrero-Suarez, S., and Martín-Hernández, F., 2012. Magnetic anisotropy of hematite natural crystals: Increasing low-field strength experiments. International Journal of Earth Sciences, 101(3), pp.625-636. https://doi.org/10.1007/s00531-011-0666-y

Hamilton, M., Evans, S.C., and Elmore, R.D., 2018. Magnetic and geochemical characteristics of alteration and weathering at the Cambrian unconformity, northeastern Oklahoma. Abstract GP43C-0788 presented at 2018 AGU Fall Meeting, Washington D.C., 10-14 Dec.

Hamilton, M., Chadima, M., Jackson, M., and Elmore, R.D., 2019. Investigation of Strongly Negative Field-Dependence of AC Magnetic Susceptibility. Abstract GP13A-04 presented at 2019 AGU Fall Meeting, San Francisco CA, 9-13 Dec.

Hamilton, M., Carpenter, B., Johnston, C., Kolawole, F., Evans, S., and Elmore, R.D., 2021. Fractured, altered, and faulted basement in northeastern Oklahoma: Implications for induced seismicity. Journal of Structural Geology, 147, 104330. https://doi.org/10.1016/j.jsg.2021.104330

Hrouda, F., 2002. Low-field variation of magnetic susceptibility and its effect on the anisotropy of magnetic susceptibility of rocks. Geophysical Journal International, 150(3), pp.715-723. https://doi.org/10.1046/j.1365-246X.2002.01731.x

Hrouda, F., 2011. Models of frequency-dependent susceptibility of rocks and soils revisited and broadened. Geophysical Journal International, 187(3), pp.1259-1269. https://doi.org/10.1111/j.1365-246X.2011.05227.x

Hrouda, F., Chlupáčová, M., and Mrázová, S., 2006. Low-field variation of magnetic susceptibility as a tool for magnetic mineralogy of rocks. Physics of the Earth and Planetary Interiors, 154, pp.323-336. https://doi.org/10.1016/j.pepi.2005.09.013

Hrouda, F., Pokorný, J., Ježek, J., and Chadima, M., 2013. Out-of-phase magnetic susceptibility of rocks and soils: A rapid tool for magnetic granulometry. Geophysical Journal International, 194(1), pp.170-181. https://doi.org/10.1093/gji/ggt097

Hrouda, F., Pokorný, J., and Chadima, M., 2015. Limits of out-of-phase susceptibility in magnetic granulometry of rocks and soils. Studia Geophysica et Geodaetica, 59, 284–308. http://dx.doi.org/10.1007/s11200-014-0948-5

Hrouda, F., Chadima, M., Ježek, J., and Pokorný, J., 2017. Anisotropy of out-of-phase magnetic susceptibility of rocks as a tool for direct determination of magnetic subfabrics of some minerals: An introductory study. Geophysical Journal International, 208, pp.385-402. https://doi.org/10.1093/gji/ggw399

Jackson, M., 2004. Imaginary susceptibility: A primer. The IRM Quarterly, 13(4), pp.1, 10-11. https://conservancy.umn.edu/handle/11299/171293

Jackson, M., and Sølheid, P., 2010. On the quantitative analysis and evaluation of magnetic hysteresis data. Geochemistry, Geophysics, Geosystems, 11(4), Q04Z15. https://doi.org/10.1029/2009GC002932

Jackson, M., Moskowitz, B., Rosenbaum, J., and Kissel, C., 1998. Field-dependence of AC susceptibility in titanomagnetites. Earth and Planetary Science Letters, 157(3-4), pp.129-139. https://doi.org/10.1016/S0012-821X(98)00032-6

Koch, C.B., Oxborrow, C.A., Mørup, S., Madsen, M.B., Quinn, A.J., and Coey, J.M.D., 1995. Magnetic properties of feroxyhyte (δ-FeOOH). Physics and Chemistry of Minerals, 22(5), pp.333-341. https://doi.org/10.1007/BF00202774

Liu, Q., Barrón, V., Torrent, J., Eeckhout, S.G., and Deng, C., 2008. Magnetism of intermediate hydromaghemite in the transformation of 2-line ferrihydrite into hematite and its paleoenvironmental implications. Journal of Geophysical Research: Solid Earth, 113, B01103. https://doi.org/10.1029/2007JB005207

McCracken, M.H., 1964. The Cambro-Ordovician rocks of northeastern Oklahoma and adjacent areas. Tulsa Geological Society Digest, 32, 49-75.

Moskowitz, B.M., Jackson, M. and Kissel, C., 1998. Low-temperature magnetic behavior of titanomagnetites. Earth and Planetary Science Letters, 157(3-4), pp.141-149. https://doi.org/10.1016/S0012-821X(98)00033-8

Mullins, C.E., and Tite, M.S., 1973. Magnetic viscosity, quadrature susceptibility, and frequency dependence of susceptibility in single-domain assemblies of magnetite and maghemite. Journal of Geophysical Research, 78(5), pp. 804–809. https://doi.org/10.1029/jb078i005p00804

Özdemir, Ö., and Dunlop, D.J., 2010. Hallmarks of maghemitization in low-temperature remanence cycling of partially oxidized magnetite nanoparticles. Journal of Geophysical Research: Solid Earth, 115, B02101. https://doi.org/10.1029/2009JB006756

Özdemir, Ö., Dunlop, D.J. and Berquó, T.S., 2008. Morin transition in hematite: Size dependence and thermal hysteresis. Geochemistry, Geophysics, Geosystems, 9(10), Q10Z01. https://doi.org/10.1029/2008GC002110

Petrovský, E. and Kapička, A., 2006. On determination of the Curie point from thermomagnetic curves. Journal of Geophysical Research: Solid Earth, 111, B12S27. https://doi.org/10.1029/2006JB004507

Tauxe, L., Mullender, T.A.T. and Pick, T., 1996. Potbellies, wasp-waists, and superparamagnetism in magnetic hysteresis. Journal of Geophysical Research: Solid Earth, 101(B1), pp.571-583. https://doi.org/10.1029/95JB03041

Worm, H.U., 1991. Multidomain susceptibility and anomalously strong low field dependence of induced magnetization in pyrrhotite. Physics of the Earth and Planetary Interiors, 69(1-2), pp.112-118. https://doi.org/10.1016/0031-9201(91)90157-D

Worm, H.U., 1998. On the superparamagnetic-stable single domain transition for magnetite, and frequency dependence of susceptibility. Geophysical Journal International 133, pp. 201-206. https://doi.org/10.1046/j.1365-246X.1998.1331468.x

CHAPTER 5

RECONNAISSANCE PALEOMAGNETIC AND MAGNETIC FABRIC STUDY OF THE SPAVINAW GRANITE

ABSTRACT

This report summarizes current knowledge regarding the Spavinaw Granite and provides new paleomagnetic and rock magnetic data from two block samples. Anisotropy of magnetic susceptibility measurements show an oblate fabric with nearly horizontal Kmin. Paleomagnetic measurements yield remanence directions similar to those of early Cambrian igneous rocks from southern Oklahoma. Rock magnetic analysis indicates that the magnetic susceptibility and remanence are controlled by magnetite and (previously unrecognized) maghemite. The new data indicate that, contrary to previous reports, the magnetism of the Spavinaw Granite is not completely incoherent. While there is variation between the two blocks, both are internally consistent and yield directions similar to those of the Cambrian units in southern Oklahoma. The paleomagnetic data suggest that the Spavinaw Granite was remagnetized during the early Cambrian, with some samples also carrying a partial later overprint. The strike of the magnetic susceptibility foliation plane also aligns with known structural trends from the Wichita and Arbuckle Mountains areas as well as subsurface faults in northeastern Oklahoma, suggesting that tilting and/or deformation along similar structures took place during or prior to the early Cambrian. This reconnaissance study indicates that the Spavinaw Granite locality likely preserves magnetic data which could shed light on the poorly-known Cambrian (and possibly Precambrian) tectonic history of northeastern Oklahoma.

INTRODUCTION

The Spavinaw Granite is one of Oklahoma's longest-studied outcrops. The existence of granite in the area was first documented by Owen (1860) through second-hand samples left over from shaped millstones. Owen died during the writing of his report without providing a detailed description, and a follow-up expedition was unable to locate the outcrop. The first published description of the Spavinaw Granite's location and petrography was that of Drake (1897), who also gave the rock its name. The age was debated vigorously in the first few decades of the 20th century (see summary by Ireland, 1930), with many arguing that the granite was a Paleozoic intrusion. Ham and Dott (1943) demonstrated that the granite was older than the surrounding Ordovician Cotter Dolomite and believed it to be Precambrian; this was confirmed by a Rb-Sr isotopic age of 1,326±58 million years (recalculated from Muehlberger et al., 1966). The Rb-Sr date is now known to be also slightly too young, and the most accurate published age determination is a U-Pb zircon date of 1,370±20 Ma (Bickford and Lewis, 1979).

In an early study of the relationships between magnetic field anomalies and the magnetism of igneous rocks, Hawes (1952) discovered numerous intense, closely spaced anomalies associated with the Spavinaw Granite, and additionally found the rock to be strongly magnetized in seemingly random directions. A subsequent attempt to determine a paleomagnetic pole position from the Spavinaw Granite (Spall and Noltimier, 1972) likewise found what appeared to be stable magnetizations with high intensities and scattered directions, which the authors were unable to explain.

As part of a larger project investigating alteration and tectonics in Oklahoma basement rocks, the present study was undertaken as a pilot test to determine whether more modern analyses might yield different results or an explanation for the magnetization of the granite, and

also to determine whether the Spavinaw Granite has a consistent magnetic fabric. Paleomagnetic analyses can yield information on the timing of alteration in rocks (e.g., Elmore et al., 1998) and measurements of the anisotropy of magnetic susceptibility have shown value in understanding the emplacement and/or subsequent deformation of rocks (e.g., Tarling and Hrouda, 1993; Bouchez 1997, 2000).

GEOLOGICAL SETTING

The Spavinaw Granite is the only Precambrian exposure in northeastern Oklahoma. The outcrop consists of five knobs which protrude through the Cotter Dolomite on the west side of the town of Spavinaw in easternmost Mayes County (Ireland, 1930). The granite forms the apparent core of a gentle asymmetric anticline striking 30-40° NE with a slight (~5°) tilt to the northwest (Drake, 1897; Ireland, 1930; Huffman, 1958). In the local subsurface, the granite is interpreted to form a steep ridge that was buried by the onlap of the early Ordovician Cotter Dolomite (Ham and Dott, 1943).

The Spavinaw Granite is highly granophyric/micrographic in texture (Drake, 1897; Merritt, 1960) and very similar rocks (dubbed the Spavinaw Granite Group) comprise the uppermost basement of much of northeastern Oklahoma (Fig. 1; Denison 1966, 1981). This group has been interpreted as granite sills emplaced at shallow depths within contemporaneous volcanic rocks known as the Washington Volcanic Group (Denison, 1966; 1981). Denison inferred that the regional volcanic-intrusive complex was uplifted into a broad anticline and the volcanics were eroded from the central area. All U-Pb radiometric ages for the Spavinaw Granite Group and the Washington Volcanic Group are essentially identical and are very near 1,370 Ma (see compilation in Bickford et al., 2015).

Regionally, the granite is considered to form part of the 1,370±30 Ma Southern Granite-Rhyolite Province (Van Schmus et al., 1996), a Mesoproterozoic basement terrane dominated by granites and rhyolites which stretches from northwestern Alabama through Oklahoma and the Texas Panhandle and likely including parts of southeastern Colorado and eastern New Mexico. The tectonic origin of this province has been debated, with many authors preferring to ascribe it to an intraplate/continental rift setting (e.g., Lidiak, 1996), with others preferring to interpret it as resulting from the accretion of volcanic arcs and post-arc extensional magmatism (e.g., Bickford et al., 2015).

Essentially nothing is known of the tectonic history between the Mesoproterozoic emplacement of the Spavinaw Granite and the Ordovician onlap of the Cotter Dolomite. The granite lies within the Ozark Uplift (Fig. 1), which was uplifted in the late Paleozoic during the Ouachita Orogeny. Paleozoic strata in the area contain unconformities in every era, including a prominent truncation of pre-Late Devonian strata and several erosional unconformities within the Mississippian (Huffman, 1958).

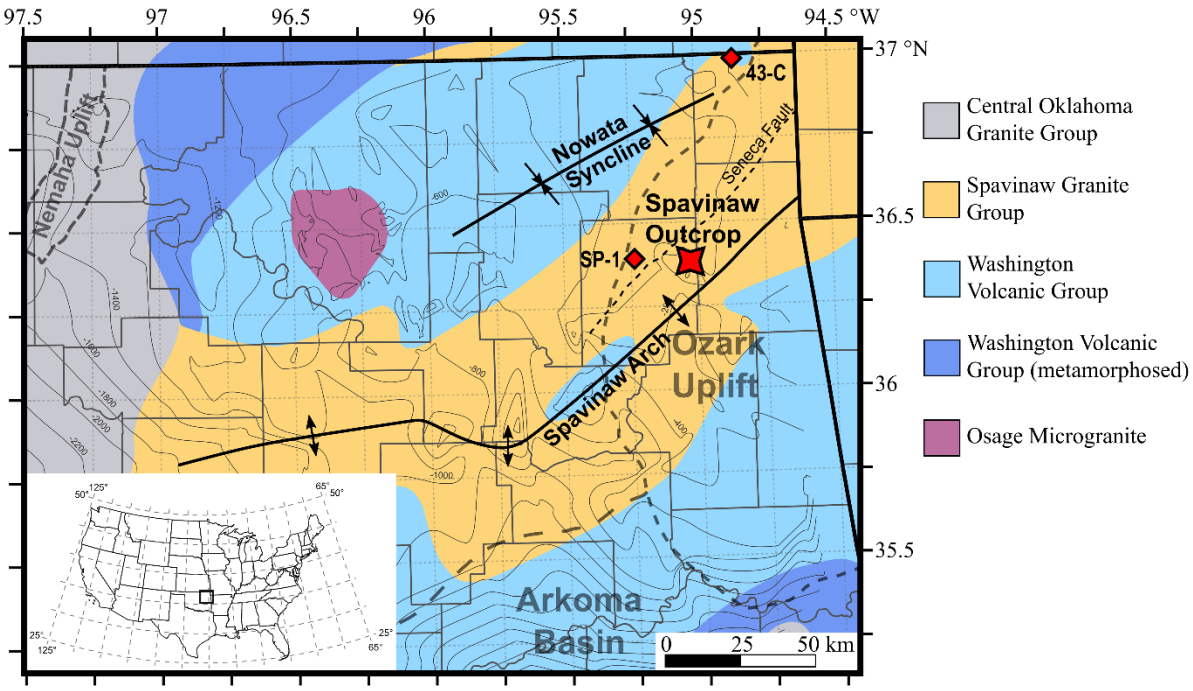


Figure 1. Uppermost basement lithology, regional structure, and topography of northeastern Oklahoma. Lithology after Denison (1966, 1981) with Woodson County Granite included in the Spavinaw Group. Basement topography contoured in meters relative to sea level from borehole contacts listed in Campbell and Weber (2006). Tectonic provinces from Northcutt and Campbell (1995). Spavinaw Arch and Nowata Syncline from Denison (1981). Locations of subsurface cores of the Spavinaw Granite Group discussed in this article are shown with red diamonds.

The abundant granophyre and association with abundant volcanic rocks led Denison (1981) to draw parallels with the much younger (early Cambrian) granites and rhyolites of the Wichita Mountains in southwestern Oklahoma. In contrast to the Cambrian suite, however, Denison noted that mafic rocks (basalts, diabases, gabbros) appear to be essentially absent in the northeastern Oklahoma basement. Additionally, it is worth pointing out that while the Spavinaw Granite Group has some textural similarity to the Wichita Granite Group, it is mineralogically distinct. Using the modal analyses of Merritt (1960) and Denison (1981), and modern classifications (Le Maitre, 2002), it is evident that the Spavinaw Granite Group mostly consists of monzogranites and syenogranites, with only a few alkali feldspar granites (Fig. 2). In contrast, modal analyses from the Wichita granites (e.g., Ham et al., 1964) universally plot as alkali

feldspar granites; they are also typically richer in quartz than the Spavinaw group. Notably, the textural descriptions provided by Denison (1981) for low-plagioclase samples of the Spavinaw Granite Group more closely resemble the Osage Microgranite and/or rhyolites of the Washington Volcanic Group than they do the rest of the Spavinaw Group; their inclusion seems to have been based on geography.

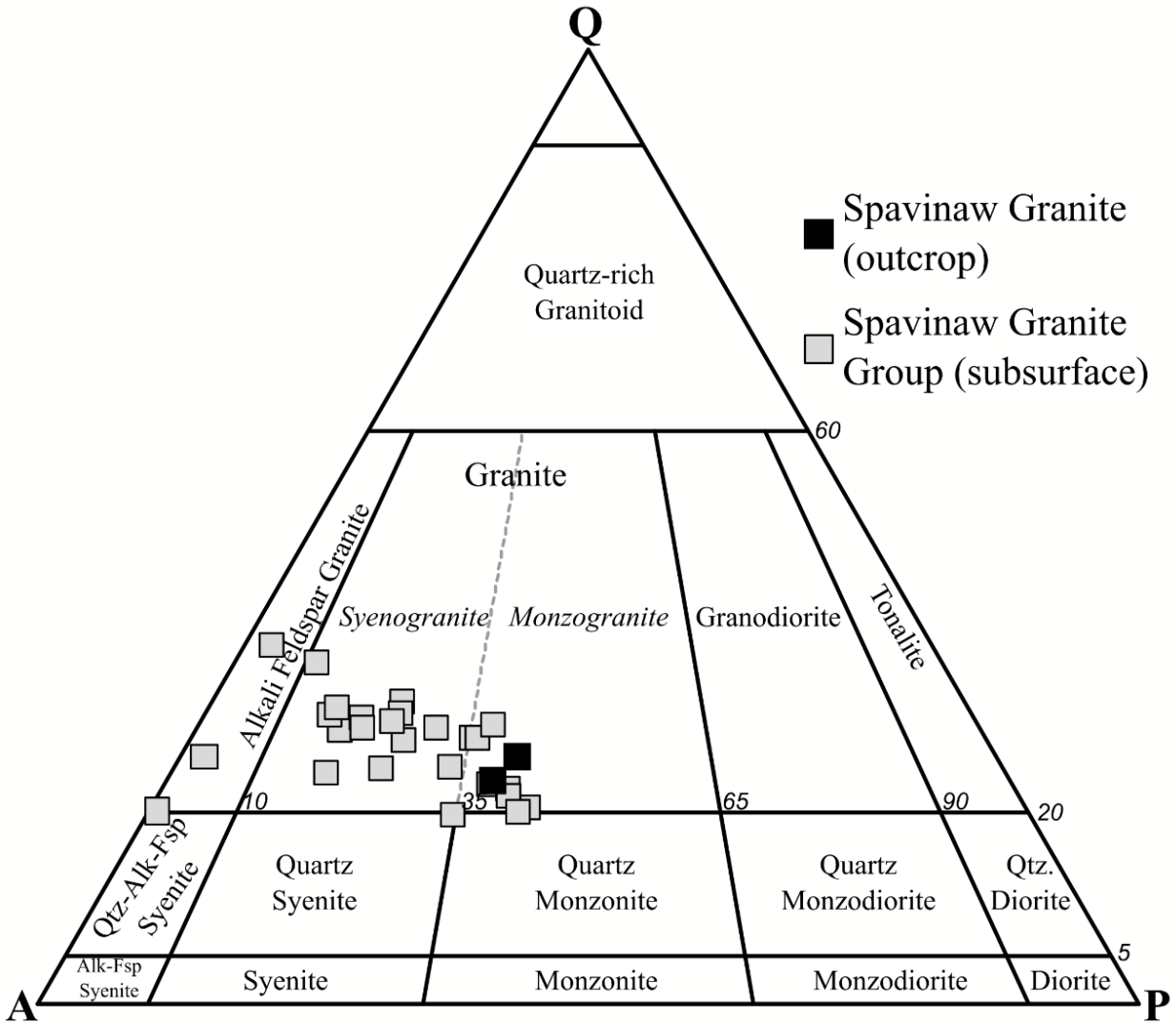


Figure 2. Classification of the Spavinaw Granite Group using the Quartz-Alkali Feldspar-Plagioclase scheme (Le Maitre, 2002 after Streckeisen, 1976). Modal analyses from Spavinaw outcrop (Merritt, 1960; Denison, 1981) as well as subsurface samples (Denison, 1981). Modal proportions calculated assuming granophyric groundmass proportions of 60% alkali feldspar, 40% quartz (Barker, 1970).

METHODS AND MATERIALS

Two blocks of Spavinaw Granite were taken from the outcrop along Spavinaw Creek by Stacey Evans of the Oklahoma Geological Survey. These blocks were oriented in the field with a Brunton compass and brought back to the University of Oklahoma, where a drill press with a water-cooled, nonmagnetic coring bit was used to extract specimens for paleomagnetic analysis. These specimens were cut into cylinders of 2.5 cm diameter and approximately 2.1 cm length. A small number of petrographic thin sections were prepared from an unoriented sample obtained at the same outcrop.

Magnetic susceptibility and anisotropy of magnetic susceptibility (AMS) were measured with a MFK1 Kappabridge using a 200 A/m alternating current magnetic field with a frequency of 976 Hz. The AMS data were analyzed using Anisoft 5.1 software available from AGICO Inc. Remanent magnetizations were measured using a 2G cryogenic magnetometer housed in a magnetically shielded room. Specimens were progressively stepwise demagnetized. Alternating field (AF) demagnetization proceeded in 10 mT steps to a maximum of 120 mT for most specimens; some were treated up to 150 mT. For thermal treatments, samples were baked in a magnetically shielded oven between measurements. Temperature steps varied, with intervals of 50 °C up to 300 °C, then intervals of 25 °C until reaching 500 °C. Above 500 °C, temperature intervals of 20 °C were used until a maximum temperature of 680 °C, at which point no samples retained a coherent magnetization.

Additional rock magnetic experiments were performed at the Institute for Rock Magnetism (IRM) at the University of Minnesota. Room-temperature hysteresis and backfield remanence curves were measured using Princeton Instruments and Lake Shore vibrating sample magnetometers (VSMs). VSM data were processed using in-IRM software with nonlinear slope

corrections for hysteresis loops (Jackson and Sølheid, 2010). High-temperature magnetic susceptibility (up to 700 °C) was measured using a KLY-2 Kappabridge with an applied field amplitude of 300 A/m at a frequency of 300 Hz. Samples were measured during heating to 350 °C, cooling to 50 °C, re-heating up to 700 °C and final cooling to ~50 °C. Low-temperature remanence cycles used a Quantum Design MPMS3 in VSM mode. for low-temperature remanence cycling. A 2.5 Tesla saturation isothermal remanent magnetization (SIRM) was applied at room temperature and remanent magnetization was measured continuously during cooling to 10 K and warming back to 300 K.

One small specimen from each of two subsurface cores of the Spavinaw Granite Group, the AMAX SP-1 and the Eagle-Picher 43-C Anna Beaver (Fig. 1) was also measured for magnetic susceptibility and natural remanent magnetization intensity. These specimens were irregularly shaped and unoriented, and therefore were only measured for bulk properties. Hysteresis and backfield remanence measurements were also made on a specimen of the SP-1.

RESULTS

Petrographic Observations

The petrography of the Spavinaw Granite has been well-documented by previous workers (e.g., Merritt, 1960; Denison, 1981) and this study offers little beyond their observations. In outcrop, the rock is pink to red, much like the granites of the Wichitas (Fig. 3A). In thin section, the rock contains numerous phenocrysts of plagioclase and alkali feldspars along with chlorite, hornblende, and opaque minerals which have been reported to be magnetite (Hawes, 1952; Merritt, 1960). Apatite is also present. Phenocrysts are set in a granophyric groundmass of quartz and alkali feldspar (Fig. 3B-D). Granophyric intergrowths account for the vast majority of quartz, though some free quartz is present. Quartz commonly has slightly undulose extinction.

Evidence for alteration is abundant. Virtually all of the feldspars have been altered to some degree and have prominent red to brown “dusting” in thin section (Fig. 3B, C). Iron oxides occur along grain boundaries and fill in microscopic fractures (Fig. 3C). Abundant chlorite is present as a replacement product of primary hornblende and possibly biotite as well; opaque minerals and titanite commonly co-occur with chlorite as additional replacement minerals. Plagioclase is commonly at least partially altered to epidote and/or sericite (Fig. 3D) and sometimes carbonate. Epidote appears in a variety of forms in this rock – Merritt (1960) considered epidote to be an alteration of hornblende, though in the thin sections investigated here it seems to occur mainly as an alteration of plagioclase and as either a magmatic or early hydrothermal mineral in patches with a more pegmatitic texture. Magnetite grains are commonly rimmed by fine-grained titanite. Traces of violet fluorite were also found in one thin section as a partial replacement of feldspar.

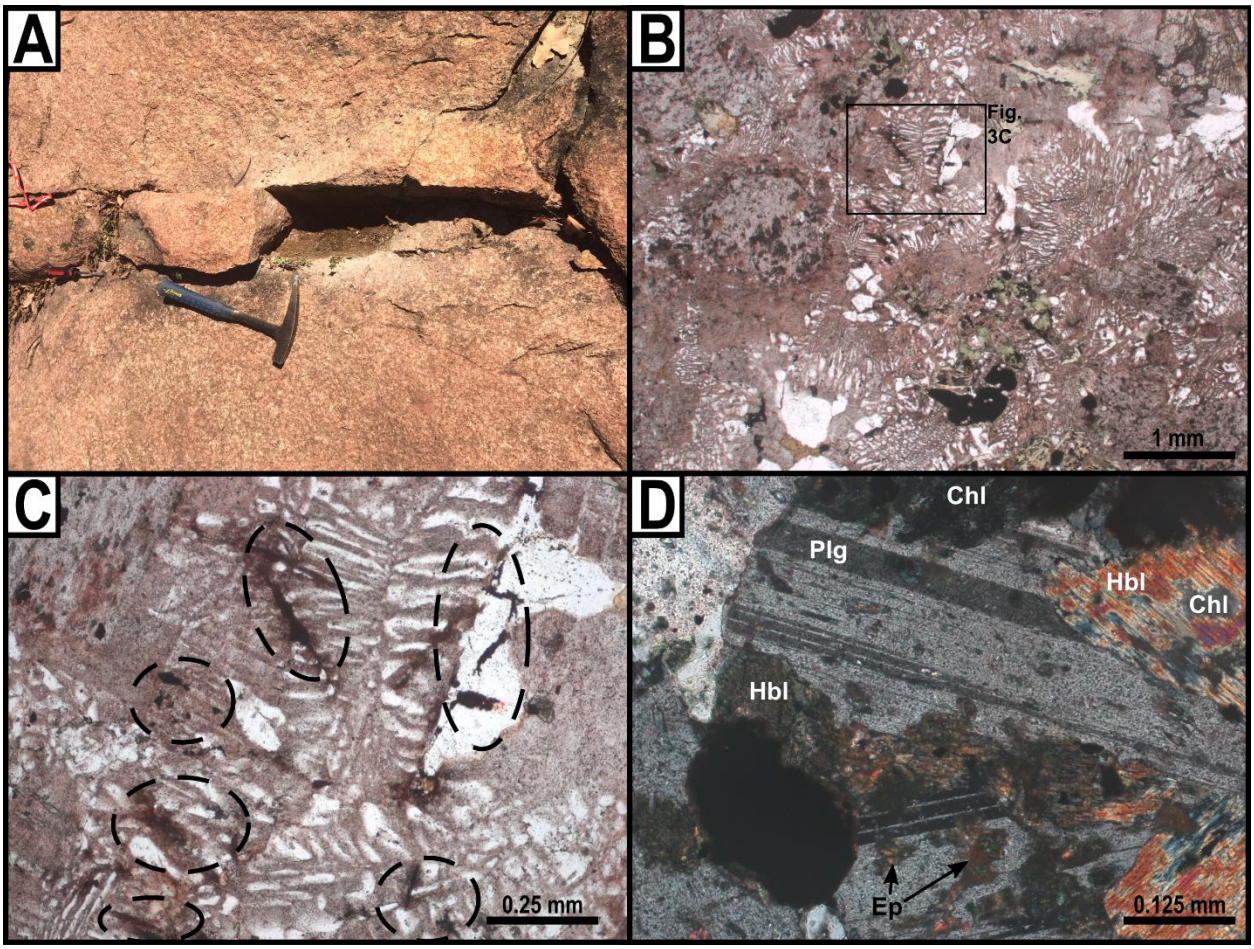


Figure 3. Petrographic character of the Spavinaw Granite. (A) The Spavinaw Granite in outcrop. Photo by Stacey Evans. (B) Typical view of Spavinaw Granite in thin section, plane light. Note darkened feldspars, granophyric texture, abundant opaque minerals and green chlorite. Inset box is area of Fig. 3C. (C) Iron oxides (selected grains circled) dusting feldspars and filling microcracks, plane light. (D) Alteration of hornblende (Hbl) to chlorite (Chl) and plagioclase (Plg) to epidote (Ep) and sericite, cross-polarized light. Also note fine-grained rim of high-birefringence material surrounding the opaque grain in the lower left– this is secondary titanite/sphene.

Bulk Magnetic Susceptibility and Anisotropy

Average mass-normalized magnetic susceptibility (χ) values are 9.94×10^{-6} m^3/kg for specimens from the first block (SPV-1) and 9.74×10^{-6} m^3/kg for the second (SPV-2). Volume-normalized values (K), assuming a density of 2.69 g/cm^3 (the average of values reported for the outcrop by Denison, 1981), are 2.67×10^{-2} SI and 2.62×10^{-2} SI respectively. These are comparable to susceptibility values reported by Denison (1981), slightly higher than those reported by Spall

and Noltimier (1972), and about twice the average reported by Hawes (1952). The sample from the AMAX SP-1 has a value of $6x10^{-6}$ m^3/kg / $1.6x10^{-2}$ SI, slightly lower than reported by Denison (1981). The specimen from the Eagle-Picher 43-C has a notably lower value of $1.49x10^{-6}$ m^3/kg ($3.95x10^{-3}$ SI); no prior magnetic data for this core were found.

AMS is represented by a second-rank tensor, which is commonly described by the directions of the principal axes and scalar factors describing the shape and magnitude of the resulting ellipsoid. This study uses the scalar factors P_j and T of Jelínek (1981). The corrected anisotropy degree P_j is calculated in order to incorporate the contribution of the intermediate principal axis of susceptibility and can range from 1.0 to infinity. The shape factor T represents the shape of the susceptibility ellipsoid and ranges from -1 to 1, with more negative values corresponding to prolate (lineation-dominant, cigar/rod-shaped) susceptibility ellipsoids and more positive values corresponding to oblate (flattened, disc-shaped) ellipsoids and T near 0 corresponding to neutral/triaxial shapes (Jelínek, 1981).

The AMS fabric for both blocks is relatively weak but consistent. The mean susceptibility tensor for block SPV-1 has a corrected degree of anisotropy value (P_j) of 1.014 (i.e., a 1.4% anisotropy) and a shape factor (T) of 0.435 which corresponds to a triaxial-oblate fabric. Block SPV-2 has a P_j value of 1.011 and a T value of 0.417. There is no relationship between the susceptibility and degree of anisotropy in individual specimens of either block, nor is there a relationship between P_j and the shape factor T. Susceptibility, degree of anisotropy, and shape factor of individual specimens have very similar values and distributions for both blocks (Fig. 4). The low values of anisotropy are still significant – the control software performs a statistical F-test of anisotropy during the measurement process, and the manufacturer recommends only considering samples with F-values greater than 5. The minimum F-value obtained was 983.

The principal susceptibility axes from both blocks show streaking of the maximum and intermediate (K_1 and K_2) axes, with a clustered minimum (K_3) axis that is more clustered but slightly elongated in the direction of K_2. This represents a fabric intermediate between oblate and triaxial in shape – a well-defined plane of foliation formed by the minimum and intermediate axes is characteristic of oblate fabrics, while in triaxial fabrics it is typical for both K_1 and K_3 to be elongated in the direction of K_2 (Tarling and Hrouda, 1993). For both blocks, the minimum susceptibility axis is shallowly inclined and plunges to the southeast at an angle of 28° for SPV-1 and 5° (within error of horizontal) for SPV-2. The K_3 plunge directions for SPV-1 and SPV-2 are very similar (142° and 146°, respectively) as are the strikes of magnetic foliation (233° and 236°) (Fig. 4). The primary difference is the degree of plunge – the foliation plane is inclined by 62° for SPV-1, while it is nearly vertical for SPV-2. Bulk susceptibilities are given in Table 1, the principal susceptibility axis orientations and scalar anisotropy parameters are given in Table 2. Two specimens with anomalous data from SPV-1 and six from SPV-2 were disregarded as outliers.

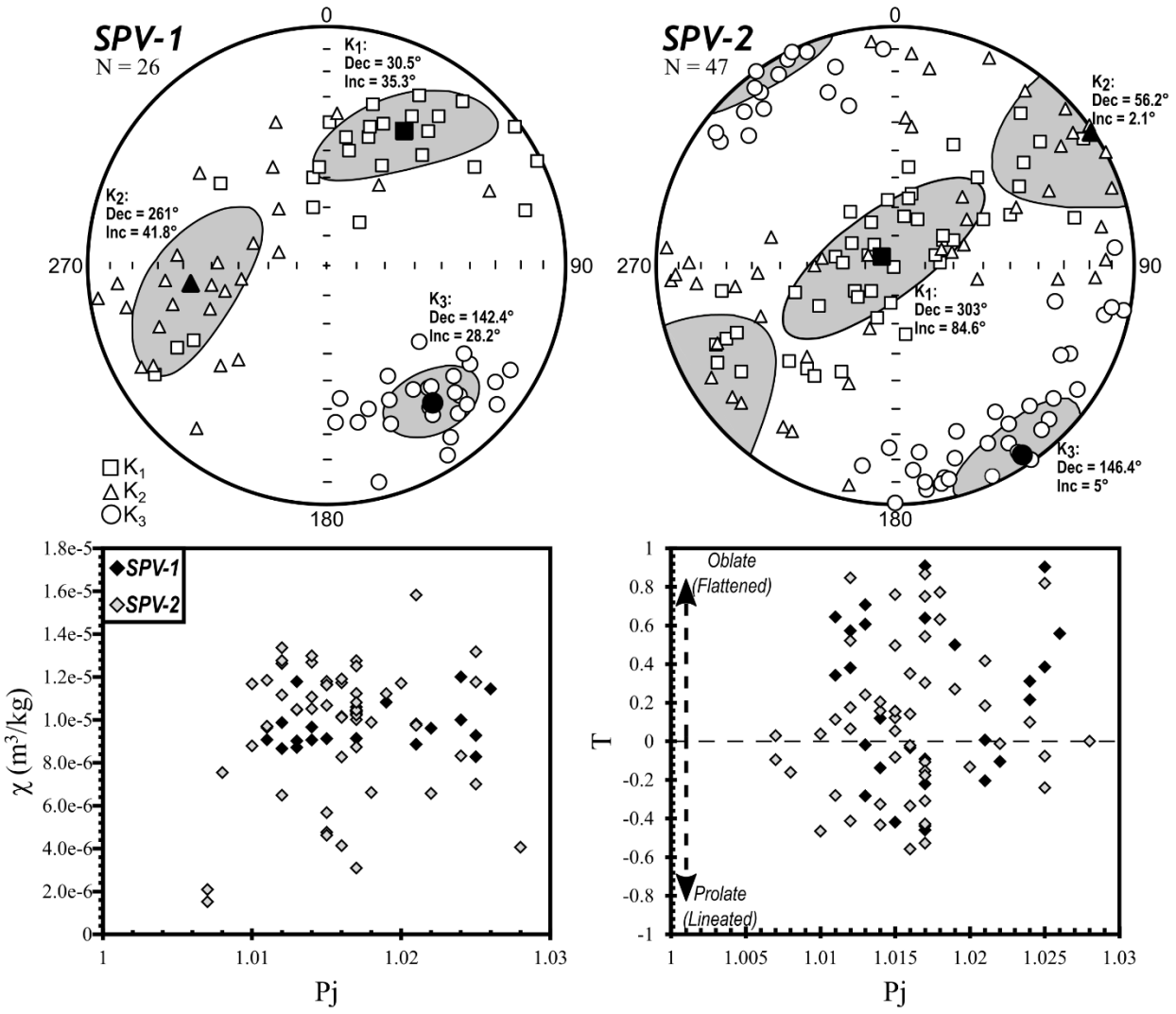


Figure 4. AMS of the Spavinaw Granite. (Top) Lower-hemisphere equal-area projections of principal susceptibility axes of individual samples as well as those of the mean tensor, with mean tensor confidence ellipses shaded. (Bottom) Plots of mass-normalized susceptibility vs. degree of anisotropy (left) and shape factor vs. anisotropy (right) for individual specimens. No correlation is evident in either plot, and there is little difference between the two granite blocks.

High-Temperature Susceptibility

Susceptibility increases during warming at lower temperatures, and notable "bumps" are present when heating from ~150 to 450 °C (Fig. 5). Some susceptibility is permanently lost on cooling, and the bumps reappear during the second heating cycle with another permanent reduction in susceptibility after cooling from 700 °C. Susceptibility is almost completely lost before 600 °, and inspection of its temperature-derivative indicates the maximum loss rate occurs

at 576 ℃ for the SPV-1 sample and 566 ° for the SPV-2 one (Fig. 5, right), close to the Curie point for magnetite. A local minimum just above 80 ℃ is also seen in the derivative curves for both specimens which may indicate a minor presence of the yet-unidentified phase responsible for unusual field-dependence behavior in subsurface rocks from the area (See Chapter 4), though this accounts for less than 1% of the total susceptibility.

The humps seen during heating between 150 and 450 ℃ are typically interpreted as a consequence of partially-oxidized (i.e., maghemitized) magnetite (Özdemir and Dunlop, 2010). The initial rise is due to thermal annealing of stresses between the more-oxidized outer shell and the less-oxidized core of magnetic grains, while the subsequent irreversible decrease is due to inversion of maghemite to hematite (Kontny and Grothaus, 2017; Bilardello, 2020). The irreversible losses are substantially higher in the SPV-1 sample (≈28%) compared to SPV-2 (≈5%). The SPV-2 sample also yielded a local peak in susceptibility just below the Curie point which is absent in the SPV-1 data; this is likely a "Hopkinson peak" generated by thermal activation of very fine-grained magnetite (e.g., Dunlop, 2014).

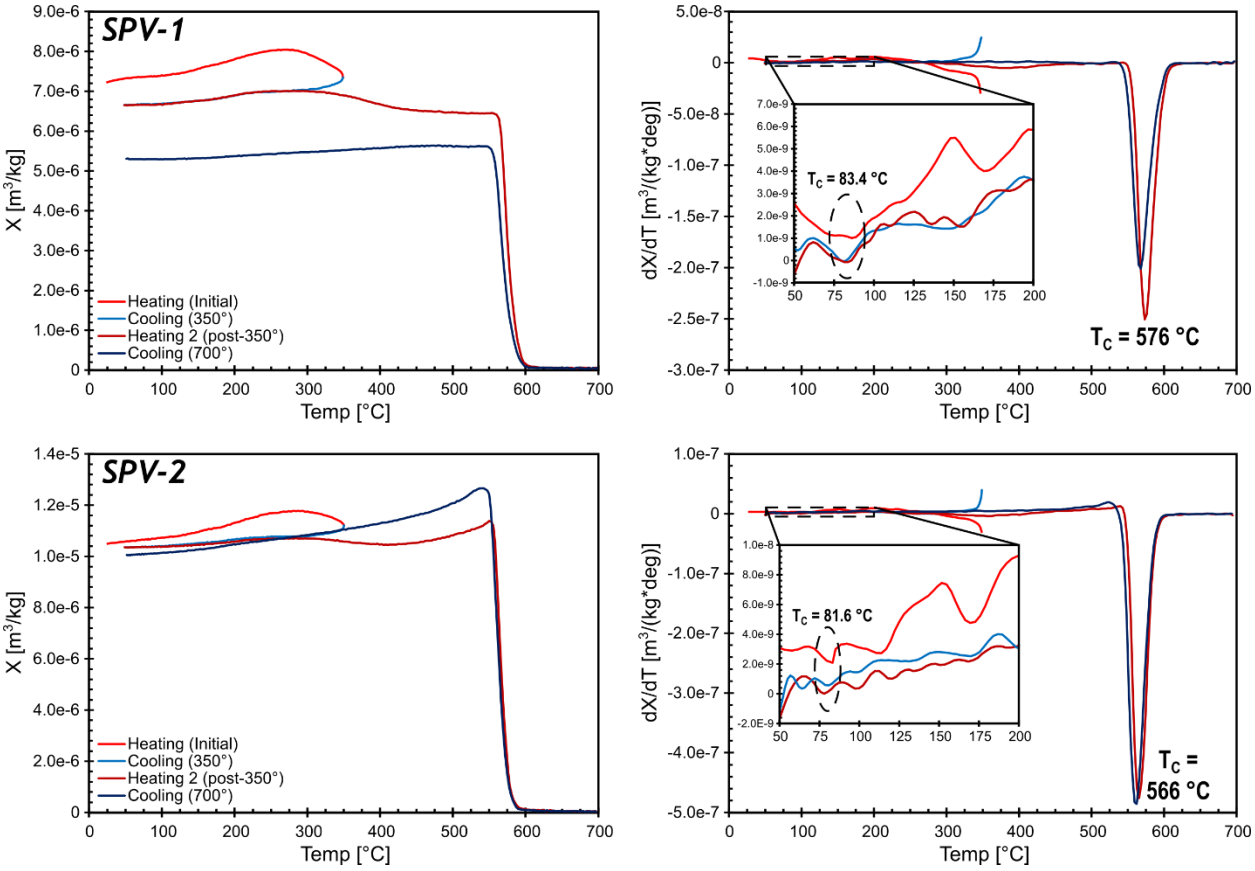


Figure 5. High-temperature magnetic susceptibility behavior of Spavinaw Granite samples. Plots on left are direct measurements of susceptibility as a function of temperature. Plots on right are the temperature-derivative of susceptibility, used to identify Curie temperatures (T_C).

Hysteresis

Samples of Spavinaw Granite yield hysteresis loops which have fairly low coercivities (Bc = 4.5 to 5.5 mT), are effectively saturated at fields of ~300 mT, and show little high-field paramagnetic contribution (less than 1%) relative to their ferromagnetic response (Fig. 6). Saturation remanence (Mr) values are on the order of 20-30 mA*m^2/kg for outcrop specimens and 50 mA*m^2/kg for one from the AMAX SP-1 core; saturation magnetization (Ms) values are some 20-25 times higher.

Backfield data indicate coercivity of remanence (Bcr) values of 40-50 mT for outcrop specimens and <20 mT for the subsurface sample. The derivative of backfield remanence with respect to the logarithm of applied field shows moderately broad coercivity distributions with

peaks of 20-30 mT in outcrop samples and just over 10 mT from the SP-1. The distribution in the SPV-2 sample is noticeably broader than the other two. Both outcrop samples still have reasonable populations with coercivities above 100 mT, while almost all remanence is gone from the core sample at that point. The SPV-2 and core samples both show a higher proportion of very low-coercivity (1-5 mT) behavior relative to the SPV-1 outcrop sample.

Hysteresis loop shape can be quantified using the σ_{hys} parameter in order to make inferences about the domain state of the magnetic mineralogy (Fabian, 2003). Loops from the outcrop samples yield values of σ_{hys} from 0.01-0.03, indicating they are essentially undistorted. The SP-1 sample yielded σ_{hys} = -0.14, indicating that its loop is very slightly "potbellied". Potbellied loops may originate from either mixtures of superparamagnetic (SP) grains with larger grains or from mixtures of independent coercivity distributions (e.g., Fabian, 2003). Given the lack of distinct populations in the backfield data as well as the presence of abundant SP material higher up in the core (Chapter 4), the former hypothesis seems more likely. The low ratios of Mr to Ms and the high ratio of hysteresis median destructive field (Brh) to coercivity of remanence (Bcr) are characteristics consistent with loops dominated by multidomain magnetic material (Dunlop and Özdemir, 1997; Fabian, 2003), though the population of coercivities from 30-100+ mT seen in the backfield coercivity distribution would seem to require a significant additional contribution from stable single-domain grains (Dunlop and Özdemir, 1997).

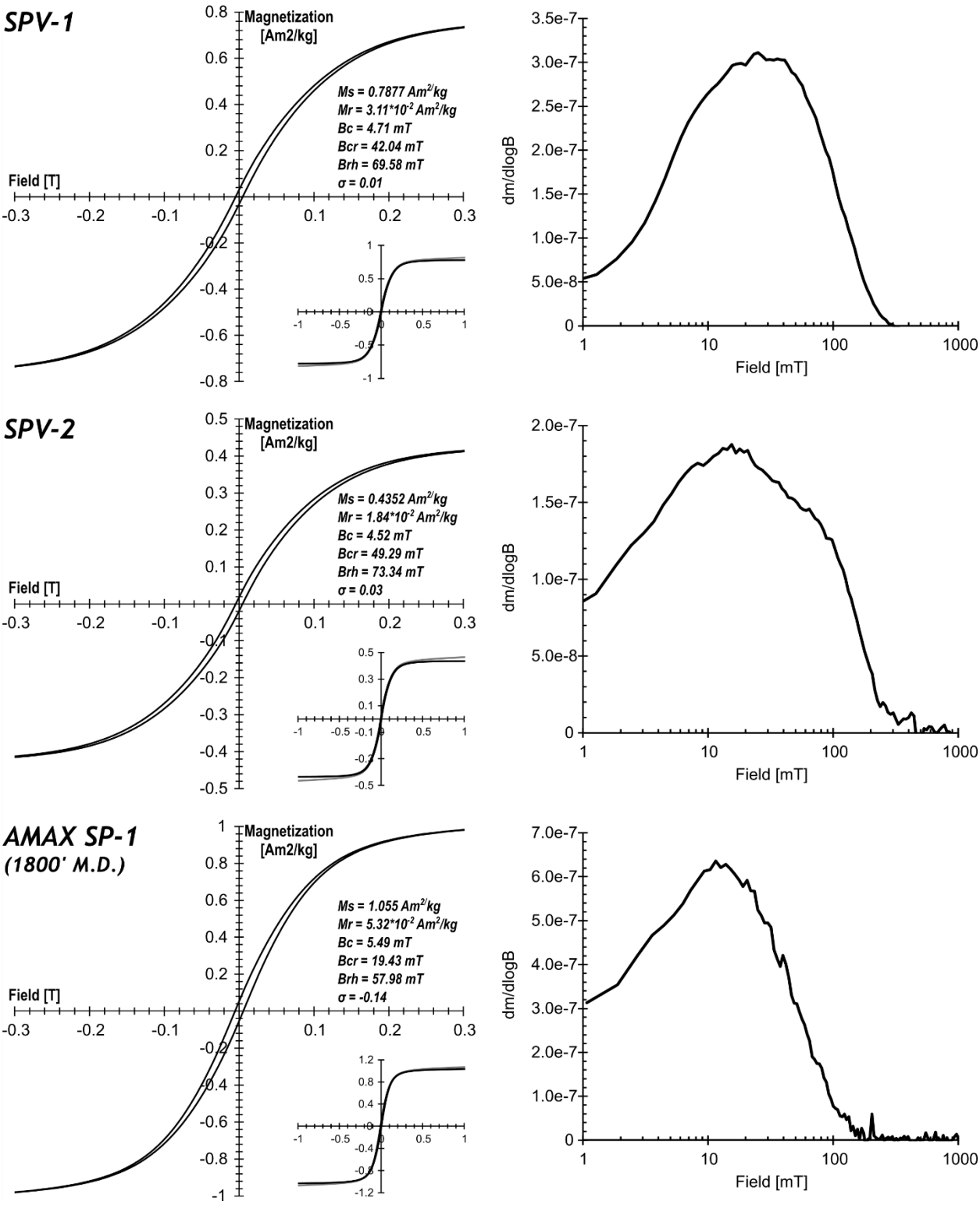


Figure 6. Hysteresis measurements of Spavinaw Granite Samples. Left: Mass-normalized, slope-corrected hysteresis loops and calculated parameters. Inset plots on lower right show data before (gray) and after (black) slope correction out to fields of 1 Tesla. Right: Derivative (un-normalized, smoothed using a 3-point moving average) of VSM backfield remanence with respect to log of applied field illustrating coercivity distributions.

Low-Temperature Remanence Cycling

During cooling of room-temperature SIRM, samples from both blocks demagnetize at very similar rates until reaching ~125 K, just below the isotropic point of magnetite (Fig. 7). Below this temperature, the SPV-1 sample continues to demagnetize smoothly and equilibrates just below 100 K. The SPV-2 sample begins to demagnetize more gradually and pauses its demagnetization between ~105-100 K, then continues demagnetization and equilibrates at ~85 K. Both samples equilibrate at ~34% of their initial magnetization at low temperatures.

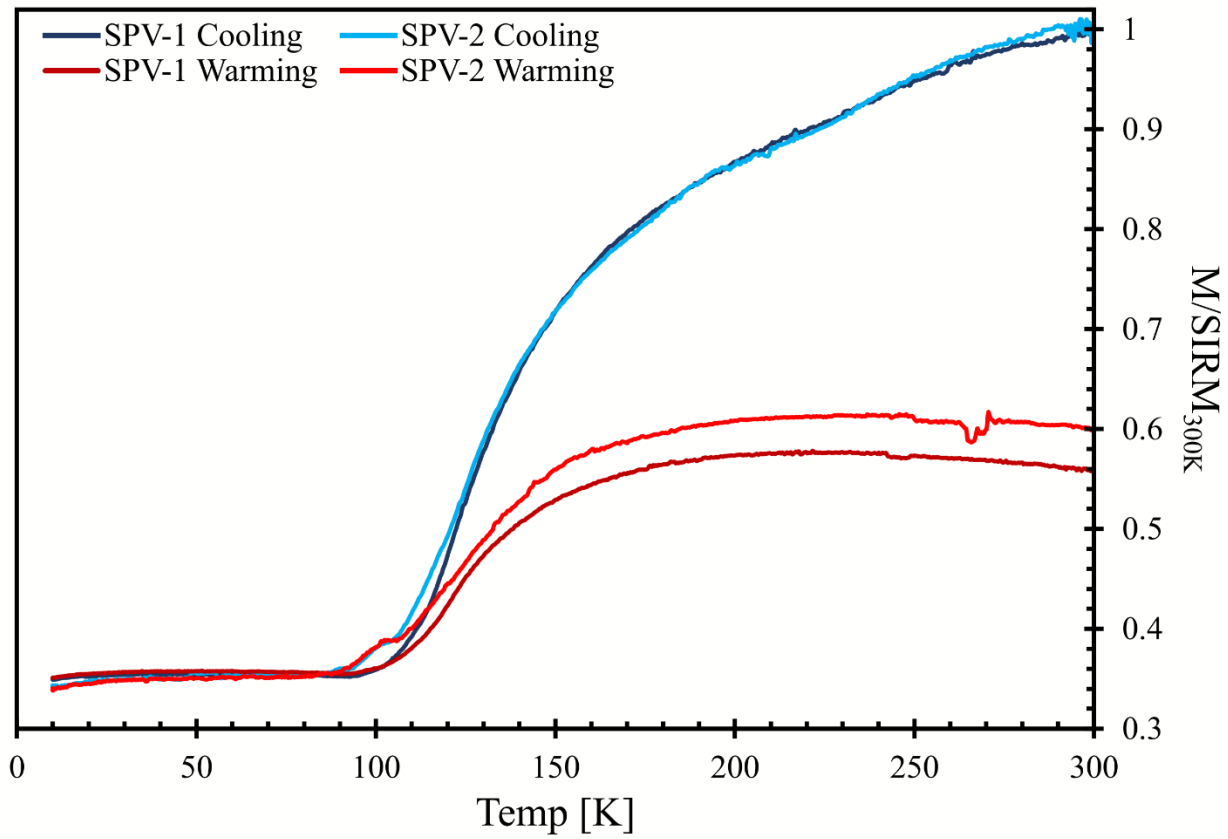


Figure 7. Low-temperature cycling of room-temperature saturation remanence. Values are normalized to initial intensity of RTSIRM. Noisy intervals may be due to particle motion caused by operating the instrument in VSM mode. Note step features in SPV-2 data and slight downward curvature of both warming curves.

During warming, remanence begins to increase in both samples at roughly the same temperatures at which they equilibrated on cooling. The two-step feature seen in the SPV-2

cooling curve is also present in the warming curve. Upon reaching 300 K, magnetization has recovered to 56% of its original value in the SPV-1 sample and 60% in the SPV-2. Both warming curves have a slight hump shape, which may be due to the presence of maghemite (Özdemir and Dunlop, 2010).

Paleomagnetic Results and Interpretations

Natural remanent magnetization (NRM) intensities are quite high, averaging 2.06×10^{-3} Am^2/kg for SPV-1 and 2.8×10^{-3} Am^2/kg for SPV-2. These values are roughly half the average (but are well within the range) documented by Spall and Noltimier (1972). NRM directions for each block were well-grouped, with a southwesterly and shallow down direction for block SPV-1 and southeasterly and moderately steep down for SPV-2. This is in stark contrast to the previous studies, which reported essentially random directions even for subspecimens from the same core samples. NRM intensities were combined with the susceptibility measurements to calculate the ratio of the remanent magnetization to that induced by the Earth's ambient field (the Koenigsberger ratio, Q') for comparison with previous studies. Block SPV-1 has an average Q' value of 5.11 (range from 4.68 to 5.74) while SPV-2 has an average Q' of 6.57 (range from 5.26 to 10.52). The sample from the Eagle-Picher 43-C core showed a Q' value of 13.4 and the one from the AMAX SP-1 has a Q' of 1.9. For comparison, Hawes (1952) reported an average Q' of 25.4, while Spall and Noltimier (1972) reported average Q' of 3.7 for specimens with downward inclinations and 12.1 for those with upward inclinations.

Similar to the observation of Spall and Noltimier (1972), remanent directions changed relatively little over the course of progressive demagnetization. Use of automated principal component analysis (Kirschvink, 1980) nearly always results in a single component from approximately 200 °C or 10 mT to the origin unless a very restrictive maximum angular

deviation (MAD) cutoff is used. Despite the subtle but visually apparent changes in the decay directions, automated PCA does not detect the changes unless a MAD cutoff of 1° is used, at which point it attempts to break the magnetization into multiple 3-point components. Consequently, components of the remanent magnetization were chosen manually. The highest MAD value of any of the chosen components is 5.1°; the vast majority are less than 3° and several are less than 1°. NRM intensities and Q' values are given in Table 1, mean magnetic component directions and the computed virtual geomagnetic poles are given in Table 2. Mean directions, precision parameters (k) and confidence intervals of magnetization components were calculated after Fisher (1953).

An unstable component was removed in samples from both blocks by 20 mT of applied alternating field (AF) demagnetization or thermal treatment to 250 °C (Fig. 8A, B). Both blocks show similar intensity decay profiles regardless of demagnetization method, though SPV-2 loses a slightly larger amount of its intensity at lower treatments (Fig. 8C). Analysis of AF demagnetization trends shows a subtle (8-10°) steepening of inclination starting at 60-80 mT applied fields for SPV-1, while in SPV-2 there is a 15-20° counterclockwise shift in declination in the same field range (Fig. 8B). Confidence intervals for low-field (20 to 60-80 mT) and high-field (60-80 mT +) components do not overlap for either block (Fig. 8D).

In order to test whether differing magnetic components were carried in magnetite vs. hematite, magnetic components from thermal demagnetization sequences were independently chosen for temperatures up to 580 °C (likely to be dominated by magnetite) and for temperatures from 600 to 680 °C (above the magnetite Curie temperature and most likely carried by hematite) (Fig. 8A). In both blocks, the confidence intervals of the sub-580° and supra-580° directions significantly overlap each other and they therefore do not likely represent separate components.

Confidence intervals of thermally-determined components do however overlap those of both apparent AF components (Fig. 8D; Table 2).

Table 1: Bulk magnetic properties of the Spavinaw Granite Group				
	SPV-1 Average	SPV-2 Average	AMAX SP-1 1802' Depth	EP 43-C 1638' Depth
χ (m^3/kg)	9.940×10^{-6}	9.741×10^{-6}	5.996×10^{-6}	1.485×10^{-6}
NRM (Am^2/kg)	2.062×10^{-3}	2.798×10^{-3}	4.545×10^{-4}	7.965×10^{-4}
Q'	5.11	6.57	1.89	13.41

Table 2: Directional magnetic properties of Spavinaw Granite outcrop samples

AMS Mean Tensor

			Dec.	Inc.	Conf. Ellipses
SPV-1	P_j = 1.014	K_1	30.1	35.3	33.4/12.5
	T = 0.435	K_2	261.0	41.8	33.4/15.1
	N/N_0 = 26/28	K_3	142.4	28.2	15.4/12.1
SPV-2	P_j = 1.011	K_1	303.0	84.6	42.0/14.8
	T = 0.417	K_2	56.2	2.1	42.0/18.9
	N/N_0 = 47/53	K_3	146.4	5.0	19.1/14.7

Remanence Directions

		In Situ		*Tilt-Corrected*				
		Dec.	Inc.	Dec.	Inc.	α_{95}	k	N/N_0
SPV-1	AF (low)	239.6	9.9	239.5	7.2	5.6	116.6	7/7
	AF (high)	248.2	18.8	247.7	16.3	5.5	107.5	7/7
	Thermal (≤580 °C)	244.6	16.4	245.4	10.7	4.2	209.1	7/7
	Thermal (≥600 °C)	245.8	24.6	247.0	9.5	7.6	63.4	7/7
SPV-2	AF (low)	134.2	41.2	138.0	45.5	3.8	188.3	9/9
	AF (high)	117.3	39.6	119.7	45.0	3.2	263.8	9/9
	Thermal (≤580 °C)	122.6	39.7	126.1	43.7	5.1	168.8	7/7
	Thermal (≥600 °C)	128.0	41.3	132.4	46.3	5.0	202.1	6/7

Virtual Geomagnetic Poles

		In Situ		*Tilt-Corrected*		
		Lat. (°N)	Lon. (°E)	Lat. (°N)	Lon. (°E)	α_{95}
SPV-1	AF (low)	-20.7	198.3	-21.7	197.3	3.3
	AF (high)	-11.2	196.1	-12.5	195.4	3.4
	Thermal (≤580 °C)	-14.9	197.6	-16.0	195.0	2.4
	Thermal (≥600 °C)	-10.3	200.3	-11.8	197.2	4.7
SPV-2	AF (low)	16.0	128.0	15.2	123.0	4.2
	AF (high)	6.6	140.6	5.3	136.2	3.5
	Thermal (≤580 °C)	11.0	136.9	10.0	132.5	5.7
	Thermal (≥600 °C)	13.3	134.3	12.0	126.8	6.0

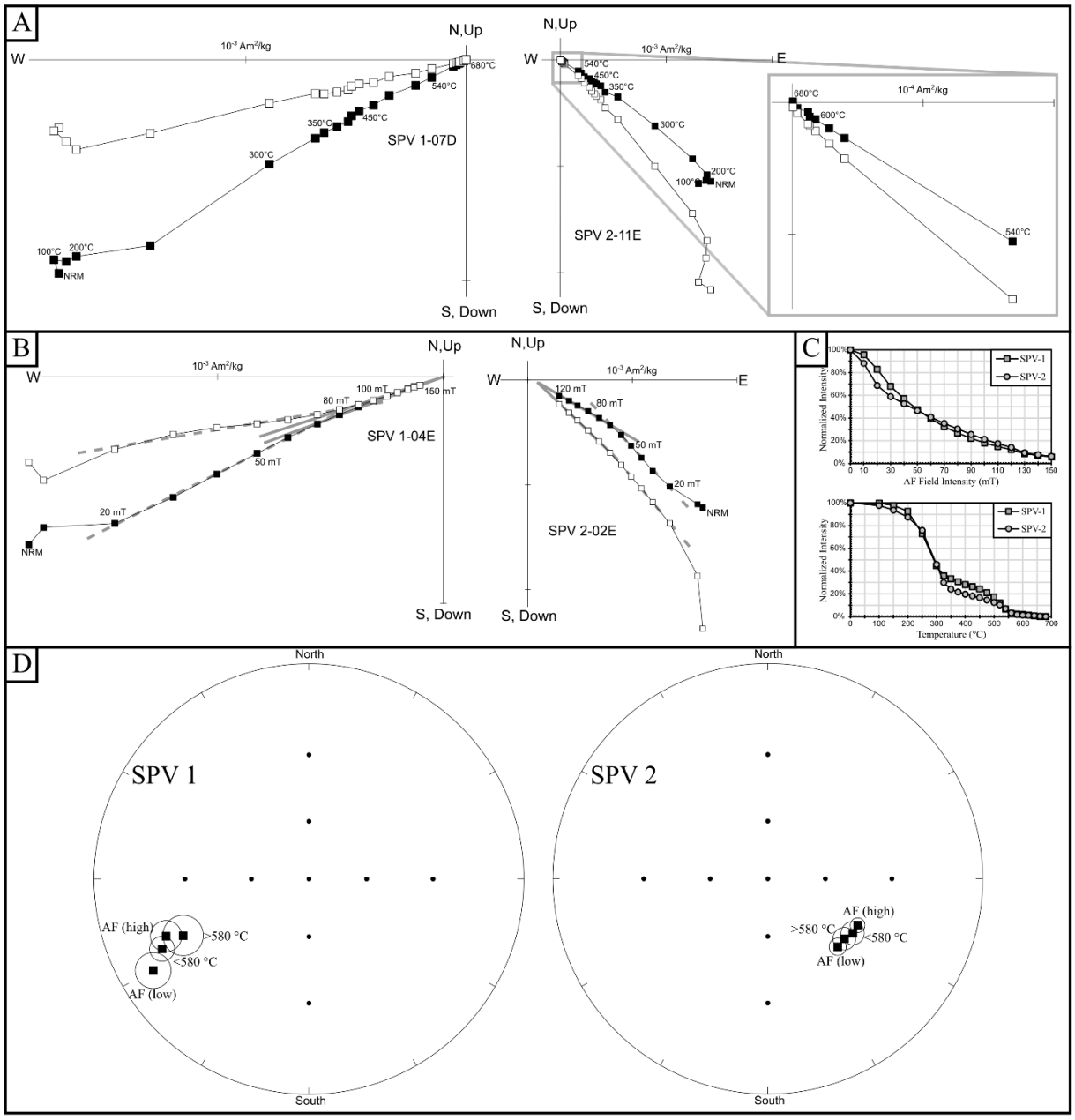


Figure 8. Demagnetization analysis of the Spavinaw Granite. (A) Orthogonal projection diagrams, aka "Z-plots" (Zijderveld, 1967) of thermal demagnetization. Inset on right shows continued decay to 680°C. (B) Z-plots for AF demagnetization, showing low-field (20 to 60-80 mT, dashed grey lines) and high-field (>60-80 mT, solid grey lines) components Left plots in A, B are specimens from SPV-1; plots on right are from SPV-2. (C) Averaged magnetic decay profiles for both blocks demonstrating similar decay behavior. (D) Equal-area projections of in-situ magnetic components identified for each block. Low-field and high-field AF components have non-overlapping confidence intervals; thermal components are not statistically distinct from one another and overlap both AF components.

The directions for each specimen were used to calculate virtual geomagnetic poles (VGPs) and the mean VGPs were compared to the Phanerozoic apparent polar wander path (APWP) for North America (Torsvik et al., 2012) to check for the possibility of Phanerozoic remagnetization of the granite. VGPs were calculated for both the in-situ remanence directions as well as directions which were adjusted for the approximate tilts reported by Ireland (1930) and Huffman (1958). These tilts are slight, and had relatively little influence on the results – most VGPs were shifted a few degrees west and very slightly southward (Fig. 9). For initial analysis, the four components previously calculated (low-field and high-field AF, sub- and supra-580 °C thermal; Table 2) were treated as independent rather than combined.

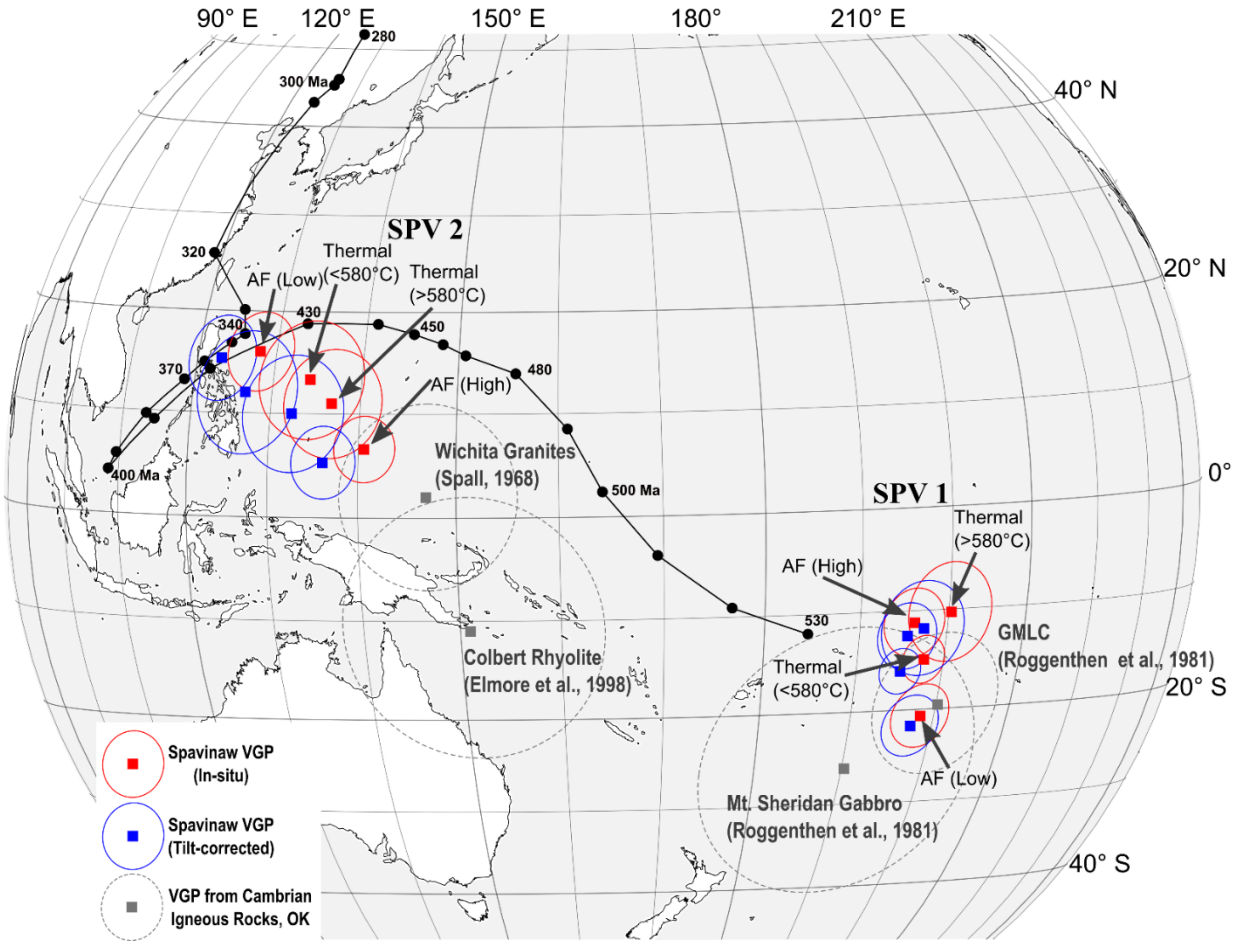


Figure 9. Virtual geomagnetic poles from in-situ and tilt-corrected directions from the Spavinaw Granite compared to the Phanerozoic apparent polar wander path for North America (drawn after Torsvik et al., 2012). Previous paleomagnetic results for early Cambrian igneous rocks of the Southern Oklahoma Aulacogen included for comparison.

The VGPs computed from remanent magnetizations identified for SPV-1 lie somewhat to the east of the oldest point (530 Ma) on the APWP and form a slight north-south streak. All four components either lie within or overlap the confidence interval of previous paleomagnetic results from the Glen Mountains Layered Complex in southern Oklahoma (Roggenthen et al., 1981).

VGPs from SPV-2 form a streak which mostly lies to the south of the Ordovician-Silurian part of the APWP, with the low-field AF component overlapping a bend in the APWP consistent with ages of either 420-430 Ma or 360-330 Ma. The high-field AF component plots

within the confidence interval of an average pole from the Wichita Granite Group in southwestern Oklahoma obtained by Spall (1968).

DISCUSSION

Observed magnetic intensities for the Spavinaw Granite are in the lower part of the ranges observed by previous workers, and susceptibility values are comparable. The samples used in the present study do not however show the extreme dispersion of directions observed by Hawes (1952) and Spall and Noltimier (1972). Instead, they show well-grouped directions (albeit different between blocks) with well-defined directional components. The variance found by previous workers could potentially be explained by the effects of lightning strikes, which induce strong intensities and can produce random directions (Dunlop and Özdemir, 1997). Lightning was discounted by Spall and Noltimier (1972), partly on the basis of these directions appearing over the spread of the Spavinaw outcrops as well as magnetic anomalies extending below sedimentary cover, but largely on the basis of a personal communication by R.E. Denison that high magnetic intensities and random directions were also characteristic of the Spavinaw Granite Group in the subsurface.

Magnetic susceptibility data were reported in publications by Denison (1966, 1981), but no measurements of intensity or directions of remanent magnetization were mentioned in his reports. The new measurements in this study confirm a high intensity in the Eagle-Picher 43-C core, though its direction could not be constrained, and a reasonable intensity (if significantly lower than the outcrop values) in the AMAX SP-1. The specimen from the SP-1 was oriented with respect to vertical and had an inclination of -79° (though it may have been upside down). This suggests that it might have been overprinted with a vertical drilling-induced isothermal remanent magnetization during the coring process (e.g., de Wall and Worm, 2001), which has

been commonly encountered in attempts by the authors to paleomagnetically evaluate multiple cores from the Washington Volcanic Group.

Average NRM intensity is approximately 7% of saturation remanence (as determined by hysteresis) for specimens from SPV-1 and 15% of saturation remanence for SPV-2. Thermal remanence in granitoids can be reasonably expected to reach 5% or more of saturation remanence, while lightning overprints usually result in NRM intensity >20% of saturation remanence (e.g., Dunlop et al., 1984). Given sample heterogeneity and the fact that absolute values of magnetic measurements are difficult to compare directly between instruments, the values from SPV-1 can be considered within expected values. SPV-2 remains uncertain, as its intensities and Q' values are lower than expected for lightning overprints but higher than expected for thermal or chemical remanence. NRM intensity for the subsurface sample is less than 1% of saturation remanence determined by hysteresis.

The magnetization of the Spavinaw Granite is most likely dominantly carried by magnetite, as approximately 85% of the magnetization is removed by alternating field treatment to 120 mT and 98% is removed by thermal treatment to 580 °C. Hawes (1952) documented that magnetic separations of crushed granite samples were able to extract 1.8% of the total weight as magnetite. Thermomagnetic measurements and reflected light petrography were considered by Spall and Noltimier (1972) to show that magnetite and hematite are the dominant carriers, with some goethite also identified petrographically. Goethite does not contribute substantially to the magnetization of the Spavinaw Granite – it has a very weak saturation magnetization relative to magnetite and is typically completely demagnetized by thermal treatment to 100 °C, which only removes approximately 1% of the initial intensity of the granite.

Rock magnetic results from this study yield a slightly different interpretation. High-temperature susceptibility and low-temperature remanence data are consistent with magnetic properties dominated by magnetite but also show a contribution from maghemite. While the overall coercivity and blocking temperature ranges of magnetite and maghemite are similar, maghemite may in some instances exhibit a higher coercivity and carry remanence to temperatures of 660 °C or more (Dunlop and Özdemir, 1997). The coercivity distributions and relatively low saturating fields determined by VSM measurements, along with the absence of Morin transitions in low-T remanence data, suggest that hematite has little if any contribution to remanence. The persistence of remanence in the Spavinaw Granite at high alternating fields and temperatures above 580 °C is therefore best explained by maghemite as a carrier.

The paleomagnetic results from the Spavinaw Granite are strikingly similar to those reported from the much younger early Cambrian rocks of the Southern Oklahoma Aulacogen. The poles calculated from SPV-1 are indistinguishable from a mean pole from the Glen Mountains Layered Complex (Roggenthen et al., 1981). The results from SPV-2 are more complicated. At high AF fields, it yields a VGP which overlaps results from the Cambrian Wichita granites (Spall, 1968). The eastward track of the SPV-2 virtual poles from their intersection with the Paleozoic APWP to their overlap with the Wichita granites can be followed further and intersects with results from Cambrian rhyolite in the Arbuckle Mountains area (Elmore et al., 1998). Recent radiometric analyses have yielded very precise dates of 530.5 Ma for some Wichita Granites, 532.5 Ma for the Glen Mountains Layered Complex, and 539 Ma for the Colbert Rhyolite in the Arbuckle Mountains (Wall et al., 2021).

The similarity of the Spavinaw results, particularly those from block SPV-1, to those from igneous rocks from the Southern Oklahoma Aulacogen strongly suggests that the Spavinaw

Granite was remagnetized during the early Cambrian. There is little direct evidence for tectonic activity in northeastern Oklahoma during the early Cambrian, as there are no known rocks of that age in the area. Sub-Arbuckle sandstones are typically assigned to the late Cambrian, though they lack fossils and therefore are poorly constrained in maximum age. There is however indirect evidence – the main axis of the Southern Oklahoma Aulacogen trends toward an azimuth of 115°/295°, which is also the primary axis of a large number of faults and diabase dikes exposed in the Arbuckle Mountains area of southern Oklahoma (Denison, 1995). This direction and another which trends approximately 60°/240°, possibly a conjugate shear, correspond to the primary orientations of seismogenic faults throughout Oklahoma as well as fractures mapped on granite outcrops in the Arbuckles and in the subsurface through seismic analysis (Kolawole et al., 2019). The same set of directions is prominent in linear aeromagnetic anomalies in northern Oklahoma (Shah and Keller, 2017), basement faults and aeromagnetic anomalies in the furthest southeast of Kansas and southwest of Missouri (Berendsen and Blair, 1991), and linear topographic features in northeastern Oklahoma and western Arkansas (Labusch, 2016).

Early Cambrian tectonism in southwestern Oklahoma has usually been interpreted as a failed rift arm from a triple junction; however, an alternative interpretation considers the aulacogen to be an intracratonic fault system parallel to a large rift transform (reviewed in Thomas, 2014). Extension alone in southern Oklahoma does not seem likely to yield significant tectonic activity as far away as the Spavinaw Granite locality. Active motions within a large regional system of transforms and transform-parallel faults such as that proposed by Thomas could however be reasonably expected to result in early Cambrian fault motions in northeastern Oklahoma. Hydrothermal activity associated with regional faulting could provide a mechanism for remagnetization of the granite.

The virtual geomagnetic poles of specimens from block SPV-2 streak between directions obtained from early Cambrian granites and rhyolites in southern Oklahoma and those consistent with later Paleozoic sections of the apparent polar wander path. The APWP has a sharp bend at 400 Ma and doubles back on itself, and the Spavinaw direction removed at low AF fields overlaps with intervals of both Silurian and Mississippian age. This is tentatively interpreted as a substantial but incomplete later Paleozoic overprint of a Cambrian remagnetization. There are large gaps in the Silurian stratigraphic record in northeastern Oklahoma, and multiple unconformities present within the Mississippian as well (Huffman, 1958), making it difficult to identify a specific event. Additional complications arise from the fact that North American paleomagnetic data from the Silurian to the early Mississippian is of rather poor quality – the running mean poles for this time interval used by Torsvik et al. (2012) have large confidence ellipses (A_{95} >20° for 410-420 Ma) and large sections are interpolated due to lack of data.

A Mississippian age is tentatively favored for the later Paleozoic remagnetization. While the bulk of Ouachita deformation is usually assigned to the Pennsylvanian, the numerous unconformities in the Mississippian suggest tectonic activity in that interval as well. Additionally, Mississippian sediments in the Ouachita Mountains of southeastern Oklahoma contain interbedded tuffs with ages in the interval from 328-320 Ma (Shaulis et al., 2012) which are considered to have erupted during pre-collisional subduction. Shaulis et al. (2012) also inferred an increase in Mississippian sedimentation rates starting at around 338 Ma, interpreted to be due to the initial stages of ocean basin closure. It seems plausible that the Spavinaw Granite records a hydrothermal response to the initial stages of the Alleghenian Orogeny that has been largely overprinted by the subsequent Ouachita-Marathon activity. The alignment of the magnetic components of SPV-2 between a likely Mississippian component and the felsic igneous

rocks of the Southern Oklahoma Aulacogen also suggests the possibility that the SOA rocks may have a similar (if less extensive) partial magnetic overprint, which could explain their divergence from the APWP. The APWP of Torsvik et al. (2012) is only constrained by a single point prior to 510 Ma (a 530 Ma pole from granites and syenites in Quebec reported by McCausland et al., 2007), however, and paleomagnetic results from the early Cambrian are an ongoing source of debate. A possible slight lightning overprint also cannot be ruled out for SPV-2.

The magnetic fabric results are somewhat tricky to interpret. The AMS of granitic rocks is usually inferred to be primarily controlled by the conditions of their emplacement (Bouchez, 1997, 2000). For epizonal sheet-like granite sills, the current interpretation for the Spavinaw Granite Group, the expected average fabric is an oblate shape with K_3 nearly vertical (e.g., Ferré et al., 1999). The fabric of the Spavinaw granite is oblate to triaxial, and K_3 is shallowly inclined to nearly horizontal. If the AMS is dominated by the rock's original emplacement fabric, this suggests that the Spavinaw Granite is dipping steeply (between 60° to subvertical) to the northwest relative to its initial orientation. The direction of inferred dip is consistent with the anticlinal Spavinaw Arch (Fig. 1) interpreted by Denison (1966, 1981). The strike of the magnetic foliation is quite similar to one of the major basement fault/lineation directions, and the granite may well be tilted along one of those faults. Interestingly, if the AMS fabric is used as a pseudo-tilt correction for the paleomagnetic data of SPV-1, the resulting direction is still compatible with early Cambrian remagnetization due to the similar directions of the declination of the magnetic component and the strike of magnetic foliation.

Alternatively, the Spavinaw Granite outcrop may have instead been intruded as a steeply-dipping dike, and the AMS may simply record the plane of the dike. If this is the case, it then suggests that the structural trends noted in the basement rocks date back to at least the time of

emplacement (~1,370 Ma). This is consistent with interpretations that a certain percentage of the diabase dikes in the Arbuckle Mountains area date to the Mesoproterozoic (e.g., Denison, 1995), though the actual ages are poorly constrained and at least most are now thought to be Cambrian. Additionally, the structural features inferred by Denison (1966, 1981) do not suggest that any of the basement rocks should be tilted so steeply.

AMS fabrics of rocks are also affected by and commonly used to study deformation. Some work has been done on modeling the effects of post-emplacement deformation on the AMS of granites. Unfortunately, virtually all the well-developed models are based on so-called paramagnetic granites, which essentially lack magnetite and have magnetic fabrics controlled by the alignment of paramagnetic minerals such as biotite, chlorite and amphiboles. For ferromagnetic granites (those with significant magnetite), the AMS fabrics are instead typically controlled by shape alignments of magnetite, and the theoretical models are rather poorly developed. While amphibole and chlorite are present, the Spavinaw Granite is definitely of ferromagnetic character and application of models devised for paramagnetic granites must be done with caution.

Numerical modeling indicates that in an oblique transpressional setting, a primary oblate fabric with vertical or inclined K_3 can evolve to a triaxial (and eventually back to oblate) fabric with horizontal K_3 (Schulmann and Ježek, 2012). These models were developed for paramagnetic granites, but may help partly explain the fabric observed in the Spavinaw Granite. While internal deformation is not extreme enough to yield macroscopic indicators, the strained extinction of quartz indicates that deformation is present and may have an effect on the AMS fabric. The Schulmann & Ježek model could explain the near-vertical AMS foliation of SPV-2 if that block has been slightly more strained than SPV-1; the higher dispersion, lower mean tensor

shape factor and streaking of K_3 towards K_2 indicate that it has. Any possible relation between this inferred additional strain and the apparent Mississippian magnetic overprint is impossible to evaluate at present. The magnetic fabric is presently interpreted to mostly represent an emplacement fabric with some subsequent tectonic modification.

CONCLUSION

The interpretations from this study are admittedly speculative, as the data set is far too small to draw rigorous conclusions. The primary observation is that, contrary to previous reports, the Spavinaw Granite very likely does preserve meaningful paleomagnetic information. The present work was largely performed as a pilot test to see whether the Spavinaw Granite is worth further paleomagnetic work; the preliminary data strongly indicate that it is. Further sampling would ideally be conducted by drilling in place and orienting with a sun compass. The present samples were oriented using a magnetic compass, and Spall and Noltimier (1972) report up to 10° of declination error due to the intensity of the rocks. Declination variance of this magnitude was modeled during data analysis and does not significantly affect the preliminary interpretations, though a declination shift of SPV-2 could potentially provide stronger support for Mississippian vs. Devonian or Silurian remagnetization. Drilling in place may prove difficult though, as the exposures are on private land in a residential area; most are literally in back yards.

The scattered directions reported by previous workers were not reproduced, possibly due to the low sample numbers, though the prior reports documented substantial variance even in subsamples of individual cores. The preliminary data of this study indicate that the Spavinaw Granite carries a chemical remanent magnetization that was acquired during the early Cambrian. Some of the granite contains another partial magnetic overprint, which is likely Mississippian in age but could possibly be late Silurian. The magnetizations are carried by both magnetite and

maghemite. Magnetic fabric data suggest that the granite is slightly deformed and steeply tilted to the northwest, with a tilt axis that corresponds to a prominent fault set in the region. The results from this pilot study indicate that a larger study could yield a great deal of information regarding the tectonic history of northeastern Oklahoma and potentially central North America.

REFERENCES

Barker, D.S., 1970. Compositions of granophyre, myrmekite, and graphic granite. Geological Society of America Bulletin, 81(11), pp.3339-3350. https://doi.org/10.1130/0016-7606(1970)81(3339:COGMAG)2.0.CO;2

Berendsen, P. and Blair, K.P., 1991. Interpretive subcrop map of the Precambrian basement in the Joplin 1° x2° Quadrangle. Kansas Geological Survey Subsurface Geology Series 14.

Bickford, M.E. and Lewis, R.D., 1979. U-Pb geochronology of exposed basement rocks in Oklahoma. Geological Society of America Bulletin, 90(6), pp.540-544. https://doi.org/10.1130/0016-7606(1979)90<540:UGOEBR>2.0.CO;2

Bickford, M.E., Van Schmus, W.R., Karlstrom, K.E., Mueller, P.A. and Kamenov, G.D., 2015. Mesoproterozoic-trans-Laurentian magmatism: A synthesis of continent-wide age distributions, new SIMS U–Pb ages, zircon saturation temperatures, and Hf and Nd isotopic compositions. Precambrian Research, 265, pp.286-312. https://doi.org/10.1016/j.precamres.2014.11.024

Bilardello, D., 2020. Practical Magnetism II: Humps and a bump, The maghemite song. IRM Quarterly, 30(1), pp.1, 15-16.

Bouchez, J.L., 1997. Granite is never isotropic: an introduction to AMS studies of granitic rocks. In Granite: from segregation of melt to emplacement fabrics (pp. 95-112). Springer, Dordrecht. https://doi.org/10.1007/978-94-017-1717-5_6

Bouchez, J.L., 2000. Anisotropie de susceptibilité magnétique et fabrique des granites. Comptes Rendus de l'Académie des Sciences-Series IIA-Earth and Planetary Science, 330(1), pp.1-14. https://doi.org/10.1016/S1251-8050(00)00120-8

Campbell, J.A. and Weber, J.L., 2006. Wells Drilled to Basement in Oklahoma. Oklahoma Geological Survey Special Publication 2006-1.

de Wall, H. and Worm, H.U., 2001. Recognition of drilling-induced remanent magnetization by Q-factor analysis: A case study from the KTB-drillholes. Journal of Applied Geophysics, 46(1), pp.55-64. https://doi.org/10.1016/S0926-9851(00)00039-2

Denison, R.E., 1966. Basement rocks in adjoining parts of Oklahoma, Kansas, Missouri, and Arkansas. (Ph.D. dissertation) University of Texas at Austin.

Denison, R.E., 1981. Basement rocks in northeastern Oklahoma. Oklahoma Geological Survey Circular 84.

Denison, R.E., 1995. Significance of air-photograph linears in the basement rocks of the Arbuckle Mountains. Oklahoma Geological Survey Circular 97, pp.119-131.

Drake, N.F., 1897. A geological reconnaissance of the coal fields of the Indian Territory. Proceedings of the American Philosophical Society, 36(156), pp.326-419.

Dunlop, D.J., 2014. High-temperature susceptibility of magnetite: a new pseudo-single-domain effect. Geophysical Journal International, 199(2), pp.707-716. https://doi.org/10.1093/gji/ggu247

Dunlop, D.J. and Özdemir, Ö., 1997, Rock magnetism: Fundamentals and frontiers. Cambridge University Press, Cambridge, UK.

Dunlop, D.J., Schutts, L.D. and Hale, C.J., 1984. Paleomagnetism of Archean rocks from northwestern Ontario: III. Rock magnetism of the Shelley Lake granite, Quetico

Subprovince. Canadian Journal of Earth Sciences, 21(8), pp.879-886. https://doi.org/10.1139/e84-094

Elmore, R.D., Campbell, T., Banerjee, S. and Bixler, W.G., 1998. Palaeomagnetic dating of ancient fluid-flow events in the Arbuckle Mountains, southern Oklahoma. Geological Society, London, Special Publications, 144(1), pp.9-25. https://doi.org/10.1144/GSL.SP.1998.144.01.02

Fabian, K., 2003. Some additional parameters to estimate domain state from isothermal magnetization measurements. Earth and Planetary Science Letters, 213(3-4), pp.337-345. https://doi.org/10.1016/S0012-821X(03)00329-7

Ferré, E.C., Wilson, J. and Gleizes, G., 1999. Magnetic susceptibility and AMS of the Bushveld alkaline granites, South Africa. Tectonophysics, 307(1-2), pp.113-133. https://doi.org/10.1016/S0040-1951(99)00122-5

Fisher, R.A., 1953. Dispersion on a sphere. Proceedings of the Royal Society of London Series A: Mathematical and Physical Sciences, 217(1130), pp.295-305. https://doi.org/10.1098/rspa.1953.0064

Ham, W.E. and Dott, R.H., 1943. New evidence concerning age of Spavinaw granite, Oklahoma. AAPG Bulletin, 27(12), pp.1626-1631. https://doi.org/10.1306/3D933630-16B1-11D7-8645000102C1865D

Ham, W.E., Denison, R.E., and Merritt, C.A., 1964. Basement Rocks and Structural Evolution of Southern Oklahoma. Oklahoma Geological Survey Bulletin 95.

Hawes, J., 1952. A magnetic study of the Spavinaw granite area, Oklahoma. Geophysics, 17(1), pp.27-55. https://doi.org/10.1190/1.1437738

Huffman, G.G., 1958. Geology of the flanks of the Ozark uplift, northeastern Oklahoma. Oklahoma Geological Survey Bulletin 77.

Ireland, H.A., 1930. Oil and gas in Oklahoma: Mayes, Ottawa, and Delaware Counties. Oklahoma Geological Survey Bulletin 40-NN.

Jackson, M., and Sølheid, P., 2010. On the quantitative analysis and evaluation of magnetic hysteresis data. Geochemistry, Geophysics, Geosystems, 11(4), Q04Z15. https://doi.org/10.1029/2009GC002932

Jelínek, V., 1981. Characterization of the magnetic fabric of rocks. Tectonophysics, 79(3-4), pp.T63-T67. https://doi.org/10.1016/0040-1951(81)90110-4

Kirschvink, J., 1980. The least-squares line and plane and the analysis of palaeomagnetic data. Geophysical Journal International, 62(3), pp.699-718. https://doi.org/10.1111/j.1365-246X.1980.tb02601.x

Kolawole, F., Johnston, C.S., Morgan, C.B., Chang, J.C., Marfurt, K.J., Lockner, D.A., Reches, Z. and Carpenter, B.M., 2019. The susceptibility of Oklahoma's basement to seismic reactivation. Nature Geoscience, 12(10), pp.839-844. https://doi.org/10.1038/s41561-019-0440-5

Kontny, A. and Grothaus, L., 2017. Effects of shock pressure and temperature on titanomagnetite from ICDP cores and target rocks of the El'gygytgyn impact structure, Russia. Studia Geophysica et Geodaetica, 61(1), pp.162-183. https://doi.org/10.1007/s11200-016-0819-3

Labusch, L., 2016. Linear Trend Analysis: Implications for a Structural Fracture System and Applications of Subsurface Fluid Migration, Northwest Arkansas and Eastern Oklahoma. (M.Sc. Thesis) University of Arkansas.

Le Maitre, R.W., 2002. Igneous Rocks: A Classification and Glossary of Terms: Recommendations of the International Union of Geological Sciences Subcommission on the Systematics of Igneous Rocks, 2nd ed., Cambridge University Press, Cambridge, UK.

Lidiak, E.G., 1996. Geochemistry of subsurface Proterozoic rocks in the eastern Midcontinent of the United States: Further evidence for a within-plate tectonic setting. Geological Society of America Special Paper, 308, pp.45-66. https://doi.org/10.1130/0-8137-2308-6.45

McCausland, P.J., Van der Voo, R. and Hall, C.M., 2007. Circum-Iapetus paleogeography of the Precambrian–Cambrian transition with a new paleomagnetic constraint from Laurentia. Precambrian Research, 156(3-4), pp.125-152. https://doi.org/10.1016/j.precamres.2007.03.004

Merritt, C.A., 1960. Petrography of the Spavinaw Granite. Oklahoma Geology Notes, 20(9), pp.224-228.

Muehlberger, W.R., Hedge, C.E., Denison, R.E. and Marvin, R.F., 1966. Geochronology of the midcontinent region, United States: 3. Southern area. Journal of Geophysical Research, 71(22), pp.5409-5426. https://doi.org/10.1029/JZ071i022p05409

Northcutt, R.A. and Campbell, J.A., 1995. Geologic provinces of Oklahoma. Oklahoma Geological Survey Open File Report 5-95.

Owen, D.D., 1860. Second report of a geological reconnoissance (sic) of the middle and southern counties of Arkansas, made during the years 1859 and 1860. C. Sherman and Sons, Philadelphia.

Özdemir, Ö. and Dunlop, D.J., 2010. Hallmarks of maghemitization in low-temperature remanence cycling of partially oxidized magnetite nanoparticles. Journal of Geophysical Research: Solid Earth, 115, B02101. https://doi.org/10.1029/2009JB006756

Roggenthen, W.M., Fischer, J.F., Napoleone, G. and Fischer, A.G., 1981. Paleomagnetism and age of mafic plutons, Wichita Mountains, Oklahoma. Geophysical Research Letters, 8(2), pp.133-136. https://doi.org/10.1029/GL008i002p00133

Schulmann, K. and Ježek, J., 2012. Some remarks on fabric overprints and constrictional AMS fabrics in igneous rocks. International Journal of Earth Sciences, 101(3), pp.705-714. https://doi.org/10.1007/s00531-011-0681-z

Shah, A.K. and Keller, G.R., 2017. Geologic influence on induced seismicity: Constraints from potential field data in Oklahoma. Geophysical Research Letters, 44(1), pp.152-161. https://doi.org/10.1002/2016GL071808

Shaulis, B.J., Lapen, T.J., Casey, J.F. and Reid, D.R., 2012. Timing and rates of flysch sedimentation in the Stanley Group, Ouachita Mountains, Oklahoma and Arkansas, USA: Constraints from U-Pb zircon ages of subaqueous ash-flow tuffs. Journal of Sedimentary Research, 82(11), pp.833-840. https://doi.org/10.2110/jsr.2012.68

Spall, H., 1968. Paleomagnetism of basement granites of southern Oklahoma and its implications: Progress report. Oklahoma Geology Notes, 28(2), pp.65–80.

Spall, H. and Noltimier, H.C., 1972. Some curious magnetic results from a Precambrian granite. Geophysical Journal of the Royal Astronomical Society, 28(3), pp.237-248. https://doi.org/10.1111/j.1365-246X.1972.tb06126.x

Streckeisen, A., 1976. To each plutonic rock its proper name. Earth-Science Reviews, 12(1), pp.1-33. https://doi.org/10.1016/0012-8252(76)90052-0

Tarling, D.H. and Hrouda, F., 1993. The Magnetic Anisotropy of Rocks. Chapman and Hall, London.

Thomas, W.A., 2014. The Southern Oklahoma transform-parallel intracratonic fault system. Oklahoma Geological Survey Guidebook 38, pp.375-388.

Torsvik, T.H., Van der Voo, R., Preeden, U., Mac Niocaill, C., Steinberger, B., Doubrovine, P.V., Van Hinsbergen, D.J.J., Domeier, M., Gaina, C., Tohver, E., Meert, J.G., McCausland, P.J.A., and Cocks, R.M., 2012. Phanerozoic polar wander, palaeogeography and dynamics. Earth-Science Reviews, 114(3-4), pp.325-368. https://doi.org/10.1016/j.earscirev.2012.06.007

Van Schmus, W.R., Bickford, M.E. and Turek, A., 1996. Proterozoic geology of the east-central Midcontinent basement. Geological Society of America Special Paper, 308, pp.7–32. https://doi.org/10.1130/0-8137-2308-6.7

Wall, C.J., Hanson, R.E., Schmitz, M., Price, J.D., Donovan, R.N., Boro, J.R., Eschberger, A.M. and Toews, C.E., 2021. Integrating zircon trace-element geochemistry and high-precision U-Pb zircon geochronology to resolve the timing and petrogenesis of the late Ediacaran–Cambrian Wichita igneous province, Southern Oklahoma Aulacogen, USA. Geology, 49(3), pp.268-272. https://doi.org/10.1130/G48140.1

Zijderveld, J.D.A., 1967. A.C. demagnetization of rocks: Analysis of results. In: Collinson, D.W., Creer, K.M., and Runcorn, S.K., eds., Methods in Paleomagnetism. Elsevier, Amsterdam, pp 254–286. https://doi.org/10.1016/B978-1-4832-2894-5.50049-5

CHAPTER 6

PALEOMAGNETISM AND MAGNETIC FABRICS OF THE EARLY CAMBRIAN GLEN MOUNTAINS LAYERED COMPLEX AND ASSOCIATED MAFIC-INTERMEDIATE UNITS, WICHITA MOUNTAINS, OKLAHOMA

ABSTRACT

The behavior of Earth's magnetic field during the early Cambrian is a subject of controversy and ongoing study, and results from North America at this time are poorly constrained. This work presents new paleomagnetic, rock magnetic and magnetic fabric data from the 532.49 Ma Glen Mountains Layered Complex and associated mafic-intermediate rocks in southwestern Oklahoma. These results suggest the presence of a primary, early Cambrian magnetization in several sites which is similar to results from contemporaneous rocks in Quebec. Additionally, some sites carry a late Paleozoic overprint while others carry a component yielding pole positions some 90° from those of the inferred primary directions. This component is interpreted as an early Devonian (~400 Ma) overprint which seems to have affected the granites of the area as well. Rock magnetic analysis indicates all components are carried in magnetite, much of it single-domain. Magnetic fabrics indicate a dip magnitude consistent with previous reports but suggest a much more easterly mean dip azimuth. Initial results suggest the possibility of using AMS as a proxy for tilt corrections as well.

INTRODUCTION

The period of Earth's history spanning the Ediacaran to the early Cambrian was one of great changes. This time coincides with the diversification of macroscopic animal life (e.g., Grotzinger et al., 1995) as well as the last stages of the breakup of the Precambrian

supercontinent of Rodinia (Dalziel, 1997; Cawood et al., 2001). Understanding these events requires some knowledge of the paleogeographic context of the associated rocks.

Paleomagnetism has long been one of the primary methods used in paleogeographic reconstructions, particularly due to the relationship between magnetic inclination and paleolatitude (e.g., Irving, 1956; Butler, 1992). This method has however found difficulty in application to the Ediacaran-Cambrian boundary. Rocks of this age are relatively rare and often have been affected by remagnetization. In studies where the magnetization appears primary, there is often a wide spread in results. The variability of Ediacaran-early Cambrian paleomagnetic results is problematic (e.g., McCausland et al., 2007, 2011) and has led to numerous hypotheses attempting to explain it such as rapid inertial interchange true polar wander (Kirschvink et al., 1997; Mitchell et al., 2015), non-uniformitarian geodynamo behavior including an equatorial axial dipole (Abrajevitch and Van der Voo, 2010), and more recently the possibility that the solid inner core began growth during or shortly before this time (Bono et al., 2019; Thallner et al., 2021).

The uncertainty in early Cambrian paleomagnetism is particularly apparent for Laurentia (i.e. North America). While numerous studies have been conducted, most have run into issues with either remagnetization or unusual directions. Relatively few reconstructions of the apparent polar wander path for Laurentia extend to this time period, and the currently most-accepted version (Torsvik et al., 2012) only includes a single constraint older than 510 Ma – a study of 530 Ma syenites from Quebec (McCausland et al., 2007).

This study presents new paleomagnetic, rock magnetic, and magnetic fabric data from early Cambrian igneous rocks of the Southern Oklahoma Aulacogen, with a major emphasis on the mafic rocks of the Glen Mountains Layered Complex. Several previous paleomagnetic

studies have been performed on the granites, rhyolites and gabbros of this area (e.g., Ku et al., 1967; Spall, 1968; Vincenz et al., 1975; Roggenthen et al., 1981; Elmore et al., 1998; Hamilton et al., 2016), some of which show a measure of consistency with each other, but which do not agree with the data from the roughly coeval Quebec syenites. The new data agree with some previous studies and (in combination with rock magnetic measurements) also yield some possible explanations for disagreement with other prior results and interpretations. Additionally, the magnetic fabric data provide information concerning the structural character of this area.

GEOLOGICAL BACKGROUND

The Southern Oklahoma Aulacogen (SOA) is an inverted early Paleozoic structure, juxtaposing Cambrian igneous rocks against a thick sequence of sediments (Shatski, 1946). It was considered to have formed from the failed arm of a Cambrian rift system by Hoffman et al. (1974), and this interpretation has been accepted by most workers. An alternative interpretation is that the structure originated from inward extension of a "leaky" transform zone from the rifted margin of Laurentia (Thomas, 1991, 2014). It has been pointed out that these models are not necessarily exclusive (e.g., Hanson et al., 2013) and for the sake of comparison with most literature on the area the rift interpretation and the aulacogen name are retained here.

During the early Cambrian, a very large volume of igneous rock was emplaced into the rift zone (Ham et al., 1964; Gilbert, 1983). The magmatism is largely considered bimodal between mafic and felsic lithologies, though there are minor instances of intermediate rocks in outcrop and they have been reported from the subsurface as well (Ham et al., 1964; Hanson et al., 2013). Current estimates of the total volume of igneous material approach or exceed 250,000 km^3, with mafic rocks accounting for about 80% of that (Hanson et al., 2013). After magmatic activity ceased, the area began to subside and was progressively buried from the Upper

Cambrian through most of the Paleozoic before being uplift during the late Pennsylvanian (Ham et al., 1964). Uplift and structural inversion at this time is generally associated with Ancestral Rocky Mountain uplifts across southern North America (Kluth and Coney, 1981). Following the end of the late Paleozoic orogenies, the area rapidly subsided due to the relaxation of horizontal stresses and the large mass of mafic rock in the subsurface, preserving an early Permian landscape which is slowly being re-exposed in the present (Gilbert, 1982; Soreghan et al., 2012).

The sequence of igneous events in the SOA is generally considered to begin with the emplacement of the Glen Mountains Layered Complex (GMLC), a large body of layered anhydrous igneous rocks consisting primarily of anorthosite and lesser amounts of troctolite and gabbro. The GMLC makes up the majority of exposed mafic rock in the SOA with a total area of ~150 km^2, though geophysical data and drilling penetrations indicate a substantially larger extent in the subsurface with a likely thickness of several kilometers (Ham et al., 1964; Powell, 1986). The GMLC has four major exposures in the Wichita Mountains area. The eastern exposures have very limited accessibility due to being on either large gated ranches or the wildlife refuge. The present study therefore sampled areas of the western and largest exposure area (Fig. 1).

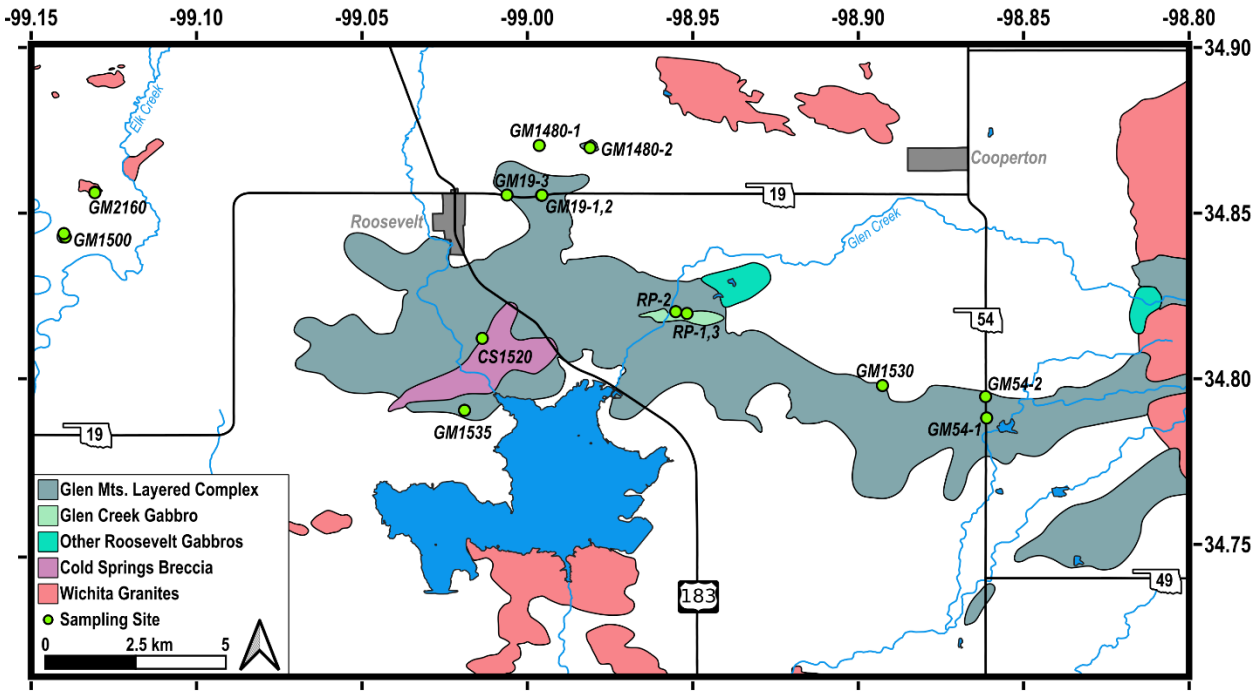


Figure 1. Generalized map of igneous unit outcrops in the study area, with sampling locations indicated. After Merritt (1958) and Gilbert (1982, 2014).

On the basis of layering attitudes, the GMLC is inferred to have been tilted to the north before being intruded by a younger group of mafic rocks which commonly contain primary hydrous minerals such as amphiboles and biotite, referred to as the Roosevelt Gabbros (Ham et al., 1964; Powell et al., 1980a, 1980b). Field relations indicate that the GMLC was exposed by uplift and erosion prior to the eruption of the Carlton Rhyolite Group, and the Wichita Granite Group was subsequently emplaced as sheets along the base of the rhyolite flows (Ham et al., 1964; Hogan and Gilbert, 1997). The relative timing of the Roosevelt Gabbros is more difficult to discern – it was long assumed that they were emplaced after tilting but before erosion of the GMLC (Ham et al., 1964; Gilbert, 1983; Powell, 1986), but later field observations indicate that at least some of the Roosevelt Gabbros were intruded against the granites (e.g., Price et al., 1998). While extrusive mafic rocks are entirely absent in outcrop, a series of basalts in the Wichita Mountains area referred to as the Navajoe Mountain Basalt-Spilite Group has been

encountered in boreholes and has long been assumed to be cogenetic with the GMLC (Ham et al., 1964), and more recently basalt flows have been found to be interbedded with rhyolite in the subsurface throughout the SOA (Hanson et al., 2013; Brueseke et al., 2016).

The absolute time frame of SOA magmatism is only now beginning to be well-understood. For decades, the age of the GMLC was poorly constrained and thought was split between those who thought it likely 10-20 million years older than the granites (e.g., Ham et al., 1964) and those who considered it likely Precambrian (e.g., Powell and Phelps, 1977; Roggenthen et al., 1981). Subsequent radiometric dating using the Sm-Nd system indicated a latest Precambrian to early Cambrian age but with a relatively large error (577 ±165 Ma whole rock, 528 ±29 Ma internal isochron; Lambert et al., 1988). Most recently, high-resolution U-Pb data from zircons have yielded an age of 532.49 ±0.12 Ma for the GMLC and 530.23 ±0.14 Ma for the youngest of the granites (Wall et al., 2021), indicating a very compressed timeline for igneous evolution of the SOA. This poses some major tectonic issues – for instance, Powell and Phelps (1977) concluded on the basis of phase chemistry that at least 2-4 kilometers of the uppermost GMLC (and likely at least as much overburden) was eroded between its emplacement and the eruption of the rhyolites. The estimated age difference of up to ~50 million years between 577 Ma anorthosite and 525 ±25 Ma granite and rhyolite (Tilton et al., 1962) was not deemed sufficient to account for this denudation by McConnell and Gilbert (1990), who instead invoked block rotation models. The new geochronology of Wall et al. (2021) allows for less than 2.5 million years, a constraint which must (but has yet to) be incorporated into models of the evolution of the SOA.

The GMLC is typically mapped into four major units referred to as the K-, L-, M-, and N-Zones (Gilbert, 1960; Spencer, 1961; Powell et al., 1980a, 1980b; Powell, 1986) and this

terminology is retained here for convenience. A very different terminology was used in mapping by Cooper (1991), whose units do not correspond to or correlate with those of other workers. While the trend of layering may be locally quite variable (e.g., McConnell and Gilbert, 1990), most workers have interpreted the overall dip of the GMLC to be between 5 and 20° to the north or NNE (e.g., Ham et al., 1964; Powell et al., 1980a, 1980b; Cooper, 1991). The western outcrop area, the area of the present study, is typically considered to be the center of a broad anticline and the area of maximum uplift (Ham et al., 1964; Scofield, 1975).

METHODS

Samples were collected in the field using a gas-powered coring drill and oriented using a Pomeroy device with a sun compass. A total of 17 sites were drilled for this study (Fig. 1). Regarding site names, most sites are adjacent to roads and are therefore numbered according to the highway or county road they lie along. Most sites sampled the Glen Mountains Layered Complex, though one site sampled a granodiorite/quartz monzonite (hereafter "granitoid") of the type associated with the Cold Springs Breccia, two sites sampled the Glen Creek Gabbro, and one site appears to have sampled another of the Roosevelt Gabbros. Mafic sites are abbreviated "GM" for Glen Mountains; the site of Cold Springs granitoid is instead abbreviated "CS". This convention is not followed for sampling sites from the aggregate quarry known as Reid's Pit (e.g., Powell and Gilbert, 1982), which are abbreviated as "RP."

After drilling, samples were cut down to standard paleomagnetic cylinders, and it was often possible to get multiple specimens per core. For most sites, polished thin sections were prepared from remaining pieces by a commercial vendor and inspected using a petrographic microscope. Bulk low-field magnetic susceptibility and anisotropy of magnetic susceptibility (AMS) were measured at room temperature using an AGICO MFK1 Kappabridge with a

measuring field amplitude of 200 A/m and frequency of 976 Hz. Data were processed using AGICO's Anisoft 5 software, with scalar AMS parameters (corrected degree of anisotropy Pj and shape factor T) calculated following Jelínek (1981). Remanent magnetizations were measured using a 2G cryogenic magnetometer housed in a magnetically shielded room. Following measurement of the natural remanent magnetization (NRM), samples were progressively demagnetized and measured between treatment steps. Thermal demagnetization treatments used an ASC TD-48 magnetically shielded oven. Due to a problem with temperature control, the actual temperatures for most measurement steps at most sites are not clear and may have been considerably (possibly as much as 50 °C at high temperatures) cooler than the set temperature. Samples were re-treated at 580 and 600 °C following resolution of the problem. Selected specimens were instead subjected to alternating field (AF) demagnetization. Paleomagnetic data analysis utilized Super-IAPD software, with data plotted on orthogonal projection diagrams (a.k.a. Z-plots, after Zijderveld, 1967). Magnetization components were chosen manually with maximum angular deviation (MAD; Kirschvink, 1980) less than 10° for all considered components; most have MAD <5°. Group statistics are calculated after Fisher (1953).

Additional rock magnetic data were collected at the Institute for Rock Magnetism (IRM). Hysteresis and backfield remanence data were measured for 1 to 3 samples per site using Princeton Measurements and Lake Shore vibrating sample magnetometers with maximum applied fields of 1-2 Tesla; plots are truncated at 1 T for uniformity as all samples were fully saturated at that point. Hysteresis data processing was done with IRM in-house software which applies a non-linear high-field lope correction (Jackson and Sølheid, 2010). Low-temperature remanence measurements utilized a Quantum Design MPMS-XL. Samples were given a 2.5

Tesla saturation isothermal remanent magnetization (SIRM) at a temperature of 300 Kelvin. Remanence was measured at 5 K intervals during cooling to 10 K, at which point another 2.5 T SIRM was applied and then remanence was measured at the same interval while warming back to 300 K. Samples for VSM and MPMS measurements consisted of small amounts of rock chips (~0.2 – 0.3 grams) packed into gel caps.

RESULTS AND INITIAL INTERPRETATIONS

Due to the substantial variation in data, results are presented site-by-site and combined as appropriate. Non-GMLC sites will be discussed first. Paleomagnetic results are summarized in Table 1, magnetic susceptibility and NRM intensity results are summarized in Table 2 and AMS mean tensor parameters in Table 3. Mean values in Table 2 and subsequent text are calculated from mean of logarithms, on the assumption that χ and intensity have lognormal distributions.

Table 1: Paleomagnetic Results of GMLC and Associated Sites

Site	Dec	Inc	N/N_0	k	α95	VGP Lat (°N)	VGP Lon (°E)	VGP α95
RP-2	256.7	21.9	5/15	114.7	7.2	-4	188	5.1
GM19-2 (1)	111.8	36.1	6/9	46.1	10	5.1	142.1	10.7
GM19-2 (2)	38.5	-30.1	4/9	174.3	7	-27.2	218.9	6
GM19-3	229.6	-50.4	8/13	90. 5	5.9	-48.9	161.3	6.8
GM54-1	251.3	5.2	8/10	75.6	6.4	-13.7	184.1	5.9
GM54-2	52.4	-19.2	11/11	254.9	2.9	-23.3	202.8	2.8
GM1480-1	101.6	70	4/4	91.3	9.7	-21.4	119.1	16.5
GM1480-2	214.7	1.1	4/8	175.3	7	-42	211	6
GM1500-1 (1)	96.4	-14.4	4/10	207.9	6.4	9.4	173.4	4.7
GM1500-1 (2)	83.1	-28	3/10	396.1	6.2	3	187.1	6
GM1500-2 (1)	117.1	-8.1	5/11	311.2	4.3	24.4	158.2	3.3
GM1500-2 (2)	53.9	-39.7	6/11	132.9	5.8	-13.5	211.6	5.9
GM1530	119.2	61.6	13/13	21.0	9.3	-7.4	121	13.5
GM1535	147.4	67.9	4/8	174.0	7	-0.5	100.9	11.5
GM2160-1	47.8	-26.3	10/10	121.1	4.4	-23.5	209.5	4.2
GM2160-2	208	57.4	8/9	113.0	5.2	-12.2	238.6	6.3
CS1520	60.1	6.5	8/11	252.1	3.5	-26.2	186.4	3.1
GM19-1	149.9	-5	6/11	41.2	10.6	128.6	47.3	9
RP-3	153.1	19.2	8/19	52.1	7.7	38.5	115.8	6.3

Table 2: Magnetic Susceptibility (χ) and NRM Intensity of GMLC and Associated Sites

Site	Mean χ (m^3/kg)	Mean NRM (Am^2/kg)	Avg. Q
RP-2	$1.24x10^{-6}$	$6.22x10^{-4}$	17.2
GM19-2	$3.05x10^{-6}$	$8.68x10^{-5}$	0.9
GM19-3	$3.47x10^{-6}$	$1.99x10^{-3}$	20.6
GM54-1	$2.66x10^{-6}$	$2.74x10^{-3}$	31.4
GM54-2	$1.61x10^{-6}$	$1.74x10^{-3}$	46.0
GM1480-1	$1.85x10^{-6}$	$2.03x10^{-3}$	28.4
GM1480-2	$7.91x10^{-6}$	$3.32x10^{-3}$	9.5
GM1500-1	$9.99x10^{-7}$	$2.55x10^{-4}$	6.9
GM1500-2	$1.43x10^{-6}$	$1.34x10^{-4}$	3.4
GM1530	$4.92x10^{-6}$	$2.62x10^{-3}$	16.5
GM1535	$3.87x10^{-7}$	$7.14x10^{-4}$	48.6
GM2160-1	$9.77x10^{-7}$	$4.18x10^{-4}$	14.9
GM2160-2	$4.51x10^{-6}$	$1.12x10^{-3}$	6.4
CS1520	$2.75x10^{-6}$	$3.86x10^{-4}$	3.6
GM19-1	$1.38x10^{-5}$	$7.16x10^{-5}$	0.2
RP-1	$1.96x10^{-5}$	$7.59x10^{-4}$	1.5
RP-3	$2.17x10^{-5}$	$1.26x10^{-3}$	2.9

Table 3: AMS Mean Tensor Parameters of GMLC and Associated Sites

Site	Pj	T	Kmax Dec	Kmax Inc	Kint Dec	Kint Inc	Kmin Dec	Kmin Inc
RP-2	1.102	0.342	67.7	30.9	327.1	17.7	212.4	53.7
GM19-2	1.131	0.291	328.5	3.4	237.1	21.8	67.0	67.9
GM19-3	1.164	0.677	55.4	2.3	324.6	20.0	151.8	69.9
GM54-1	1.093	0.398	10.7	10.5	105.3	23.6	258.4	63.9
GM54-2	1.097	0.616	233.2	10.2	324.2	5.2	80.6	78.5
GM1480-1	1.065	-0.486	162.5	13.6	39.2	66.2	257.3	19.1
GM1480-2	1.093	-0.573	219.8	53.2	334.5	17.3	75.4	31.3
GM1500-1	1.061	-0.098	191.3	9.0	101.2	0.6	7.2	81.0
GM1500-2	1.127	0.427	191.4	0.9	101.0	20.3	283.8	69.6
GM1530	1.077	0.667	103.4	17.2	199.2	18.0	332.5	64.6
GM1535	1.129	0.809	85.6	15.8	353.8	6.5	242.3	72.8
GM2160-1	1.061	0.017	78.5	50.4	276.5	38.2	179.4	8.9
GM2160-2	1.036	-0.638	49.8	27.3	156.6	29.3	284.9	47.9
CS1520	1.085	0.869	235.9	4.8	133.6	68.5	327.8	20.9
GM19-1	1.023	0.583	315.8	77.4	221.7	0.9	131.5	12.6
RP-1	1.051	0507	144.8	12.6	49.8	21.2	263.4	65.0
RP-3	1.029	0.343	32.4	58.8	179.0	26.8	276.6	14.7

Site CS1520, Cold Springs Granitoid

The lithology sampled here is a fine- to medium-grained slightly pink granitoid and lacks the inclusions of anorthosite and/or microdiorite for which the Cold Springs Breccia is known. While point counts were not performed, examination of a thin section of the rock indicates the bulk of the mass is made of slightly sericitized plagioclase with subordinate alkali feldspar, quartz, green to brown hornblende and biotite. Petrographically, the rock is very similar to the description of Cold Springs intermediate rocks given by Powell et al. (1980a, 1980b) and Vidrine and Fernandez (1986).

Mass-normalized bulk low-field magnetic susceptibility (χ) for this site has a mean value of 2.75×10^{-6} m^3/kg as determined with the MFK1 Kappabridge. Initial susceptibility estimated from hysteresis data is within the range measured using the kappabridge, and high-field susceptibility accounts for only about 2.25% of the total. The hysteresis loop is essentially closed by 150 mT and saturates at around 300 mT (Fig. 2, left). Bulk coercivity (Bc) is low, just above 3 mT. Backfield remanence measurements indicate a bulk coercivity of remanence (Bcr) of about 31 mT. A plot of the derivative of backfield remanence against the logarithm of the applied field (Fig. 2, right) can be used to estimate the coercivity spectrum (e.g., Egli, 2003), and indicates a reasonably broad single distribution from about 5 to 100 mT with a peak at 20 mT. A minor noisy component is apparently present above 500 mT and may correspond to a small contribution from a much higher-coercivity phase. The low coercivities and ratio of saturation remanence to saturation magnetization (Mr/Ms) are consistent with an abundance of multi-domain (MD) grains of ferrimagnetic minerals (Dunlop and Özdemir, 1997; Dunlop, 2002).

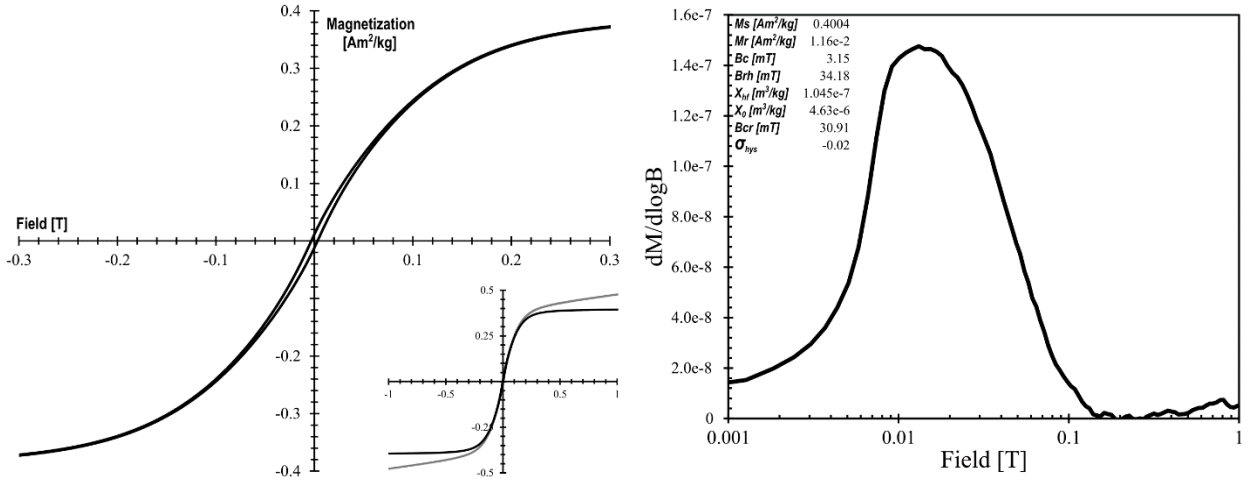


Figure 2. Hysteresis and backfield remanence data for a sample of Cold Springs granitoid at site CS1520. (Left) Slope-corrected high-field hysteresis loop. Data truncated at ±300 mT for visibility. Lower right inset shows data before (gray) and after slope correction (black) out to 1 T. (Right) Derivative of backfield remanence data plotted against logarithm of applied field in order to visualize coercivity distribution. Inset table gives calculated hysteresis parameters. Backfield values reflect raw moment and are not normalized.

A low-temperature remanence sweep was performed for this sample (Fig. 3). On cooling, the room-temperature saturation isothermal remanent magnetization (RTSIRM) demagnetizes nonlinearly, with peak loss rate between 150-100 K. Warming of low-T SIRM shows a sharp remanence loss above 90 K, corresponding to the Verwey transition of magnetite. Use of IRM data analysis software yields a Verwey transition temperature (T_V) of 103.8 K, noticeably lower than the usual value given for pure magnetite (≈119 K). Lower values of T_V are commonly associated with partial oxidation of magnetite (see review by Jackson and Moskowitz, 2021). While hematite would explain the apparent high-coercivity component seen in backfield data, no Morin transition is evident in low-T remanence data, suggesting that if hematite is present it is either so minor as to be invisible to the low-T remanence data or is sufficiently fine-grained that the Morin transition is absent (e.g., Özdemir et al., 2008).

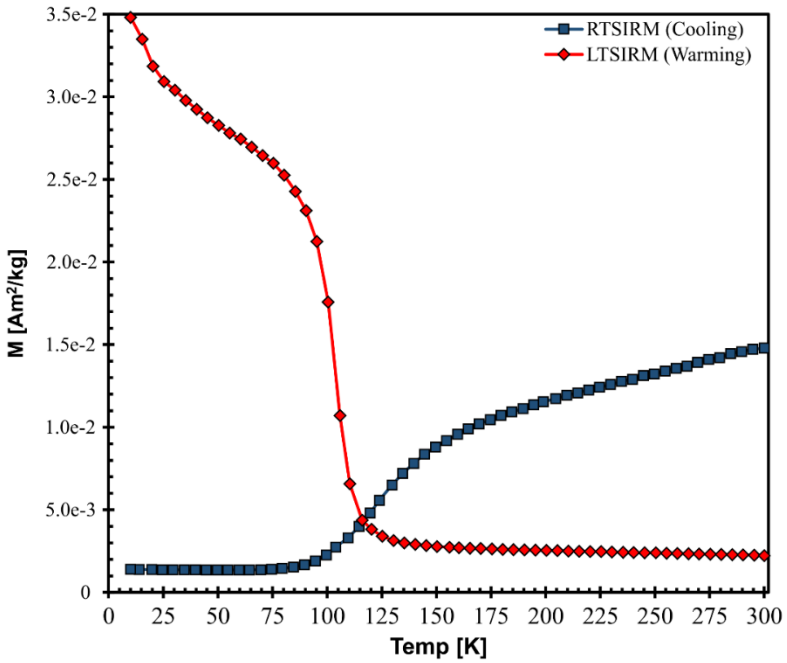


Figure 3. Low-temperature remanence measurements for Cold Springs granitoid, site CS1520. Blue curve is low-temperature demagnetization from cooling of room-T SIRM. Red curve is measured on warming after application of low-T SIRM. Steep drop of remanence on warming corresponds to Verwey transition at a temperature of 103.8 K.

AMS data for this site show a consistent, strongly oblate fabric (Fig. 4). All samples have values of shape factor $T > 0.5$, and the overall mean tensor for the site has $T \approx 0.87$. The corrected degree of anisotropy Pj ranges from 1.06 to nearly 1.14 (i.e., 6 to ~14% anisotropy). This indicates that most of the anisotropy must be carried by the ferrimagnetic mineral fraction (i.e., magnetite and possibly maghemite) – while biotite and amphibole are both present and both known to carry magnetic fabrics in igneous rocks (e.g., Rochette et al., 1992; Tarling and Hrouda, 1993), the degree of anisotropy (site mean Pj = 1.085) is significantly larger than the total paramagnetic contribution to susceptibility as inferred from hysteresis data (~2.25%). There is an apparent correlation between bulk susceptibility and Pj and likewise a correlation between Pj and T. Correlation of Pj with bulk susceptibility is typically interpreted as the degree of anisotropy being controlled by the abundance of the carrier mineral (Tarling and Hrouda, 1993).

Oblate fabrics are common in granitoids and in igneous intrusives in general, and it is common for the minimum principal axis of susceptibility (variously referred to as K_3 or K_{min}) to be perpendicular to the plane of the dike (Rochette et al., 1992; Bouchez, 1997). In the case of horizontal sills, as many of the Wichita Granites are interpreted, this means the plane of magnetic foliation should be near-horizontal and K_{min} should be near-vertical. K_{min} at this site is shallow (~21°) and the foliation plane dips steeply to the southeast (Fig. 4). Whether this fabric represents a dike plane, substantial tilting, or something else is presently unclear.

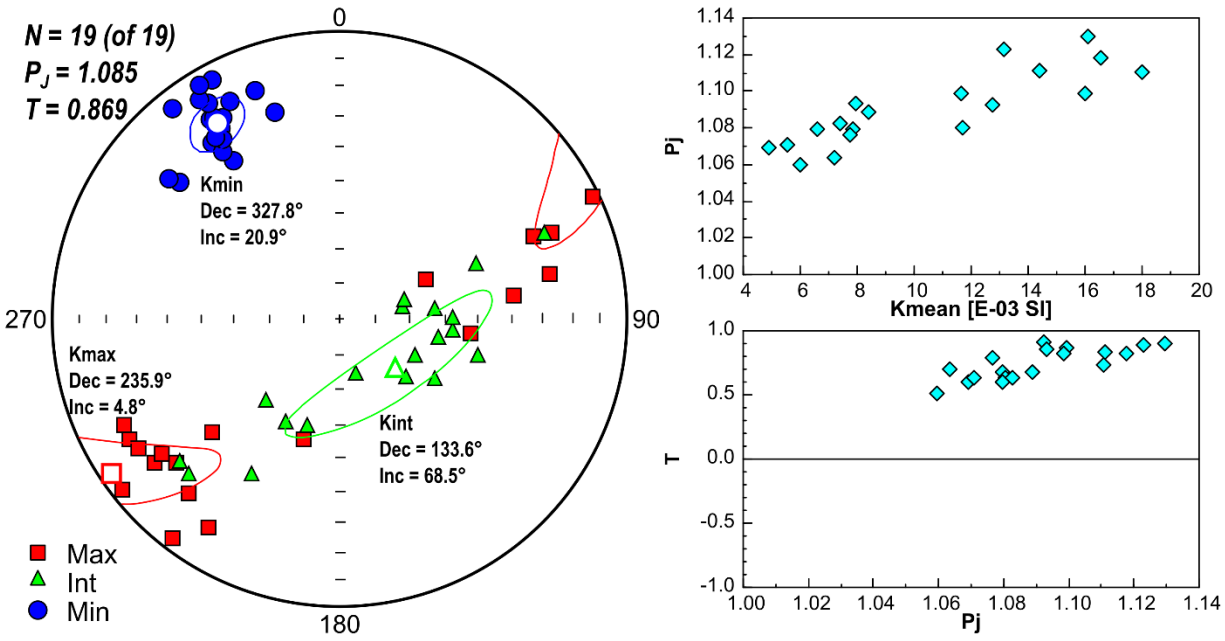


Figure 4. AMS results for site CS1520. (Left) Equal area diagram showing principal axes for individual samples as well as the site mean tensor and statistics. (Right) Jelínek-type crossplots of corrected degree of anisotropy Pj against mean volume-normalized susceptibility (Kmean) (top) and shape factor T against Pj (bottom). A moderate correlation is present.

Demagnetization of specimens from this site yielded consistent behavior and paleomagnetic directions. Due to the previously mentioned problem with the demagnetizing oven, actual temperatures for most points are not known but treatment at 580 °C after fixing the oven completely removed the little magnetization remaining. AF demagnetization to 120 mT removes 90 to 95% of the remanence. A characteristic remanent magnetization (ChRM) with

shallow inclination and a northeasterly declination is progressively unblocked from an apparent temperature of about 300 °C (Fig. 5A). Thermal and AF demagnetization yield essentially the same direction, but the two samples subject to AF treatment showed noticeably steeper inclinations and were not included in the mean. The mean *in-situ* direction has a declination of 60.1° and an inclination of 6.5° and is well-grouped (Fig. 5B; Table 1). Calculation of virtual geomagnetic pole (VGP) locations from the ChRM directions yields a mean pole at 26.2 °S, 186.4 °E with a confidence interval α_{95} = 3.1°. Comparison with the Phanerozoic apparent polar wander path (APWP) for North America of Torsvik et al. (2012) shows that this position is broadly similar to the only constraint at 530 Ma (McCausland et al., 2007) but lies south and slightly east of that pole (Fig. 5C).

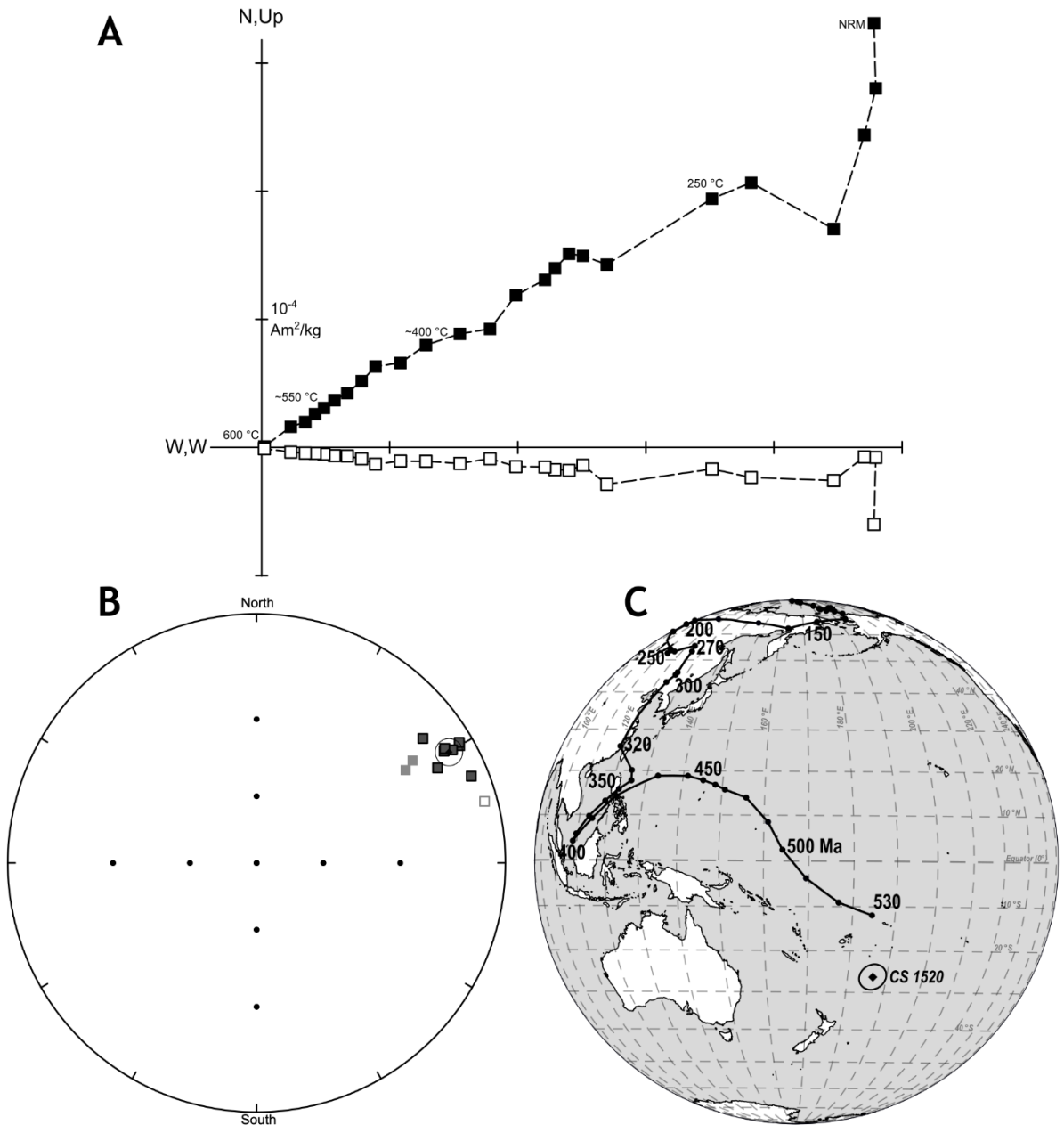


Figure 5. Paleomagnetic results from site CS1520. (A) Representative Zijderveld diagram obtained from thermal demagnetization data. (B) Equal-area plot of all characteristic remanent magnetizations determined for this site and the calculated mean direction. Data outlined in light gray were not included in the mean. (C) Mean virtual geomagnetic pole calculated from in-situ ChRM directions compared to APWP of Torsvik et al. (2012). APWP is the recommended spline path but has been tied to the only constraint used in its calculation beyond 510 Ma.

Sites RP-1 and RP-3, Glen Creek Gabbro

These two sites sampled Glen Creek Gabbro in the eastern part of the Reid's Pit locality, near where it intrudes anorthositic rocks of the Glen Mountains Layered Complex. These rocks are coarse-grained olivine-bearing gabbros. Biotite and amphibole are also obvious in thin section, and opaque minerals are abundant. Needle-like opaque inclusions in plagioclase (likely magnetite) are abundant (e.g., Scofield and Roggenthen, 1986) and are found in all thin sections from mafic lithologies in the current study. An excellent overview of the site and the petrography in general is given by Powell and Gilbert (1982). As these sites were collected very near each other and sampled effectively the same lithology, they are discussed together here.

The mean value of χ is 2.06×10^{-5} m^3/kg and individual specimens range from slightly less than half to slightly more than twice that. Comparison of high-field and initial susceptibilities determined from hysteresis data indicate that paramagnetic minerals contribute less than 2% of the total at low fields in all specimens and less than 1% for most. Hysteresis loops close by about 150 mT and are effectively saturated around 300 mT, with Bc values from 5 to 9 mT (Fig. 6). Backfield remanence indicates a moderately wide coercivity spectrum with an average of about 20-25 mT; bulk values of Bcr are comparable 18-26 mT. Lack of high-coercivity contributions suggests the ferrimagnetic mineralogy is dominated by magnetite.

Hysteresis loop shape can be used to identify additional magnetic fractions. The parameter σ_{hys} is a quantitative indicator of the departure of hysteresis loop shape from that expected by simple domain theory, with positive values corresponding to "wasp-waisted" or constricted loops and negative values corresponding to "potbellied" loops (Fabian, 2003). All hysteresis loops from the Glen Creek Gabbro show values of σ_{hys} near -0.3, corresponding to a somewhat potbellied shape (Fig. 6). Both potbellied and wasp-waisted lops arise from either

mixtures of substantially different coercivity populations or from the presence of superparamagnetic (SP) mineral grains (Tauxe et al., 1996). The backfield data suggest a single dominant coercivity population with some contribution from an overlapping very low-coercivity population but do not indicate distinct groupings, making the superparamagnetic contribution seem more likely. Notably, initial tests for frequency-dependence of susceptibility did not yield any significant variation, though such tests are actually only sensitive to a rather narrow size range relative to the full range of superparamagnetic grain sizes (Hrouda, 2011).

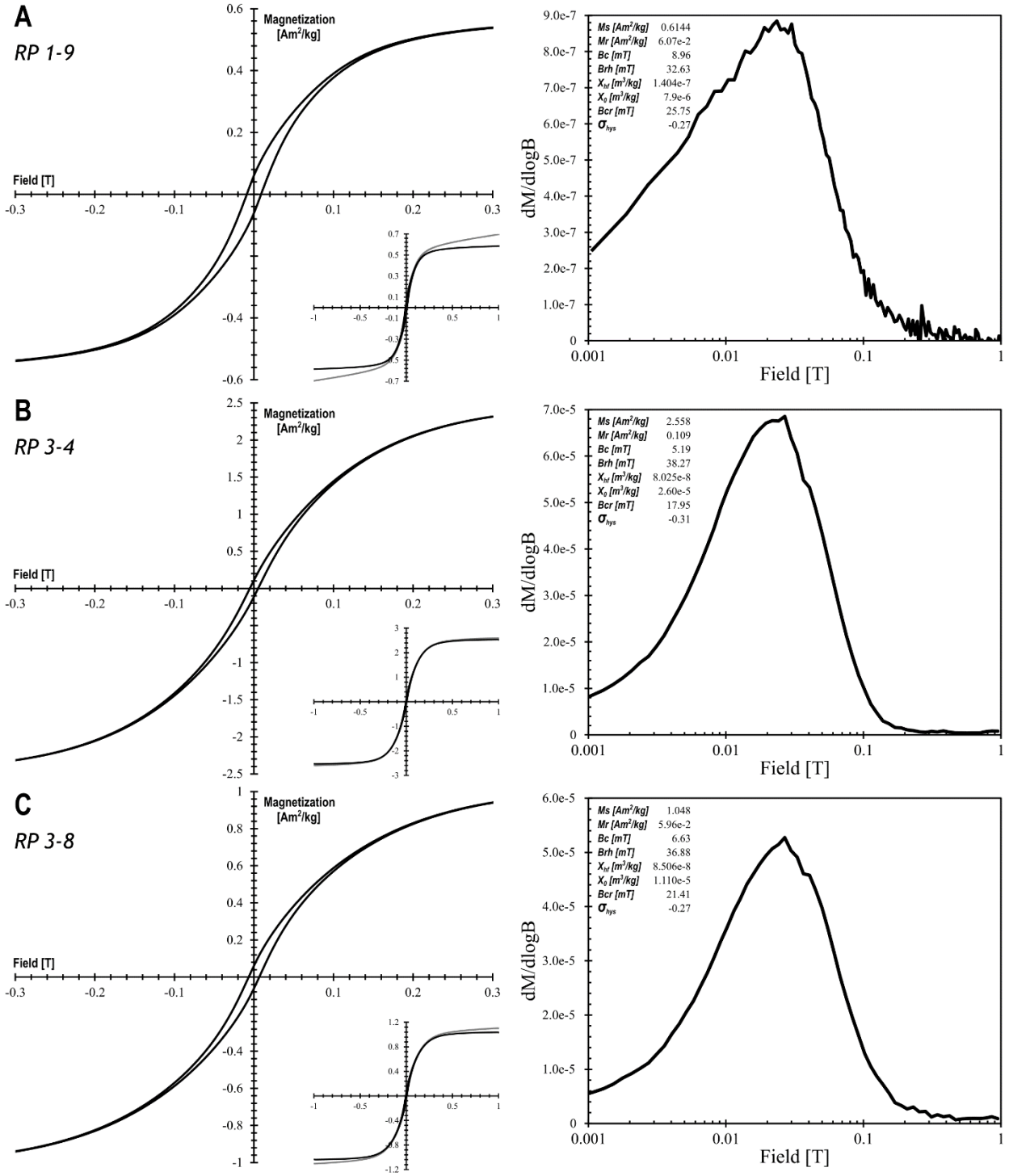


Figure 6. Hysteresis and backfield remanence data for samples of Glen Creek Gabbro at sites RP-1 and RP-3. (Left) Slope-corrected high-field hysteresis loops. (Right) Derivative of backfield remanence curves vs. log applied field. Additional features as in Fig. 2.

AMS data for these sites are complex and are quite noisy at the site level. Individual specimen anisotropies exceed the total paramagnetic contributions by a considerable margin, suggesting the fabric is carried by magnetite. No correlations exist between Pj and total susceptibility or between Pj and T. Site RP-1 shows an oblate fabric with a foliation plane that dips ~25° eastward (Fig. 7). RP-3 nominally has a triaxial to oblate fabric based on T of the mean tensor, but the scatter of individual samples and the very large error ellipses around the principal axes indicate that the susceptibility fabric at this location is effectively incoherent.

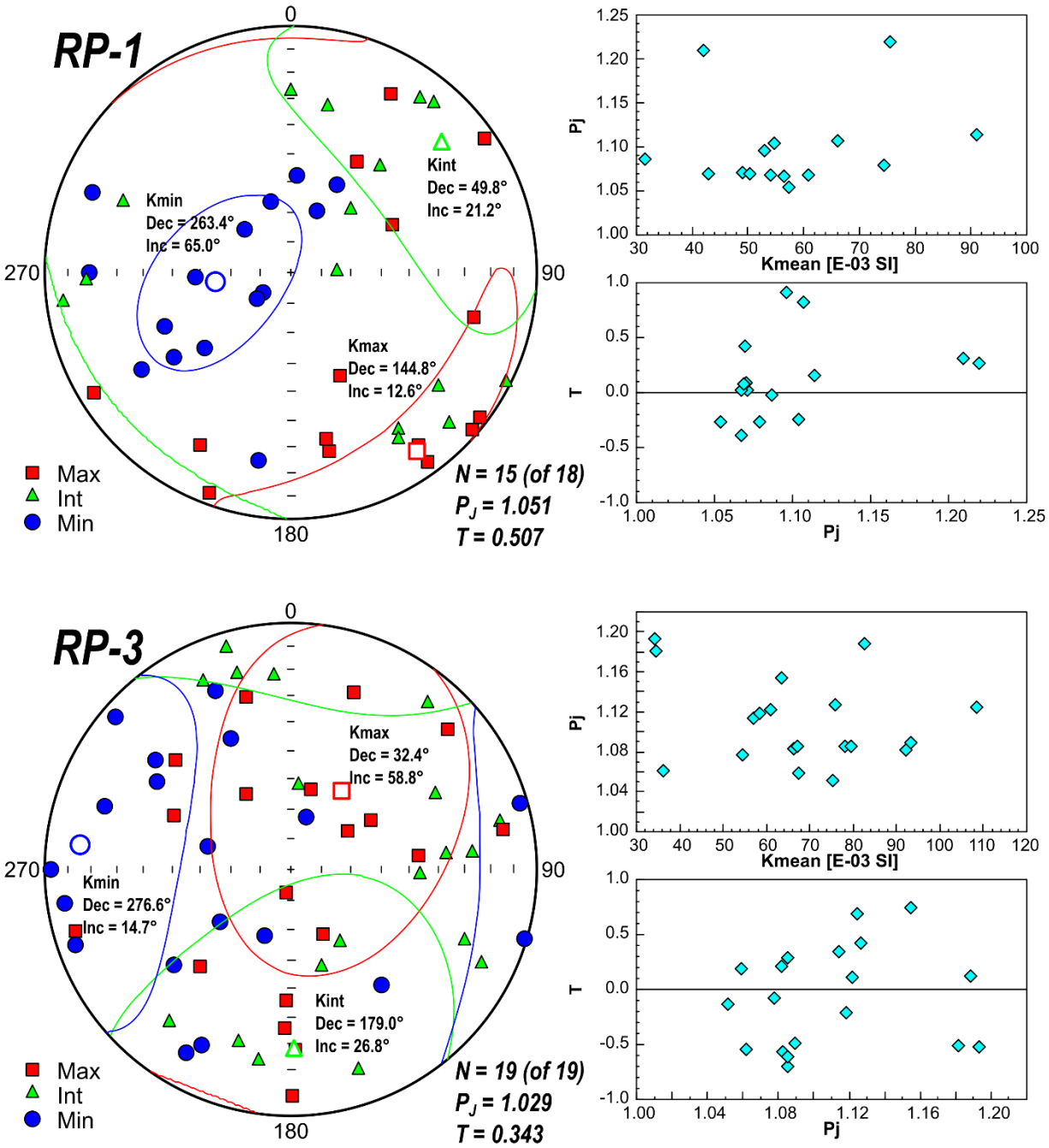


Figure 7. AMS results for Glen Creek Gabbro sites RP-1 and RP-3. (Left) Equal area diagrams showing individual samples and site mean tensor. Some outliers were removed from data for RP-1. (Right) Jelínek-type crossplots of Pj vs. Kmean and T.

Remanence measurements for these sites yielded some unusual results. Normalized magnetization values vary by over an order of magnitude within site RP-3, and large variations are present in RP-1 as well. It was apparent (particularly for RP-3) that the intensity seemed to be

higher in specimens from the outer part of the drilled cores, i.e. nearest the surface. Specimens from this site were measured for length with calipers in order to get the depth below the surface at their center (1mm gaps were assumed for saw cuts). Remanence and bulk susceptibility were measured in order to calculate the ratio of remanence to the induced moment (Q, a.k.a. the Koenigsberger Ratio, after Koenigsberger, 1938). Bulk susceptibility values do not change on average, though the range increases, while Q increases by over an order of magnitude within a couple of centimeters of the surface (Fig. 8). This indicates that remanence alone is responsible, rather than a change in magnetic mineralogy.

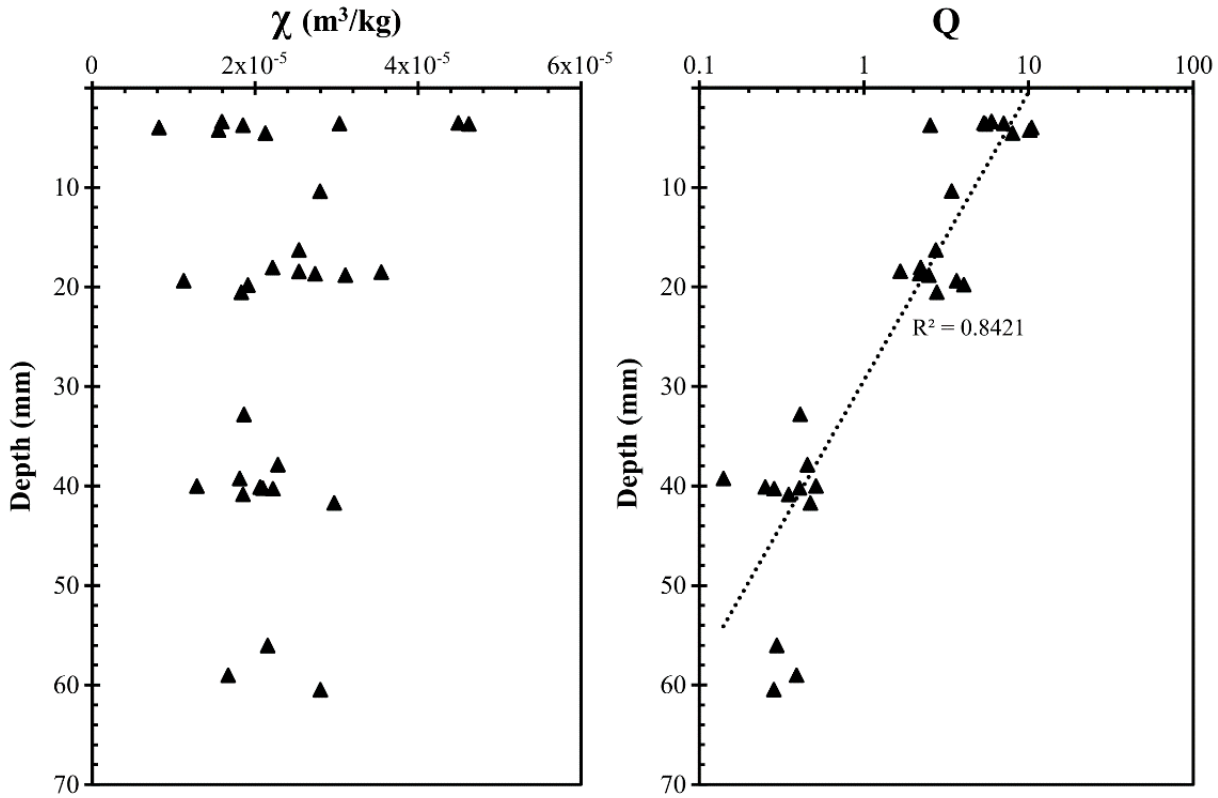


Figure 8. Bulk susceptibility (left) and Q-factor (right) as a function of distance below the outcrop surface at site RP-3.

Specimens from site RP-1 were tested using low-temperature demagnetization in liquid nitrogen followed by AF demagnetization. Remanence values dropped by an average of 66% during the first treatment alone. Analysis of demagnetization data did not yield stable

magnetizations, and specimens began to acquire strong gyroremanent magnetizations at about 40 mT. Samples from site RP-3 were subjected to thermal demagnetization; this site was not affected by the temperature issue. The resulting magnetizations vary considerably, but following the results of the Q analysis it was noted that specimens from deeper in the original plugs yielded a significantly better grouping. In general, a southeasterly and moderately shallow downwardly-inclined magnetization is removed between 200 and 500 °C, at which point the rock is effectively demagnetized (Fig. 9A). Considering only the deeper specimens, the mean direction has a declination of 153.1° and inclination of 19.1° (Fig. 9B).

The average VGP for the site lies at 38.5 °N, 115.8 °E (α_{95} = 6.3°), near the 320-310 Ma segment of the APWP (Fig. 9C). This suggests that the Glen Creek Gabbro was at least partially remagnetized during the late Paleozoic. This has been seen in the granites of the Southern Oklahoma Aulacogen by previous workers (e.g., Ku et al., 1967; Spall, 1968; Vincenz et al., 1975; Hamilton et al., 2016). The VGP determined from the Glen Creek Gabbro at this site overlaps remagnetized granite pole positions from those studies.

The enhanced remanent intensity and the high scatter of the directions obtained from the uppermost specimens are interpreted as most likely due to a nearby lightning strike. Lightning strikes impart an isothermal remanent magnetization (IRM) which can be much stronger than the natural remanent magnetization, and depending on conditions the resulting direction may be uniform or essentially randomized (Dunlop and Özdemir, 1997). The retention of the earlier remanence and the fact that the IRM disappears within a few centimeters of the surface suggests that the overprint was probably from a surface current rather than a direct strike.

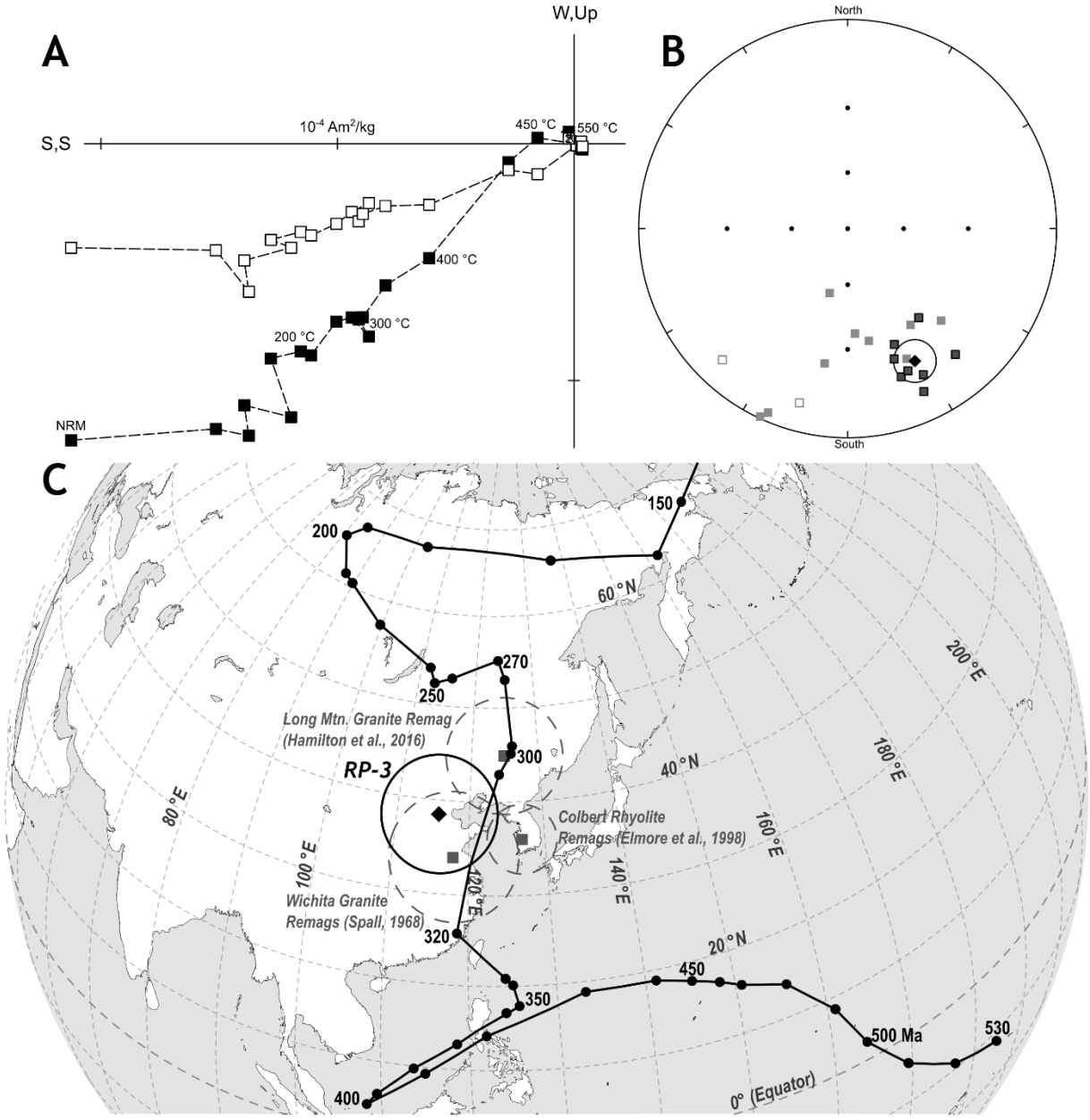


Figure 9. Paleomagnetic results from Glen Creek Gabbro, site RP-3. (A) Representative Zijderveld diagram. (B) Equal area plot of all data and mean; only specimens outlined in black were used. (C) Mean in-situ VGP compared with the North American apparent polar wander path (Torsvik et al., 2012) and previous results from remagnetized early Cambrian granites and rhyolites in the Southern Oklahoma Aulacogen.

Site GM19-1, Unnamed Roosevelt Gabbro

This site sampled a small pod of gabbro on the north side of Oklahoma Highway 19.

Most of the outcrops here are anorthosite from the layered complex, but at this spot there was a

small area which resembles the Glen Creek Gabbro. This is several kilometers from that body's mapped extent and is therefore unlikely to be a part of it. Petrographically, the rock is medium- to coarse-grained and consists mostly of plagioclase, clinopyroxene, brown amphibole (which appears to be replacing pyroxene in places) and orthopyroxene. Opaque minerals are abundant, and olivine, biotite and apatite are also present in reasonable amounts.

The mean value for χ is 1.38×10^{-5} m^3/kg, with a narrow range between 1.07×10^{-5} to 1.60×10^{-5}. Comparison of high-field and initial susceptibilities calculated from hysteresis data indicate the paramagnetic contribution is on the order of 1.2% of the total. Hysteresis data (Fig. 10) is similar to that from RP-3, though Bc and Bcr at this site are slightly higher and σ_{hys} is closer to zero, indicating less of a potbellied character. Saturation remanence (Mr) is slightly less than 10% of saturation magnetization (Ms). Backfield remanence data indicate a moderately broad coercivity with a peak at 30 mT, near the value of Bcr.

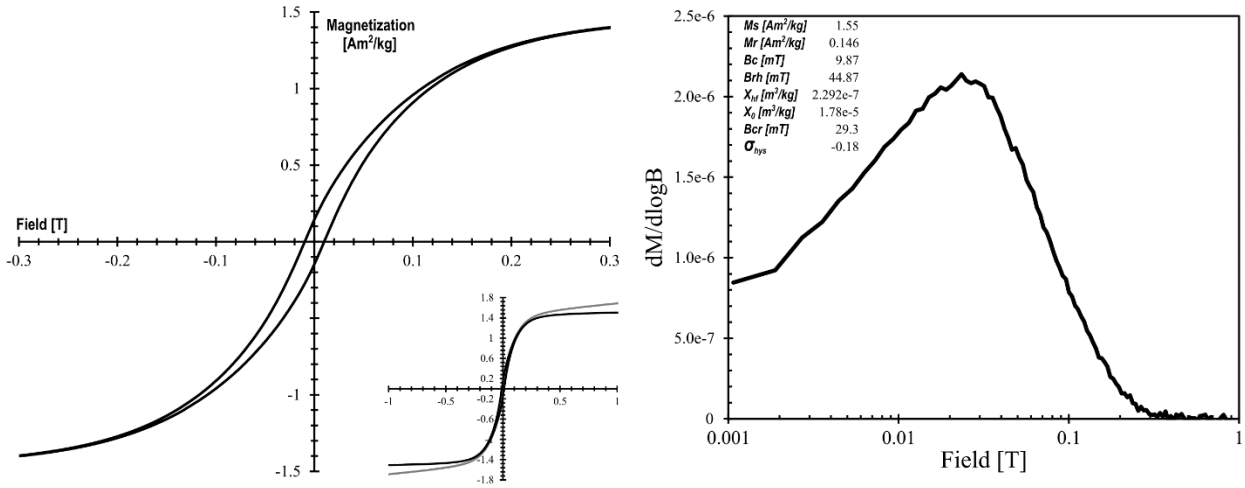


Figure 10. Hysteresis loop and remanent coercivity spectrum for Roosevelt Gabbro at site GM19-1.

AMS data reveal a well-developed oblate fabric with a foliation that plunges steeply to the northwest (Fig 11). Degree of anisotropy is lower than in previously-described sites, with most samples showing Pj between 1.02 and 1.036. This is still higher than the total paramagnetic

contribution, indicating the fabric is carried in the ferrimagnetic fraction. There is essentially no correlation between Pj and Kmean or T. As discussed for the Cold Springs site, oblate fabrics are commonly seen in igneous intrusions, with foliation planes parallel to the dike plane. While dike geometry was not clearly observed at this location (possibly due to the poor quality of most of the exposure), it would explain the limited apparent extent of this particular gabbro and the steep plunge of the foliation. Additionally, the strike of the foliation is very similar to that of the Cold Springs granitoid site (Fig. 4). Following data analysis, a description which appears to correspond to this site was found in Powell et al. (1980b) in which it is interpreted as a dike.

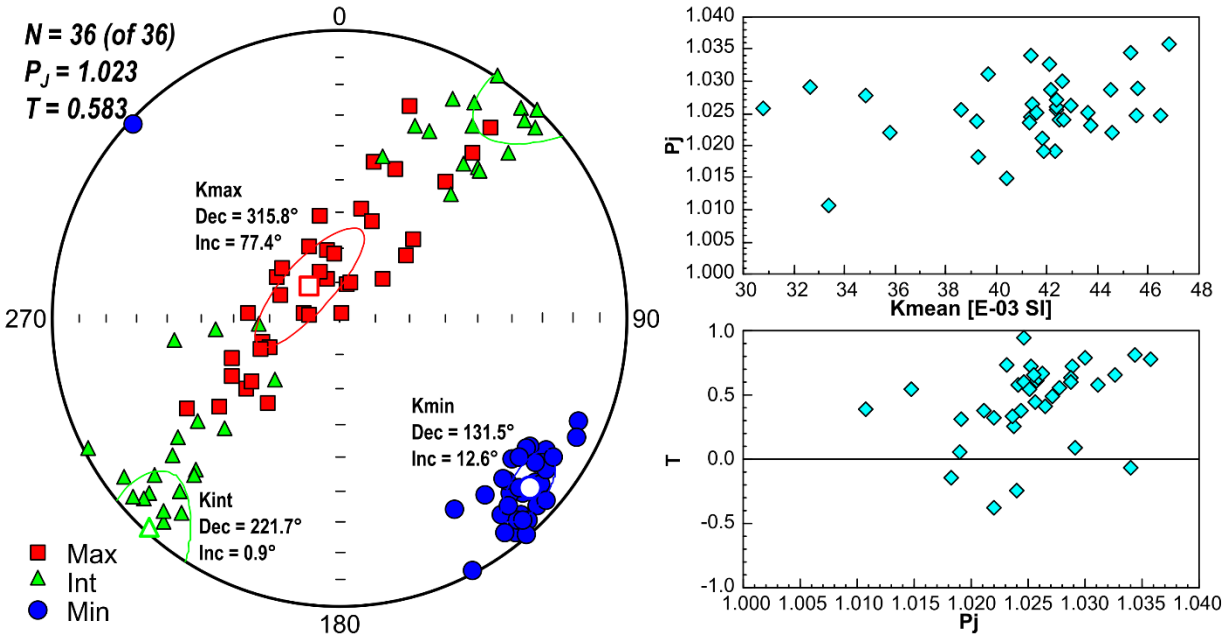


Figure 11. AMS results for Roosevelt Gabbro at site GM19-1.

NRM intensity is unusually low for this site with an average value of 7.70×10^{-5} Am^2/kg, yielding an average Q-factor of 0.16. This site was affected by the problem with the oven, and actual temperatures are not clear for much of the data. Treatment at 600 °C after fixing the oven issue removed virtually all remaining remanence. AF demagnetization resulted in samples being effectively demagnetized by 25 mT and acquiring gyroremanent magnetizations beginning at about 40 mT. While several samples from this site yielded either unstable or highly curved decay

paths, noisy components (MAD up to 10°) were identifiable at higher temperatures in thermal demagnetization data for some samples and generally point southeasterly and shallow, with a mix of positive and negative inclinations (Fig. 12A, B). The mean direction for the site after data selection is declination 149.9°, inclination -5°, corresponding to a mean VGP at 47.3 °N, 128.6 °E (α_{95} = 9°). This plots near the 300 and 290 Ma poles on the APWP (Fig. 12C) and is very similar to the VGP position of remagnetized red Long Mountain Granite from the southwestern Wichita Mountains area (Hamilton et al., 2016). This site appears to have been remagnetized at about the same time, though the rock sampled does not appear nearly as weathered as the granite.

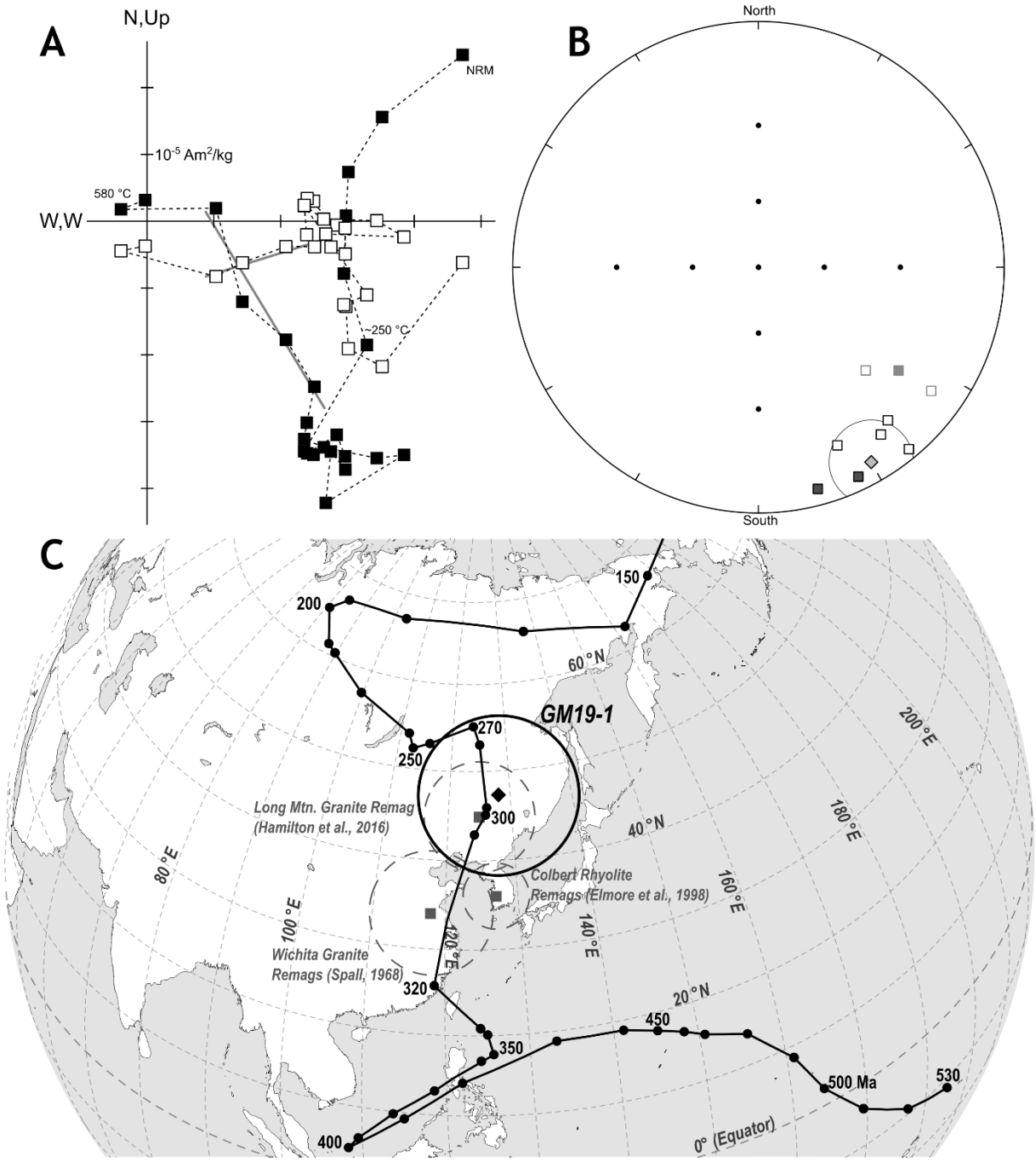


Figure 12. Paleomagnetic results from unnamed Roosevelt Gabbro, site GM19-1. (A) Representative Zijderveld diagram. Solid lines indicate the chosen ChRM. (B) Equal area plot of all data and mean; only specimens outlined in black were used. (C) Mean in-situ VGP compared with the North American apparent polar wander path (Torsvik et al., 2012) and previous results from remagnetized early Cambrian granites and rhyolites in the Southern Oklahoma Aulacogen.

Site RP-2, Glen Mountains Layered Complex

This site sampled anorthosite of the GMLC at the Reid's pit location, just west of the contact with the Glen Creek Gabbro. The outcrop here is mapped as part of the "M-Zone" of the layered series (Powell et al., 1980a, 1980b; Gilbert, 1982). Primary mineralogy consists of medium-grained plagioclase with minor amounts of opaque minerals and ophitic pyroxene. Plagioclase has been partially sericitized and recrystallized along some fractures, and some pyroxene has been replaced by chlorite. Minor carbonate veins are also present.

Values of χ range from 5.1×10^{-7} to 5.2×10^{-6} m^3/kg, with a mean of 1.24×10^{-6}. Paramagnetic minerals contribute less than 1% of this. Bulk coercivity is low (5 to 9 mT). Hysteresis and backfield data for two samples from this site show some variation – roughly a factor of two difference in Bc and Bcr. The sample with higher Bc and Bcr has a σ_{hys} value of -0.2, indicating a slightly potbellied character, and a coercivity spectrum with a single peak near 70 mT (Fig. 13A). The low-Bc, low-Bcr sample has σ_{hys} of essentially zero and a broader coercivity spectrum which likely includes multiple components (Fig 13B). High Mr/Ms and low Bc indicates bulk hysteresis properties are likely controlled by MD grains, though the high coercivity population revealed from backfield data is consistent with remanence properties dominated by single-domain (SD) particles of magnetite and/or titanomagnetite (Dunlop and Özdemir, 1997; Dunlop, 2002).

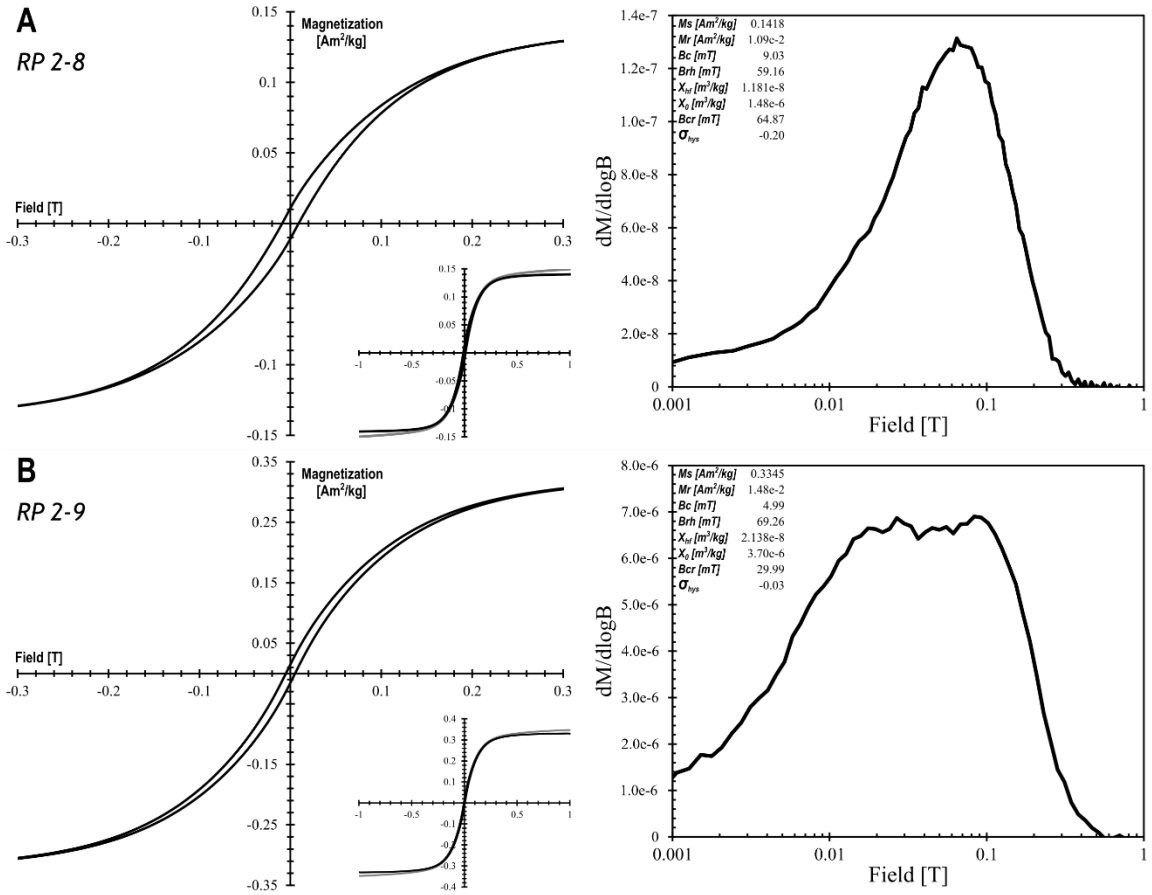


Figure 13. Hysteresis loops and backfield coercivity spectra of anorthosite samples from site RP-2.

The AMS data from this site indicate a triaxial-oblate fabric (mean tensor T = 0.342) with a foliation plane dipping 37° to the northeast (Fig. 14). Individual specimens have Pj ranging from 1.05 to 1.35 (though most are less than 1.15), indicating the fabric is carried by ferrimagnetic minerals. No correlation is apparent between Pj and Kmean or T. Values of T range from -0.6 to 0.6 for individual specimens, despite the mostly oblate character of the site-level fabric.

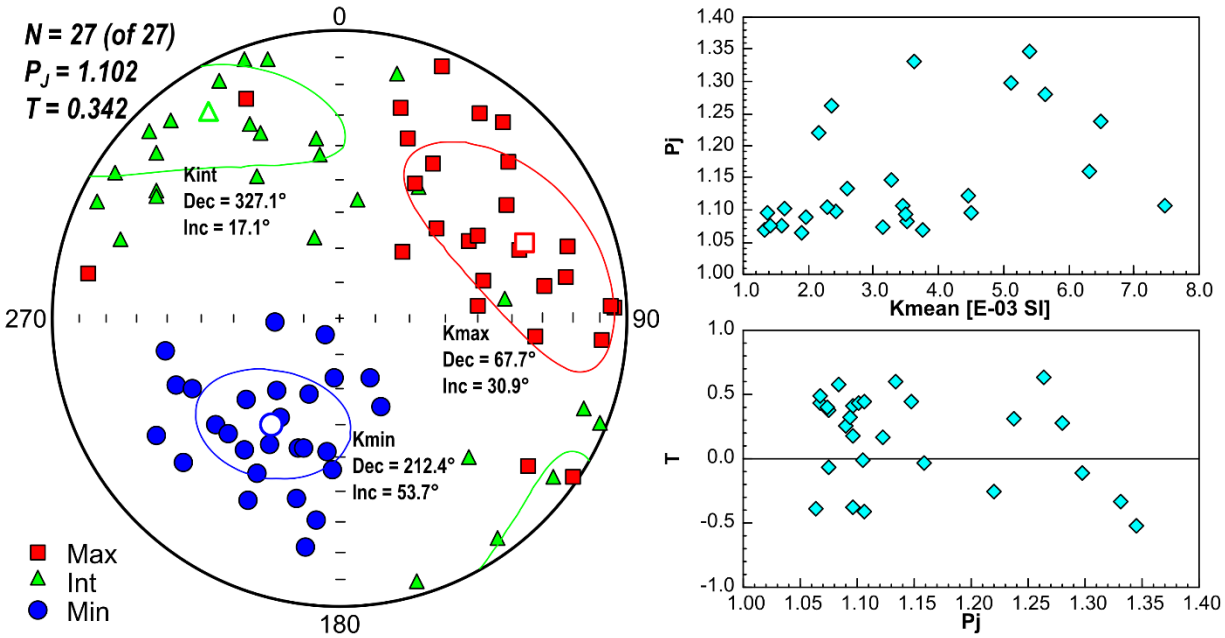


Figure 14. AMS data from Glen Mountains Layered Complex anorthosite at site RP-2.

Low-temperature demagnetization of pilot specimens in liquid nitrogen removed about a third of the NRM intensity. About half of the samples from this site have high remanent intensities and directions which point upwards near-vertically. This is most likely due to a nearby lightning strike. Many samples – both those with the apparent lightning overprint and without – were essentially unaffected by thermal demagnetization to 575 °C (this site was not affected by the oven issue), and components for those were not chosen. The rest have a southeasterly and moderate to shallow down ChRM that is removed between 400 and 550 °C (Fig. 15A). Blocking temperatures, low-T demagnetization results and hysteresis properties suggest it is housed in magnetite. Picked ChRMs seem to form a streak with a relatively consistent declination and shallow to moderate inclinations; the steepest two specimens were not included in calculation of mean directions and VGP. The mean *in*-situ direction has a declination of 256.7° and inclination of 21.9° (Fig. 15B), corresponding to an average VGP at 4 °S, 188 °E (α_{95} = 5.1°). This position is similar to but slightly north-northeast of the 530 Ma pole of McCausland et al. (2007) (Fig. 15C).

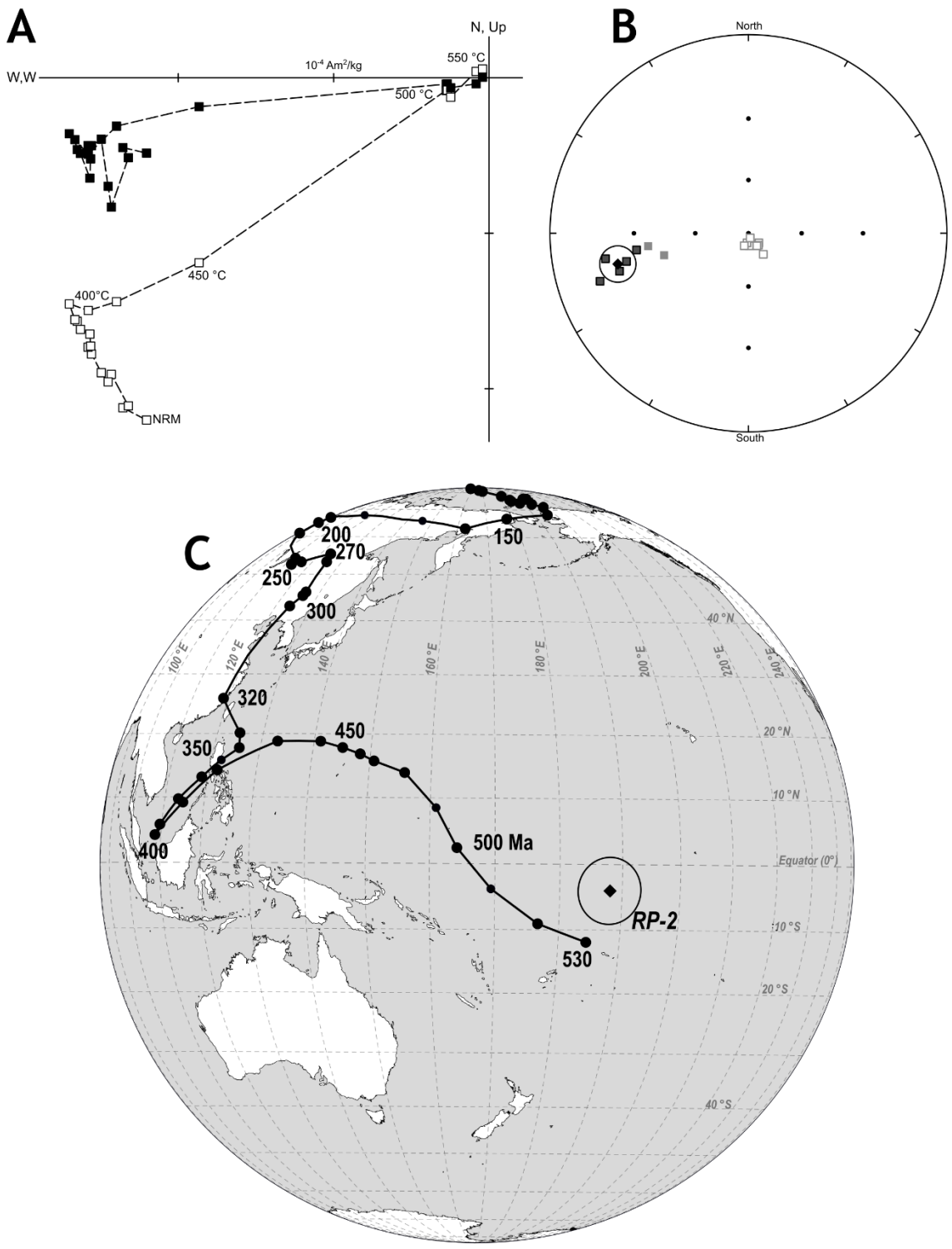


Figure 15. Paleomagnetic results for GMLC anorthosite at site RP-2. (A) Representative Zijderveld diagram. (B) Equal area plot of identified ChRMs. (C) Comparison of mean in-situ VGP to Phanerozoic APWP of North America.

Site GM19-2, GMLC

This site sampled anorthosite along the north side of Oklahoma Highway 19 just east of site GM19-1. Previous drill holes were found at this locality, possibly those of Roggenthen et al. (1981). The rock is medium-grained and medium to light gray in color, with localized areas nearly white. No thin section was made for this site. This location is mapped as part of the M-Zone of the layered series (Gilbert, 1982).

Values of χ range from 7.75×10^{-7} to 2.05×10^{-5} m^3/kg, with a mean of 3.05×10^{-6}. Paramagnetic minerals contribute about 1% of this. Hysteresis data indicate Bc < 4 mT, with Bcr of 12.6 mT and the backfield coercivity spectrum is dominated by a peak of about the same value (Fig. 16). The hysteresis loop is very slightly potbellied (σ_{hys} = -0.08), most likely due to a small contribution from SP grains as there are no distinct high-coercivity populations. Low Mr/Ms, low Bc, and the low Bcr are suggestive of MD (titano)magnetite.

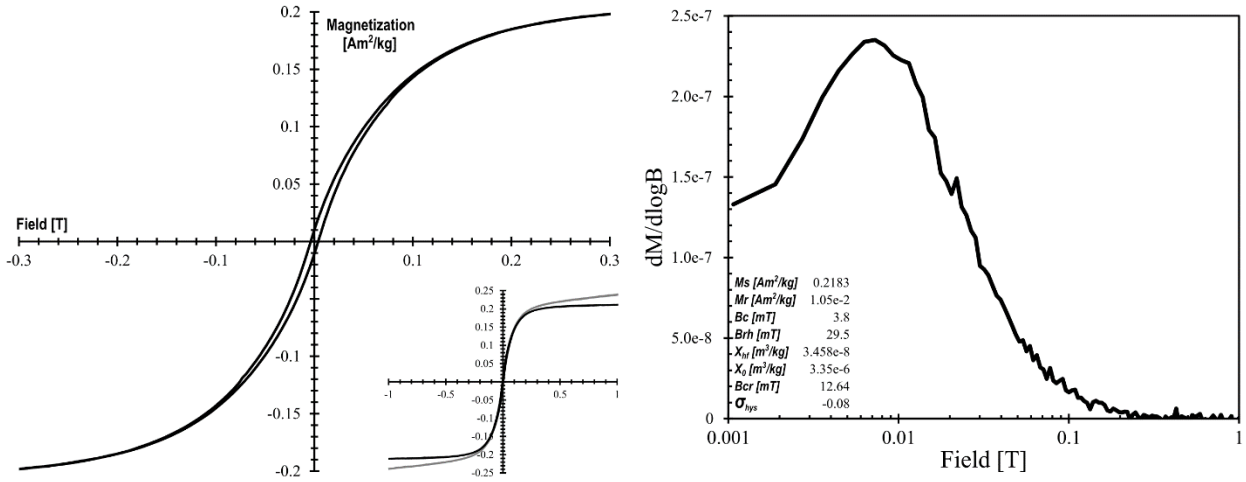


Figure 16. Hysteresis loop and remanent coercivity spectrum for GMLC anorthosite at site GM19-2.

AMS data for this site are somewhat complex. As a whole, the site possesses a reasonably well-defined triaxial-oblate fabric with a foliation plane dipping ~20° to the southwest (Fig. 17A). Individual specimen anisotropy values range from 1.06 to 1.32 and almost

all are triaxial to oblate; comparison with the paramagnetic contribution to susceptibility indicates that the fabric is carried in the ferrimagnetic fraction.

Examination of the Pj- Kmean plot shows the possible presence of two different trends; Kmin axes also appear to form two diffuse groups. One set of specimens has relatively low susceptibility and a reasonable correlation of Pj and Kmean, while the other has higher susceptibility and a weaker correlation of these parameters (Fig. 17A, right). One specimen with Kmean intermediate between these groups showed directions misaligned with the others and was not assigned to either. Samples with Kmean $<5x10^{-3}$ SI show a consistent fabric with a foliation dipping slightly (~7°) to the WNW (Fig. 17B). Specimens with higher Kmean ($>10x10^{-3}$ SI) show a fabric with a foliation dipping much more steeply (~41°) to the southwest (Fig. 17C). The individual groups each show a more oblate character, higher mean tensor Pj, and more tightly-clustered Kmin directions than the site as a whole. The origin of this apparently split fabric is unclear and is not tied to particular drill cores – specimens from both groups are found in several individual cores.

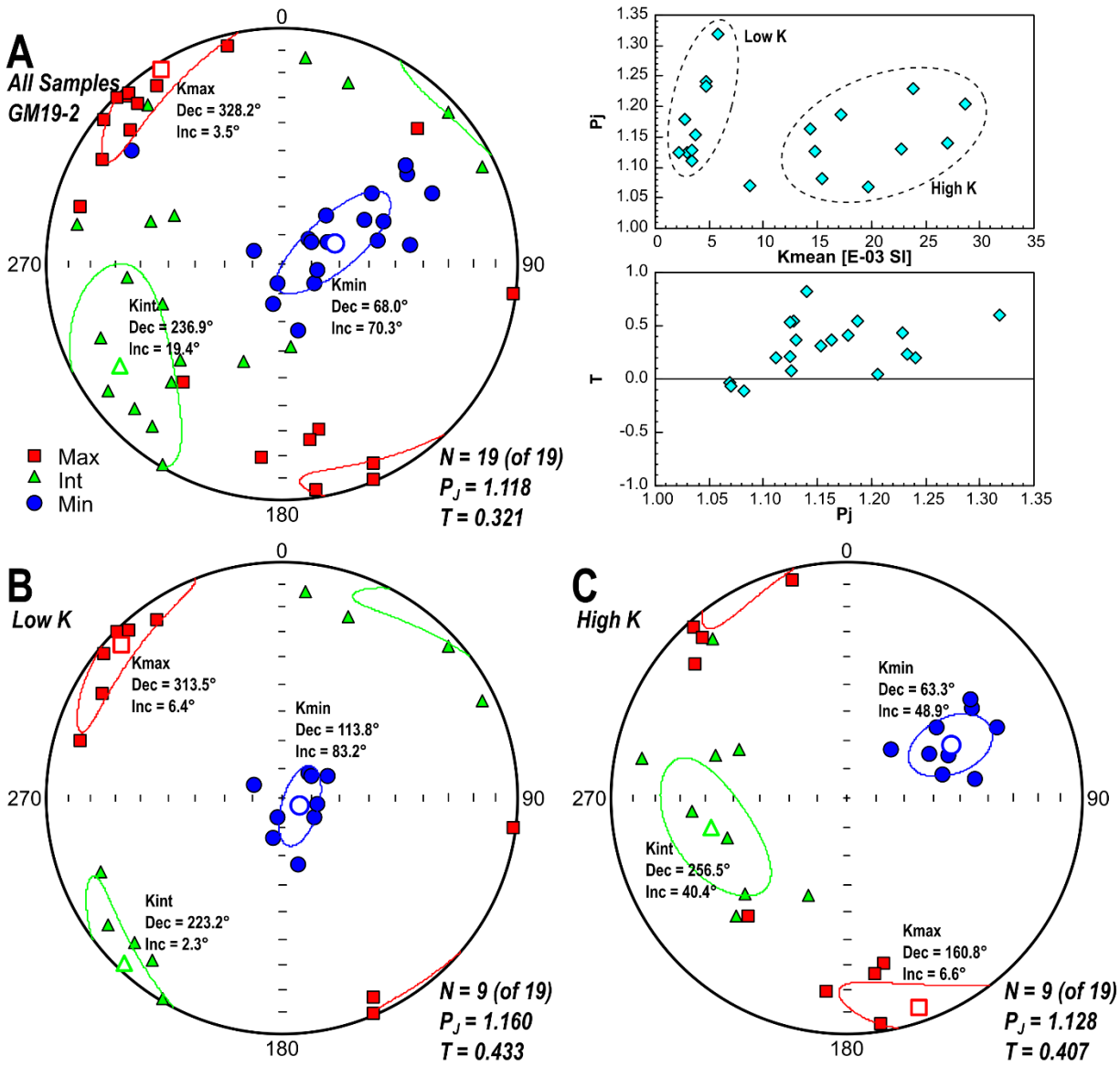


Figure 17. AMS results for site 19-2, GMLC. (A) Equal area plot and scalar crossplots for all samples. Note two populations in Pj-K plot. (B) Equal area plot for low-K specimens. (C) Equal area plot for high-K specimens.

Remanence intensities are not particularly high at this site, and the average Q is less than 1. This site was affected by the temperature control issue, and blocking temperatures are therefore only estimates but seem to be near 500 °C. Two distinct magnetic components are present (Fig. 18A). Component 1 has a southeasterly declination and moderately down inclination (mean D = 111.8°, I = 36.1°, α_{95} = 10°), while component 2 points northeast and up (mean D = 38.5°, I = -30.1°, α_{95} = 7°) (Fig. 18A, B). Both components are present in several

samples, while in others only component 1 is found. Where both are present, component 1 is removed at lower temperatures (Fig. 18A). Component 1 yields a mean VGP at 5.1 °N, 142.1 °E (α_{95} = 10.7°), which lies south of the Ordovician segment of the APWP and overlaps with previous results for granites and rhyolites of the Southern Oklahoma Aulacogen (Spall, 1968; Elmore et al., 1998; Hamilton et al., 2016). Component 2 yields a mean VGP at 27.2 °S, 218.9 °E (α_{95} = 6°), considerably to the southeast of the 530 Ma constraint (Fig. 18C). Comparison of remanence results with measured susceptibilities indicates that component 2 is likely preferentially associated with lower susceptibilities; in all measured specimens where $\chi > 1.5 \times 10^{-6}$ m^3/kg, only component 1 was recovered.

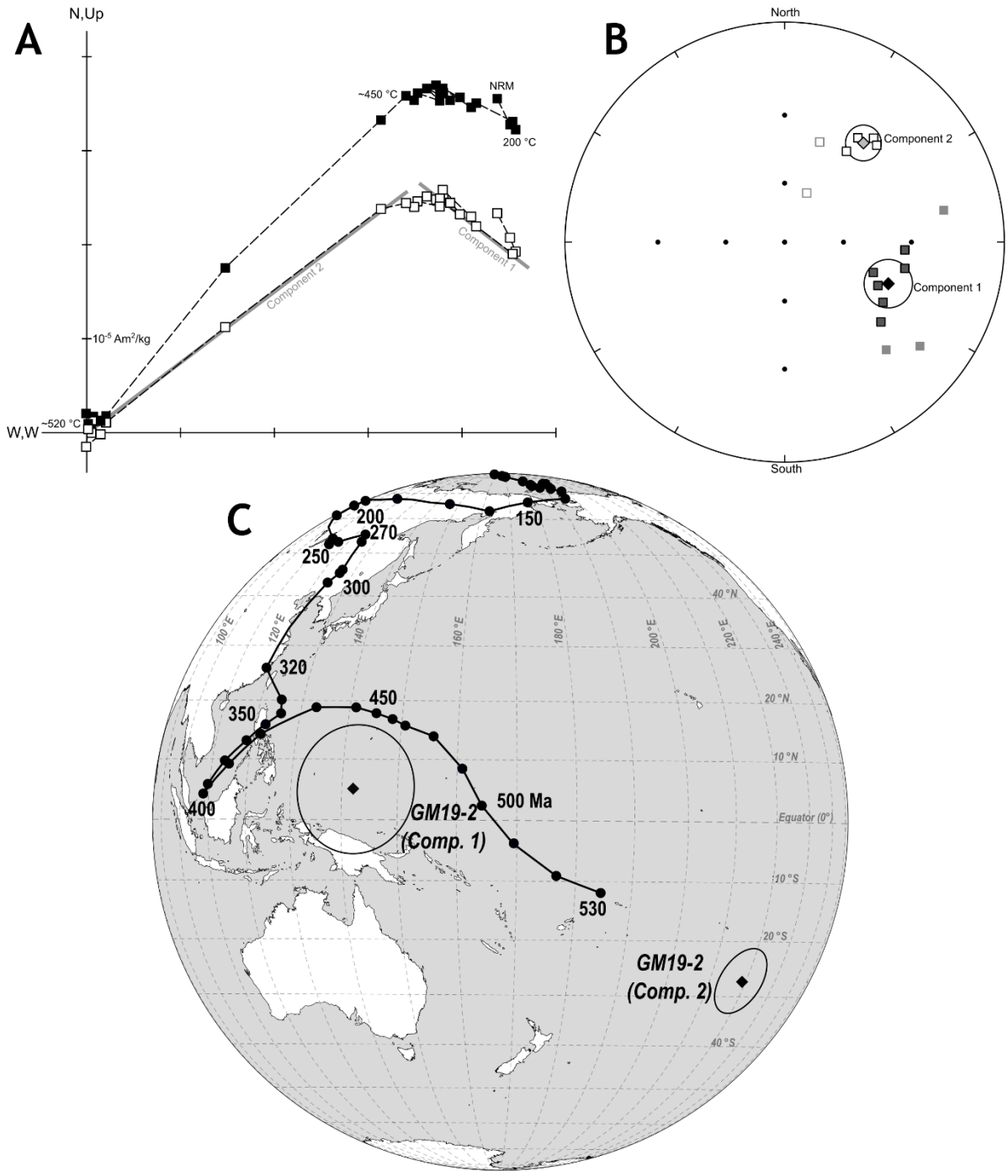


Figure 18. Paleomagnetic results for GMLC site GM19-2. (A) Representative Zijderveld diagram showing two components of the magnetization. (B) Equal area plot of determined magnetic directions. (C) Comparison of mean in-situ VGPs with the North American APWP.

Site GM19-3, GMLC

This site sampled anorthosite along the north side of Oklahoma Highway 19 approximately 1 km west of site GM19-2. The rock is medium to coarse-grained and dark to medium gray in color. No thin section was made for this site. This location is mapped as part of the M-Zone of the layered series (Gilbert, 1982). The outcrop sampled here most likely corresponds to the GMLC sampling location of Wall et al. (2021).

Values of χ range from 1.49×10^{-6} to 6.02×10^{-5} m^3/kg, with a mean of 3.47×10^{-6}. Hysteresis data indicate that paramagnetic minerals contribute less than 0.1% of the initial susceptibility, and nonlinear slope correction in fact yields a negative high-field susceptibility for one sample. Bc and Bcr are exceptionally low at 1.8 and 6.18 mT respectively, and the backfield coercivity spectrum is overwhelmingly composed of a low-coercivity component with an average of about 7 mT (Fig. 19). Hysteresis loops are non-distorted to slightly potbellied (σ_{hys} = -0.01 to -0.19), most likely due to a small contribution from SP grains in the absence of distinct high-coercivity populations. Ms and Mr values are comparable to or higher than those of samples from the Roosevelt Gabbros, with Mr/Ms ≈0.03. This ratio likely indicates a very large contribution from MD magnetite or titanomagnetite (e.g., Dunlop, 2002). The initial susceptibility measured by VSM is higher than any observed for large samples with the MFK1, and it is probable that the hysteresis sample was not representative of the site as a whole.

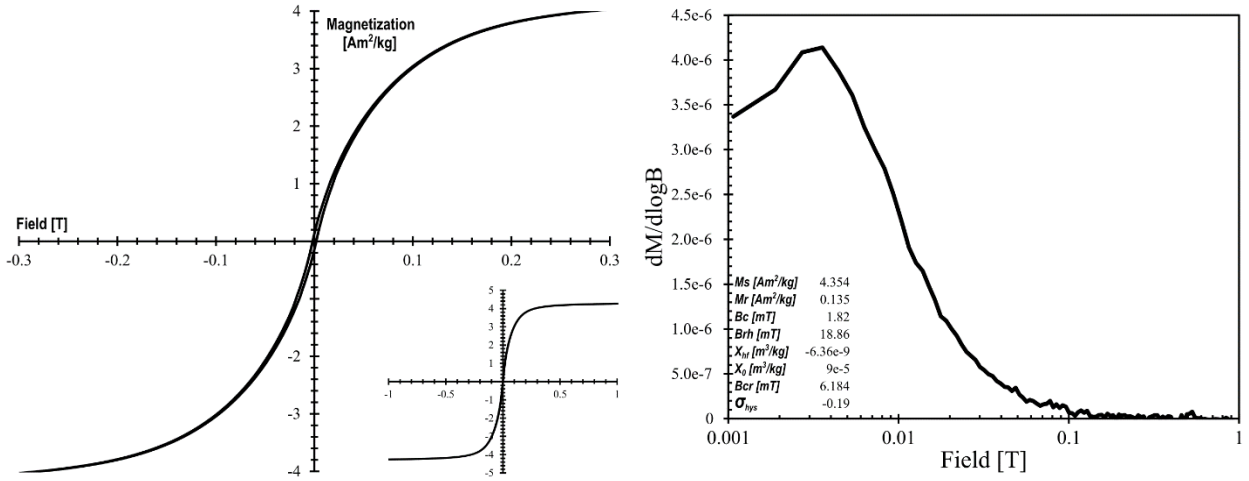


Figure 19. Hysteresis loop and backfield remanence coercivity spectrum for anorthosite at site GM19-3.

AMS data yield a reasonably well-defined oblate fabric (Tmean = 0.677) with a foliation that plunges ~20° to the NNW (Fig. 20). Individual specimen values of Pj range from 1.1 to 1.57. The degree of anisotropy indicates the fabric is carried in ferrimagnetic minerals. No relationships are evident between Pj and Kmean or T.

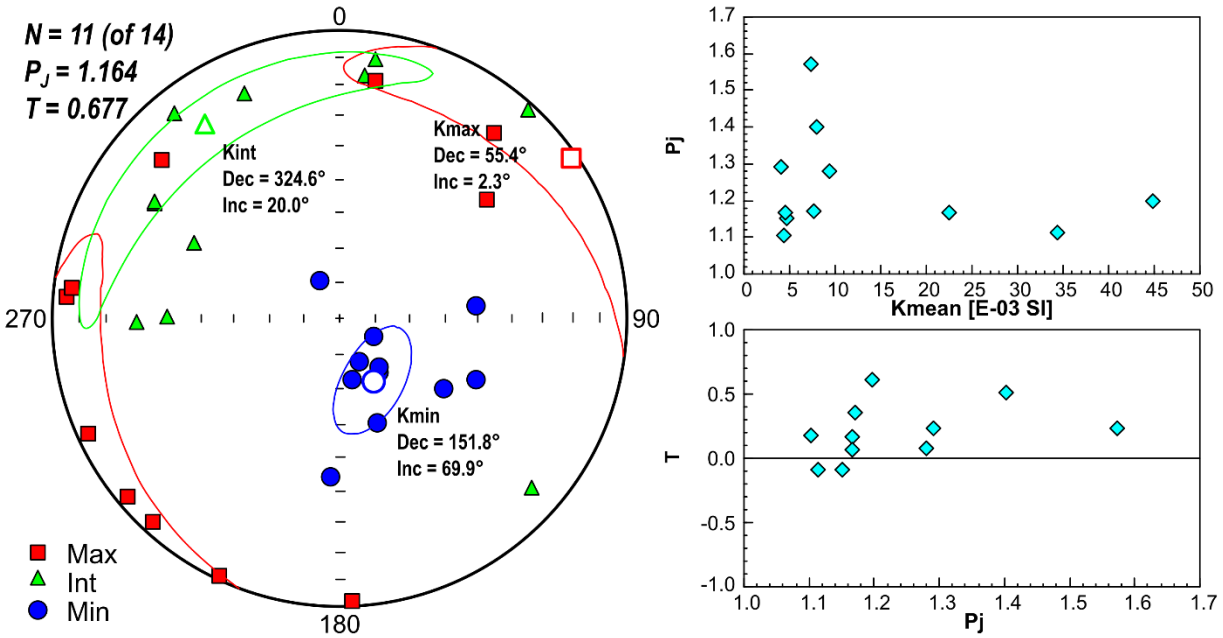


Figure 20. AMS results for GMLC site 19-3.

NRM intensities are high for this site, and the average value of Q is over 20. This site was affected by the temperature control issue, but blocking temperatures were likely near 570-580

°C. Thermal demagnetization yields a consistent southwesterly and moderately steep upward direction (Fig. 21A) which is only removed at relatively high-temperature treatments, likely beginning in the range of 450 – 500 °C. This ChRM has a mean declination of 229.6° and inclination -50.6° (Fig. 21B), corresponding to a mean VGP at 48.9 °S, 161.3 °E (α_{95} = 6.8°) (Fig. 21C). The mean VGP position is a considerable distance south of the APWP and does not align with previous results, making it difficult to interpret. The steep inclination could be explained by a partial lightning overprint. Average remanent intensity is roughly 2% of saturation remanence Mr, which is well within the bounds of expected thermal remanent magnetization intensities and well below the proportion expected for a lightning IRM (Dunlop et al., 1984; Dunlop and Özdemir, 1997). It could be that the overprint was only partial and that the strike happened long enough ago that the multidomain magnetite (inferred from hysteresis results) has had time to lose much of its remanence. This is admittedly speculative, and this site's remanence cannot be well explained at present.

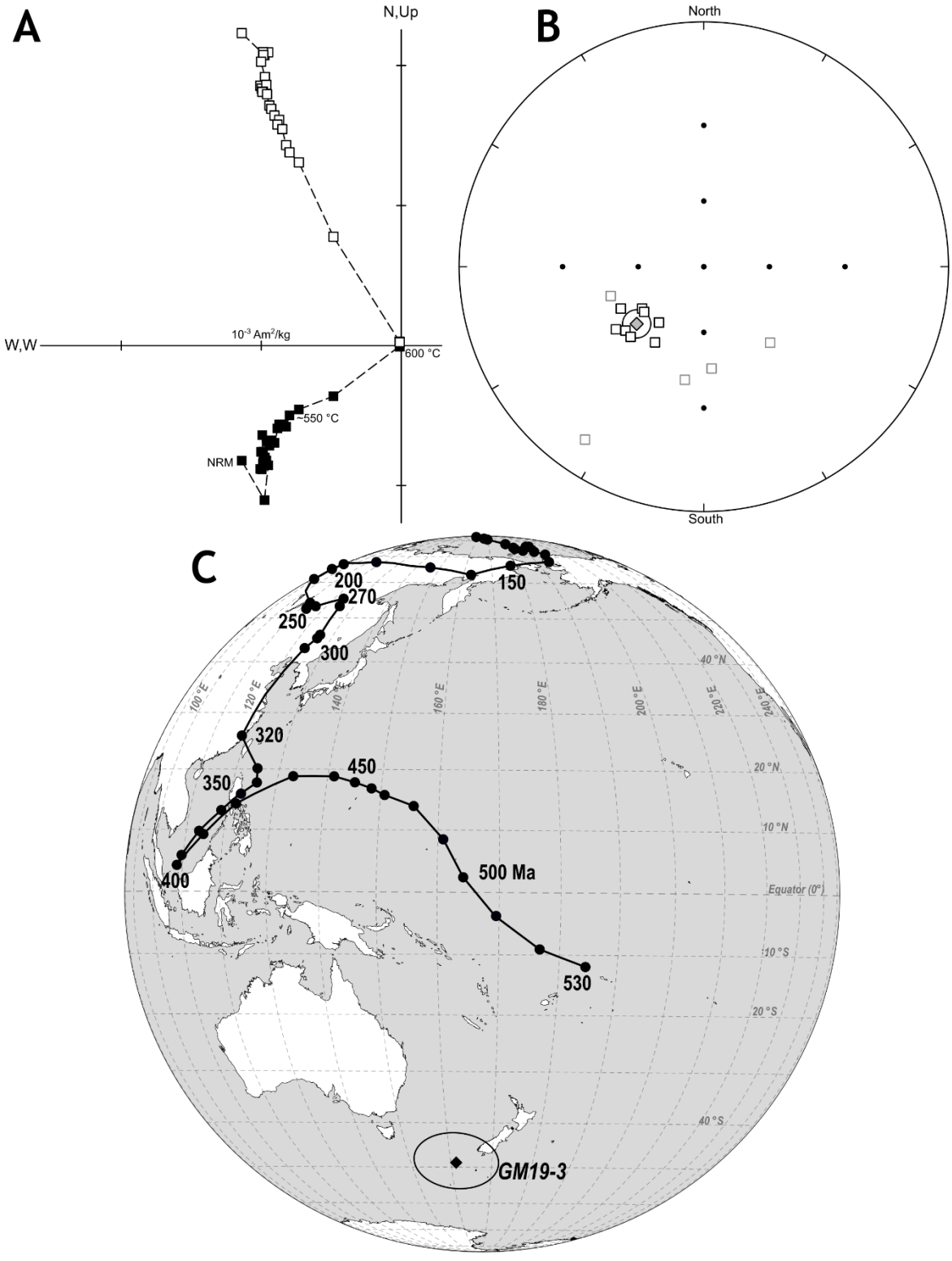


Figure 21. Paleomagnetic results from GMLC site GM19-3. (A) Representative Zijderveld diagram showing the typical southwesterly and up ChRM. (B) Equal area plot of identified ChRMs for this site. (C) Comparison of mean in-situ VGP with North American APWP.

Site GM1535, GMLC

This site sampled the layered series along a county road southwest of Cold Springs. The rock is medium to coarse-grained and medium gray in color with white color around small fractures; much of the outcrop is weathered. No thin section was prepared for this site; the rock appears to be an anorthosite. The location is mapped as belonging to the L-Zone of the layered series by Gilbert (1982).

Magnetic susceptibility χ is relatively uniform with a mean value of 3.87×10^{-7} m^3/kg, by far the lowest for any site sampled during this study. Hysteresis data indicates paramagnetic minerals account for ~1% of this. The hysteresis loop acquired for this site closes at about 250 mT and has Bc = 26.8 mT and Mr/Ms = 0.38, suggesting a high contribution from SD magnetite (Dunlop, 2002). The loop is slightly potbellied (σ_{hys} = -0.15), and the backfield coercivity spectrum shows a moderate dispersion with a peak near 30 mT (Fig. 22).

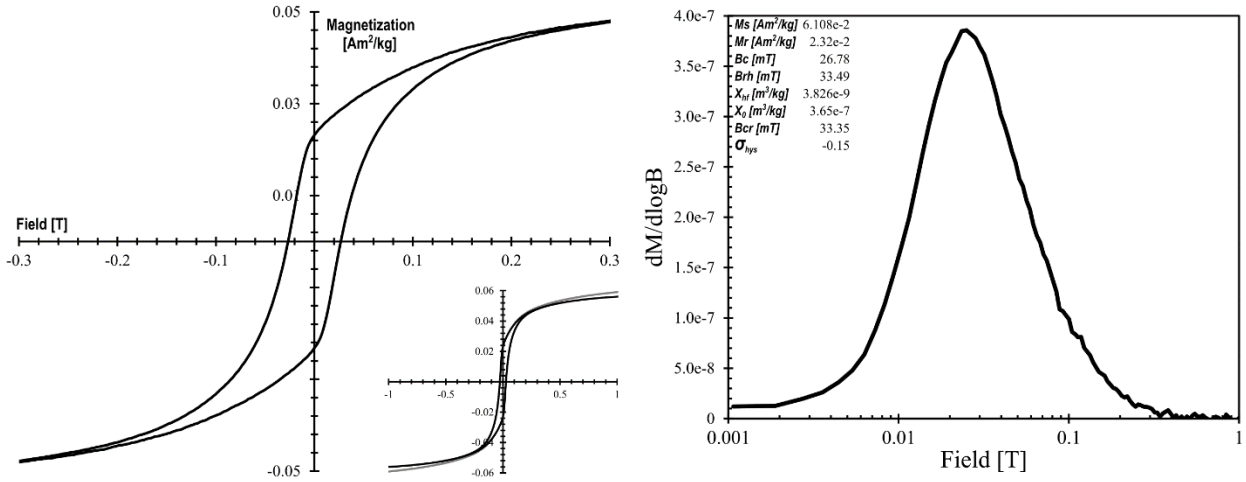


Figure 22. Hysteresis loop and backfield coercivity spectrum for sample from GMLC site GM1535.

AMS data show a very well-defined oblate fabric (Tmean = 0.809) with foliation dipping ~17° to the east (Fig. 23). The individual samples are very similar compared to other sites – Pj

ranges from 1.11 to 1.16, and all values of T are above 0.5. No interdependence of parameters is observed.

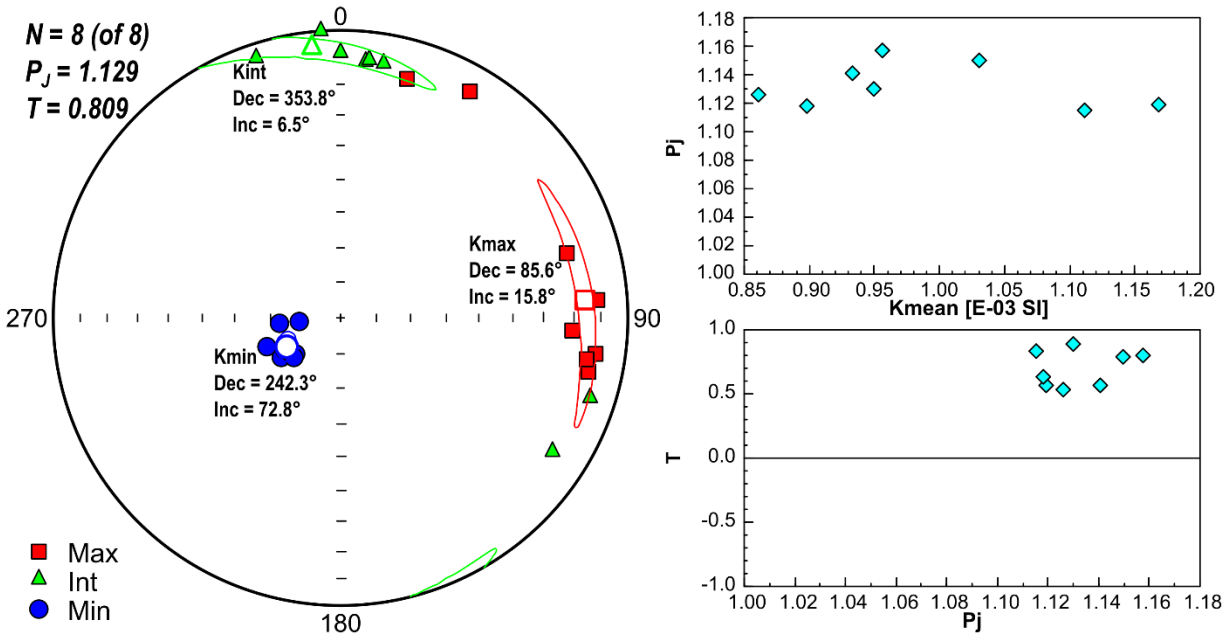


Figure 23. AMS Results from GMLC site GM1535.

Remanence data are somewhat less well-behaved. Q values are very high, with an average of 48.6. Thermal demagnetization has little effect up until an estimated temperature of 550 °C or so; temperature control issues make it presently impossible to quantify. The characteristic remanent magnetization has southeasterly declinations and steep down inclination (Fig. 24A). Mean declination is 147.4° with an inclination of 67.9° (Fig. 24B). AF demagnetization yielded southerly and southwesterly declinations which were disregarded in this calculation. The corresponding mean VGP lies at 0.5 °S, 100.9 °E, near the 400 Ma position of the apparent polar wander path (Fig. 24C).

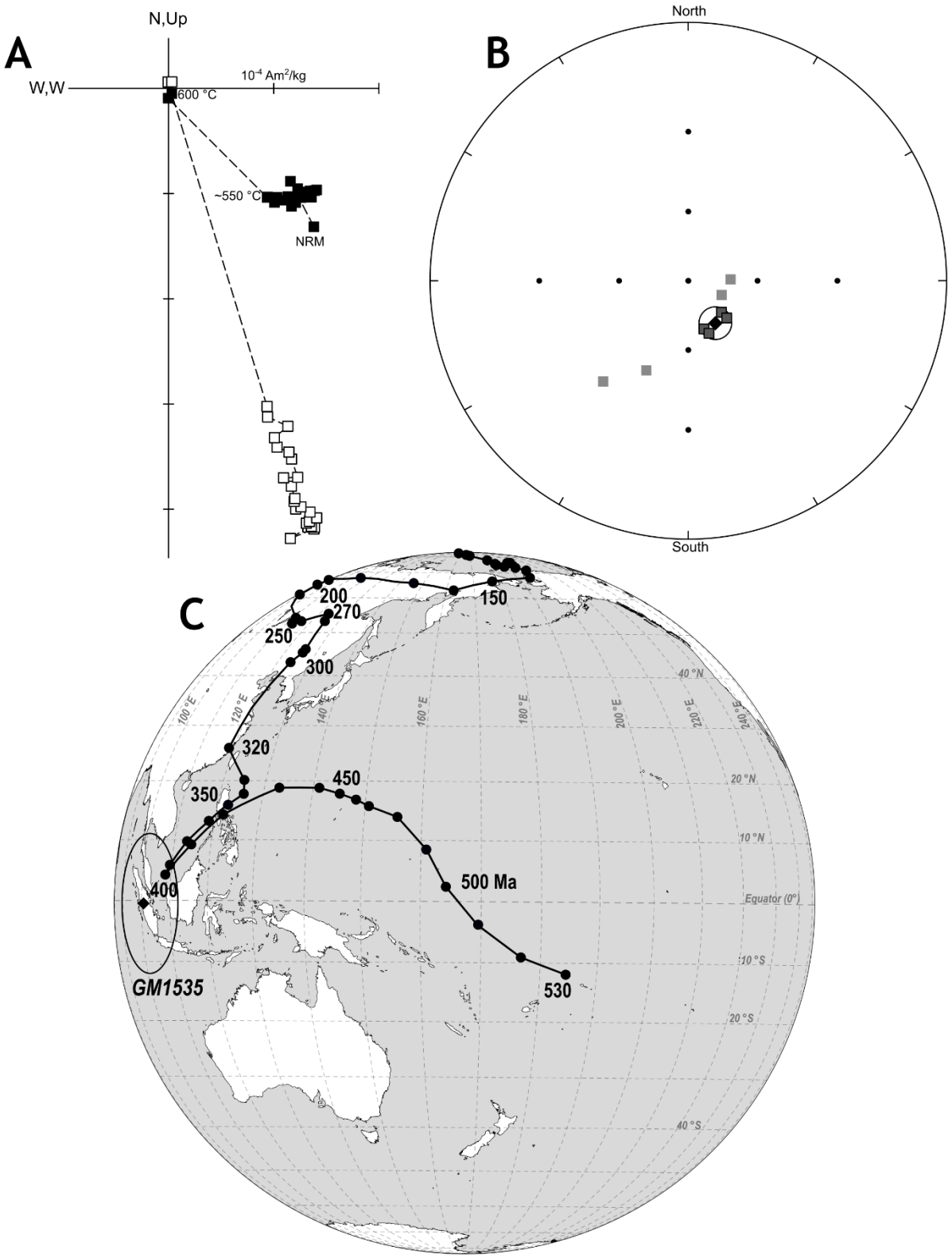


Figure 24. Paleomagnetic results from site GM1535. (A) Representative Zijderveld diagram. (B) Equal area plot of ChRMs from this site. (C) Comparison of mean in-situ VGP to North American APWP.

This particular pole position is curious – it does not correspond to known tectonic events or recognized remagnetizations in the area. The steep inclinations could potentially be due to a partial lightning overprint, though this usually results in vertically *up* directions such as those seen in RP-2 samples (Fig. 15A). The ratio of NRM intensity to saturation remanence is about 3%, much like site GM19-3, though the hysteresis data do not indicate nearly as much contribution from MD magnetite to explain the low intensity relative to lightning-saturated samples identified by Dunlop et al. (1984).

Site GM1530, GMLC

This site sampled the layered series along the north side of a county road approximately 6 km ESE of Reid's Pit. Old drill holes found near this site likely correspond to sampling location "I" of Vincenz et al. (1975). This location is mapped as part of the M-Zone of the layered series (Gilbert, 1982). The rock is medium to coarse-grained and medium gray in color. In thin section, the rock is dominantly comprised of foliated plagioclase. Ophitic clinopyroxene is present in abundance, and the variable plane-light colors and pleochroism suggest a range of composition. Some are heavily populated by opaque inclusions. Clinopyroxene and opaque minerals also occur as intercumulus phases. Traces of biotite and amphibole are present, likely as alteration products, as are traces of chlorite and calcite.

The mean value of χ at this site is 4.92×10^{-6} m^3/kg; individual data points are spread across two orders of magnitude from 3.34×10^{-7} to 3.47×10^{-5}. Unlike previous sites, hysteresis data indicates a considerable paramagnetic contribution, with high-field susceptibility equal to 24% of the low-field value. Saturation is not achieved until nearly 400 mT (Fig. 25). Mr/Ms is reasonably high (~0.3) and Bc exceeds 30 mT. The coercivity spectrum forms a skewed distribution with a peak near 70 mT (Fig. 25). Overall, the hysteresis and backfield data indicate

the ferrimagnetic assemblage has a high contribution from SD particles, much like site GM1535 but without the apparent potbellied character (σ_{hys} = -0.03).

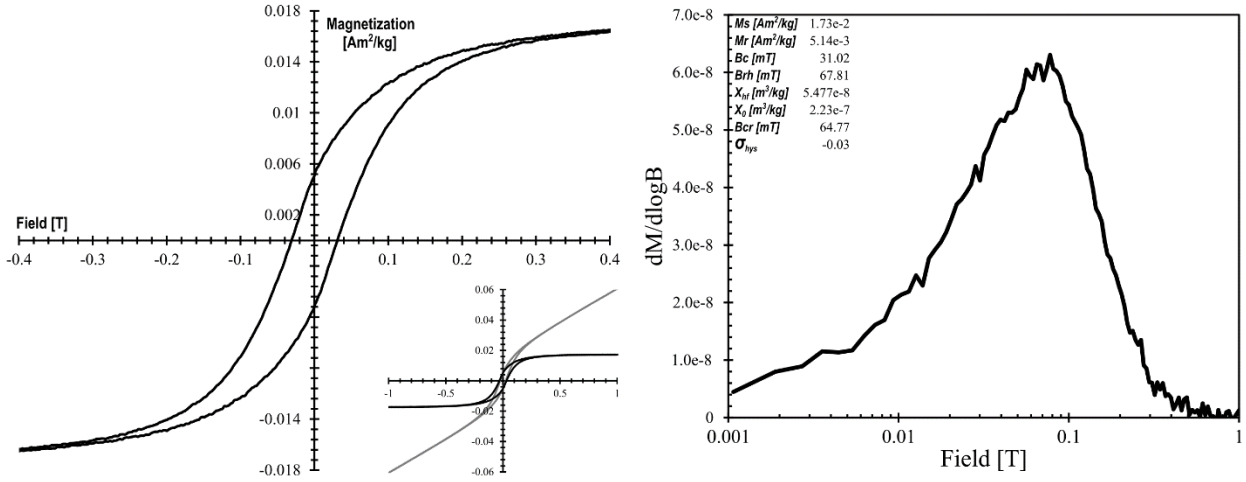


Figure 25. Hysteresis and backfield coercivity results for site GM1530.

AMS data indicate a noisy fabric with an oblate shape and a foliation plane dipping ~25° to the southeast (Fig. 26). No correlations are seen between Pj and Kmean or T. Error ellipses on all principal axes are relatively large. Individual values of Pj range from ~1.05 to about 1.35. The site mean fabric appears to be largely controlled by samples with lower values of χ. Coarse grain size and the relatively high paramagnetic contribution may be factors in the high dispersion of principal axes.

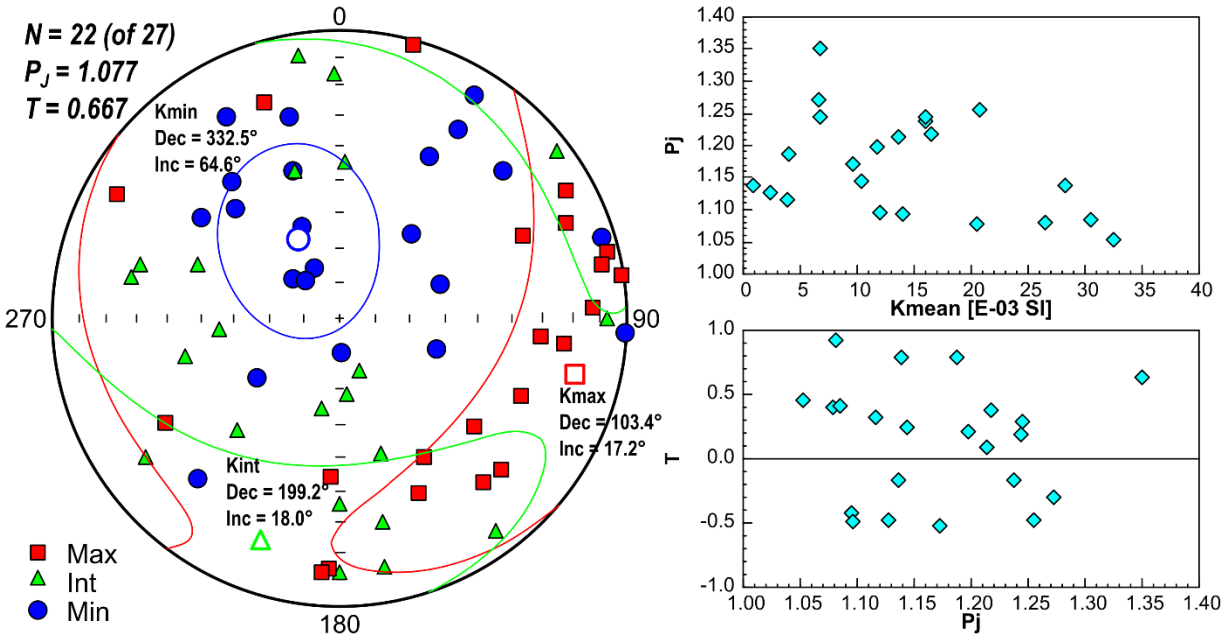


Figure 26. AMS results for GMLC site GM1530.

Remanence is strong, with average values of Q approaching 16.5. A ChRM is removed during thermal demagnetization at temperatures between 450-580 °C, with the largest drops near 540 °C (Fig. 27A). This ChRM is somewhat dispersed, averaging to an ESE and steep down direction (mean D = 119.2°, I = 61.6°, α_{95} = 9.3°) (Fig. 27B) and corresponds to a mean VGP at 7.4 °S, 121 °E (α_{95} = 13.5°) (Fig. 27C). This position is southeast of the 400 Ma point of the APWP and is similar to that encountered at site GM1535.

On initial inspection, the average NRM intensity is over 50% of the saturation remanence determined from hysteresis, which would greatly exceed expected intensity for anything natural other than a lightning strike. However, the initial susceptibility of the hysteresis specimen is lower than any of the bulk samples, and it is likely that the small chip used for VSM measurements is not suitably representative of the site. Additional data on hysteresis of higher-susceptibility specimens and remanence of low-susceptibility ones is required to evaluate whether this apparent saturation is accurate. Given the similarity of the VGP to site GM1535, it seems more likely that it is not.

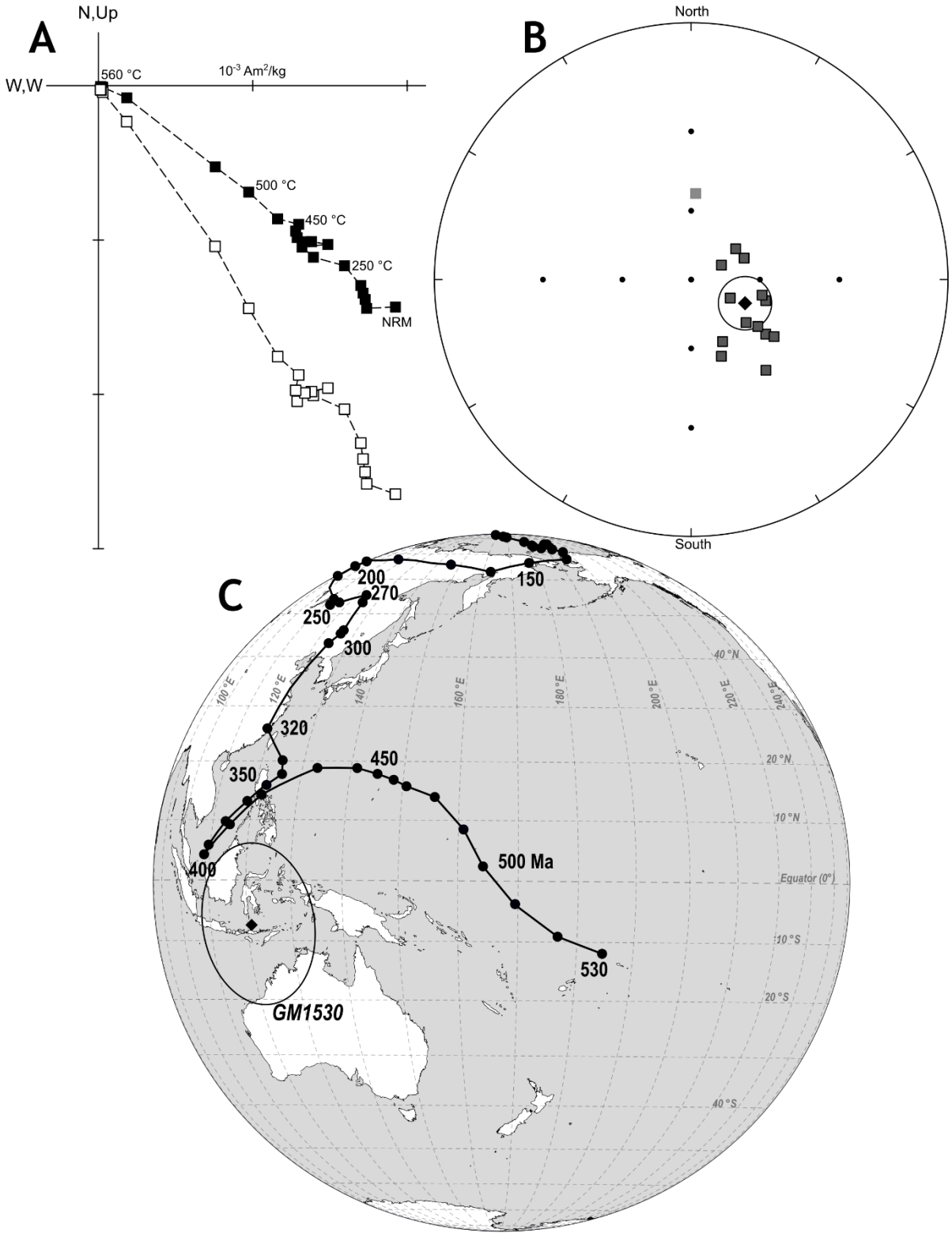


Figure 27. Paleomagnetic results for GMLC site GM1530. (A) Representative Zijderveld diagram with typical southeasterly and steep down directions. (B) Equal area plot of ChRMs determined for this site. (C) Comparison of mean in-situ VGP to North American APWP.

Site GM1480-1, GMLC

This site sampled the layered series at the western of two small hills along a county road about 2.9 km northeast of the town of Roosevelt. Outcrops in this area are mapped as belonging to the M-Zone (Gilbert, 1982). Rock at this location is medium to pale gray in color and appears to be a medium-grained anorthosite; no thin section was prepared.

Mean χ at this site is 1.85×10^{-6} m^3/kg; individual specimens range from 6.64×10^{-7} to 6.58×10^{-6}. High-field susceptibility measured with the VSM is less than 1% of its low-field value. The hysteresis loop obtained for this site appears to close at about 200 mT and bulk coercivity is just under 12 mT (Fig. 28). Mr is about 12% of Ms. The remanent coercivity spectrum derived from backfield data has its highest peak near 20 mT but shows a slight hump at higher fields which suggests a notable contribution from higher-coercivity (~60-70 mT) grains. The loop is slightly potbellied (σ_{hys} = -0.20), possibly due to the apparent mix of coercivity distributions. The coercivity distribution and Mr/Ms ratio suggest a significant contribution from single-domain grains. It is worth pointing out that the value of initial susceptibility estimated from hysteresis data is at the lower end of the range determined for this site from measurements of larger specimens with the MFK-1 and the hysteresis properties reported here may therefore not be a good representation of the site.

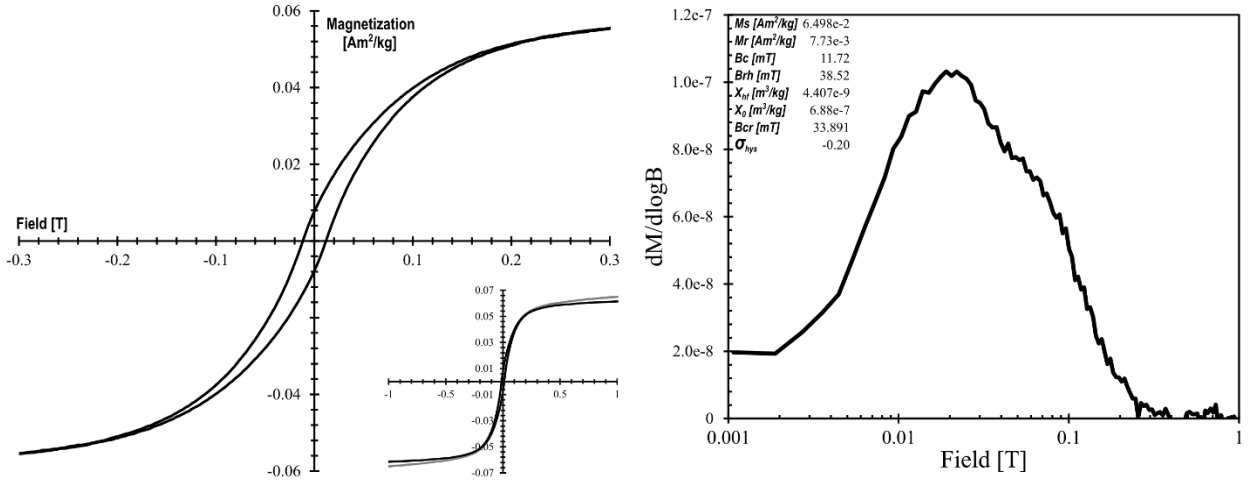


Figure 28. Hysteresis and remanent coercivity spectrum for a sample from GMLC site GM1480-1.

Measurements of AMS at this site indicate the presence of a triaxial-prolate fabric (Tmean = -0.486) with a lineation plunging slightly (~13°) to the south-southeast. There appears to be a reasonable correlation between Pj and both Kmean and T if one high-susceptibility sample is ignored. Pj ranges from ~1.02 to 1.36 and the low paramagnetic contribution indicates the fabric is carried in the ferrimagnetic minerals. All three principal axes show large error ellipses and are streaked. While single-domain magnetite can in principle lead to AMS fabric inversion from oblate to prolate (e.g., Ferré, 2002), the streaking of all axes is more characteristic of triaxial fabrics which may result from deformation (Tarling and Hrouda, 1993). Relatively few samples were collected at this site, and interpretation of the fabric is presently unclear.

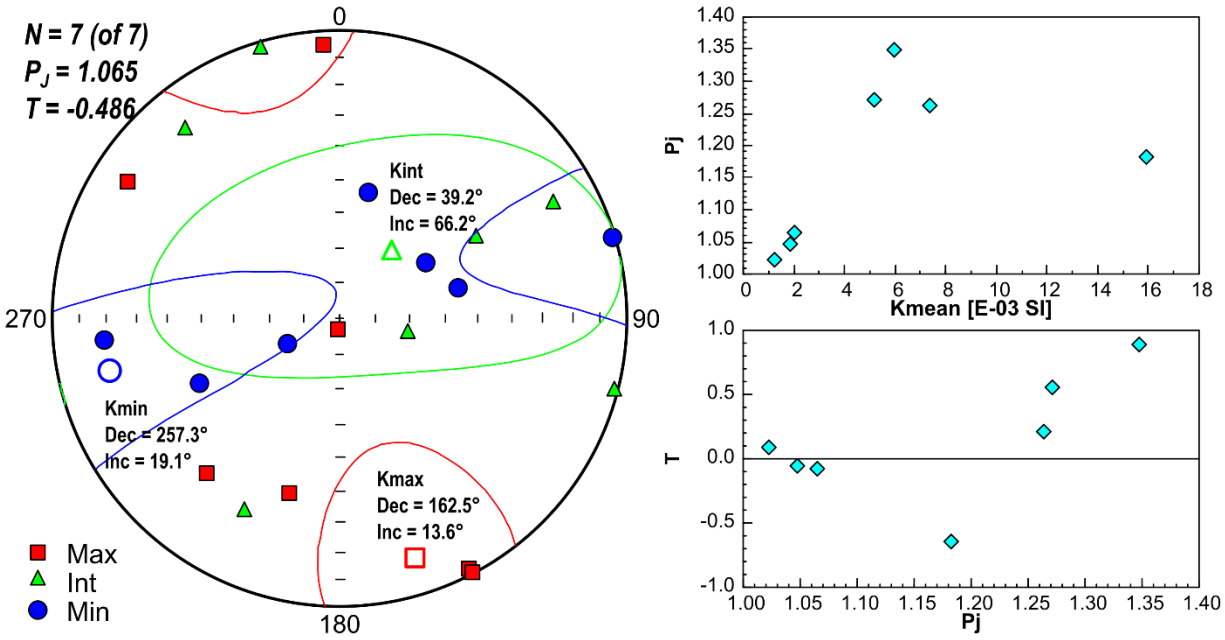


Figure 29. AMS results from site GM1480-1.

The NRM of these rocks has a high intensity, with an average value of ~28 for Q. Thermal demagnetization removes a magnetic component with easterly and steep down declination (Fig. 30A, B). This site was affected by temperature control issues and blocking temperatures are only an estimate, but the ChRM was probably mostly removed between 450 and 520 °C. The ChRM directions (mean D = 101.6°, I = 70°, α_{95} = 9.7°) correspond to a mean VGP at 21.4 °S, 119.1 °E (α_{95} = 16.5°), which lies south and east of the 400 Ma segment of the APWP (Fig. 30C). This position is similar to those obtained from sites GM1530 and GM1535. Average NRM intensity is 26% of Mr as determined for the hysteresis specimen, but its representativeness is in doubt and cannot be taken for clear evidence of lightning.

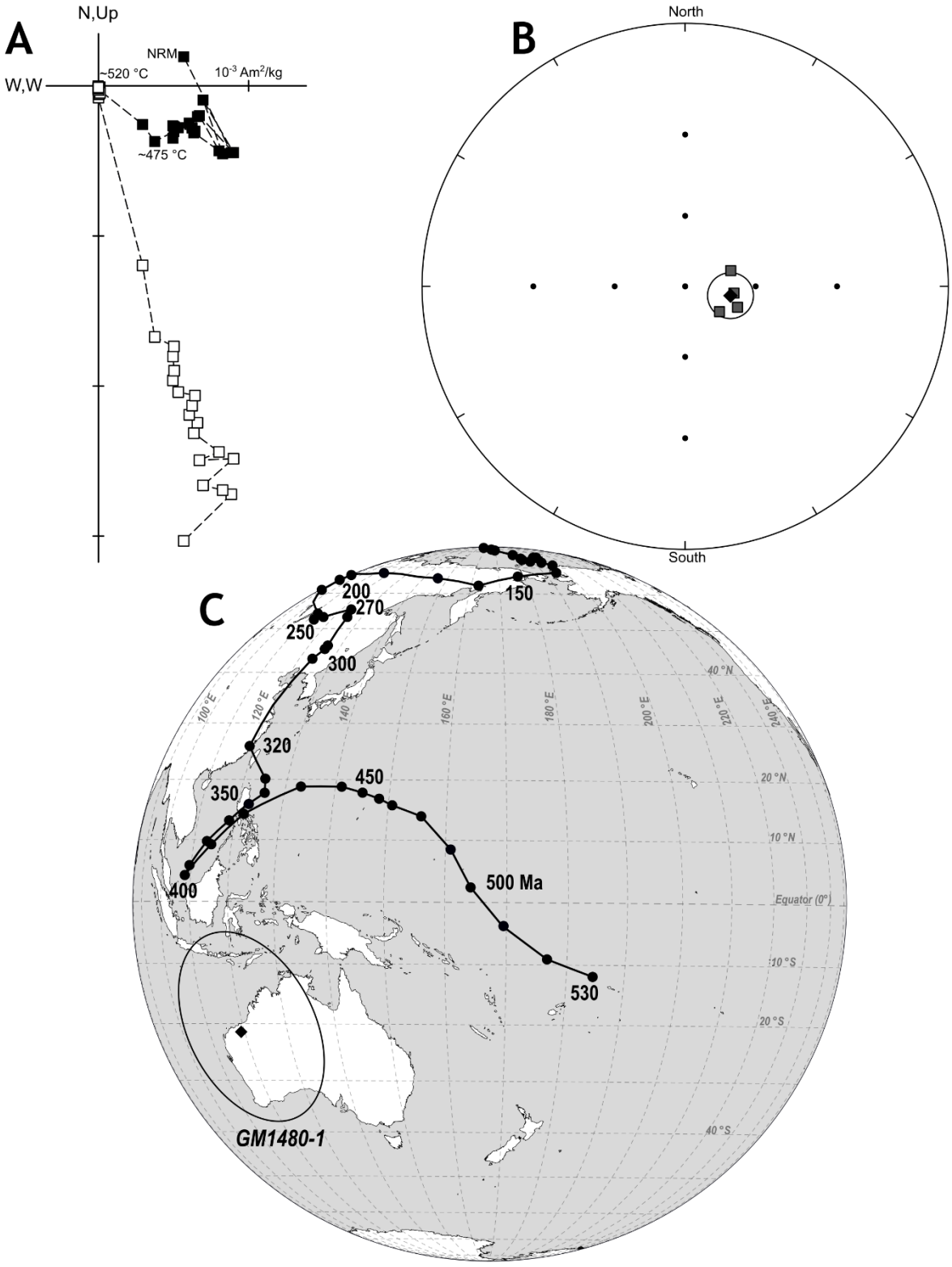


Figure 30. Paleomagnetic results from site GM1480-1. (A) Representative Zijderveld diagram with easterly and steep down ChRM. (B) Equal area plot of identified ChRMs. (C) Comparison of calculated mean in-situ VGP with North American apparent polar wander path.

Site GM1480-2, GMLC

This site sampled the layered series at the eastern of two small hills along a county road northeast of Roosevelt, about 1.4 km east of site GM1480-1. Rock at this location is medium-grained, medium to pale gray in color and appears to be anorthosite, though some pyroxene crystals are visible in places; no thin section was prepared. This location also appears to be classified as part of the M-Zone of the GMLC (Gilbert, 1982).

Mean χ at this site is 7.91×10^{-6} m^3/kg with individual specimens ranging from one-fifth to five times this value. Hysteresis data (Fig. 31) indicate that paramagnetic minerals account for barely 0.1% of this. The hysteresis sample for this site yielded an initial susceptibility toward the high end of the observed range. Bulk coercivity is rather low (Bc = 2.9 mT) and Mr/Ms is very low (0.027), suggesting a large contribution from MD grains. Backfield remanence data yield a value of 43.6 mT for Bcr, and the remanent coercivity spectrum is unusually narrow with a peak very close to this value (Fig. 31). The loop does not visually appear distorted, but quantitative analysis indicates a slightly wasp-waisted shape with $\sigma_{hys} = 0.26$. This site did not yield any reason to suspect a significant amount of SP material, and the backfield data do not support mixed coercivities.

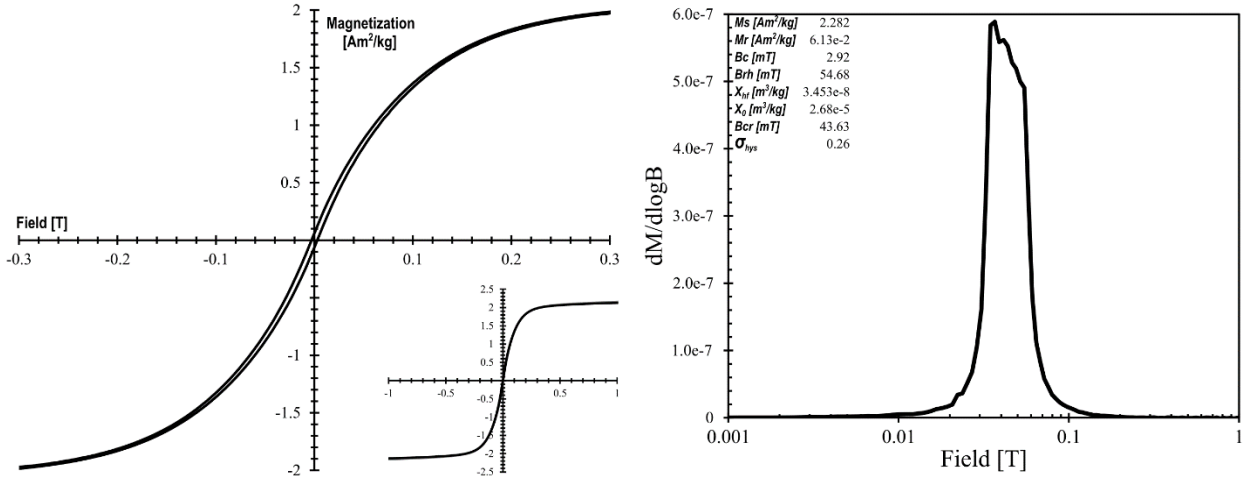


Figure 31. Hysteresis and remanence coercivity spectrum for sample from site GM1480-2.

A low-temperature remanence sweep was performed on the specimen used for hysteresis measurements. On cooling, the sample shows a small but sharp drop in intensity between 250 – 240 K (Fig. 32). While this is slightly below the usual temperature of the Morin transition in hematite, it has been shown that sub-micron hematite grains may undergo this transition at reduced temperatures (Özdemir et al., 2008). The presence of hematite could explain the elevated σ_{hys} value, and it may be that the backfield remanence measurements simply missed it due to using a peak field of 1 T. This was the only sample for which remanence curves indicate a Morin transition.

Low-temperature SIRM is considerably stronger than the RTSIRM. On warming, there is a large drop in intensity consistent with passing through the Verwey transition of magnetite. The calculated T_V is 98.2 K, considerably lower than the typical value for stoichiometric magnetite, and likely indicates a degree of oxidation (Jackson and Moskowitz, 2021) which would also be consistent with the apparent presence of hematite.

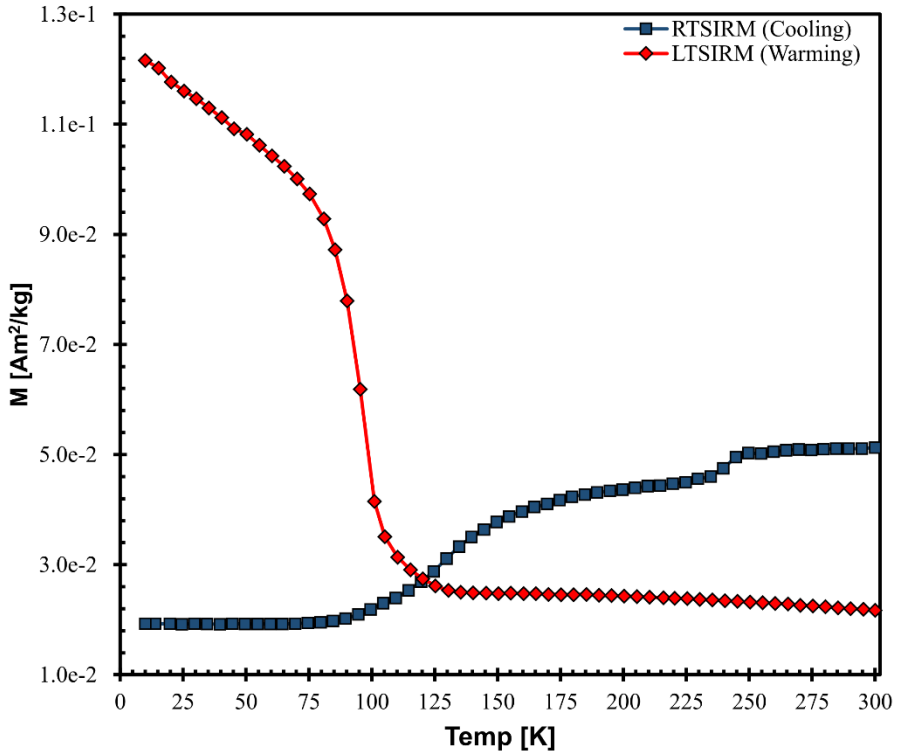


Figure 32. Low-temperature remanence curves for sample from site GM1480-2. Blue curve shows low-T demagnetization of room-temp SIRM; red curve shows thermal demagnetization of low-T SIRM.

AMS results indicate a triaxial-prolate fabric (Tmean = -0.219) with a lineation plunging ~55° to the WSW (Fig. 33). Individual values of Pj range from 1.09 to 1.35, suggesting the fabric is carried by ferrimagnetic minerals, and individual values of T are variable. No correlation is apparent between Pj and Kmean or T. Error ellipses are large for all principal axes, and all axes show streaked distributions. The azimuth of the lineation is nearly orthogonal to that of the lineation from site GM1480-1.

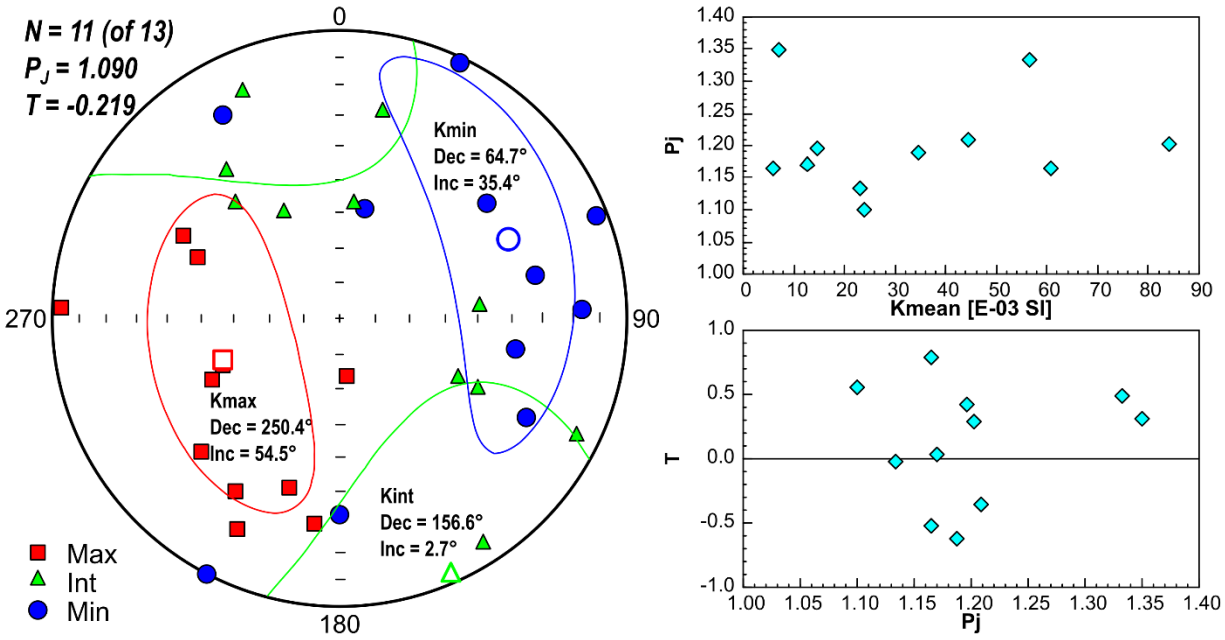


Figure 33. AMS results for GMLC site GM1480-2.

Remanent intensities are moderate to high, with average Q just below 10. During thermal demagnetization, a ChRM is progressively removed from low temperatures (Fig. 34A). It appears to become well-defined above ~350 °C and unblocks by about 520 °C, though these are estimates due to the temperature issue. The direction is southwesterly and very shallow (mean D = 214.7°, I = 1.1°, α_{95} = 7°) (Fig. 34B), with a corresponding mean VGP at 42 °S, 211 °E. The mean VGP is considerably southeast of the 530 Ma point on the apparent polar wander path (Fig. 34C).

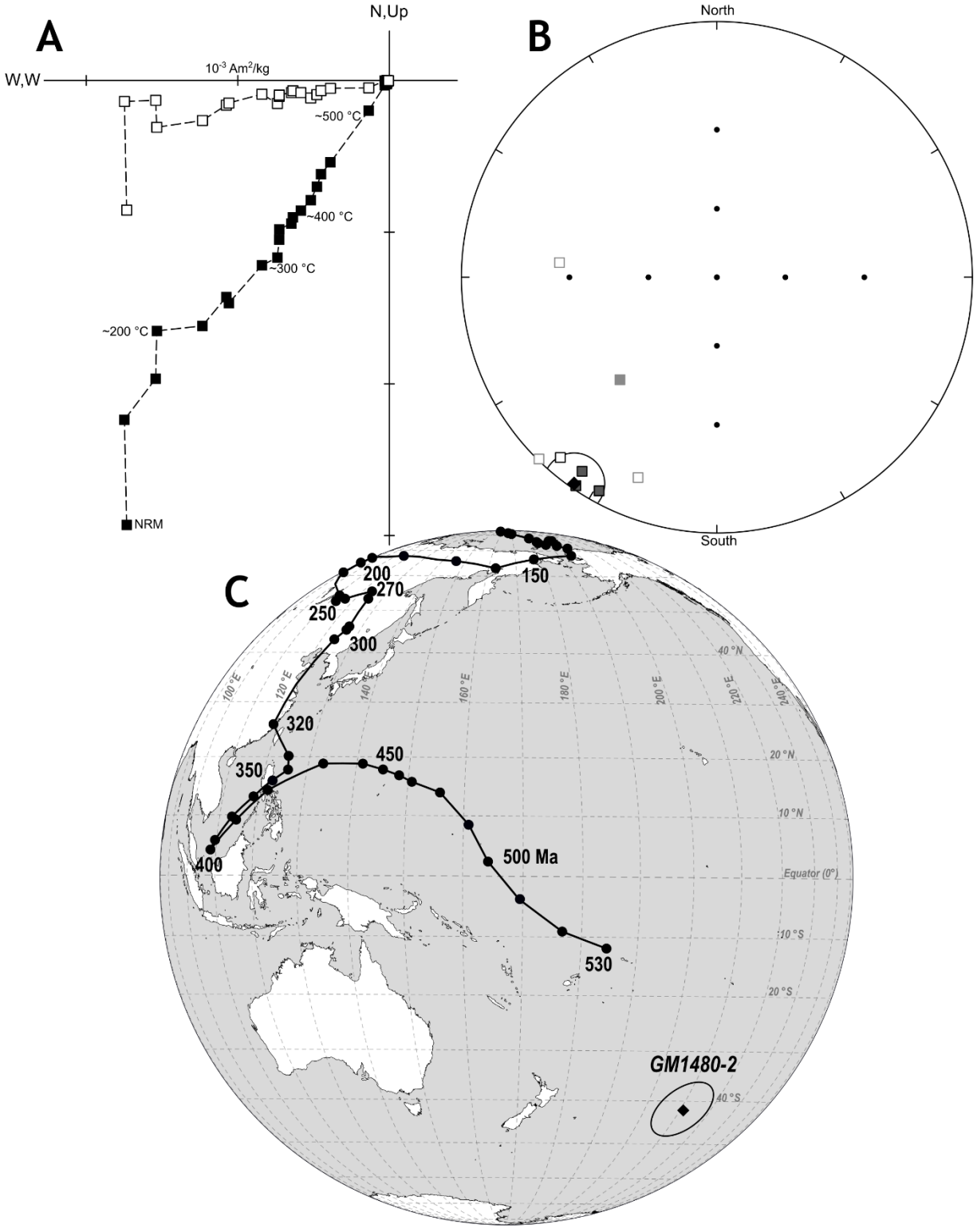


Figure 34. Paleomagnetic results from site GM1480-2. (A) Representative Zijderveld diagram with southwesterly and shallow ChRM. (B) Equal area plot of identified ChRMs. (C) Comparison of calculated mean in-situ VGP with North American APWP.

Site GM54-1, GMLC

This site sampled the layered series along the east side of Oklahoma Highway 54, about 8.4 km south of the town of Cooperton. This area is mapped as part of the N-Zone of the layered series, near the transition from M- to N-Zone (Gilbert, 1982, 2014). The rock is a medium to coarse anorthosite with intercumulus pyroxene. Trace pyroxene-oxide symplectite appears to have replaced olivine, and minor chlorite is present as an alteration product of pyroxene. Plagioclase contains abundant needle-like opaque mineral grains, and opaque inclusions are present in pyroxene as well.

Values of χ at this site range from 9.32×10^{-7} to 2.22×10^{-5} m^3/kg with a mean value of 2.66×10^{-6}. Paramagnetic minerals contribute about 0.3% of this. Hysteresis measurements yield a slightly potbellied loop (σ_{hys} = -0.19) with Bc = 14.6 mT and Mr/Ms = 0.13 (Fig. 35). Backfield remanence measurements yield a bulk Bcr of 48.2 mT, but inspection of the coercivity spectrum indicates that the distribution is actually bimodal with a peak just above 10 mT and another between 60 – 70 mT. Coercivity and remanence properties are consistent with SD (titano)magnetite.

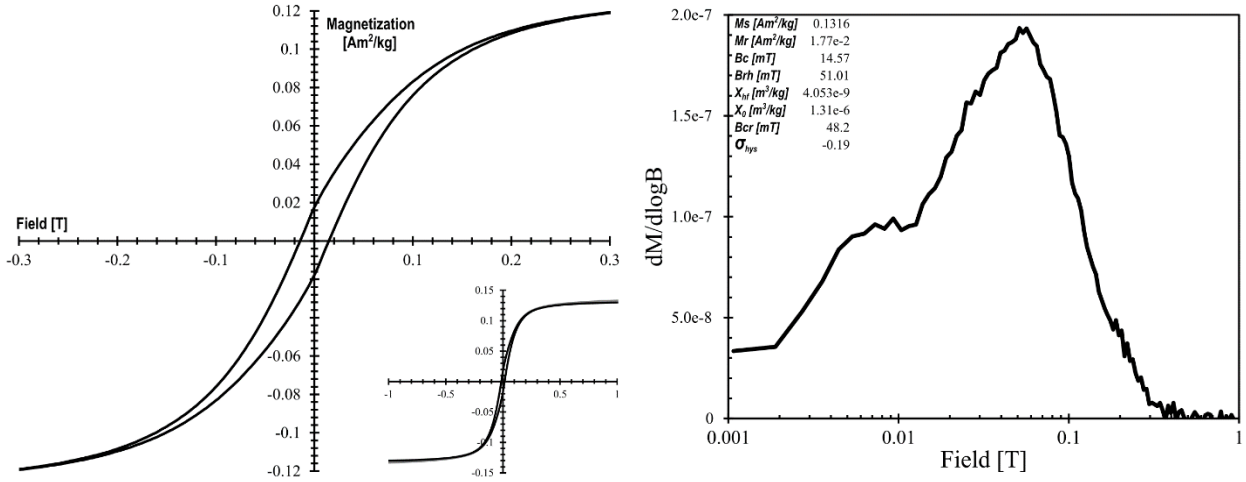


Figure 35. Hysteresis and remanent coercivity spectrum for anorthosite sample from site GM54-1.

Low-T remanence data for this sample shows nonlinear demagnetization during cooling and a large demagnetization on warming consistent with the Verwey transition of magnetite (Fig. 36). On cooling, remanence holds steady and actually slightly increases (<1%) before dropping. This may be a very subtle cooling-curve "hump" of the sort associated with maghemitization (Özdemir and Dunlop, 2010). LTSIRM is slightly weaker than RTSIRM, and exhibits a remanence minimum just above T_V, which is calculated at 120 K and lines up well with the expected T_V for stoichiometric magnetite.

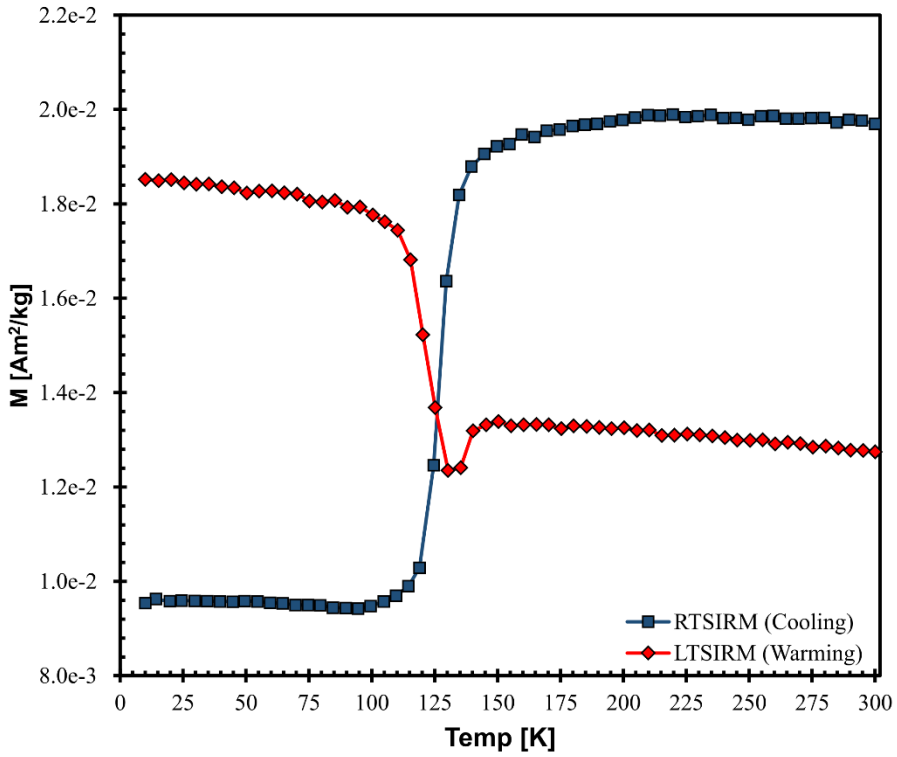


Figure 36. Low-T remanence data for anorthosite sample from site GM54-1.

AMS data show a slightly triaxial oblate fabric with a foliation plunging ~25° to the east (Fig. 37). There is essentially no correlation between Pj and Kmean. Samples with lower Pj (1.05 to ~1.13) have a broad distribution of T, while high-Pj (up to ~1.4) samples have negative or near-zero values for T. Orientations of principal axes are somewhat disperse, and Kmin seems to streak slightly towards Kmax. The overall fabric may be a composite fabric - mixtures of single-

domain and multi-domain ferromagnetic grains can result in "intermediate" fabrics due to partial development of an inverse fabric (Ferré, 2002), and both are clearly present here. The second population in the coercivity distribution may also be a factor.

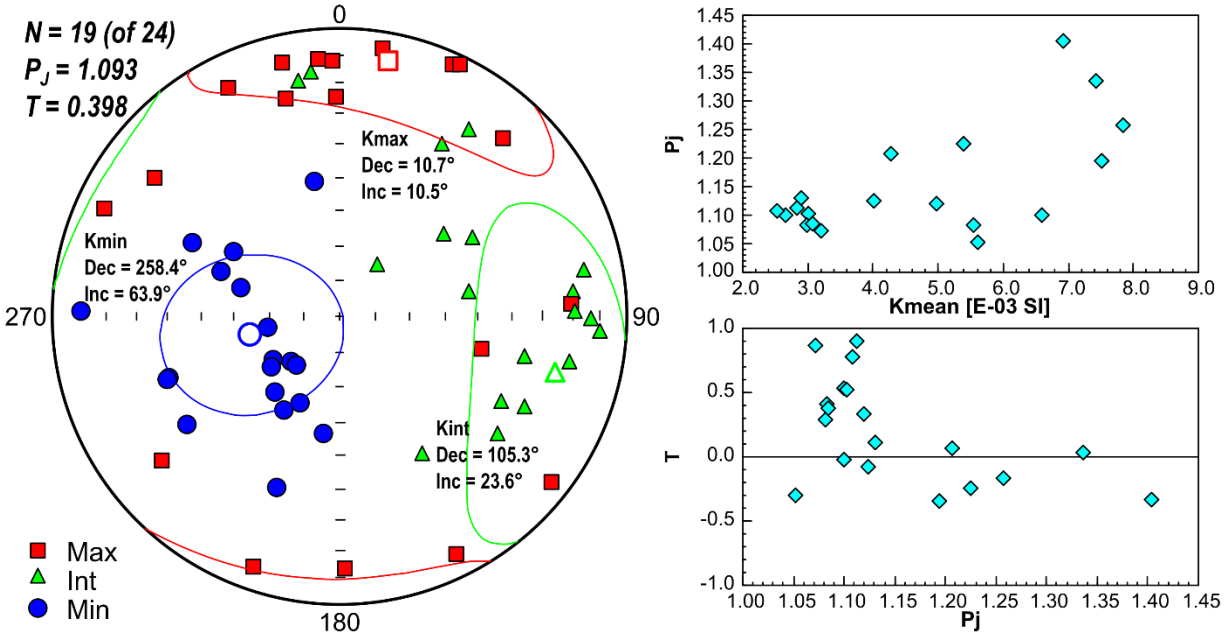


Figure 37. AMS results for anorthosite at site GM54-1.

Remanent intensity is high at this site, with average Q of about 31 and NRM is roughly 15% of saturation remanence. This is towards the upper end of values expected for samples with abundant single-domain magnetite (Dunlop et al., 1984). Thermal demagnetization reveals a southwesterly and shallow ChRM which mostly unblocks between 500 – 560 °C (Fig. 38A, B). This direction (mean D = 247.5°, I = 4.4°, α_{95} = 4.6°) yields a mean VGP at 17 °S, 186.2 °E that lies very near the 530 Ma pole of McCausland et al. (2007) (Fig. 38C).

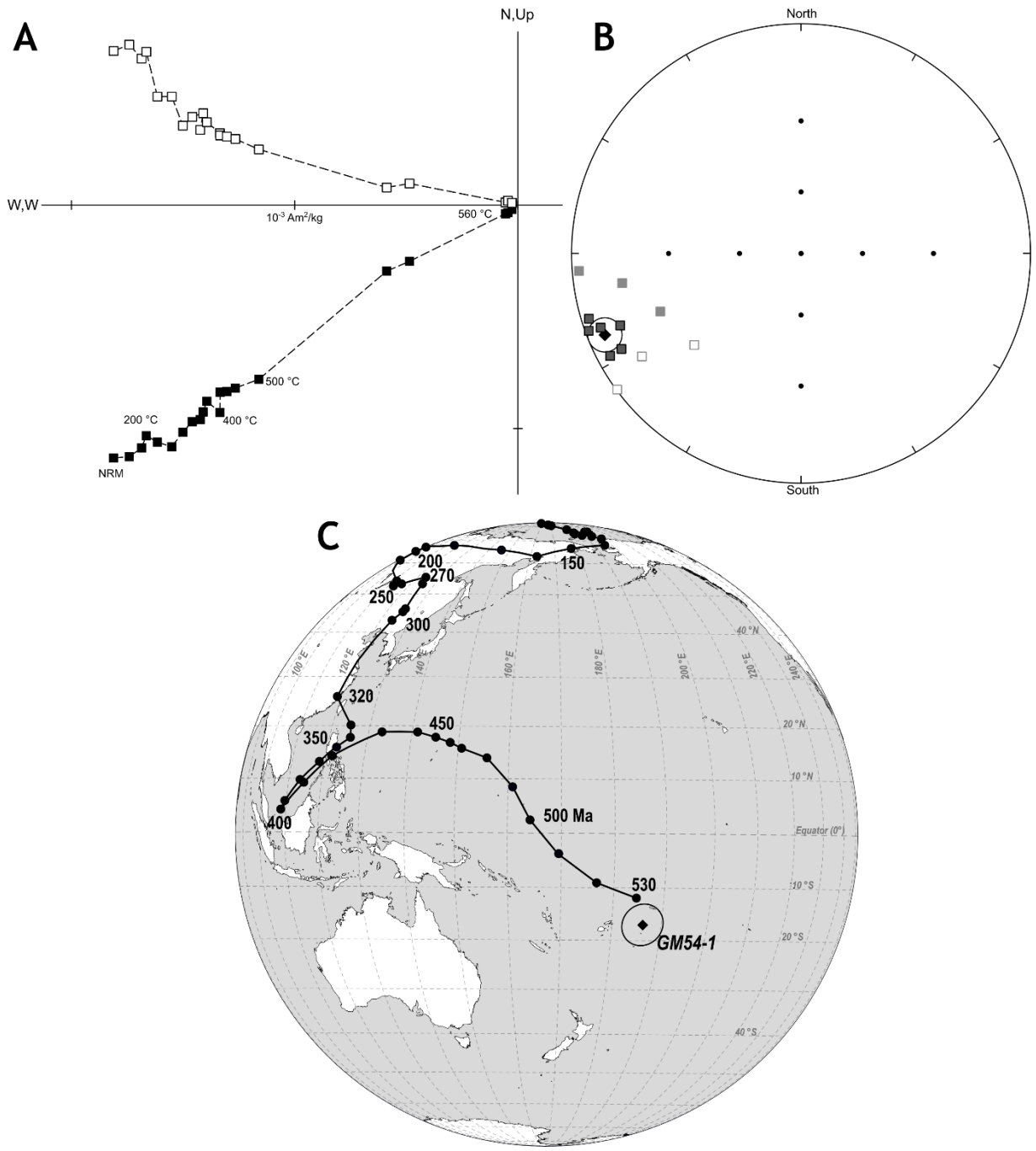


Figure 38. Paleomagnetic results for GMLC anorthosite at site GM54-1. (A) Representative Zijderveld plot showing southwest and shallow direction, (B) Equal area plot of ChRMs, (C) Comparison of mean in-situ VGP to the APWP for North America.

Site GM54-2, GMLC

This site sampled the layered series along the west side of Oklahoma Highway 54, about 0.7 km to the north of site GM54-1. The location is mapped as part of the N-Zone of the GMLC (Gilbert, 1982). Old drill holes found at this site likely correspond to site W-4 of Roggenthen et al. (1981). The rock is a medium-grained anorthosite with clear evidence of deformation and alteration. Microfractures are abundant and many plagioclase grains have bent or wedged twin planes. The original mafic silicates (most likely intercumulus augite) have been replaced by epidote, chlorite, and trace amphibole. Intercumulus opaque minerals remain. Traces of carbonate and zeolites are also present along fractures. Zeolite veins are present at the outcrop, and natrolite-cemented breccia is found along the west side of the road about 100 m south.

Values of χ range from 3.56×10^{-7} to 1.06×10^{-5} m^3/kg with a mean value of 1.61×10^{-6}. The paramagnetic contribution accounts for 14.5% of initial susceptibility in the hysteresis sample used for this site, though it is worth noting that the initial susceptibility measured by VSM is near the low end of values measured for larger samples and this ratio is unlikely to be representative. The hysteresis loop is slightly potbellied ($\sigma_{hys} = -0.16$) and does not close until about 300 mT, reaching saturation near 400 mT (Fig. 39). This sample has the highest Bc measured in this study at nearly 36 mT, and Mr/Ms has a value of nearly 0.24, indicating a significant contribution from SD grains (likely magnetite or titanomagnetite).

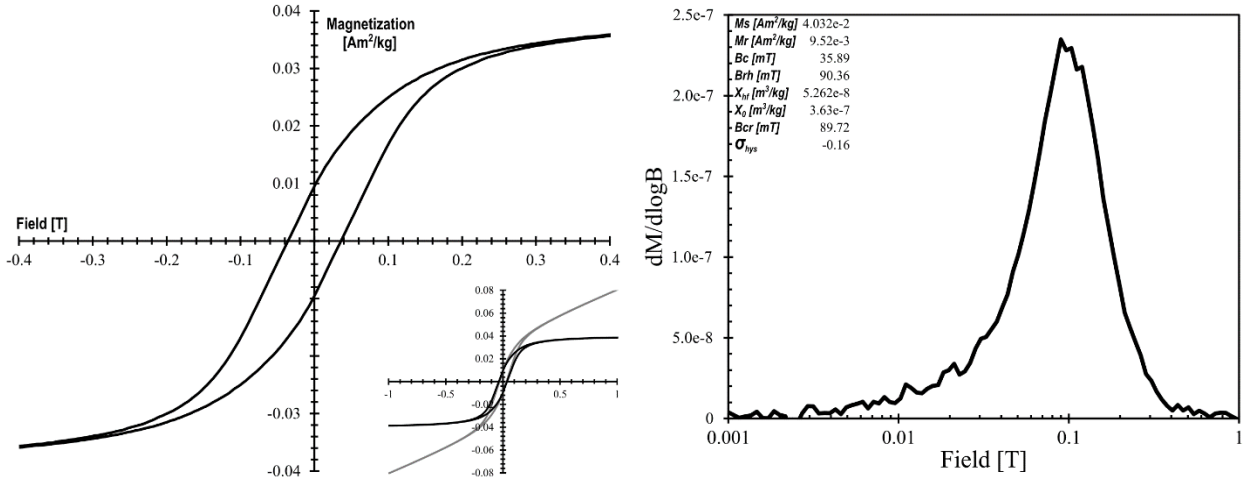


Figure 39. Hysteresis and backfield remanence coercivity spectrum for anorthosite from site GM54-2.

The cooling curve of low-T demagnetization of RTSIRM shows a slight increase of remanence on cooling with a peak value just under 2% higher than initial, resulting in a faint hump shape indicative of the presence of maghemite (Özdemir and Dunlop, 2010). Application of LTSIRM results in somewhat higher intensity than for RTSIRM (Fig. 40). Calculated T_V for this sample is 123.4 K, slightly higher than the average for magnetite but within the range reported by Jackson and Moskowitz (2021).

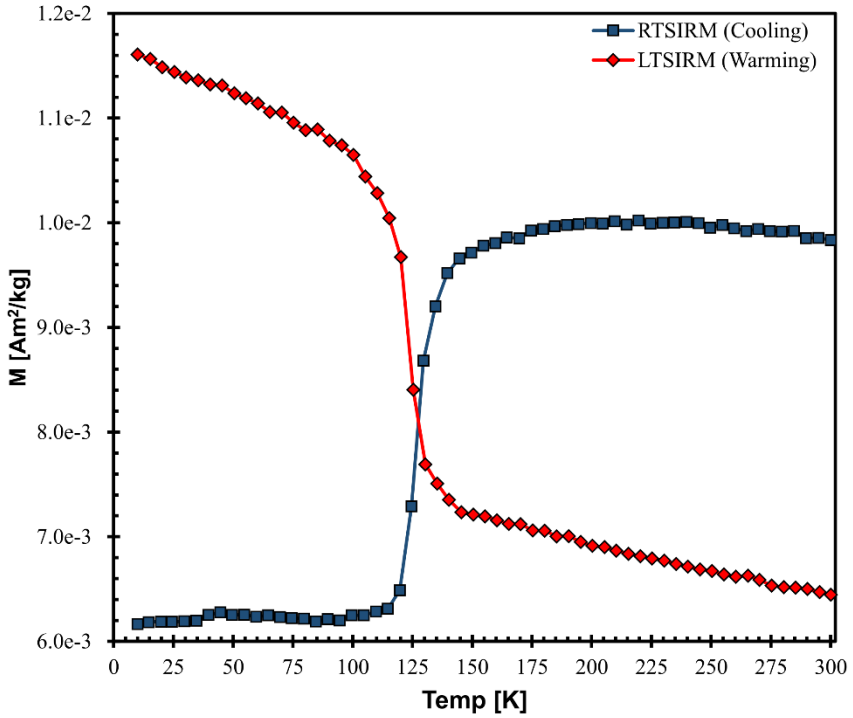


Figure 40. Low-T remanence curves for anorthosite from site GM54-2.

AMS data for this site show a weak correlation between Pj and Kmean. Nearly all specimens from this site have positive values of T. The overall fabric is oblate with a foliation dipping ~12° to the west (Fig. 41). Kmin is slightly streaked towards Kint. Due to the apparent (if weak) correlation between Pj and Kmean, the high values of Pj and the high values of Kmean for many samples, it is likely that the fabric is carried in magnetite.

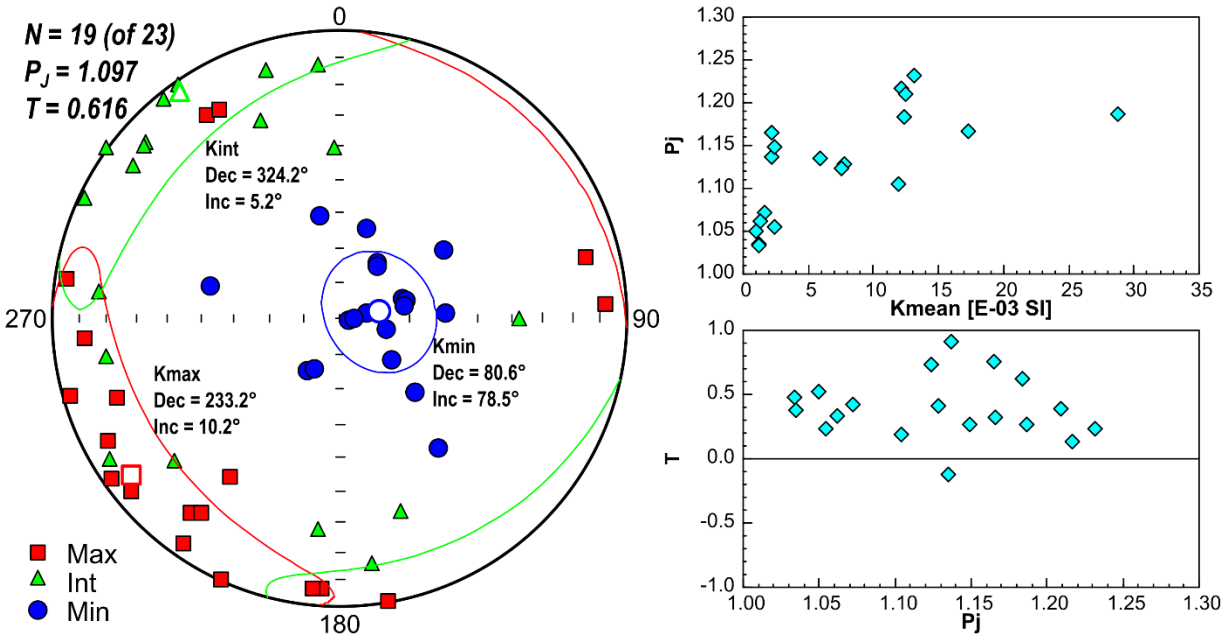


Figure 41. AMS results for GMLC anorthosite at site GM54-2.

NRM intensity at this site is high with a median Q of ~30, but this is not evenly distributed – Q varies from about 4 to over 130 at this site, and shows a power-law correlation with χ. The mean NRM is about 18% of the saturation remanence inferred from hysteresis, though this value is not likely representative. This site yields a very consistent northeasterly and shallow up ChRM which likely unblocks from 500 to 580 °C (only an estimate, due to temperature control issue) (Fig 42A, B). The same direction is removed by AF demagnetization and shows high coercivity, with ~28% of the NRM remaining after treatment at 120 mT. This ChRM (mean D = 52.4°, I = -19.2°, α_{95} = 2.9°) yields a mean VGP position of 23.3 °S, 202.8 °E (α_{95} = 2.8°), to the southeast of the 530 Ma pole of the APWP (Fig. 42C).

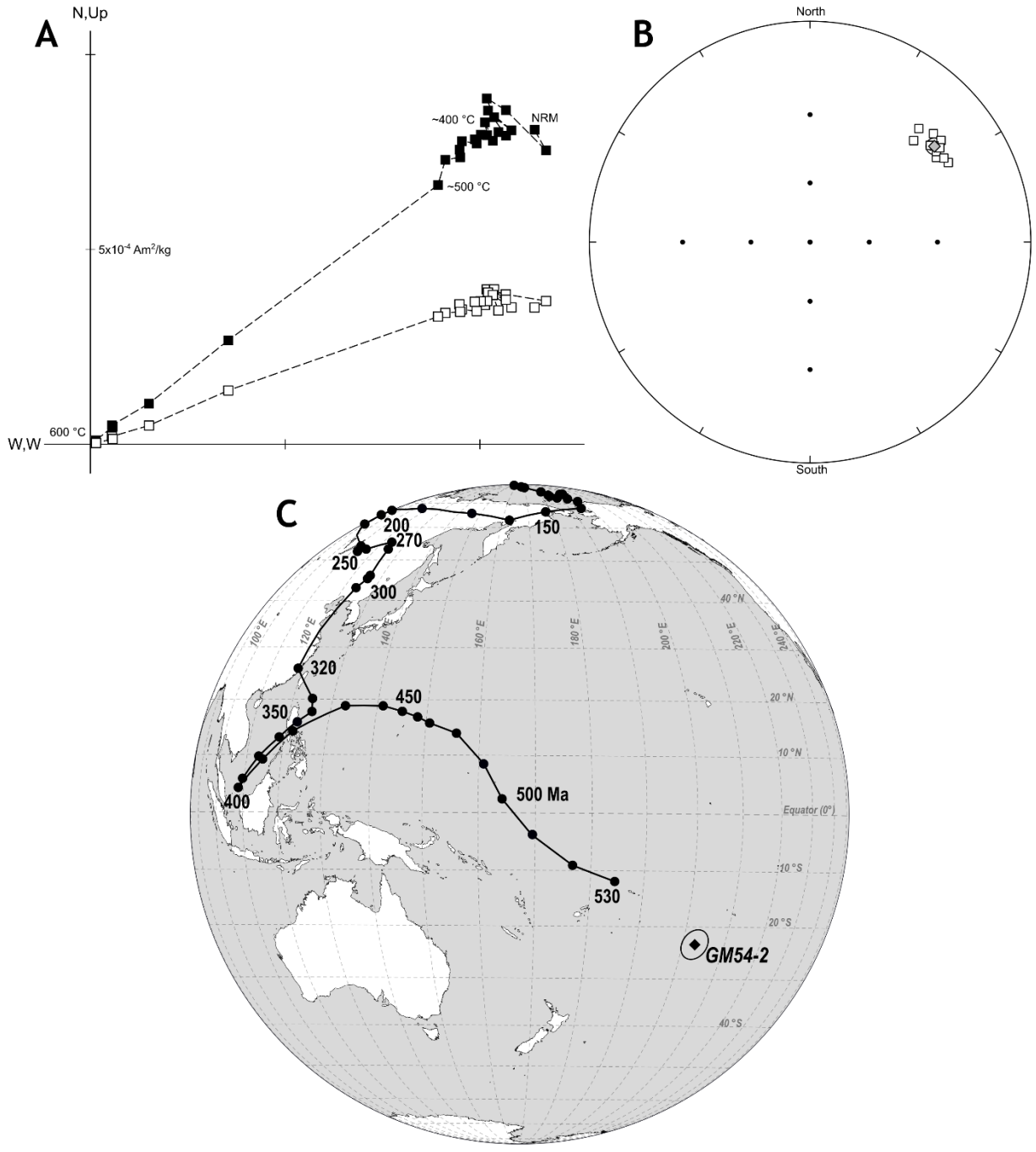


Figure 42. Paleomagnetic results from site GM54-2. (A) Representative Zijderveld diagram with northeasterly and shallow up directions. (B) Equal area plot of ChRMs. (C) Comparison of mean in-situ VGP with North American apparent polar wander path.

Sites GM1500-1 and GM1500-2, GMLC

These sites (~120 m apart) likely sampled the layered series at an isolated hill of anorthosite 10.9 km west and slightly south of the intersection between Oklahoma Highway 19 and U.S. Highway 183 in Roosevelt. This location is not included in maps of the GMLC; the nearest exposure seen on the maps of Gilbert (1982, 2014) is just over 7 km southeast. The hill does not seem to have been studied in reports more recent than that of Merritt (1958), whose map shows it to be the westernmost outcrop of anorthosite in the general Wichita Mountains area. The southern and southwestern sides of this hill are the original locations from which zeolite-opal rocks were first reported (Merritt and Ham, 1939, 1941).

In general, any significant exposure of anorthosite in the region has been assigned to the GMLC and thus this location is most likely a part of it, and possibly its most western exposure. The rock here is a fine- to medium-grained anorthosite with scattered very coarse crystals of plagioclase up to a few centimeters long. As it has not been petrologically investigated since before their adoption, it is not clear which (if any) of the zones of Powell et al. (1980a, 1980b) it corresponds to. Initial field and petrographic examination suggest the L-Zone is the closest fit, though the diagnostic large pyroxenes of the L-Zone are absent, and some features are more similar to the M-Zone.

Merritt (1958) reported an absence of foliation and alteration features; he must have sampled a different spot on the hill. The rocks show at least localized lamination of plagioclase, and the thin sections from both sites show minor sericitization and chlorite replacement of primary mafic silicates. Biotite (likely deuteric) is also present in trace amounts in the section from GM1500-2. In hand sample, local color gradations from medium-dark gray to near white

also appear to be a consequence of alteration. The hill is cut by several north-south trending granite dikes on its west side, which may be the origin of the alteration.

Values of χ range from 3.11×10^{-7} to $1.45 \times 10^{-5} m^3/kg$ (mean value 9.99×10^{-7}) for site GM1500-1 and range from 2.37×10^{-7} to $3.38 \times 10^{-5} m^3/kg$ (mean value 1.43×10^{-6}) for GM1500-2. VSM data indicate that paramagnetic minerals contribute 1.2 to 2.4% of this. The hysteresis samples are not likely representative – the sample for GM1500-1 yields an initial susceptibility value lower than any measured on bulk samples, while the one for GM1500-2 has a value that is within range (barely) but is still five times higher than the mean. They may however capture the range of properties likely to be present.

The low- χ sample, from GM1500-1, has relatively low Bc (~ 9mT) but a reasonably high Bcr of about 70 mT. The remanence coercivity spectrum has its largest peak near 70 mT, but has a humped shape which suggests a significant contribution from a much lower-coercivity population (Fig. 43A). The high- χ sample (GM1500-2) has even lower Bc (~4 mT) and much lower Bcr (~14 mT). The coercivity spectrum is narrow and oddly shaped. It may be due to a mixture of two populations, but both would be less than 20 mT (Fig. 43B). Both loops have values of σ_{hys} which are very close to zero. Mr/Ms is rather low for both (~0.07 to 0.1). The hysteresis results suggest bulk properties are controlled by MD grains in high-susceptibility samples with SD particles having a larger contribution to remanence in low-susceptibility samples.

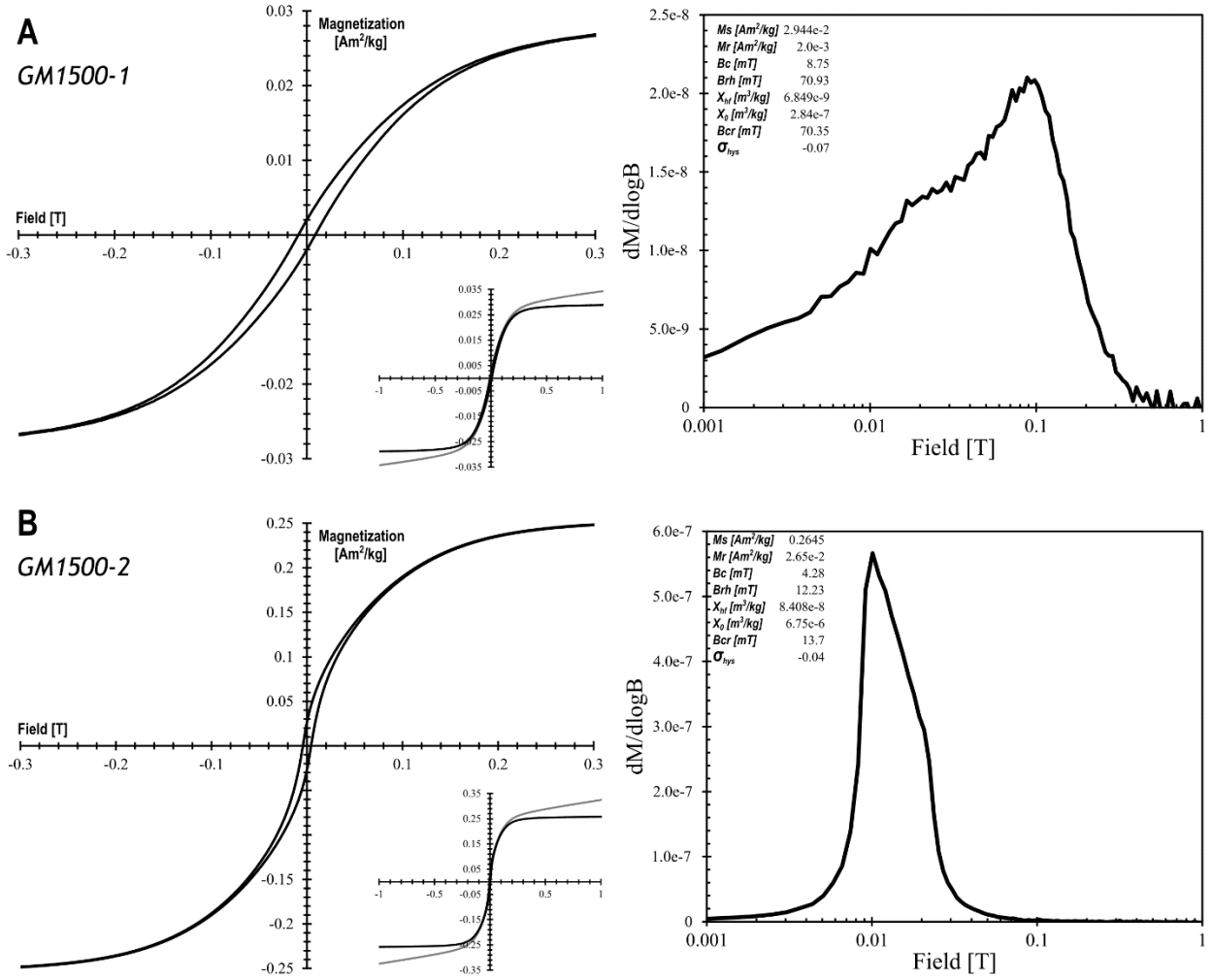


Figure 43. Hysteresis and remanent coercivities from samples of the anorthosite hill at sites GM1500-1 and GM1500-2. (A) GM1500-1, showing moderate Bc and a contribution from a high-Bcr component. (B) GM1500-2 with low Bc and a narrow coercivity distribution.

AMS for both sites yields moderately-defined fabrics with a large dispersion of principal axes (Fig. 44). There is essentially no correlation between Pj and Kmean. Individual samples yield Pj up to ~1.25 at GM1500-1 and up to 1.5 at GM1500-2; the fabric is most likely carried by (titano)magnetite. The site mean fabric is triaxial at GM1500-1 and triaxial-oblate at GM1500-2. Kmin shows noticeable streaking towards Kint for both sites. The overall fabric appears to be an oblate fabric with a moderate dip (~15-20°) to the east with a triaxial overprint.

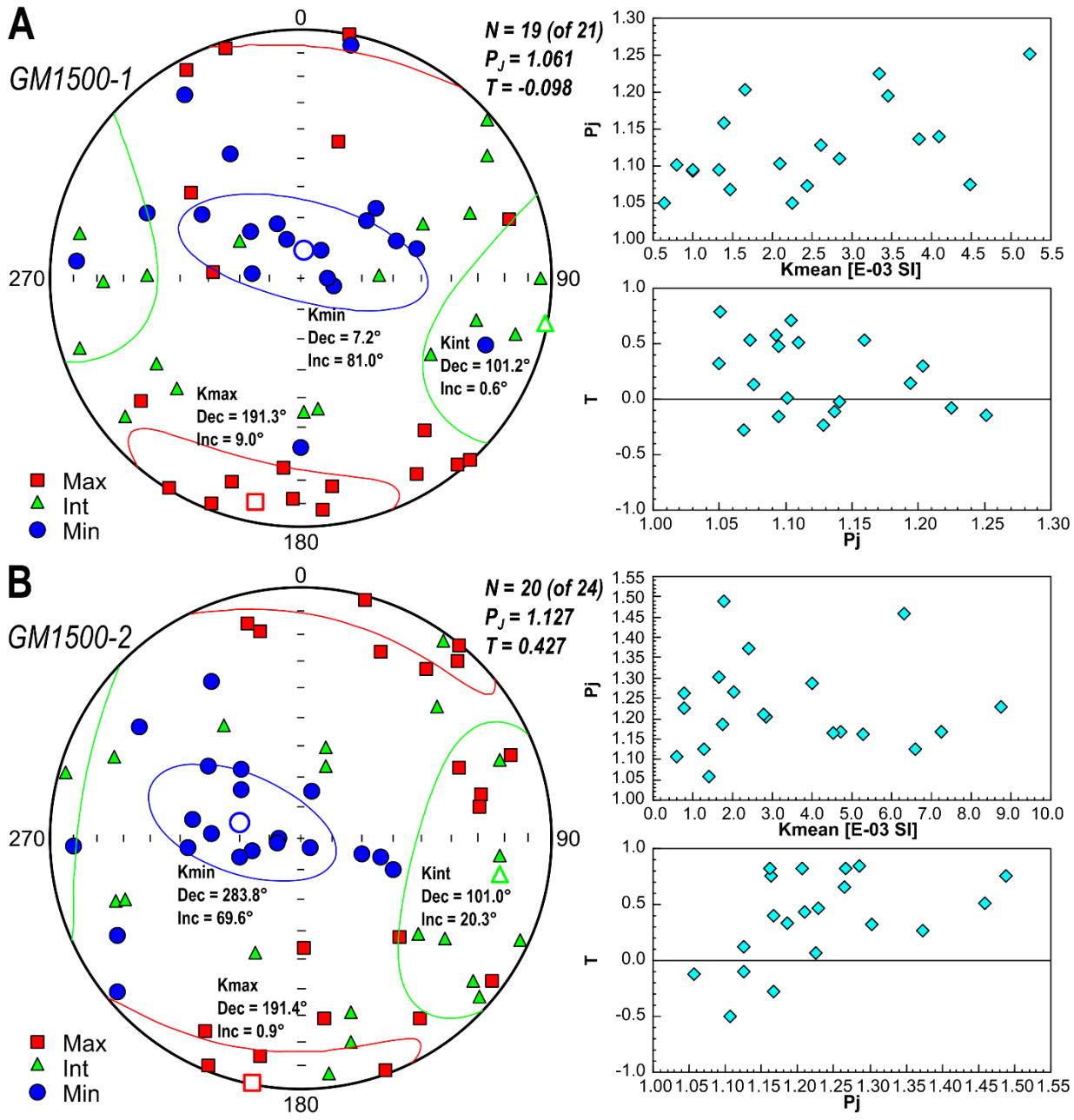


Figure 44. AMS results for anorthosite hill sites GM1500-1 and GM1500-2.

Remanence is lower than for most sites. Average Q for GM1500-1 is ~7 and ~3.5 for GM1500-2. Demagnetization of samples from GM1500-1 consistently yields easterly and shallow to intermediate up directions (Fig. 45A). These appear to form two clusters – one with a slightly shallower and more southerly declination, and another with a slightly steeper and more northerly inclination (Fig. 45B). The ChRM is mostly revealed above about 450 °C, though this

is an estimate due to temperature control issues. Mean VGPs for both groups plot north of the Cambrian segment of the APWP (Fig. 45C). Three samples yielded ChRMs with a much more southeasterly declination which were not considered in the means; in AF demagnetization of one sample this component was revealed at fields up to 30 mT, at which point the steeper ChRM began to demagnetize. Similar but quite noisy directions are seen at low temperatures in thermal demagnetization plots for some samples as well (e.g., Fig. 45A).

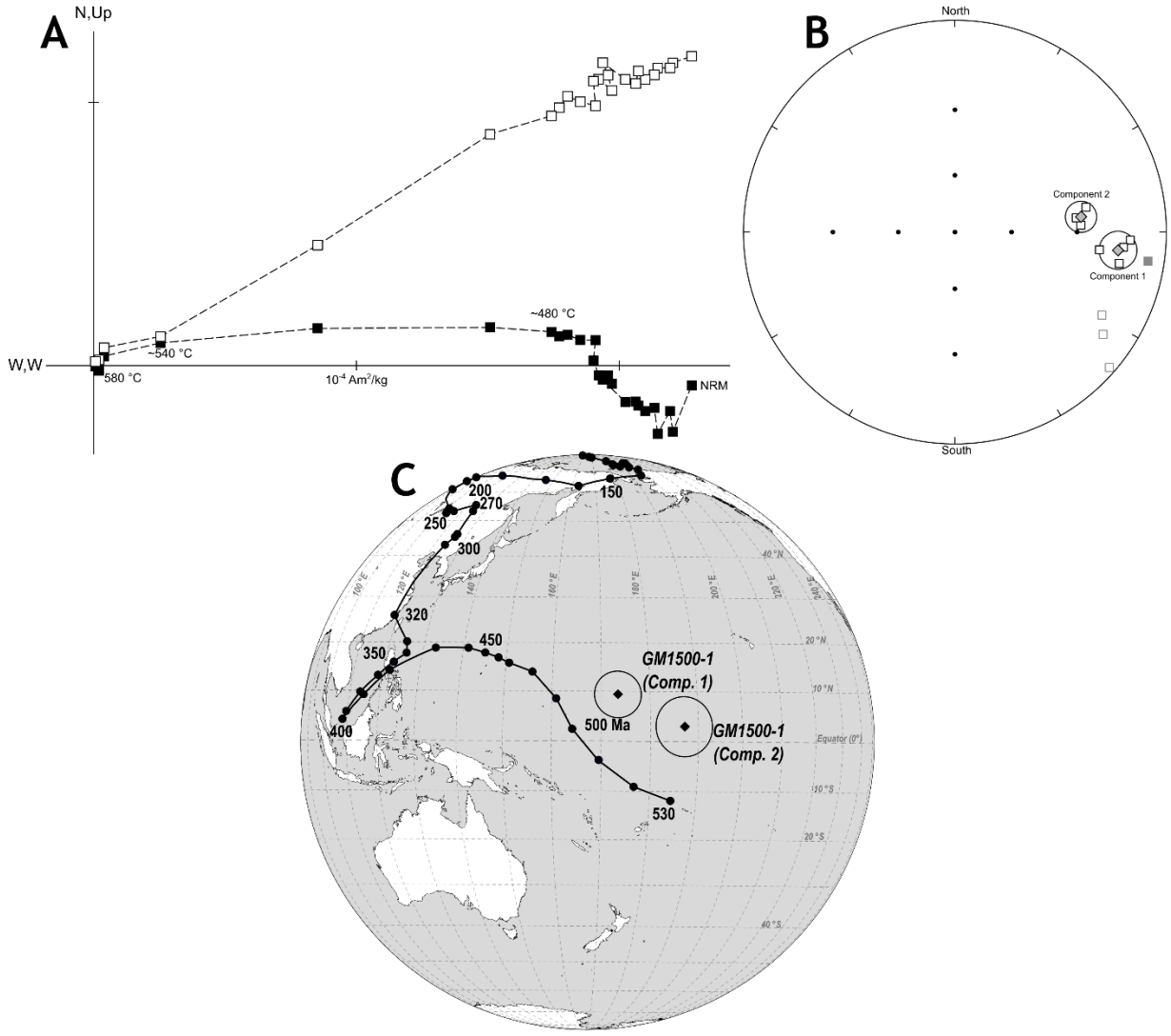


Figure 45. Paleomagnetic results for site GM1500-1. (A) Representative Zijderveld diagram. (B) Equal area plot of ChRMs with groups identified. (C) Comparison of mean in-situ VGPs with the North American APWP.

GM1500-2 yields two apparent components as well. At low temperatures (from ~100 to ~460 or 480 °C), a southeasterly and shallow up direction is removed which is essentially the same as the disregarded southeastern directions from GM1500-1 but is usually less noisy. In a couple of samples, it is the only component present. Beginning at roughly 480 °C (temperature control issues prevent precision), a more northeasterly and intermediate up ChRM is removed (Fig. 46A). The rocks are typically demagnetized by an estimated 560 °C. These form relatively well-grouped clusters (Fig. 46B). The northeasterly ChRM (mean D = 53.9°, I = -39.7°, α_{95} = 5.8°) yields a mean VGP at 13.5 °S, 211.6 °E which lies east and slightly south of the 530 Ma point of the APWP (Fig. 46C). The lower-temperature component (mean D = 117.1°, I = -8.1°, α_{95} = 4.3°) has a corresponding mean VGP at 24.4 °N, 158.2 °E which lies to the north of the Ordovician segment of the APWP (Fig. 46C).

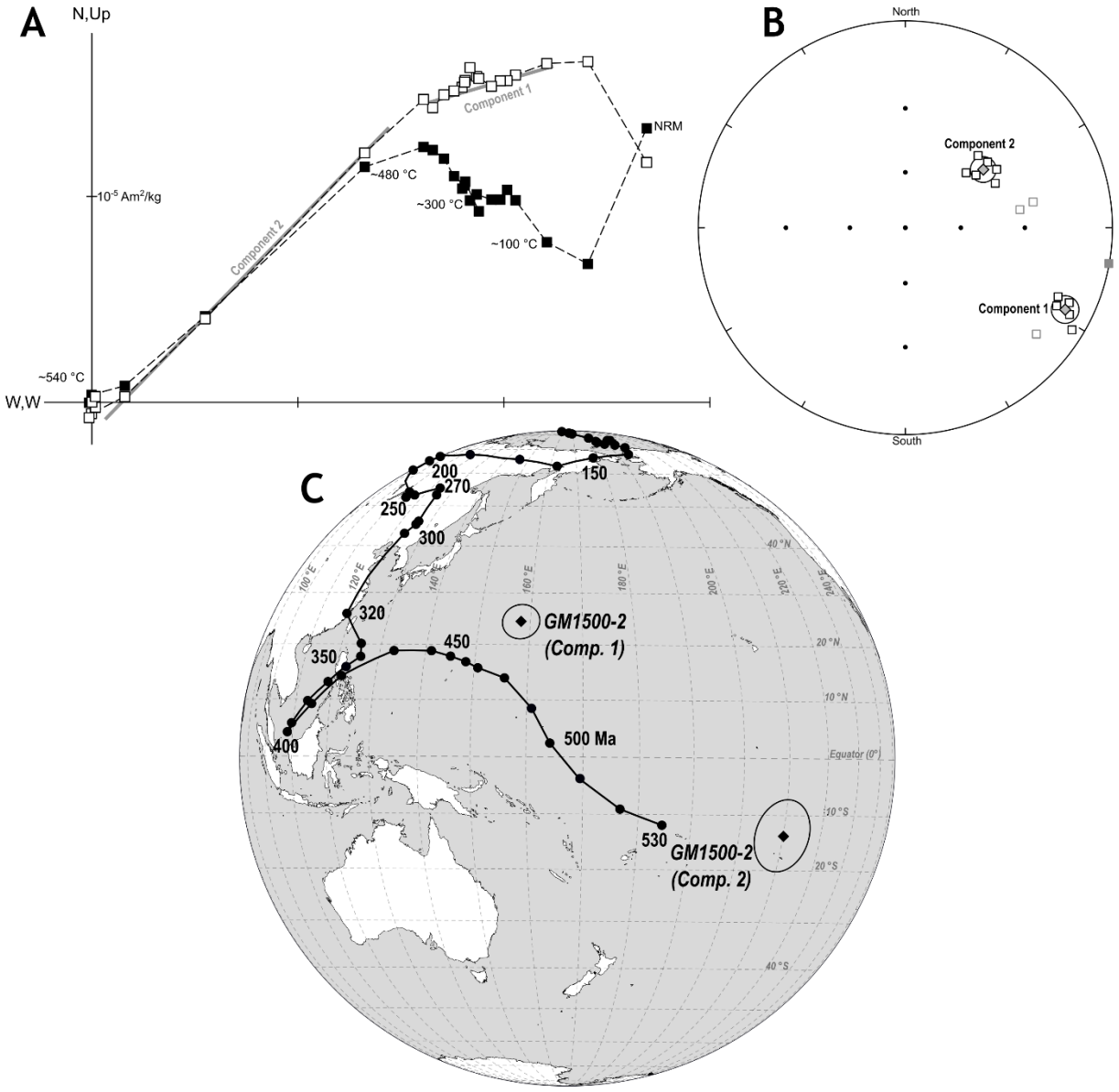


Figure 46. Paleomagnetic results for site GM1500-2. (A) Representative Zijderveld diagram. (B) Equal area plot of determined magnetization components with groups identified. (C) Comparison of mean in-situ VGPs with the Phanerozoic North American apparent polar wander path.

Site GM2160-1, GMLC

This site sampled anorthosite at the base of a granite hill referred to in older publications as "Mount Powwow" (Merritt, 1958) located approximately 1.7 km northeast of the anorthosite hill of the previous sites. As with that location, this site lies outside the area normally assigned to

the layered series and at least the mafic rock here does not appear to have been studied in the last 60+ years. Two sites were sampled here some 20 meters apart; due to variation in lithology and results, they will be discussed separately. This site is tentatively considered part of the layered series, as a thin section showed the lithology to consist almost entirely of medium-grained plagioclase with abundant acicular inclusions of opaque minerals and anorthosites are typically referred to the GMLC. Minor amounts of opaque grains and trace pyroxene is present as well. The rock has been slightly altered – some plagioclase crystals show minor sericite, and epidote, chlorite and carbonate are present in trace amounts as well. Some plagioclase grain boundaries appear to have been recrystallized. Emplacement of the adjacent granite (mapped as Lugert Granite in Gilbert, 2014) could reasonably explain these features.

Values of χ range from 4.93×10^{-7} to 4.46×10^{-6} m^3/kg (mean value 9.78×10^{-7}), and VSM data indicate that the paramagnetic contribution is just over 1% of the total. The specimen used has an initial susceptibility toward the lower end of the range observed in larger samples. Hysteresis data yield a somewhat potbellied loop (σ_{hys} = -0.28) with Bc of 18.8 and Mr/Ms of 0.18 (Fig. 47). Backfield data yields a moderately broad, somewhat asymmetric remanent coercivity distribution with a maximum near 30 mT. The Mr/Ms ratio and the coercivity spectrum suggest a contribution from SD grains.

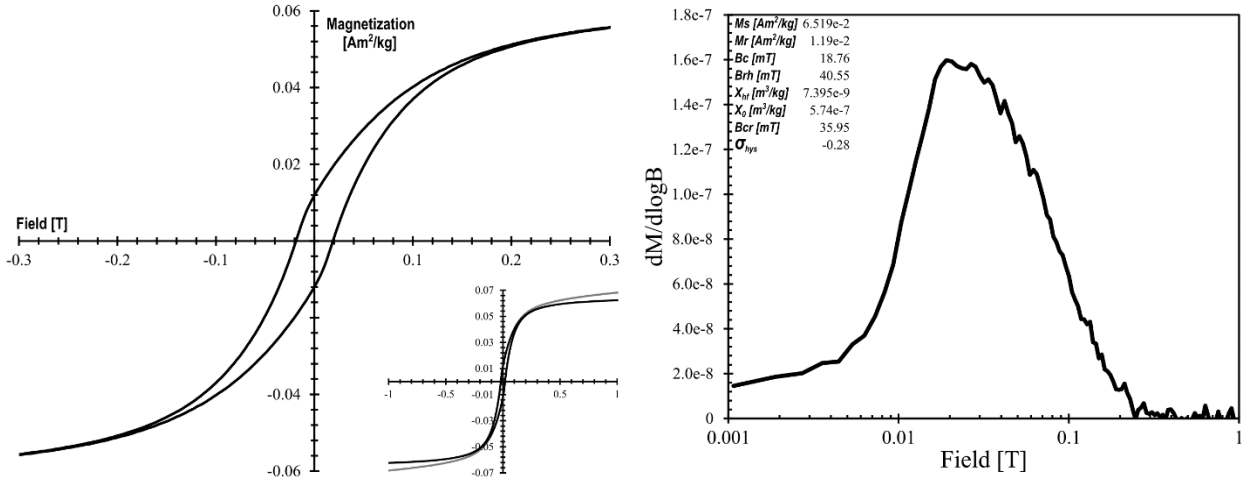


Figure 47. Hysteresis and backfield remanence coercivity data for anorthosite sample from site GM2160-1.

Low-temperature remanence measurements for this sample (Fig. 48) show a very slightly humped cooling curve from RTSIRM. LTSIRM after zero-field cooling is slightly more intense than RTSIRM. Like the data from GM54-1, there is a local minimum remanence after warming through the Verwey transition, which has a calculated T_V of 122 K. The humped cooling curve is an indicator of a degree of maghemitization (Özdemir and Dunlop, 2010), though the higher value of T_V suggests that relatively little of the magnetite is oxidized.

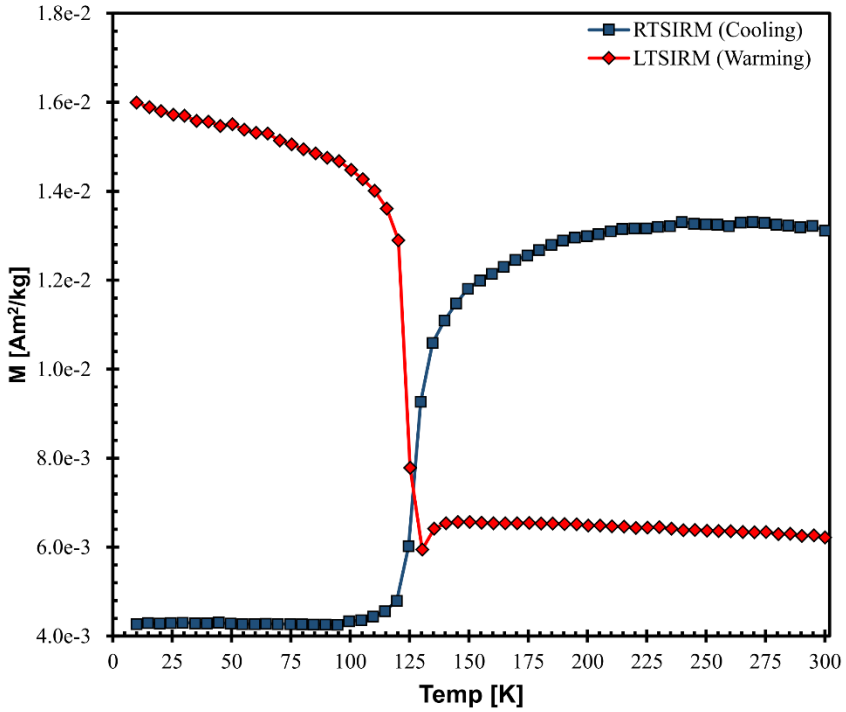


Figure 48. Low-temperature remanence data for anorthosite from site GM2160-1.

AMS measurements show that most specimens have triaxial to oblate fabric shapes, with Pj ranging from 1.03 to 1.14 and no clear correlation between scalar parameters. The mean site fabric is triaxial with both Kmax and Kmin streaking towards Kint (Fig. 49). The lineation plunges ~50° to the east. Given the reduced susceptibility of many specimens and the evidence for SD grains in the VSM data, is possible that the site mean fabric may be inverted, which would instead yield a foliation plunging ~40° to the west. The generally triaxial character of the site fabric and the fact that most specimens yield positive values of T are possible counterpoints (and certainly complicating factors) to this possibility.

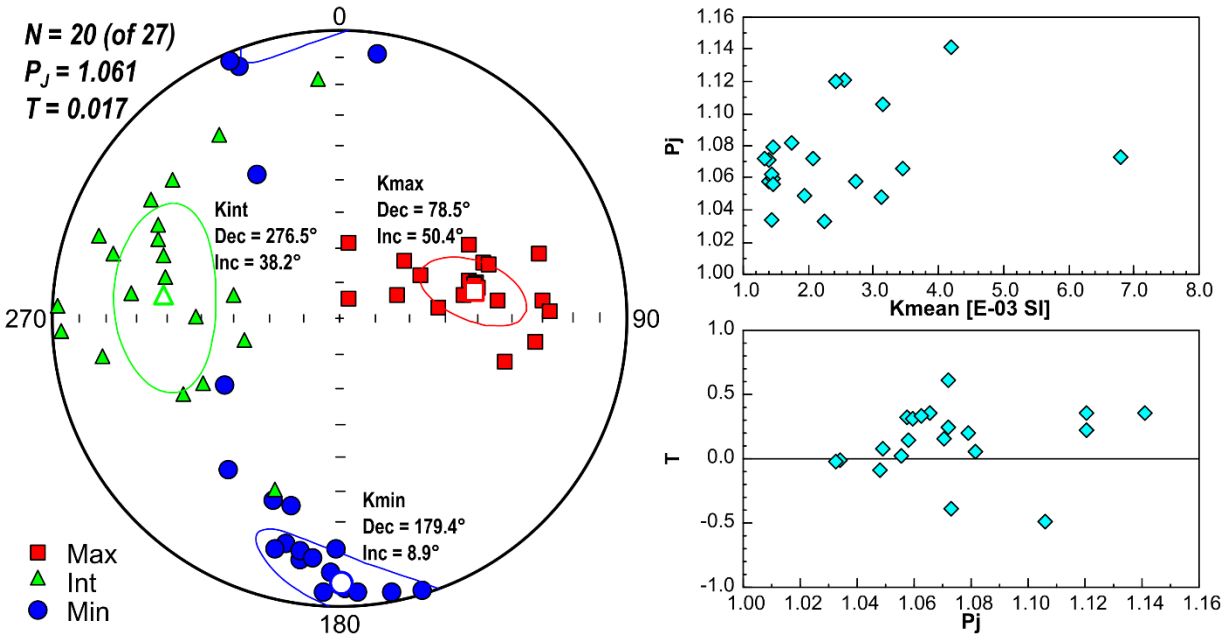


Figure 49. AMS results from anorthosite at site GM2160-1.

NRM intensity is reasonably high (averaging ~3.5% of Mr of the hysteresis sample) with a mean Q of 14.9. Thermal demagnetization has little effect until high temperatures - ~90% of the remanence is retained until an estimated temperature of about 520 °C (inexact due to oven issues). Above this temperature, a ChRM with a northeasterly and intermediate up direction is removed until the rock is fully demagnetized at 580 °C (Fig. 50A). The ChRMs are well grouped with mean D = 47.8°, I = -26.3°, α_{95} = 4.4° (Fig. 50B). The corresponding mean VGP lies to the southeast of the apparent polar wander path at 23.5 °S, 209.5 °E (Fig. 50C), like several of those previously determined.

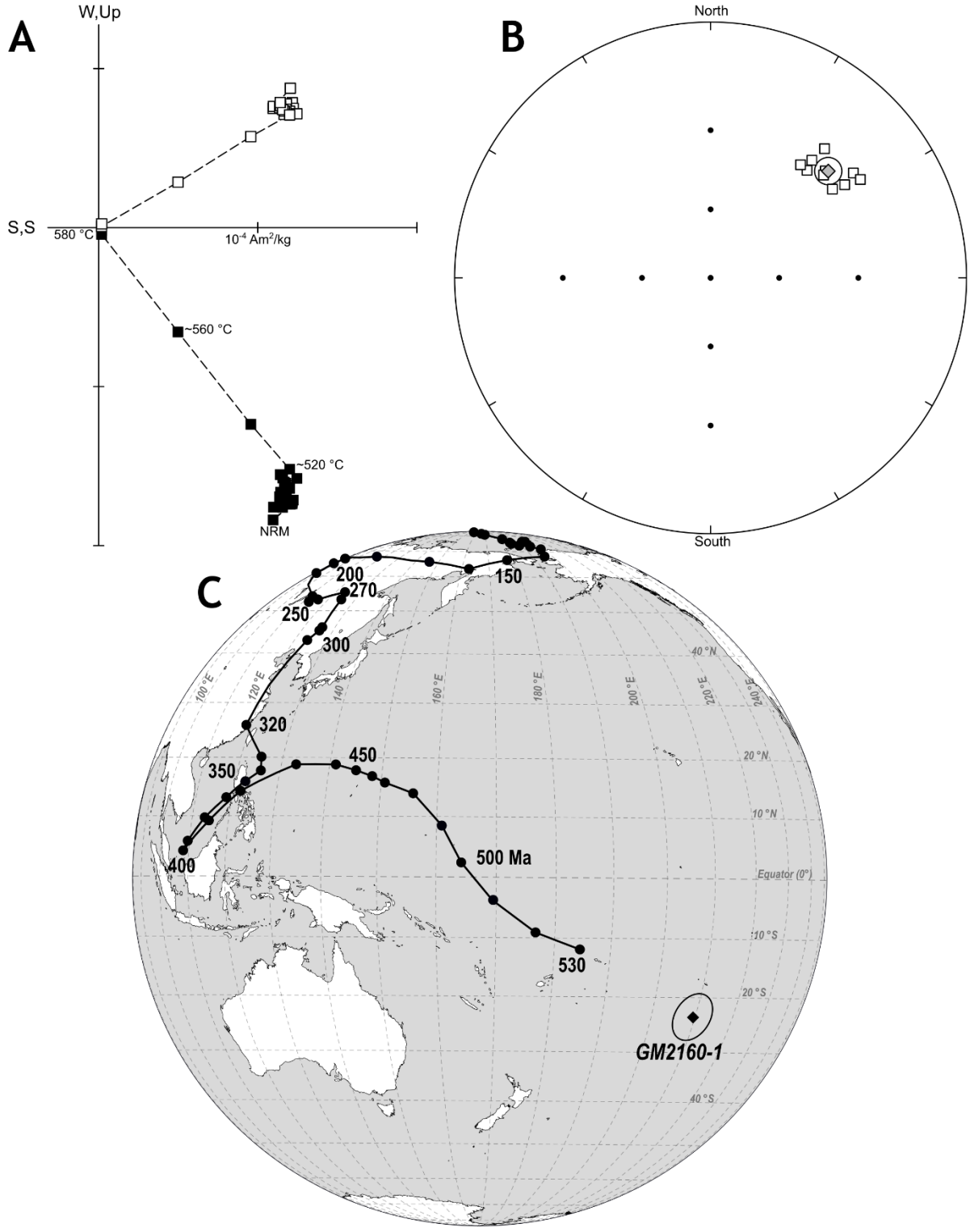


Figure 50. Paleomagnetic results for anorthosite at site GM2160-1. (A) Representative Zijderveld diagram showing northeasterly and intermediate-up ChRM. (B) Equal area plot of ChRMs determined for this site. (C) Comparison of mean in-situ VGP with Phanerozoic apparent polar wander path for North America.

Site GM2160-2, GMLC or Unnamed Roosevelt Gabbro

This site is located only ~20 meters from GM2160-1 but sampled a very different lithology. The rock here is a medium-coarse gabbroid with primary mineralogy consisting of plagioclase, clinopyroxene, olivine and opaque minerals. There is clear evidence for alteration, with olivine partly replaced by chlorite, carbonate and serpentine, plagioclase partially altered to sericite and epidote, and pyroxene partially replaced by amphibole, biotite and chlorite. It is possible that at least some of the amphibole is primary, which would contradict an affinity with the GMLC and instead would be classified as one of the Roosevelt Gabbros. The general texture of the rock is also quite similar to the Roosevelt Gabbros. Contact relations with the anorthosite were not clearly observed, and it is uncertain whether there are multiple mafic bodies at this site or simply localized segregations. At least some of the alteration is likely due to the intrusion of the large adjacent mass of granite and the numerous smaller granitic dikes found at this site.

Mean χ is 4.51×10^{-6} m^3/kg with a range of 2.52×10^{-6} to 7.36×10^{-6} m^3/kg, one of the narrower distributions of bulk susceptibility encountered. VSM data indicate a paramagnetic contribution of just over 1% of the initial susceptibility. The calculated initial susceptibility of the VSM sample is slightly higher than any of the bulk samples. Hysteresis measurements yield a weakly potbellied loop ($\sigma_{hys} = -0.12$) with $Mr/Ms \approx 0.09$ (Fig. 51). Coercivity and remanent coercivity are notably lower than the nearby anorthosite. The remanent coercivity spectrum shows a moderately broad distribution with a center near 20 mT. The reduced coercivities and Mr/Ms are likely a consequence of increased contributions from MD (titano)magnetite particles.

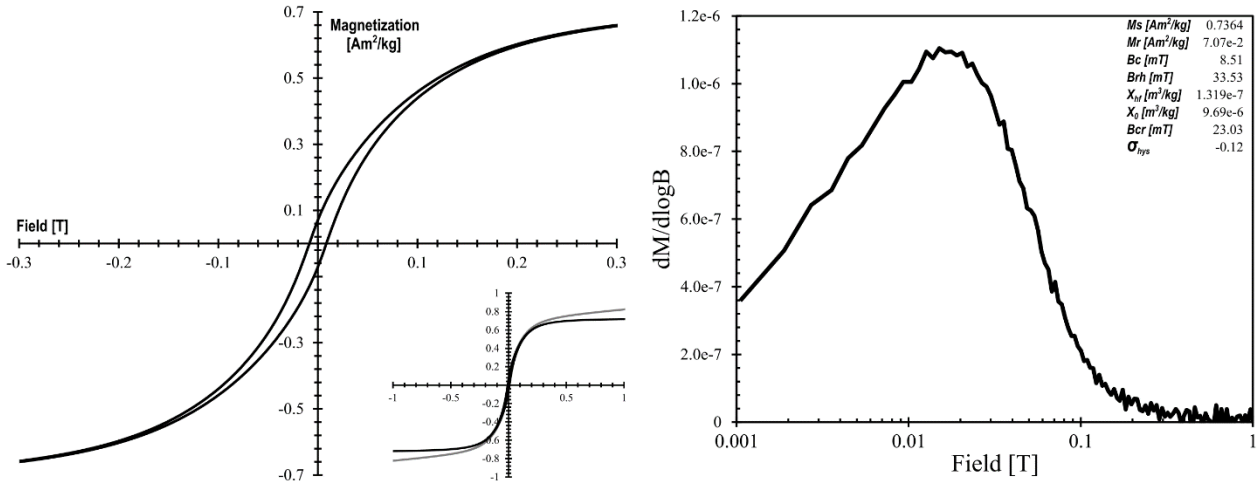


Figure 51. Hysteresis and remanent coercivity data from gabbro at site GM2160-2.

The AMS results from this site are quite noisy. Individual specimen values of Pj range from 1.03 to 1.39, though only a few are above 1.2. There is no relationship between Pj and Kmean and only a faint trend indicating that the samples with the highest Pj values have more negative values of T. Principal axis directions are highly dispersed. The site mean fabric is prolate, with a lineation plunging 27° to the northeast (Fig. 52). This fabric is almost entirely controlled by a few specimens with high Pj and negative T. Removing them from the calculation yields an essentially incoherent fabric at the site level.

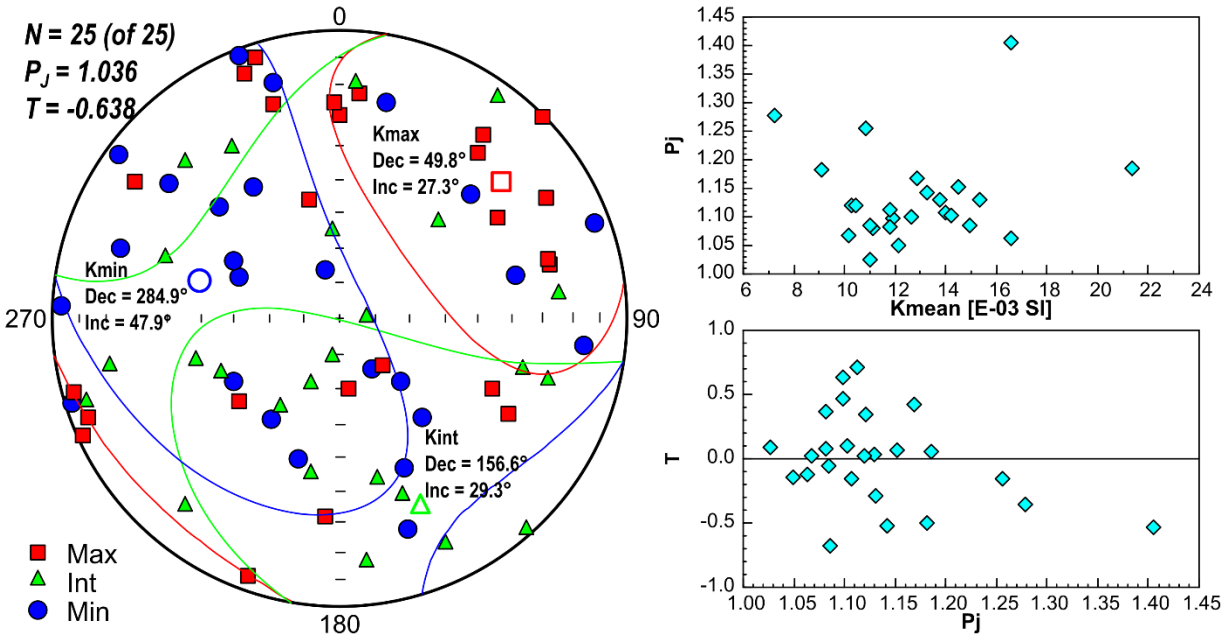


Figure 52. AMS results from gabbro at site GM2160-2.

Remanent intensities are slightly higher than those of the anorthosite, though the higher values of χ result in a lower average Q of 6.4. Thermal demagnetization progressively removes a southwesterly and moderate to steep down ChRM from low temperatures up to an estimated blocking temperature of about 540 °C (Fig. 53A). AF demagnetization attempts resulted in the samples acquiring a gyroremanent magnetization at low fields (~30-40 mT), similar to the behavior of samples from the Roosevelt Gabbros. The ChRM directions are well-grouped (Fig. 53B) and the corresponding mean VGP lies at 12.2 °S, 238.6 °E (α_{95} = 6.3°), well to the east of the 530 Ma point of the APWP (Fig. 53C).

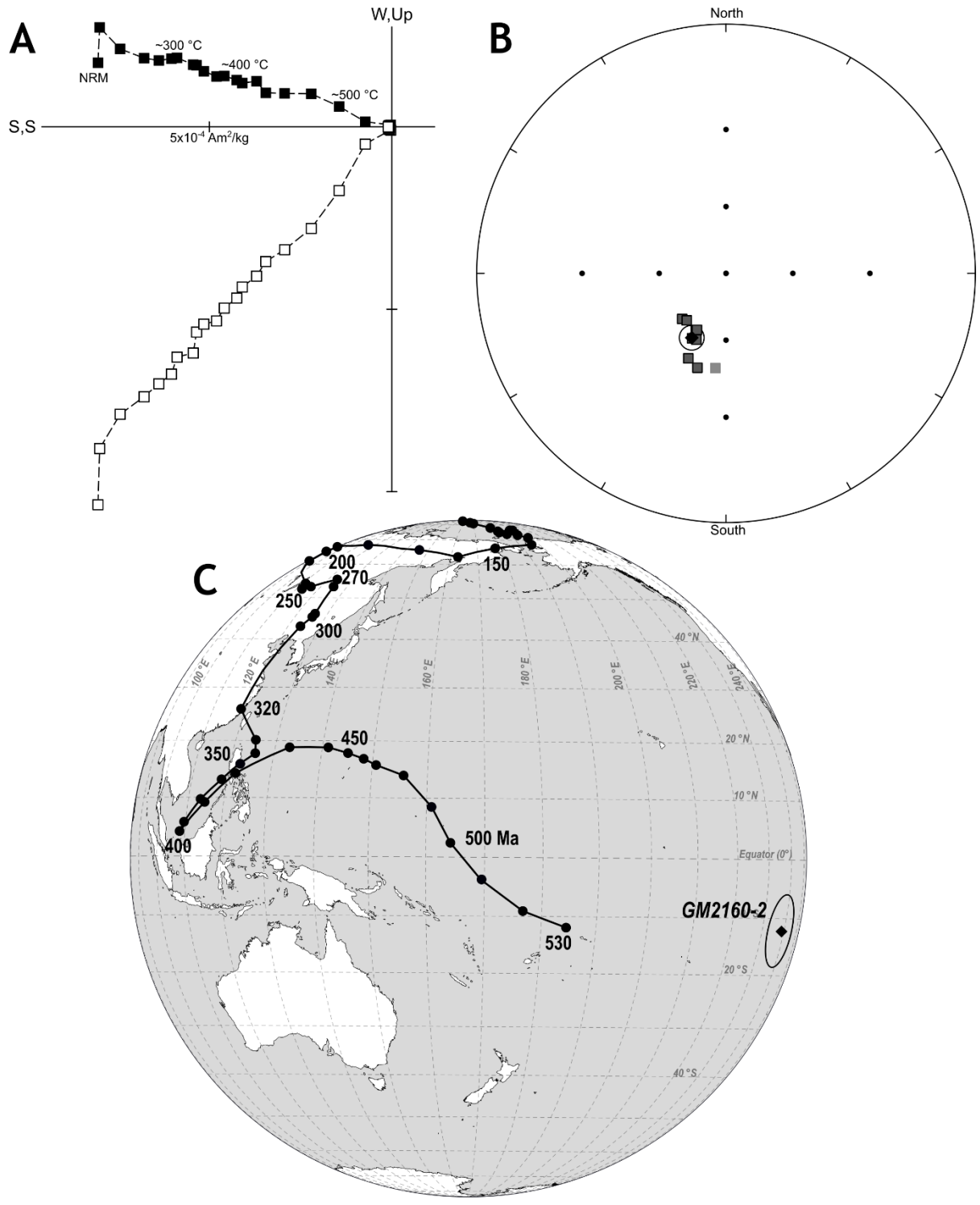


Figure 53. Paleomagnetic results for site GM2160-2. (A) Representative Zijderveld diagram showing steady removal of southwesterly and down ChRM. (B) Equal-area plot of identified ChRMs for this site. (C) Comparison of mean in-situ VGP with Phanerozoic APWP for North America.

DISCUSSION

In-Situ Paleomagnetism

Examination of the full distribution of site-mean VGPs calculated from *in-situ* remanence directions yields three major trends (Fig. 54A). A disperse group of VGPs appears to cluster to the southeast of the 530 Ma constraint of the apparent polar wander path and essentially overlaps previous results for the GMLC and the Mount Sheridan Gabbro by Roggenthen et al. (1981). The second trend is defined by components from the GM1500 sites and appears to form a NW-SE streak from the mean direction of the first group towards the 300 Ma segment of the APWP and the clearly-remagnetized sites from the Roosevelt Gabbros. A third group of VGPs with large confidence intervals is clustered approximately 80-90° to the west, approaching the 400 Ma mean pole. The large confidence intervals of three of these sites show overlap with previous results from granites of the Wichita Mountains. These results are tentatively interpreted as (1) an early Cambrian pole at 21.4 °S, 205.4 °E (α_{95} = 13°) dating to essentially the time of emplacement, (2) a partial late-Paleozoic overprint (complete, in the case of the two Roosevelt Gabbro sites) imparted during uplift, and (3) a partial middle-Paleozoic overprint which appears to have been acquired at ~400 Ma (Fig. 54B). The rock magnetic data indicate that all components are carried in magnetite and/or low-Ti titanomagnetite, some of which is partially oxidized and much of which occurs as inclusions in silicates (Scofield and Roggenthen, 1986).

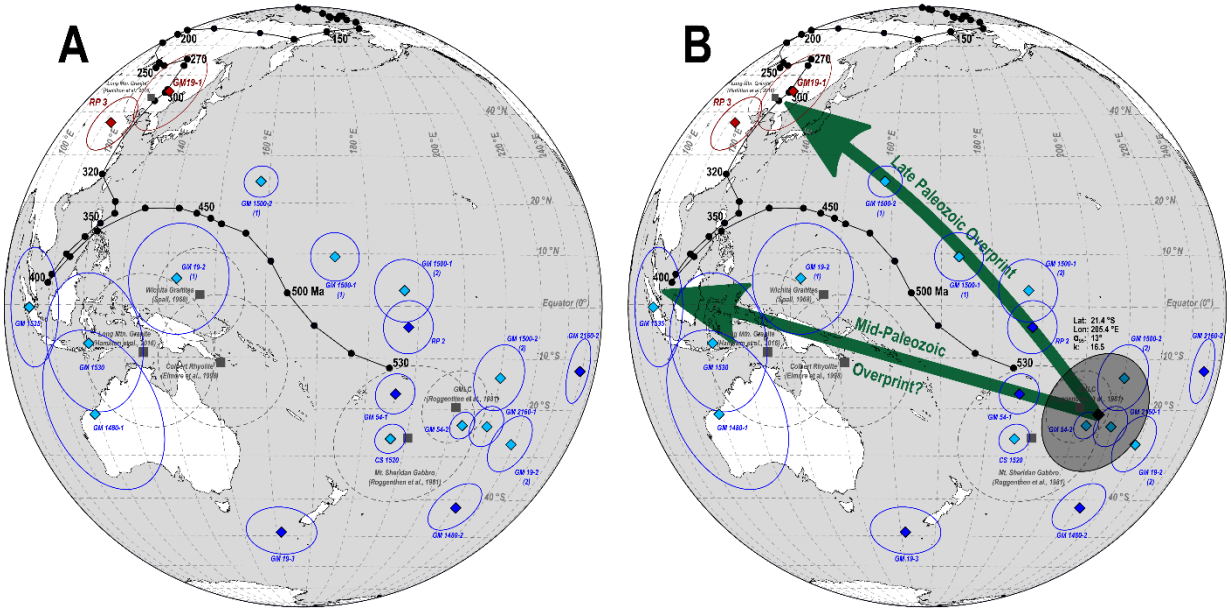


Figure 54. Compiled in-situ VGPs for all sites in this study. (A) Site mean VGPs only, with comparison to previous paleomagnetic studies of SOA igneous rocks and the apparent polar wander path of Torsvik et al. (2012). (B) Interpreted trends and primary mean VGP. Lightly-shaded markers indicate interpreted reverse polarity; dark markers indicate normal polarity.

The component which lies to the southeast of the APWP is consistent with the prior results of Roggenthen et al. (1981), the only previous paleomagnetic study with a focus on the mafic rocks of the SOA. Sites with VGPs in this group have directions with both northeasterly and southwesterly declinations which are interpreted as reversals, though (likely due to the high dispersion) they do not pass the reversal test of McFadden and McElhinny (1990) at the 95% confidence level. The presence of apparent reversals and the position of the mean VGP suggest this is an early Cambrian pole, likely as a thermoremanent magnetization during crystallization or after heating by adjacent intrusive bodies shortly after emplacement. It is also plausible that some sites instead carry a thermochemical remanent magnetization from moderate hydrothermal alteration during the same processes.

The presence of a late Paleozoic overprint at some sites is not particularly surprising. Most previous paleomagnetic studies of SOA granites and rhyolites have found remagnetizations of this age in at least some of their sampling sites (Ku et al., 1967; Spall, 1968; Vincenz et al.,

1975; Elmore et al., 1998; Hamilton et al., 2016). In the granites, this remagnetization appears to be mostly linked to low-temperature alteration at near-surface conditions (Price et al., 1998; Hamilton et al., 2016), though temperatures on the order of 300 °C were suggested by Vincenz et al. (1975) on the basis of rock magnetic data. Thin sections from the remagnetized Roosevelt Gabbros and the partially overprinted anorthosites show the rock to be remarkably fresh, in contrast to the weathering or remineralization that would be expected for mafic lithologies under groundwater or high-T hydrothermal conditions. The cause of remagnetization in these sites is presently unclear. It seems to have preferentially affected the Roosevelt Gabbro sites, possibly due to their high proportion of multidomain magnetite.

The presence of the third component is a significant point of interest. Prior paleomagnetic poles inferred to represent primary magnetization in the Wichita granites (Spall, 1968; Hamilton et al., 2016) and contemporaneous rhyolites from the eastern exposures of the aulacogen (Elmore et al., 1998) lie along a line between the inferred primary VGP of the layered complex and the gabbros which exhibit this component (Fig. 54B). Confidence intervals for some sites overlap those of the felsic rocks, and the trend suggests that igneous rocks throughout the SOA may have been subject to varying degrees of overprint by the same event.

The VGPs appear to approach the APWP near its position at 400 Ma. It is worth noting that very few paleopoles of this age range seem to have been either available or acceptable for inclusion in the calculation of the running mean, and the confidence interval for the path in Silurian to middle-Devonian time is very large (Torsvik et al., 2012). While tectonics of this area during the early Devonian are poorly understood, stratigraphic study does indicate multiple unconformities in the late Silurian and early Devonian of southern Oklahoma and at least some of these are reported to show evidence of subaerial exposure and erosion (Amsden, 1975, 1980).

The origin of this apparent uplift is unclear – speculatively, it may be associated with far-field effects of Caledonian tectonism which is inferred to have occurred at a similar time (e.g., Torsvik et al., 1996).

Remagnetization of basement rocks at this time seems the most parsimonious explanation for the observed trends and would explain the presence of this component at lower temperatures in site GM19-2. There is however another possible interpretation worth discussing. The VGP of the apparent early Devonian component is separated from that of the inferred primary VGP by nearly 90°. Clustered VGPs nearly 90° apart have been found in several studies of late Ediacaran and early Cambrian rocks across the world, forming the basis for the rapid early Cambrian inertial-interchange true polar wander hypothesis of Kirschvink et al. (1997). Bono and Tarduno (2015) investigated the occurrence of orthogonal magnetizations in the 565 Ma Sept-Îles layered intrusion of Quebec and found that only one of the components was carried in single-domain magnetite while the other was likely an overprint carried by MD grains. While this study cannot firmly confirm or refute a similar effect here, the (admittedly limited) rock magnetic data indicate that some of the affected sites (particularly GM1535) have a comparable or higher contribution from SD grains relative to most sites carrying the inferred primary direction. Recent work also indicates that the geomagnetic field was highly unstable in the late Ediacaran, and instability associated with a very high reversal rate seems to have persisted into the middle Cambrian (Gallet et al., 2019; Dudzisz et al., 2021). The trend could therefore also possibly represent a reversal path (or aborted reversals) during the early Cambrian, though no internal reversals are observed and the relatively large crystal size of most of the rocks involved suggests that they should have cooled slowly enough to average secular variation. It also fails to account

for the apparent clustering, and early Devonian remagnetization is tentatively retained as the preferred hypothesis.

Evaluation of Tilting

As previously stated, virtually all workers in the GMLC report that the layered series is tilted to the north or northeast. Unfortunately, most of these reports either only give a general range of trends or more commonly do not give numbers at all. Many are also located in the eastern exposures, which were not investigated here. Local faults have been mentioned as associated with changes in lithology and dip in several reports, but quantitative information is rarely provided and even the fault traces are often absent from published maps.

Well-developed layering was not observed at any of the drill sites in this work, making it difficult to evaluate structural corrections. The map and cross-section of Cooper (1991) lie within the present study area and indicate a dip of ~20° toward an azimuth of 19°. This trend was used as a first-order attempt at a regional tilt correction.

It has also been noted in studies of other layered intrusions that the foliation plane derived from AMS data typically coincides with mineral lamination (e.g., O'Driscoll et al., 2008, 2015; Ferré et al., 2009). While it does not appear to have been used in this manner, this suggests that AMS data might possibly be used to estimate an appropriate tilt correction in the absence of well-defined layering. To that end, an alternative regional tilt adjustment was also calculated using the average orientation of Kmin (the pole to magnetic foliation) of all GMLC sites. With outliers removed, the average pole to foliation corresponds to a dip of 9° toward an azimuth of 72°. This is considerably more easterly than dip directions typically reported in the literature, but agrees reasonably well with layering observed in a railway cut southwest of Roosevelt (F. Tetto, personal communication 2021). Notably, the large confidence interval (α_{95} = 15.2°) overlaps

zero, meaning that at the 95% certainty level there is no discernable tilt of the GMLC apparent from magnetic anisotropy.

In the event that structural complexity is considerably higher than expected or reported, individual sites were also tilt-adjusted using their particular foliation orientations (or lineations, in the case of two possible inverted fabrics). Two sites did not have well-defined foliations but were adjusted as per nearby sites. The Cold Springs site was included in these adjustments as there is evidence that mafic and felsic magmatism at that locality were simultaneous, though this is highly ambiguous (Powell et al., 1980a, 1980b; Vidrine and Fernandez, 1986). Comparison of VGPs derived from *in-situ* directions against those calculated after applying structural corrections based on the map of Cooper (1991) and magnetic fabrics are shown in Fig. 55 and discussed below.

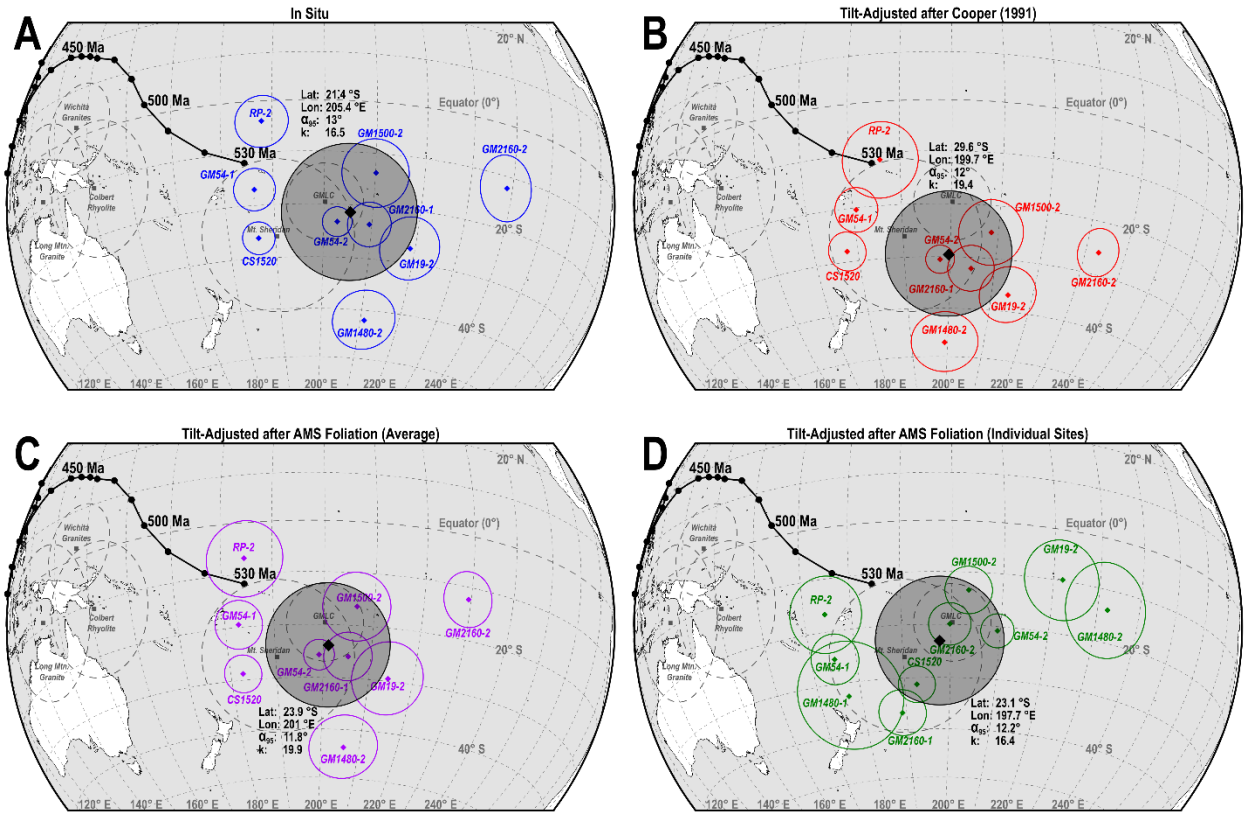


Figure 55. Comparison of in-situ VGPs to those recalculated using various structural corrections. Only those with possibly primary magnetizations are shown. (A) VGPs from in-situ directions. (B) VGPs recalculated following tilt-adjustment after Cooper (1991). (C) VGPs recalculated following tilt-adjustment using average poles to AMS foliation. (D) VGPs recalculated following tilt-adjustment using AMS foliations at individual sites.

Application of the structural correction determined from the map of Cooper (1991) results in the mean VGP being shifted southward by about 8 degrees and west by about 6 degrees relative to the *in-situ* directions (Fig. 55A, B). Individual poles mostly shift by the same amount, though there is some variance due to nonlinearity of the equations. In particular, the three most westerly VGPs are much closer to each other following this adjustment. Adjusting the *in-situ* directions instead for a regional tilt calculated from AMS foliations results in a less severe shift in roughly the same direction (2.5 ° south and 4.4° west; Fig. 55C). Tilt adjustments based on individual site AMS result in the largest changes among individual sites and also bring the VGP for site 1480-1 into the same area as those of sites thought to be primary from *in-situ* directions.

The mean VGP shifts westward just over 8° and southward by just under 2° (Fig. 55D). This approach also results in a streaked VGP distribution rather than a dispersed one; the meaning of this result (if any) is unclear. If the GM1480 sites are disregarded (likely justifiable, as the tilt adjustment requires the assumption that the fabric is inverse despite the MD magnetite clearly present in the hysteresis data), the mean pole shifts another 5° to the west and less than a degree south (23.9 °S, 192.2 °E). Regardless of the tilt correction applied, the results indicate a paleolatitude of about 6°, consistent with previous work which infers an equatorial Laurentia through the late Ediacaran to early Cambrian (e.g., Hodych et al., 2004; McCausland et al., 2007, 2011).

Due in part to the large α_{95} values, the confidence intervals for *in-situ* VGPs and those determined by the various structural corrections all show a significant degree of overlap and cannot be statistically distinguished; The relatively small changes in pole position with reasonable tilt adjustments suggest that the primary magnetization has not been significantly deflected by tectonics. The GMLC appears to preserve an essentially primary early Cambrian magnetization with a pole position similar to but southeast of that reported for roughly contemporaneous syenites by McCausland et al. (2007) and consistent with the prior results of Roggenthen et al. (1981), who also noted the minimal effect of tilt corrections. Application of tilt adjustments to most directions which appear to be the result of an early Devonian remagnetization result in VGPs even further from the APWP of Torsvik et al. (2012), possibly reflecting the inferred post-tilting age of the remanence.

SUMMARY

Paleomagnetic results from the early Cambrian have been a subject of controversy for decades, and the apparent polar wander path during that time is very poorly constrained. The

532.5 to 530 Ma igneous rocks of the Wichita Mountains area in southern Oklahoma provide an opportunity for further data regarding the APWP and paleogeography of Laurentia and possibly to test some of the hypotheses which have been developed regarding the character of the geomagnetic field at the time. The present study has focused on the anorthositic units of the Glen Mountains Layered Complex and the mafic to intermediate rocks which intrude it in its western exposures.

The results of this study yield evidence for three magnetizations in these rocks. One component appears to be a primary early Cambrian direction which is indistinguishable from a previous study of the area and is also similar to results from syenites of similar age in Canada. Application of tilt corrections does not largely affect the mean pole position of this component. The second component is a partial to complete overprint of late Paleozoic age which resembles that found in some of the Wichita granites. While that remagnetization has largely been associated with low-temperature fluid alteration in the granites, evidence for that is lacking in the mafic units sampled here and the cause remains uncertain. The third component is tentatively interpreted as a partial to complete remagnetization of some sites in the mid-Paleozoic (~400 Ma), again with unknown cause. Comparison of with previous paleomagnetic studies of Wichita granites indicates that they are likely affected by this overprint as well. Rock magnetic data indicate all remanent magnetizations are carried in magnetite or low-Ti magnetite, with evidence for minor maghemite, and most samples show a significant contribution from single-domain grains.

Anisotropy of magnetic susceptibility measurement most commonly yields oblate fabrics, though several sites have a significant triaxial or prolate overprint. Some may be inverse fabrics, but deformation or possibly magma chamber dynamics are more likely causes. The AMS

foliation planes suggest that the overall dip of the GMLC is slight and more easterly (9° dip towards an azimuth of 72°) than described from studies of local layering. The confidence interval overlaps zero. Initial tests using AMS as a proxy for paleohorizontal in tilt corrections yield very similar results to tilt corrections from inferred layering in previous studies. While this does not clearly verify the technique, it shows promise insofar as the results are not obviously wrong.

While further work is necessary to clarify blocking temperatures and search for possible field tests, this work indicates that many of the mafic and intermediate rocks of the Wichita Mountains area contain a primary magnetization that can provide information regarding the paleogeography of North America and the behavior of the geomagnetic field during the early Cambrian. Additionally, some record evidence of a late Paleozoic overprint most likely acquired shortly after uplift, and others indicate the presence of a previously unrecognized early Devonian overprint of unknown cause which has likely complicated previous work on the granites. These results provide both new information for paleogeographic and paleomagnetic work in the future as well as context for the results of past studies.

REFERENCES

Abrajevitch, A. and Van der Voo, R., 2010. Incompatible Ediacaran paleomagnetic directions suggest an equatorial geomagnetic dipole hypothesis. Earth and Planetary Science Letters, 293(1-2), pp.164-170. https://doi.org/10.1016/j.epsl.2010.02.038

Amsden, T.W., 1975. Hunton Group (Late Ordovician, Silurian, and early Devonian) in the Anadarko Basin of Oklahoma. Oklahoma Geological Survey Bulletin 121.

Amsden, T.W., 1980. Hunton Group (Late Ordovician, Silurian, and early Devonian) in the Arkoma Basin of Oklahoma. Oklahoma Geological Survey Bulletin 129.

Bono, R.K. and Tarduno, J.A., 2015. A stable Ediacaran Earth recorded by single silicate crystals of the ca. 565 Ma Sept-Îles intrusion. Geology, 43(2), pp.131-134. https://doi.org/10.1130/G36247.1

Bono, R.K., Tarduno, J.A., Nimmo, F. and Cottrell, R.D., 2019. Young inner core inferred from Ediacaran ultra-low geomagnetic field intensity. Nature Geoscience, 12(2), pp.143-147. https://doi.org/10.1038/s41561-018-0288-0

Bouchez, J.L., 1997. Granite is never isotropic: an introduction to AMS studies of granitic rocks. In Granite: From segregation of melt to emplacement fabrics (pp. 95-112). Springer, Dordrecht. https://doi.org/10.1007/978-94-017-1717-5_6

Brueseke, M.E., Hobbs, J.M., Bulen, C.L., Mertzman, S.A., Puckett, R.E., Walker, J.D. and Feldman, J., 2016. Cambrian intermediate-mafic magmatism along the Laurentian margin: Evidence for flood basalt volcanism from well cuttings in the Southern Oklahoma aulacogen (USA). Lithos, 260, pp.164-177. https://doi.org/10.1016/j.lithos.2016.05.016

Butler, R.F., 1992. Paleomagnetism: Magnetic domains to geologic terranes. Boston: Blackwell Scientific Publications.

Cawood, P.A., McCausland, P.J. and Dunning, G.R., 2001. Opening Iapetus: constraints from the Laurentian margin in Newfoundland. Geological Society of America Bulletin, 113(4), pp.443-453. https://doi.org/10.1130/0016-7606(2001)113<0443:OICFTL>2.0.CO;2

Cooper, R.W., 1991. Geology, geochemistry, and platinum-group-element mineralization of the Cambrian Glen Mountains Layered Complex and associated rocks, southwestern Oklahoma. Oklahoma Geological Survey Circular 92, pp.98-108.

Dalziel, I.W., 1997. OVERVIEW: Neoproterozoic-Paleozoic geography and tectonics: Review, hypothesis, environmental speculation. Geological Society of America Bulletin, 109(1), pp.16-42. https://doi.org/10.1130/0016-7606(1997)109<0016:ONPGAT>2.3.CO;2

Dudzisz, K., Lewandowski, M., Werner, T., Karasiński, G., Kędzior, A., Paszkowski, M., Środoń, J. and Bojanowski, M.J., 2021. Paleolatitude estimation and premises for geomagnetic field instability from the Proterozoic drilling core material of the south-western part of the East European Craton. Precambrian Research, 357, 106135. https://doi.org/10.1016/j.precamres.2021.106135

Dunlop, D.J., 2002. Theory and application of the Day plot (Mrs/Ms versus Hcr/Hc) 1. Theoretical curves and tests using titanomagnetite data. Journal of Geophysical Research: Solid Earth, 107(B3), 2056 pp.EPM4-1-EPM4-22. https://doi.org/10.1029/2001JB000486

Dunlop, D.J. and Özdemir, Ö., 1997, Rock magnetism: Fundamentals and frontiers. Cambridge University Press, Cambridge, UK.

Dunlop, D.J., Schutts, L.D. and Hale, C.J., 1984. Paleomagnetism of Archean rocks from northwestern Ontario: III. Rock magnetism of the Shelley Lake granite, Quetico Subprovince. Canadian Journal of Earth Sciences, 21(8), pp.879-886. https://doi.org/10.1139/e84-094

Egli, R., 2003. Analysis of the field dependence of remanent magnetization curves. Journal of Geophysical Research: Solid Earth, 108(B2), 2081. https://doi.org/10.1029/2002JB002023

Elmore, R.D., Campbell, T., Banerjee, S. and Bixler, W.G., 1998. Palaeomagnetic dating of ancient fluid-flow events in the Arbuckle Mountains, southern Oklahoma. Geological Society of London Special Publications, 144(1), pp.9-25. https://doi.org/10.1144/GSL.SP.1998.144.01.02

Fabian, K., 2003. Some additional parameters to estimate domain state from isothermal magnetization measurements. Earth and Planetary Science Letters, 213(3-4), pp.337-345. https://doi.org/10.1016/S0012-821X(03)00329-7

Ferré, E.C., 2002. Theoretical models of intermediate and inverse AMS fabrics. Geophysical Research Letters, 29(7), pp.31-34. https://doi.org/10.1029/2001GL014367

Ferré, E.C., Maes, S.M. and Butak, K.C., 2009. The magnetic stratification of layered mafic intrusions: Natural examples and numerical models. Lithos, 111(1-2), pp.83-94. https://doi.org/10.1016/j.lithos.2009.03.042

Fisher, R.A., 1953. Dispersion on a sphere. Proceedings of the Royal Society of London Series A: Mathematical and Physical Sciences, 217(1130), pp.295-305. https://doi.org/10.1098/rspa.1953.0064

Gallet, Y., Pavlov, V. and Korovnikov, I., 2019. Extreme geomagnetic reversal frequency during the Middle Cambrian as revealed by the magnetostratigraphy of the Khorbusuonka section (northeastern Siberia). Earth and Planetary Science Letters, 528, 115823. https://doi.org/10.1016/j.epsl.2019.115823

Gilbert, M.C., 1960. The geology of the western Glen Mountains, Oklahoma. Unpublished M.Sc. Thesis, University of Oklahoma.

Gilbert, M.C., 1982. Geologic setting of the eastern Wichita Mountains with a brief discussion of unresolved problems. Oklahoma Geological Survey Guidebook 21, pp.1-30.

Gilbert, M.C., 1983. Timing and chemistry of igneous events associated with the Southern Oklahoma Aulacogen. Tectonophysics, 94(1-4), pp.439-455. https://doi.org/10.1016/0040-1951(83)90028-8

Gilbert, M.C., 2014. The Wichita Mountains in Oklahoma: Their story through time. Oklahoma Geological Survey Guidebook 39.

Grotzinger, J.P., Bowring, S.A., Saylor, B.Z. and Kaufman, A.J., 1995. Biostratigraphic and geochronologic constraints on early animal evolution. Science, 270(5236), pp.598-604. https://doi.org/10.1126/science.270.5236.598

Ham, W.E., Denison, R.E., and Merritt, C.A., 1964. Basement Rocks and Structural Evolution of Southern Oklahoma. Oklahoma Geological Survey Bulletin 95.

Hamilton, E.M., Elmore, R.D., Weaver, B.L., Dulin, S. and Jackson, J., 2016. Paleomagnetic and petrologic study of the age, origin, and significance of early and late Paleozoic events in the Long Mountain Granite, Wichita Mountains, Oklahoma. Geological Society of America Bulletin, 128(1-2), pp.187-202. https://doi.org/10.1130/B31277.1

Hanson, R.E., Puckett Jr, R.E., Keller, G.R., Brueseke, M.E., Bulen, C.L., Mertzman, S.A., Finegan, S.A. and McCleery, D.A., 2013. Intraplate magmatism related to opening of the southern Iapetus Ocean: Cambrian Wichita igneous province in the Southern Oklahoma rift zone. Lithos, 174, pp.57-70. https://doi.org/10.1016/j.lithos.2012.06.003

Hodych, J.P., Cox, R.A. and Košler, J., 2004. An equatorial Laurentia at 550 Ma confirmed by Grenvillian inherited zircons dated by LAM ICP-MS in the Skinner Cove volcanics of western Newfoundland: implications for inertial interchange true polar wander. Precambrian Research, 129(1-2), pp.93-113. https://doi.org/10.1016/j.precamres.2003.10.012

Hoffman, P., Dewey, J.F., Burke, K., 1974. Aulacogens and their genetic relation to geosynclines, with a Proterozoic example from Great Slave Lake, Canada. In: Dott Jr., R.H., Shaver, R.H. (Eds.), Modern and Ancient Geosynclinal Sedimentation: Society of Economic Paleontologists and Mineralogists Special Publication, 19, pp. 38–55. https://doi.org/10.2110/pec.74.19.0038

Hogan, J.P. and Gilbert, M.C., 1997. Intrusive style of A-type sheet granites in a rift environment: The Southern Oklahoma aulacogen. Geological Society of America Special Paper 312, pp.299-311. https://doi.org/10.1130/0-8137-2312-4.299

Hrouda, F., 2011. Models of frequency-dependent susceptibility of rocks and soils revisited and broadened. Geophysical Journal International, 187(3), pp.1259-1269. https://doi.org/10.1111/j.1365-246X.2011.05227.x

Irving, E., 1956. Palaeomagnetic and palaeoclimatological aspects of polar wandering. Geofisica pura e applicata, 33(1), pp.23-41. https://doi.org/10.1007/BF02629944

Jackson, M.J. and Moskowitz, B., 2021. On the distribution of Verwey transition temperatures in natural magnetites. Geophysical Journal International, 224(2), pp.1314-1325. https://doi.org/10.1093/gji/ggaa516

Jackson, M. and Sølheid, P., 2010. On the quantitative analysis and evaluation of magnetic hysteresis data. Geochemistry, Geophysics, Geosystems, 11(4), Q04Z15. https://doi.org/10.1029/2009GC002932

Jelínek, V., 1981. Characterization of the magnetic fabric of rocks. Tectonophysics, 79(3-4), pp.T63-T67. https://doi.org/10.1016/0040-1951(81)90110-4

Kirschvink, J., 1980. The least-squares line and plane and the analysis of palaeomagnetic data. Geophysical Journal International, 62(3), pp.699-718. https://doi.org/10.1111/j.1365-246X.1980.tb02601.x

Kirschvink, J.L., Ripperdan, R.L. and Evans, D.A., 1997. Evidence for a large-scale reorganization of Early Cambrian continental masses by inertial interchange true polar wander. Science, 277(5325), pp.541-545. https://doi.org/10.1126/science.277.5325.541

Kluth, C.F. and Coney, P.J., 1981. Plate tectonics of the ancestral Rocky Mountains. Geology, 9(1), pp.10-15. https://doi.org/10.1130/0091-7613(1981)9<10:PTOTAR>2.0.CO;2

Koenigsberger, J.G., 1938. Natural residual magnetism of eruptive rocks: Part I. Terrestrial Magnetism and Atmospheric Electricity, 43(2), pp.119-130. https://doi.org/10.1029/TE043i002p00119

Ku, C.C., Sun, S., Soffel, H. and Scharon, L., 1967. Paleomagnetism of the basement rocks, Wichita Mountains, Oklahoma. Journal of Geophysical Research, 72(2), pp.731-737. https://doi.org/10.1029/JZ072i002p00731

Lambert, D.D., Unruh, D.M. and Gilbert, M.C., 1988. Rb-Sr and Sm-Nd isotopic study of the Glen Mountains layered complex: Initiation of rifting within the southern Oklahoma aulacogen. Geology, 16(1), pp.13-17. https://doi.org/10.1130/0091-7613(1988)016<0013:RSASNI>2.3.CO;2

McCausland, P.J., Van der Voo, R. and Hall, C.M., 2007. Circum-Iapetus paleogeography of the Precambrian–Cambrian transition with a new paleomagnetic constraint from Laurentia. Precambrian Research, 156(3-4), pp.125-152. https://doi.org/10.1016/j.precamres.2007.03.004

McCausland, P.J., Hankard, F., Van der Voo, R. and Hall, C.M., 2011. Ediacaran paleogeography of Laurentia: Paleomagnetism and 40Ar–39Ar geochronology of the 583 Ma Baie des Moutons syenite, Quebec. Precambrian Research, 187(1-2), pp.58-78. https://doi.org/10.1016/j.precamres.2011.02.004

McConnell, D.A. and Gilbert, M.C., 1990. Cambrian extensional tectonics and magmatism within the Southern Oklahoma aulacogen. Tectonophysics, 174(1-2), pp.147-157. https://doi.org/10.1016/0040-1951(90)90388-O

McFadden, P.L. and McElhinny, M.W., 1990. Classification of the reversal test in palaeomagnetism. Geophysical Journal International, 103(3), pp.725-729. https://doi.org/10.1111/j.1365-246X.1990.tb05683.x

Merritt, C.A., 1958. Igneous geology of the Lake Altus area, Oklahoma. Oklahoma Geological Survey Bulletin 76.

Merritt, C.A. and Ham, W.E., 1939. Zeolitic rocks in the Wichita Mountains, Oklahoma. Proceedings of the Oklahoma Academy of Science, 19, pp. 115-117.

Merritt, C.A. and Ham, W.E., 1941. Pre-Cambrian Zeolite-Opal Sediments in Wichita Mountains, Oklahoma. AAPG Bulletin, 25(2), pp.287-299. https://doi.org/10.1306/3D9332AC-16B1-11D7-8645000102C1865D

Mitchell, R.N., Raub, T.D., Silva, S.C. and Kirschvink, J.L., 2015. Was the Cambrian explosion both an effect and an artifact of true polar wander? American Journal of Science, 315(10), pp.945-957. https://doi.org/10.2475/10.2015.02

O'Driscoll, B., Stevenson, C.T. and Troll, V.R., 2008. Mineral lamination development in layered gabbros of the British Palaeogene Igneous Province: A combined anisotropy of magnetic susceptibility, quantitative textural and mineral chemistry study. Journal of Petrology, 49(6), pp.1187-1221. https://doi.org/10.1093/petrology/egn022

O'Driscoll, B., Ferré, E.C., Stevenson, C.T. and Magee, C., 2015. The significance of magnetic fabric in layered mafic-ultramafic intrusions. In: Charlier B., Namur O., Latypov R., and Tegner, C. (eds), Layered Intrusions (pp. 295-329). Springer, Dordrecht. https://doi.org/10.1007/978-94-017-9652-1_7

Özdemir, Ö. and Dunlop, D.J., 2010. Hallmarks of maghemitization in low-temperature remanence cycling of partially oxidized magnetite nanoparticles. Journal of Geophysical Research: Solid Earth, 115, B02101. https://doi.org/10.1029/2009JB006756

Özdemir, Ö., Dunlop, D.J. and Berquo, T.S., 2008. Morin transition in hematite: Size dependence and thermal hysteresis. Geochemistry, Geophysics, Geosystems, 9(10), Q10Z01. https://doi.org/10.1029/2008GC002110

Powell, B.N., 1986. The Raggedy Mountain Gabbro Group. Oklahoma Geological Survey Guidebook 23, pp.21-52.

Powell, B.N. and Phelps, D.W., 1977. Igneous cumulates of the Wichita province and their tectonic implications. Geology, 5(1), pp.52-56. https://doi.org/10.1130/0091-7613(1977)5<52:ICOTWP>2.0.CO;2

Powell, B.N. and Gilbert, M.C., 1982. Stop 1: Reid's Pit. Oklahoma Geological Survey Guidebook 21, pp.79-96.

Powell, B.N., Gilbert, M.C. and Fischer, J.F., 1980a. Lithostratigraphic classification of basement rocks of the Wichita province, Oklahoma: Summary. Geological Society of America Bulletin, 91(9), pp.509-514. https://doi.org/10.1130/0016-7606(1980)91<509:LCOBRO>2.0.CO;2

Powell, B.N., Gilbert, M.C. and Fischer, J.F., 1980b. Lithostratigraphic classification of basement rocks of the Wichita province, Oklahoma. Geological Society of America Bulletin, 91(9) Part II, pp.1875-1994. https://doi.org/10.1130/GSAB-P2-91-1875

Price, J.D., Hogan, J.P., Gilbert, M.C. and Payne, J.D., 1998. Surface and near-surface investigation of the alteration of the Mount Scott Granite and geometry of the Sandy Creek Gabbro pluton, Hale Spring area, Wichita Mountains, Oklahoma. In Basement Tectonics 12 (pp. 79-122). Springer, Dordrecht. https://doi.org/10.1007/978-94-011-5098-9_4

Rochette, P., Jackson, M. and Aubourg, C., 1992. Rock magnetism and the interpretation of anisotropy of magnetic susceptibility. Reviews of Geophysics, 30(3), pp.209-226. https://doi.org/10.1029/92RG00733

Roggenthen, W.M., Fischer, J.F., Napoleone, G. and Fischer, A.G., 1981. Paleomagnetism and age of mafic plutons, Wichita Mountains, Oklahoma. Geophysical Research Letters, 8(2), pp.133-136. https://doi.org/10.1029/GL008i002p00133

Scofield, N., 1975. Layered Series of the Wichita Complex, Oklahoma. Geological Society of America Bulletin, 86(6), pp.732-736. https://doi.org/10.1130/0016-7606(1975)86<732:LSOTWC>E2.0.CO;2

Scofield, N. and Roggenthen, W.M., 1986. Petrologic evolution of plagioclase-rich cumulates from the Wichita Mountains, Oklahoma: Effects upon magnetic remanence properties. Geology, 14(11), pp.908-911. https://doi.org/10.1130/0091-7613(1986)14<908:PEOPCF>2.0.CO;2

Shatski, N.S., 1946. The great Donets basin and the Wichita system; comparative tectonics of ancient platforms. Akademiya Nauk SSSR Izvestiya, Seriya Geologicheskaya, 6, pp.57-90.

Soreghan, G.S., Keller, G.R., Gilbert, M.C., Chase, C.G. and Sweet, D.E., 2012. Load-induced subsidence of the Ancestral Rocky Mountains recorded by preservation of Permian landscapes. Geosphere, 8(3), pp.654-668. https://doi.org/10.1130/GES00681.1

Spall, H., 1968. Paleomagnetism of basement granites of southern Oklahoma and its implications: Progress report. Oklahoma Geology Notes, 28(2), pp.65–80.

Spencer, A.B., 1961. Geology of the basic rocks of the eastern portion of the Raggedy Mountains, southwestern Oklahoma. Unpublished M.Sc. Thesis, University of Oklahoma.

Tarling, D.H. and Hrouda, F., 1993. The Magnetic Anisotropy of Rocks. Chapman and Hall, London.

Tauxe, L., Mullender, T.A.T. and Pick, T., 1996. Potbellies, wasp-waists, and superparamagnetism in magnetic hysteresis. Journal of Geophysical Research: Solid Earth, 101(B1), pp.571-583. https://doi.org/10.1029/95JB03041

Thallner, D., Biggin, A.J., McCausland, P.J. and Fu, R.R., 2021. New paleointensities from the Skinner Cove Formation, Newfoundland, suggest a changing state of the geomagnetic field at the Ediacaran-Cambrian transition. Journal of Geophysical Research: Solid Earth. https://doi.org/10.1029/2021JB022292.

Thomas, W.A., 1991. The Appalachian-Ouachita rifted margin of southeastern North America. Geological Society of America Bulletin, 103(3), pp.415-431. https://doi.org/10.1130/0016-7606(1991)103<0415:TAORMO>2.3.CO;2

Thomas, W.A., 2014. The Southern Oklahoma transform-parallel intracratonic fault system. Oklahoma Geological Survey Guidebook 38, pp.375-388.

Tilton, G.R., Wetherill, G.W. and Davis, G.L., 1962. Mineral ages from the Wichita and Arbuckle mountains, Oklahoma, and the St. Francis mountains, Missouri. Journal of Geophysical Research, 67(10), pp.4011-4019. https://doi.org/10.1029/JZ067i010p04011

Torsvik, T.H., Smethurst, M.A., Meert, J.G., Van der Voo, R., McKerrow, W.S., Brasier, M.D., Sturt, B.A. and Walderhaug, H.J., 1996. Continental break-up and collision in the Neoproterozoic and Palaeozoic—a tale of Baltica and Laurentia. Earth-Science Reviews, 40(3-4), pp.229-258. https://doi.org/10.1016/0012-8252(96)00008-6

Torsvik, T.H., Van der Voo, R., Preeden, U., Mac Niocaill, C., Steinberger, B., Doubrovine, P.V., Van Hinsbergen, D.J.J., Domeier, M., Gaina, C., Tohver, E., Meert, J.G., McCausland, P.J.A., and Cocks, R.M., 2012. Phanerozoic polar wander, palaeogeography and dynamics. Earth-Science Reviews, 114(3-4), pp.325-368. https://doi.org/10.1016/j.earscirev.2012.06.007

Vidrine, D.M. and Fernandez, L.A., 1986. Geochemistry and Petrology of the Cold Springs Breccia, Wichita Mountains, Oklahoma. Oklahoma Geological Survey Guidebook 23, pp.86-106.

Vincenz, S.A., Yaskawa, K. and Ade-Hall, J.M., 1975. Origin of the magnetization of the Wichita Mountains granites, Oklahoma. Geophysical Journal of the Royal Astronomical Society, 42(1), pp.21-48. https://doi.org/10.1111/j.1365-246X.1975.tb05848.x

Wall, C.J., Hanson, R.E., Schmitz, M., Price, J.D., Donovan, R.N., Boro, J.R., Eschberger, A.M. and Toews, C.E., 2021. Integrating zircon trace-element geochemistry and high-precision U-Pb zircon geochronology to resolve the timing and petrogenesis of the late Ediacaran–Cambrian Wichita igneous province, Southern Oklahoma Aulacogen, USA. Geology, 49(3), pp.268-272. https://doi.org/10.1130/G48140.1

Zijderveld, J.D.A., 1967. A.C. demagnetization of rocks: Analysis of results. In: Collinson, D.W., Creer, K.M., and Runcorn, S.K., eds., Methods in Paleomagnetism. Elsevier, Amsterdam, pp 254–286. https://doi.org/10.1016/B978-1-4832-2894-5.50049-5

CHAPTER 7

SUMMARY AND SYNTHESIS

Chapter 2 presents new observations from the Osage Microgranite. This particular body had previously been identified and interpreted as a shallowly-emplaced granite. New petrographic observations suggest that it could alternatively be interpreted as a highly-welded volcanic unit, though the limited samples render this. Hydrothermal alteration features, including secondary minerals such as chlorite and synchysite, recrystallization of quartz with fluid inclusions, and impurities in metamict zircon are also discussed. Microstructures in quartz veins indicate deformation under aseismic conditions. A new geochemical set is compared to the much younger Long Mountain Granite of the Wichita Mountains; the resemblance may indicate that both were derived from source materials of similar mineralogy and composition. A brief description of unusual magnetic properties is provided as well, which is addressed in much more detail in Chapter 4.

Chapter 3 delivers observations of basement rocks in cores from northeastern Oklahoma. As opposed to the common assumption that basement rock in Oklahoma is intact, unaltered granite, inspection of core samples shows that basement rocks are almost invariably fractured and altered. Fractures are found to be common to depths of nearly 150 meters (the limit of core recovery to date). Slip indicators are present along numerous fractures as well, and, in some instances, slip may have been under seismic conditions. All samples show some degree of alteration, and geochemical analyses suggest alteration chemistry was either highly heterogeneous or occurred during multiple events. The fractured and altered character of the upper basement present in cores is far more similar to fractured basement reservoirs than it is to

uniform undamaged granite. This chapter proposes that basement fractures may act as sources of porosity and fluid-flow pathways, a possibility which should be considered in the context of induced seismicity studies.

Chapter 4 documents and investigates some highly unusual magnetic properties associated with altered rocks along the basement-cover interface and within some fracture zones; these behaviors are also found in the lowermost clastic sediments in some cores. These rocks show a decrease in magnetic susceptibility with increasing applied fields ("negative field-dependence"), a behavior which has been observed occasionally in rock magnetic studies but has never been explained or studied in detail. This study documents a relationship between frequency-dependence of susceptibility and negative field-dependence which indicates a likely association with superparamagnetic behavior. Further investigation shows that negative field-dependence is clearly linked to an unknown phase which has an apparent Curie temperature of ~83 °C, above which frequency-dependence diminishes and negative field-dependence diminishes or disappears in most samples. Additional rock magnetic measurements indicate that this behavior is not dependent on the presence of any known magnetic minerals. The mineral responsible remains unidentified, but the fact that this behavior appears to be found only in altered rocks suggests that it may have potential as an indicator for certain chemical conditions if the origin can be constrained.

Chapter 5 presents new data from the Spavinaw Granite. Rock magnetic data suggest that the magnetism is carried by magnetite and previously unrecognized maghemite. In contrast to older studies, the results of this work indicate that the magnetic remanence of the Spavinaw Granite is not incoherent. Instead, the results are similar to those obtained from early Cambrian rocks from southern Oklahoma and it appears that the rock was remagnetized during that time,

with a possible later partial overprint during the middle to late Paleozoic. The strike of the AMS foliation plane also agrees with structural trends associated with early Cambrian tectonics in southern Oklahoma, and the dip of the plane suggests that the Spavinaw Granite may be substantially tilted. While limited sampling means these results are only preliminary, the work presented in this chapter suggests that early Cambrian tectonism affected northeastern Oklahoma as well.

Chapter 6 provides a new paleomagnetic constraint on the early Cambrian apparent polar wander path for North America using data from the Glen Mountains Layered Complex and associated mafic/intermediate rocks in southwestern Oklahoma. The apparent primary pole position is roughly similar to that of contemporaneous Cambrian rocks from Quebec and is shown to be fairly insensitive to estimates of tilt from both mapped layering and AMS foliation. Results from some sites indicate spurious directions interpreted as partial to complete late Paleozoic remagnetizations, likely associated with the last stages of uplift but the origin remains unknown. Other sites show a component with a pole position nearly 90° from the primary one that is close to the Devonian part of the path. While similar results have been used to justify hypotheses such as true polar wander and equatorial geomagnetic dipole, in this instance the parsimonious explanation is a remagnetization during the Devonian. Though no major tectonism is known for this area at that time, it is at least plausible on the basis of numerous Devonian unconformities. Previous paleomagnetic poles from the early Cambrian granites and rhyolites in southern Oklahoma lie along a line between the primary direction and the apparent Devonian one, and in some cases the confidence intervals overlap, suggesting that those rocks were partially overprinted.

Deformation and alteration in basement rocks from northeastern Oklahoma are noted in Chapter 2 and expounded in Chapter 3. Alteration is characterized via mineralogical and chemical methods in those chapters, and via magnetic methods as well in Chapters 4 and 5. Chapter 4 describes essentially unstudied magnetic phenomena associated with at least some of the alteration. Chapter 5 provides evidence for early Cambrian alteration of the Spavinaw Granite, which could plausibly provide a timing estimate for at least some of the alteration seen in the subsurface rocks. The timing and the orientation of AMS foliation also hint at a plausible connection between this alteration and tectonic activity far to the southwest. Chapter 6 yields a new paleomagnetic constraint for North America during the early Cambrian and additionally shows evidence for possibly two alteration events, Late Paleozoic and Devonian, the latter of which had not been previously documented and is enigmatic. Together, these studies highlight characteristics associated with the tectonics and alteration of Oklahoma basement rocks and show that these rocks have great relevance to larger problems.